1983

Application Of Counter-current Fluidized Cascade In Flotsam-rich Mixtures

Edward Wing-kee Chan

CANADIAN THESES ON MICROFICHE

I.S.B.N.

THESES CANADIENNES SUR MICROFICHE

National Library of Canada
Collections Development Branch

Canadian Theses on
Microfiche Service

Ottawa, Canada
K1A 0N4

Bibliothèque nationale du Canada
Direction du développement des collections

Service des thèses canadiennes
sur microfiche

NOTICE

The quality of this microfiche is heavily dependent upon the quality of the original thesis submitted for microfilming. Every effort has been made to ensure the highest quality of reproduction possible.

If pages are missing, contact the university which granted the degree.

Some pages may have indistinct print especially if the original pages were typed with a poor typewriter ribbon or if the university sent us a poor photocopy.

Previously copyrighted materials (journal articles, published tests, etc.) are not filmed.

Reproduction in full or in part of this film is governed by the Canadian Copyright Act, R.S.C. 1970, c. C-30. Please read the authorization forms which accompany this thesis.

AVIS

La qualité de cette microfiche dépend grandement de la qualité de la thèse soumise au microfilmage. Nous avons tout fait pour assurer une qualité supérieure de reproduction.

S'il manque des pages, veuillez communiquer avec l'université qui a conféré le grade.

La qualité d'impression de certaines pages peut laisser à désirer, surtout si les pages originales ont été dactylographiées à l'aide d'un ruban usé ou si l'université nous a fait parvenir une photocopie de mauvaise qualité.

Les documents qui font déjà l'objet d'un droit d'auteur (articles de revue, examens publiés, etc.) ne sont pas microfilmés.

La reproduction, même partielle, de ce microfilm est soumise à la Loi canadienne sur le droit d'auteur, SRC 1970, c. C-30. Veuillez prendre connaissance des formules d'autorisation qui accompagnent cette thèse.

THIS DISSERTATION
HAS BEEN MICROFILMED
EXACTLY AS RECEIVED

LA THÈSE A ÉTÉ
MICROFILMÉE TELLE QUE
NOUS L'AVONS REÇUE

NL-339 (r. 82/08)

Canada

APPLICATION OF COUNTER-CURRENT FLUIDIZED CASCADE IN FLOTSAM-RICH MIXTURES

by

Edward Wing-Kee Chan

Submitted in partial fulfillment
of the requirements for the degree of
Doctor of Philosophy
(Engineering)

Faculty of Graduate Studies
The University of Western Ontario
London, Ontario
December, 1982

ABSTRACT

The counter-current gas fluidized cascade is a novel pneumatic device for the separation of mixed granular solids according to density and size difference. The study presented here is restricted to the application of the cascade in flotsam-rich binary mixed solids systems.

The separation effectiveness of the cascade is dependent on the density difference and size distributions of the components in the mixed solids system, the height and speed of the paddles, the fluidization velocity and the feed and withdrawal rates of product and reject streams. The purpose of the study is to investigate the effect of these variables on the separation performance of the cascade. It was observed that while a significant density difference between the jetsam and flotsam components would usually result in strong segregation of the jetsam component in the simple fluidized be, the separation in the cascade was less predictable. Separation efficiency appeared to deteriorate as the mean particle size of the components was reduced. Experiments with various solids systems have demonstrated the importance

of paddle height, paddle speed and fluidization velocity on the separation efficiency. With the limited throughput capacity of the present system, the effect of the feed and withdrawal rate on the separation performance of the cascade could not be ascertained.

Statistical multiple regression technique was used to investigate the effect of the various variables on the cascade performance. A theoretical model was also presented to describe the performance of the cascade under total reflux conditions. The dependency of turbulent diffusivity on the horizontal convective velocity of the fluidized solids was incorporated into the model. Agreement between the theoretical model and the experimental data is reasonable.

Of the various solids systems investigated, the natural coal system is of industrial importance. The present study demonstrated the potential of the cascade as a simple and inexpensive device in coal beneficiation, despite the limitation on the purity of the product imposed by the degree of liberation of pyrite and ash from the coal matrix. Experiments with the natural coal system have also demonstrated that the separation effectiveness of the cascade could be improved by a multi-pass process in which the products and rejects were reprocessed in subsequent passes in the cascade.

The present work should be viewed as a first attempt to investigate the performance of the cascade in the separation of flotsam-rich solids systems. Continuation of the

present experimental program as well as further theoretical development is recommended for a more thorough understanding of the cascade.

ACKNOWLEDGEMENTS

The author would like to express his sincere gratitude to Dr. J.M. Beeckmans for his guidance and assistance throughout the project. The Material Science professors and personnel were also most accommodating to lend their facilities and assistance in the X-Ray analysis. I would also like to extend my appreciation and gratitude to the professors at the department, Dr. Bergougnou, Dr. Bulani, Dr. Margaritis and others, and the graduate students and associates, Dr. Tschanz, Mr. Rowe, Mr. Catros, Mr. Goransson, Dr. Abubaker, Mr. Muzyka, Mr. Creese, Mr. Jeffs and Mrs. L. Bergstrom Macy for their enthusiastic assistance, encouragement and advice throughout the project.

The staffs and colleagues at the National Research Council, Atlantic Research Laboratory in Halifax, N.S., have been most helpful in lending their facilities and assistance for the completion of the later part of the thesis. The assistance of Dr. Simpson, Dr. Whiteway, Dr. Hirajima, Dr. Leewis, Dr. Stewart, Mr. Johnson and many others is truly appreciated.

Sincere gratitude is extended to members of my family for their support during my graduate work. Their encouragement in times of difficulty is especially appreciated.

Finally, without the financial support of the Energy, Mines and Resources Canada, and the Natural Sciences and Engineering Research Council of Canada, the project would not have been possible.

TABLE OF CONTENTS

TABLE OF CONTENTS (Continued)

TABLE OF CONTENTS (Continued)

TABLE OF CONTENTS (Continued)

LIST OF TABLES

LIST OF TABLES (Continued)

LIST OF TABLES (Continued)

LIST OF TABLES (Continued)

LIST OF FIGURES

LIST OF FIGURES (Continued)

LIST OF APPENDICES

NOMENCLATURE

a (Chapter 6)	Empirical constant of Equation 6.23
A	Slope of regression line of ln(c) versus Z
A_1, A_2, A_3	Empirical constants
A_1, A_2 (Chap. 6)	Empirical constants of Equation 6.24
a_3, a_4	Empirical constants
Ash	Weight percentage or fraction of ash in coal
B	Intercept of regression line of ln(c) versus Z
b (Chapter 6)	Empirical constant of Equation 6.23
BR	Beneficiation ratio, ratio of jetsam concentration at the two ends of the cascade
C	Concentration of jetsam, %
$C_{Z=0}$	Concentration of jetsam at Z=0
$C_{Z=1}$	Concentration of jetsam at Z=1
C_{exp}	Integrated jetsam concentration based on logarithmic jetsam concentration profile, %
C_i	Local concentration of jetsam in fluidized bed, %
C_1	Empirical constant of Equation 6.13
C_2 (Chapter 6)	Empirical constant of Equation 6.13
cc	Correlation coefficient of regression line
CS	Speed of paddle chain, mm/s
D	Internal diameter of fluidized bed, m
D (Chapter 6)	Turbulent diffusivity; mm^2/s
D_{er}	Shaped corrected diameter ratio = $\phi_H d_H / \phi_L d_L$

D_1	Concentration of pyrites in product stream, %
D_2	Concentration of pyrites in reject stream, %
D_3	Beneficiation ratio of pyrite (= D_2/D_1)
D_t (Chapter 6)	Taylor diffusivity, mm^2/s
D_o (Chapter 6)	Diffusivity in the absence of horizontal velocity, mm^2/s
d_b	Mean diameter of large component in binary mixture of solids. m
d_H	Mean diameter of heavy component in binary mixture of solids, m
d_L	Mean diameter of light component in binary mixture of solids, m
d_s	Mean diameter of small component in binary mixture of solids, m
$F(U-Um_f)$	A function of $(U-Um_f)$
F_D	Diffusion flux of jetsam
F_V	Vertical flux of jetsam
F_{ratio}	Statistical parameters
$F_{0.05}$	F_{ratio} at 95% confidence
G	Total coal feed rate, kg/hr
H	Bed height of solids in fluidized bed, m
H*	Reduced aspect ratio (= 1-exp(-H/D))
I*	Normalized X-ray counts
JR	Unaccountable jetsam accumulation, %
K (Chapter 6)	Vertical mass transfer coefficient, mm/s
ℓ (Chapter 6)	Axial distance in cascade measured from flotsam-rich end, mm
L	Total length of cascade bed, mm

L_f	Height of fluidized bed, m
L_{mf}	Height of fluidized bed at ($U=U_{mf}$), m
M	Mixing index
M_1, M_2 (Chap.6)	Roots of the characteristic equation, Equation 6.13
N_f	Fluidization number ($=U/U_{mf}$)
P_r	Fraction of feed originating at product side of cascade
PSAF	Ash-free pyritic sulphur, fraction or percentage
S	Weight fraction of total sulphur
S'_o	Weight fraction of organic sulphur on an ash-free basis
S_p	Weight fraction of pyritic sulphur, as is
S_p	Weight fraction of pyritic sulphur, on an ash-free basis
S (Chapter 6)	Parameter defined by Equation 6.5
t (Chapter 6)	Time, s
U	Superficial velocity, m/sec
$\bar{U}$	Mean convective velocity of flowing fluidized solids, mm/s
U_{mf}	Minimum fluidization velocity, m/sec
U_f	U_{mf} of the more fluid component in binary mixture
U_p	U_{mf} of the more packed component in binary mixture
U_{to}	Take-over velocity at which M = 0.5
V_L, V_h (Chap. 6)	Average velocity of upper and lower stratum of cascade bed, mm/s
W	Feed rate of coal per unit width of bed, kg/m-hr

W_{opt}	Optimal fluidization velocity for maximum segregation, m/sec
W_{pr}, W_{co}	U_{mf} of aluminum fluoride and corundum, respectively, m/sec
X (Chaper 6)	Jetsam volumetric concentration in lower stratum of cascade, %
$\bar{X}$	Overall jetsam concentration, %
Y (Chaper 6)	Jetsam volumetric concentration in upper stratum of cascade, %
Y* (Chapter 6)	Equilibrium jetsam volumetric concentration in the upper stratum of a simple fluidized bed, %
Y_o (Chapter 6)	Jetsam volumetric concentration at ℓ=0, %
Z	Normalized distance from flotsam rich end of cascade

GREEK LETTERS

α (Chapter 6)	Ratio between paddle height and total bed height
ϕ_H, ϕ_L	Sphericity of heavy and light component, respectively
ρ_H, ρ_L	Density of heavy and light component, kg/m^3
μ	Viscosity of gas, poise
ΔP_b	Pressure drop in the fluidized bed of solids, mm of water
σ^2 (Chapter 6)	Variance of the tracer concentration distribution
ρ_R	Ratio of density of heavy and light component

CHAPTER ONE

INTRODUCTION

1.1 Foreword

With the dwindling availability of natural energy resources and the unstable political situation globally, in particular in the oil producing states of the middle east, the world is indeed increasingly approaching a state of crisis, the so-called "Energy Crisis". As a consequence of the phenomenal increase in the cost of petroleum and natural gas, attention is now focused on alternate energy sources which include renewable energy typified by biomass, solar, and the non-renewable but abundant fossil fuels like coal, tar-sand and shale. The recent revitalization of interest in coal is not at all surprising. North America is reputed to have an immense coal reserve, enough to meet the energy requirements of the industrial world for two to three hundred years. However, the utilization of coal is still limited because of its sulphur and ash content, which pose both environmental and technical problems.

There are basically two different modes of coal beneficiation, namely, chemical and physical separation. Chemical beneficiation usually is more efficient in separation effectiveness. Unfortunately, it is also expensive. Physical separation of ash and pyritic sulphur from the hydrocarbon matrix is based on the principle of separation due to density difference between the different components of coal. Most of the techniques in physical beneficiation are developed separation processes using water as the separation medium. Wet separation processes, until recently, have yielded better separation efficiency than the dry pneumatic type. A new device in dry pneumatic separation, the counter-current fluidized cascade separator, was recently invented and developed by Professor Beeckmans at the University of Western Ontario, and may revive interest in dry pneumatic separation. The device makes use of the fact that when a composite mixture of granular solids is fluidized in a simple fluidized bed, the heavy and large component, jetsam, tends to settle towards the bottom and the light and/or small component, flotsam, tends to settle towards the top stratum of the bed.

A sketch of the counter-current fluidized cascade is shown in Figure 1.1. It consists of a long rectangular bed containing the fluidized granular solids. The fluidization air is controlled and metered externally to the bed prior to its introduction to the wind box beneath the grid of the fluidized bed. Motion is induced in the lower stratum of the fluidized bed towards the left side by paddles which

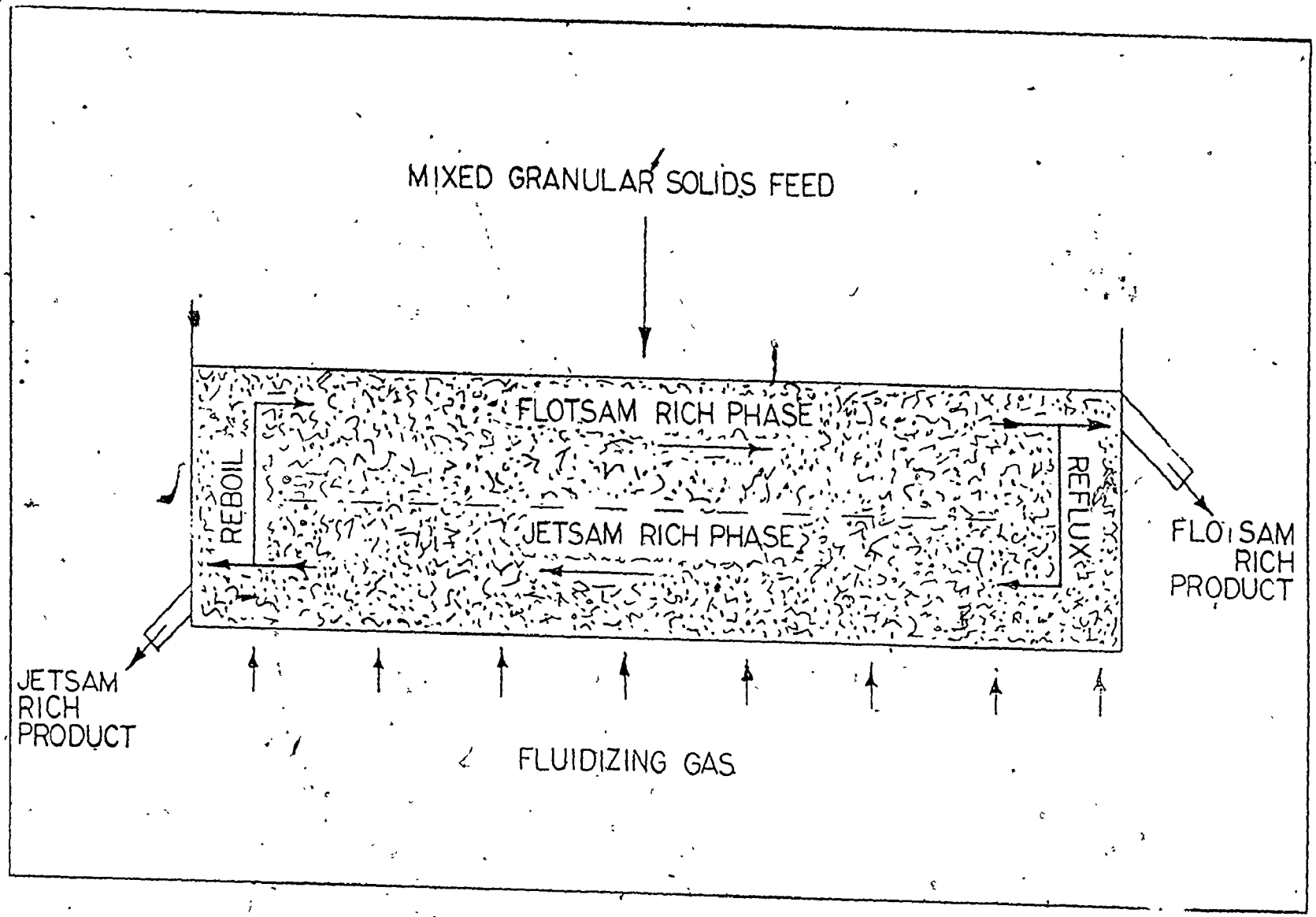

FIGURE 1.1 PRINCPLE OF THE COUNTER-CURRENT FLUIDIZED CASCADE

are attached to an endless chain completely submerged in the solids, and which is driven by an external motor. Owing to the fluid property of fluidized solids, the upper stratum of the bed moves towards the right side by gravity, resulting in a counter-current motion of the two stratified layers inside the long rectangular bed. Owing to the segregating properties resulting from the density and/or size difference between the components, the left end of the bed will be enriched in jetsam, while the right side will be, conversely, flotsam-rich with low jetsam concentration. At some point along the bed, a mixture of granular solids is introduced into the bed and constitutes the feed. There are two withdrawal ports at the two ends of the cascade. Towards the left end, the jetsam-rich side, the withdrawal port is constructed very close to the grid for the effective withdrawal of the jetsam-rich reject stream, as jetsam tends to concentrate towards the lower stratum of the bed. Towards the right side, the flotsam-rich side, the port is located close to the top surface of the fluidized bed for the withdrawal of a flotsam-rich product stream.

The operation of the counter-current fluidized cascade closely resembles that of a distillation tower. The convective flow of jetsam-rich material in the lower stratum is analogous to the liquid flow, and the counter-current flow of flotsam-rich material in the upper stratum is analogous to the vapor flow. The location where material is fed to the bed is analogous to the feedplate. The

continuous vertical exchange between the two strata of the cascade is very similar to the liquid-vapor mass transfer in each tray of the distillation tower. When material is conveyed towards either end of the cascade, only a fraction of it would be withdrawn, the remainder being recycled back into the bed. Once again, this resembles the reboiling and the refluxing operations at the reboiler and the condenser of the distillation tower. The jetsam and flotsam-rich withdrawals at the two ends of the cascade are analogous, of course, to the withdrawal of the bottom and distillate streams. By conceptually visualizing the operations of the cascade as a distillation unit, it can be deduced that the effectiveness of separation, usually measured by the beneficiation ratio, defined as the concentration ratio of jetsam in the two product streams, should be dependent on the concentration of the feed, the feed and withdrawal rates, the relative height of the two strata, the convective volumetric flow rates of the two strata (i.e. the chain speed), and the rate of the vertical exchange between the two strata, which in turn is dependent on the fluidizing velocity.

In view of the fact that part of the heavy ash and pyritic sulphur can be liberated from the hydrocarbon matrix of coal by crushing, it is logical to assume that the cascade may find application in the field of coal beneficiation. A relatively low operating cost, high separation effectiveness and the fact that it is a dry process are some of the

factors that contribute to the attractiveness of the counter-current fluidized cascade as an alternative coal cleaning machine. By optimizing the different operating conditions, the potential of the cascade to successfully compete with other coal cleaning devices can be greatly enhanced.

The objective of this study was to investigate the effect of the different operating conditions on the separation effectiveness of the cascade. Different artificial solid granular mixtures with the minor component of a higher density than that of the matrix material were used. There were also a limited number of experiments performed with natural coal. Most of the data collected were quite encouraging. However, owing to the lack of manpower and financial constraints, this investigation should be viewed only as a first attempt to study the counter-current cascade using flotsam-rich mixtures. Further work on both the theoretical and applicational aspects of the device is indeed essential to better understand its performance and limitations.

CHAPTER TWO

LITERATURE SURVEY

2.1 Fluidization

2.1.1 Definition of Fluidization

When a fluid flows upward through a bed of fine particles, the bed remains stationary while the fluid percolates through the interstitial void between the particles. The bed in this condition is called a fixed bed and its pressure versus fluid flow rate characteristics can be described by the Ergun equation.[1,2,4]

A point will be reached when the frictional pressure drop due to fluid flow is equal to the buoyant weight per unit area of the particles. At this point, the bed will be expanded slightly to a height of L_{mf}, as shown in Figure 2.1, and the particles will become re-arranged in order to minimize their resistance to fluid flow.[4] The fluid velocity at this point is called the minimum fluidization velocity (U_{mf}), or incipient fluidization velocity of the solids. Any increase in the fluid velocity will result in bed expansion and vigorous solids movement.

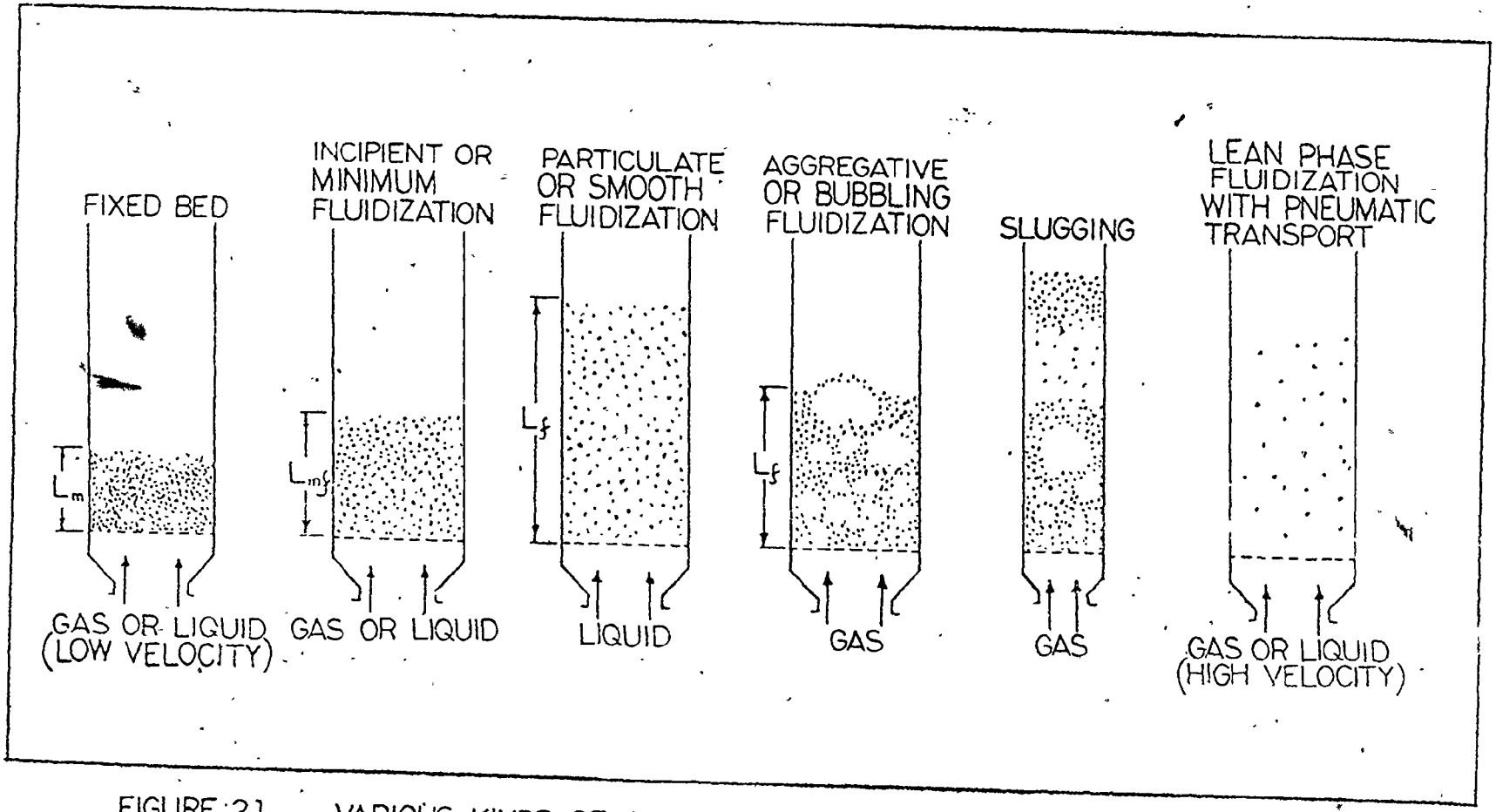

FIGURE 2.1 VARIOUS KINDS OF CONTACTING OF A BATCH OF SOLIDS BY FLUID (2)

The turbulent motion of solids and gas flow resembles a boiling liquid. The fluidity of the fluidized solids can be observed in the retention of a horizontal surface when the bed containing the fluidized solids is tipped at an angle. Furthermore, if there is a weir or opening in the side of the vessel, the fluidized solids will flow freely through it as if they were liquid. The rapid mixing of solids is responsible for very efficient mass and heat transfer which makes fluidized beds very attractive and viable in drying and reaction engineering.

A liquid-solid system is inherently different from a gas-solid system. As the fluid superficial velocity exceeds the minimum fluidization velocity of solids in the liquid-solid system, the bed height will continually increase with fluid flow rate, resulting in what is commonly called particulate fluidization (see Figure 2.1). In gas-solid systems, however, the increase in gas flow beyond the minimum fluidization velocity will lead to vigorous bubbling and channeling of gas (see Figure 2.1); L_f remains almost constant and is relatively insensitive to increases in gas flow rate. This bubbling behaviour of the gas-solid fluidized bed is commonly known as aggregative, heterogenous or bubbling fluidization.[2]

In a small diameter fluidization column, as the gas flow rate exceeds the minimum fluidization velocity of the solids, a phenomenon called slugging may occur[7] (see Figure 2.1). Slugging is due to the coalescence of gas

bubbles which results in the formation of a bubble large enough to spread across the vessel. The upward momentum of this large bubble can result in an intermittent displacement of sections of the bed, with particles raining down from the slug. Slugging may be undesirable as it reduces the contact effectiveness between solids and gas and increases the loss of solids as a result of increased entrainment. In both the liquid-solid and gas-solid system, as the fluid velocity is further increased, a point will be reached where the fluid velocity exceeds the terminal settling velocity of solids and this leads to pneumatic transport of the solid particles (Figure 2.1).

2.2 Segregation of Solids in Fluidized Beds

2.2.1 Segregation Profiles and Definitions

If a binary mixture of solid particles is fluidized at a fluid velocity slightly greater than the minimum fluidization velocity of the mixture, the larger and/or denser component tends to concentrate near the lower stratum while the smaller and/or less dense component will be enriched in the upper stratum of the fluidized bed. Rowe and coworkers[11] proposed to call the component that sinks and segregates toward the bottom "jetsam", and the component that floats "flotsam".

A typical example of a jetsam-rich system is the

fluidized bed combustor where the minor component is coal particles and the major component is limestone. Flotsam-rich systems are usually of greater industrial importance. Pyrites and ash are the minor components in coal; the fact that the pyrites and ash are heavier than the coal matrix will therefore imply a flotsam-rich system. Other naturally occurring flotsam-rich systems can be found in the impure mineral ores.

Rowe and coworkers[12] investigated the segregation of jetsam in flotsam-rich systems. Segregation profiles are shown in Figure 2.2.[13] Figure 2.2A shows a well-segregated system which is typified by a large density difference at an air velocity close to that of minimum fluidization. In this system, a pure layer of jetsam accumulates at the bottom while the remaining jetsam is distributed evenly across the top stratum of the bed. This concentration profile changes with increase in fluidization velocity. In Figure 2.2B, there is no longer the formation of a pure jetsam layer in the bottom and the concentration of jetsam in the upper stratum of the bed is substantially increased. As the fluidization velocity is further increased, a point will be reached where the bed will become perfectly mixed, as shown in Figure 2.2C.

The segregation profile of a jetsam-rich system is different from that of a flotsam-rich system. A pure layer of flotsam on the top of the bed has never been observed. This is due to the depositing of jetsam material, which is

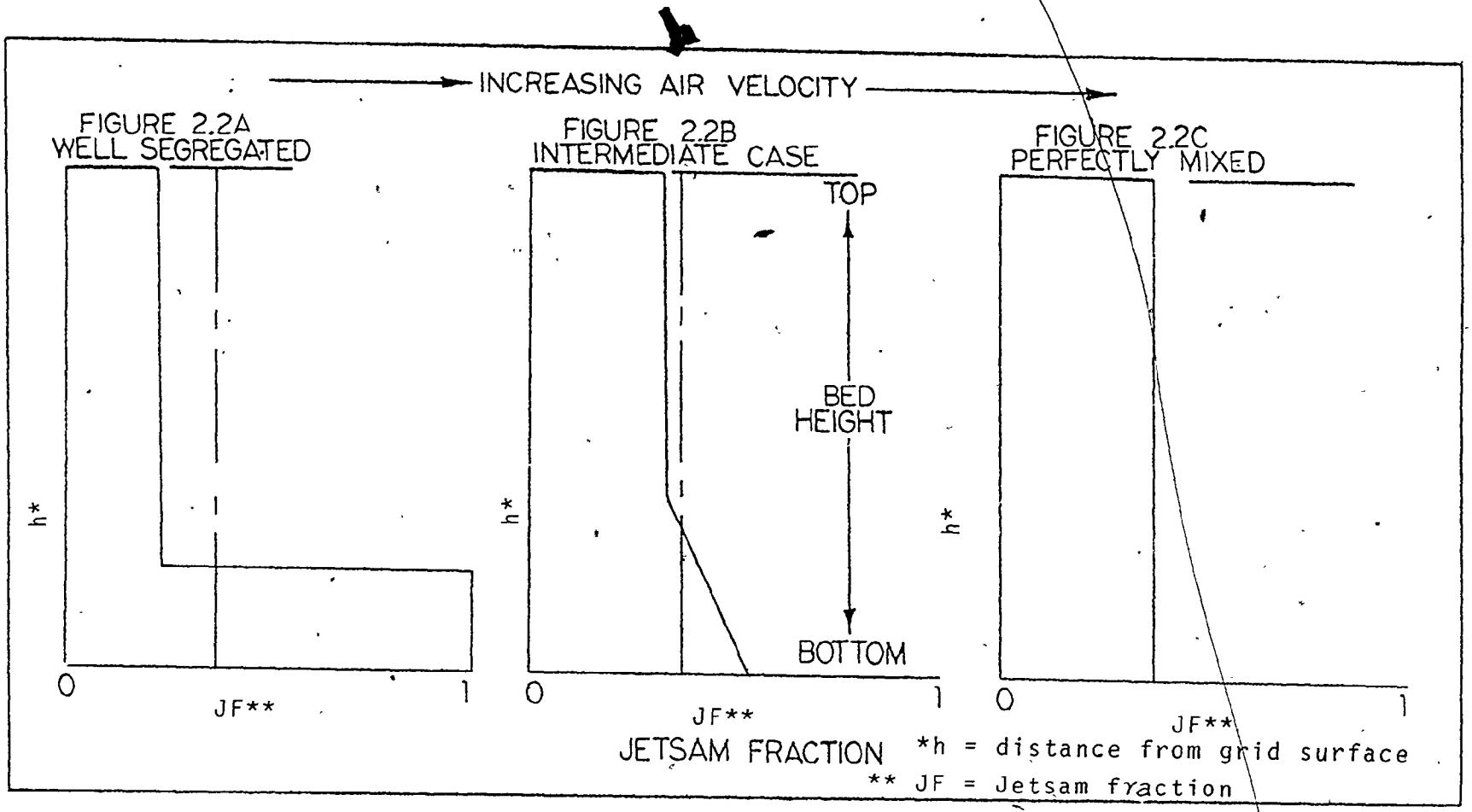

FIGURE 2.2 CONCENTRATION PROFILES IN FLOTSAM-RICH MIXTURE (13)

carried by the wakes of the bubbles, to the top of the bed. For well-segregated systems, which usually occur at low fluidization velocity and when there is a density difference between the components, the concentration of flotsam exhibits a gradient on the top of the bed while the bottom stratum of the bed is essentially devoid of flotsam component, as shown in Figure 2.3A. As the fluidization air velocity is increased, the concentration profile progresses from Figure 2.3A to Figure 2.3C. Even at high fluidization velocity, a slight jetsam concentration variation with height is still observed.

2.2.2 Empirical Equation for Solids Segregation in Gas-Fluidized Beds

For over ten years, the research team at University College, London, England, carried out detailed investigations on particle segregation in gas fluidized beds, and the effect of different operating conditions, such as fluidization velocity, particle size and density ratio, overall concentration of jetsam in the binary mixture, bed aspect ratio and other factors, on segregation effectiveness. The work pertaining to the mechanisms of segregation will be discussed later in this chapter (Section 2.24).

An empirical equation was introduced to predict the segregation effectiveness of jetsam in a binary mixture of solids.[12] The equation is based on experimental data on a wide range of binary mixtures of varying size and density

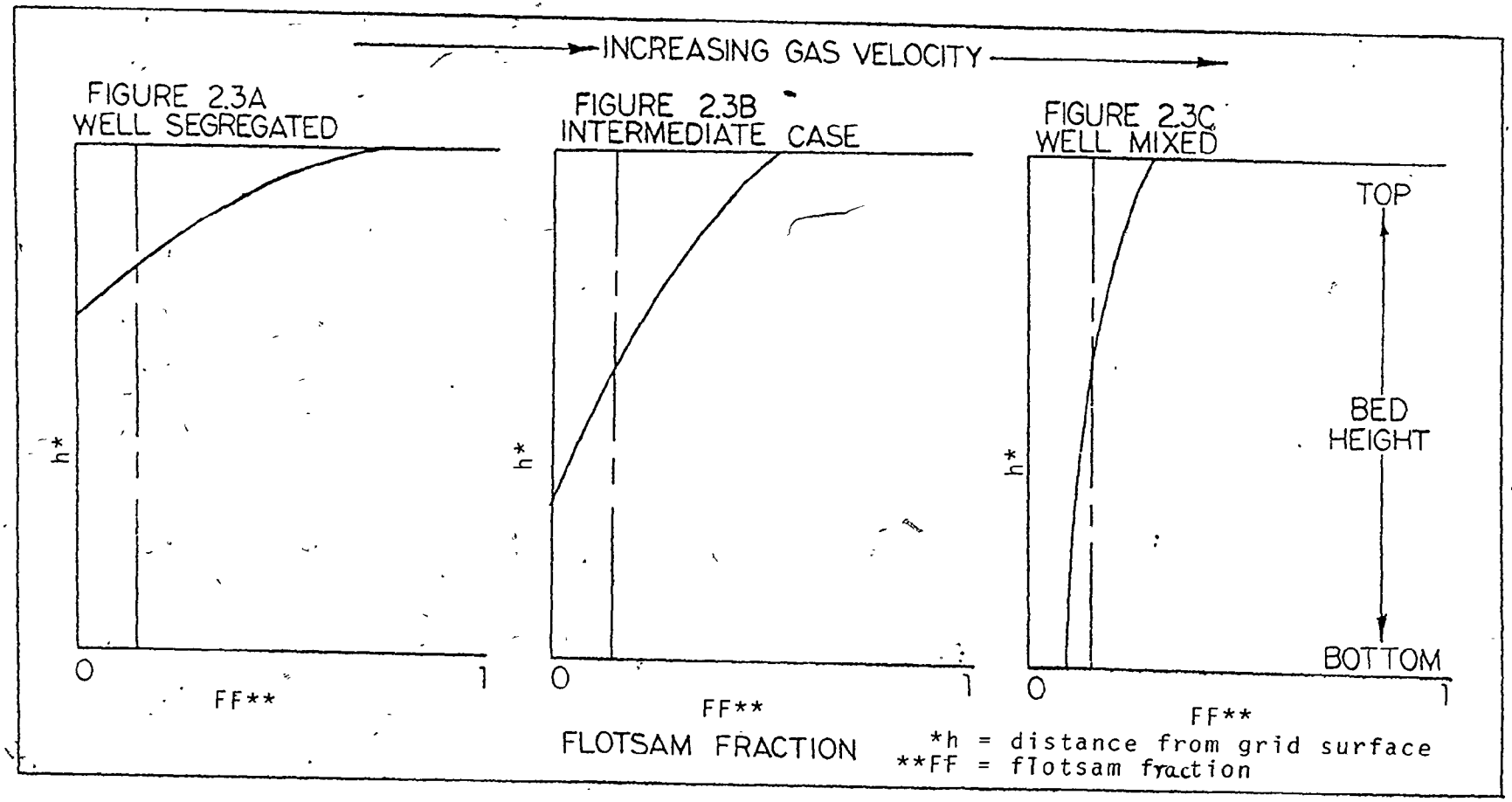

FIGURE 2.3 CONCENTRATION PROFILES IN JETSAM-RICH MIXTURES (13)

ratio, overall concentration of jetsam in the bed and the bed aspect ratio. The equation is relatively easy to use for the prediction of segregation in flotsam-rich binary mixtures, with and without a density difference, of up to about 50% by volume of jetsam. It is also claimed that the predicted mixing index would have a relatively small standard deviation of ±9% if the take-over velocity, U_{to}, and the U_{mf} of both components were known.

The effectiveness (or degree) of segregation is quantified by the mixing index M, where $M = X/\bar{X}$

X = mass fraction of jetsam in the upper uniform part of bed

$\bar{X}$ = overall mass fraction of jetsam in the bed.

M is a function of nondimensional parameter Z, which is called the reduced gas velocity.

$$M = X/\bar{X} = (1 + e^{-Z})^{-1} \qquad (2.1)$$

where $$Z = \frac{U - U_{to}}{U - U_f} \exp (U/U_{to}) \qquad (2.2)$$

and U = superficial gas velocity

$U_f = U_{mf}$ of component with the lower U_{mf} (i.e., the more fluid component)

U_{to} = take-over velocity at which M = 0.5

The take-over velocity, U_{to}, can be estimated from the empirical equation:

$$\frac{U_{to}}{U_f} = \frac{(U_p)^{1.2}}{(U_f)} + 0.9\,(\rho_R - 1)^{1.1}(Der)^{0.7} - 2.2\,(\bar{X})^{0.5}$$

$$(H^*)^{1.4} \qquad (2.3)$$

where $U_f = U_{mf}$ of the component with lower U_{mf} (fluid), m/s

$U_p = U_{mf}$ of the component with higher U_{mf} (packed), m/s

U_{to} = take-over velocity; the velocity above which mixing takes over, i.e., when M = 1/2

$\rho_R = \rho_H/\rho_L$. ρ_H = apparent density of heavy component, kg/m^3

ρ_L = apparent density of light component, kg/m^3

Der = shape-corrected diameter ratio = $\phi_H d_H/d_L \phi_L$

ϕ_H, d_H = sphericity and mean diameter of the heavy component

ϕ_L, d_L = sphericity and mean diameter of the light component

$\bar{X}$ = overall mass fraction of jetsam in the bed

H* = reduced aspect ratio = 1 -exp (-H/D)

H = bed height, m

D = bed diameter, m

It is interesting to note that the use of the empirical equation can be extended to ternary systems consisting of dense jetsam in a matrix of two flotsam components of varying sizes.[14]

For the continuous mixing of two particulate species of different densities in a gas fluidized bed, the same equations can be used to predict the concentration of the outgoing stream if the feed rate is adjusted to a level at which the mean residence time of the solids is greater than twice the time required for equilibrium to be reached in the batch test.[15]

2.2.3 The Chen and Keairns Phase Diagram

Chen and Keairns[8] studied particle segregation at low gas velocity, near the minimum fluidization velocity for mixtures of different sizes (150 to 2800 microns) and densities (720 to 2800 kg/m^3) in a gas fluidized bed. They advocated the construction of phase diagrams similar to those of liquid-solid systems. Their phase diagrams are unique in the sense that the concentration and amount of jetsam in the upper or lower strata of the fluidized bed can be determined if the overall concentration and operating gas velocity are known. With the availability of experimental data, the Chen and Keairns phase diagram approach can be used to interpolate and predict the degree of segregation of binary mixtures in fluidized beds.

2.2.4 Mechanisms of Segregation

Numerous publications on the subject of the mechanisms of segregation of solids in fluidized beds have appeared. Perhaps the work by Rowe, Nienow and coworkers at University College, England, should be described first, in view of their pioneering investigations in the area.

Using high speed photography and X-ray techniques, Rowe and coworkers[17] studied the entrainment of solids by a rising bubble. The photographs were essentially supportive of the theoretical models of bubbles by Davidson and Murray.[3,5] It was observed that the volume occupied by the wake was approximately 25% that of the entire

bubble,[16] or the lower one third of the bubble diameter. The size of the wake varies with the size and type of fluidized particles. Going from the bottom to the top of the fluidized bed, the particles inside the wake do not remain intact but are shed regularly en route while the wake is continuously replenished. "As underlying material is carried upward by the bubbles, so other material must sink to take its place. The overall effect is a kind of convection, upward along the path of bubbles and downward elsewhere."[16]

It was also observed that the initial wake material was gathered from a depth less than the bubble diameter and included material from the very bottom of the bed where the bubble emerged. It was also observed that the wake size fluctuated appreciably but did not change systematically with bed height. When the bubble reaches the top surface, it bursts and the residual momentum of the wake forces the wake material to spread over the top of the bed. When the jetsam material consists of large and dense particles, it can fall through a gas fluidized bed, much as drops of a denser immiscible liquid would fall through another liquid.[18] The segregating movement induced by single bubbles on a heap of jetsam material initially placed on top of the bed is described in detail in a paper by Nienow and coworkers.[18]

It is perhaps interesting to note that the segregation phenomenon of spouted fluidized beds is substantially different from that of ordinary fluidized beds. A paper on

the subject was published by Piccinini, et al.[19]

It is also worthwhile to note that segregation due to mechanical jigging is also mechanistically different from segregation due to bubbles in fluidized bed.[20] This may be of interest because fluidization is coupled with mechanical jigging in some fluidized bed separators (Section 2.4).

Rowe and coworkers[17] studied the segregation of jetsam in a binary mixture of solids of different densities, sizes and fluidities (i.e., U_{mf}'s). It was hypothesized that the out of balance hydrodynamic forces following the passage of bubbles caused the small and heavy jetsam particles to percolate between the interstitial spaces of their neighbours and consequently to concentrate toward the bottom stratum. Large and heavy jetsam particles, however, would tend to fall through the roof of bubbles and progressively concentrate toward the bottom in a series of jerks as a result of falling through the passing bubbles. Their physical size would prohibit them from descending through the small interstitial voids of the fluidized bed. No explanation was attempted as to the reason why the less dense particles should float on a fluidized bed of denser ones.

It has also been observed that the hindrance of particle movement due to fluidized internals (such as heat exchangers or baffles) can decrease solid mixing, and thereby enhance segregation.[23]

An attempt to quantitatively study solids segrega-

tion in fluidized beds was undertaken by Rowe and co-workers.[21] The dependency of the mixing index, which was defined earlier (section 2.2.2), on the density and size ratio was correlated. It was found that segregation was only mildly affected by the size ratio between the two components. Density ratio, however, strongly affected the segregation effectiveness. However, a limiting condition could be reached when the dominance of density ratio could be overshadowed by the large size difference. In this case, the dense component may be flotsam.[22] In all cases, segregation diminished with increase in the excess fluidization velocity, i.e., the magnitude of $(U-U_{mf})$. The functional dependency of the mixing index can be summarized in the equation

$$M = F(U - U_{mf,f})(\rho_H/\rho_L)^{-2.5}(d_b/d_s)^{-.2} \qquad (2.4)$$

Conceptually, equation 2.4 is of great importance in fluidized bed design with heterodispersed and/or composite density solid mixtures.

It has been asserted that mixing of particles in bubbling gas fluidized beds is solely caused by bubbles.[24] The rate of mixing is dependent on the total bubble flux that passes through the bed. With fine powders, increase in gas flow rate usually produces less bubbles and therefore less mixing than the same percentage increase with coarse particles. It is also interesting to note that for the fluidization of spherical particles of uniform size in a deep bed, the onset of bubble formation is usually at

about 1.3 x U_{mf}.[24]

An interesting paper was published by Nienow et al.[28] concerning the mixing and segregation of a small proportion of large particles in a gas fluidized bed of small ones. In the investigation, the large particles (flotsam) were coal in a matrix of small ash and sand (jetsam). It was observed that the bubbles tended to move away from the containing walls toward the centre of the fluidized bed so that an overall convection was set up with particles moving downward near the walls. Equilibrium distribution of particles was reached quite rapidly, usually within some tens of seconds, in most cases.

Tanimoto, et al.[31] used cine-photographic techniques to study the movement induced by the passage of single bubbles of large and heavy jetsam solids in a two-dimensional gas-fluidized bed. The average descending distance over the bubble cross sectional area was shown to be dependent on the jetsam properties.

Chiba, et al.[32,33] studied the rate of solids exchange between the bubble wake and the emulsion phase in a three-dimensional gas fluidized bed. It was found that the exchange rate decreased with increase of bubble diameter. A model was developed for the prediction of the exchange coefficient between the two phases.

In a different research area, experimental work was performed to investigate the flow of coarse particles through a fluidized bed of fines.[27,26]

Based on experimental observation and high-speed photography, distinctly different mechanisms of particle movement were identified.[13,16] As the bubble formed near the bottom of the bed, it gathered material in its wake region which occupied the lower one third of the bubble.[16] En route to the top of the bed, the wake periodically shed and recaptured material to and from neighbouring fluidized solids. Even when the pure jetsam layer in the bottom is defluidized, the bubbles originating at the interphase would still capture some jetsam in their wakes.[28] As the bubble reached the top, it would burst and deposit its wake material at the surface. Although this mechanism caused mixing, it was also the only mechanism to transport the flotsam to the top, and thereby causing segregation.

A few mathematical models were developed to describe the phenomenon of solids segregation of binary mixture in gas fluidized beds.[11,29] In one of the models, the bed is assumed to consist of two exchanging phases, the wake and bulk phase (Figure 2.4). Mixing/segregation is caused by the exchange of solids between the two phases, the overall segregation of jetsam toward the bottom stratum by falling rapidly through bubbles and percolation through the interstitial voids in the bed, and axial displacement by bubbles. The exchange between the phases and the segregation terms are approximated by the product of transfer coefficients and concentration, whilst axial mixing is approximated by the product of a pseudo-diffusivity and the

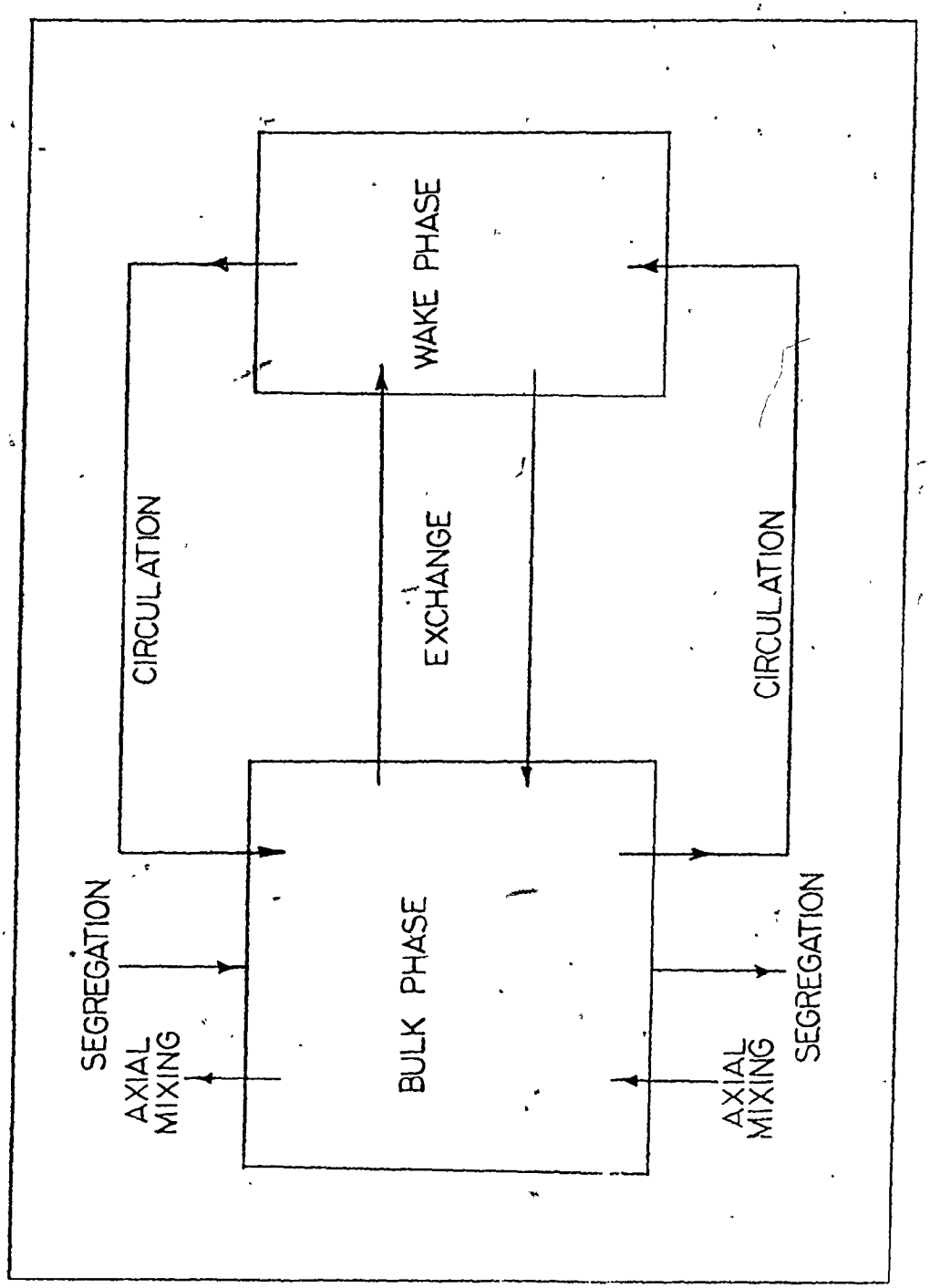

FIGURE 2.4 THE ROWE-GIBILARO SEGREGATION MODEL (13)

axial concentration gradient of jetsam. The overall convective circulation rate is assumed to take on some constant value and is independent of location in the bed. The coefficients for the exchange and segregation, the circulation rate, and the pseudo-diffusivity coefficient for axial mixing are assumed to take on some specific values, and are dependent on the bubble flow rate, i.e., the value of $(U-U_{mf})$. The model leads to two ordinary differential equations which can be solved when the appropriate boundary conditions are applied. The predicted and the experimentally obtained concentration profiles compare satisfactorily.

Burgess, et al.[30] presented a bubbling bed model on the segregation of solids in a fluidized bed. The model is unique in the assumption of the existence of two regions in the wake phase; one of them is stagnant with no mutual transfer with the bulk phase, the other is well mixed with mass exchange with the bulk phase. The assumption is also made that the segregation is dominated by the falling of jetsam through the roof of the bubbles. The predicted segregation profiles are in excellent agreement with experimental data.

Yoshida, et al.[34] incorporated a new parameter, the segregation factor R, which is defined as the ratio between the exchange rate of jetsam and that of flotsam, into the exchange term in the equations of Yoshida and Kunii.[35] The inclusion of this parameter enhances the agreement between the theoretically predicted segregation

profiles and those obtained experimentally. The validity of parameter R, however, was questioned by Beeckmans.[36]

Beeckmans and Bergstrom[36,37] studied segregation mechanisms and kinetics in a fluidized bed using segregating and non-segregating tracers. They claimed that the primary segregation mechanisms operate at the free surface of the bed in the case of jetsam-rich systems, or at the grid region in the case of flotsam-rich systems. It was found that the circulation of solids due to bubble movement was much slower in the lower stratum of the bed. A theoretical model was proposed to describe both steady state and transient segregation profiles. The model is unique in the sense that the transfer coefficient between the wake and the emulsion phase is assumed to be dependent on the location in the bed. A brief critique and survey on other theoretical models was also provided. Unfortunately, the model in its present form fails to represent the experimental data faithfully. It was speculated that the disagreement may be due to the non-homogeneity in the bubbles or solids flow across the bed cross section.

2.3 Previous Counter-Current Fluidized Cascade (CCFC) Research

Research in the application of the cascade under various conditions with synthetic and naturally occurring solids mixtures was carried out by a number of graduate students at this university.

2.3.1 Research by Minh[38,39]

Minh worked with a jetsam-rich system of activated carbon in a sand matrix using the CCFC. It was apparent that the separation effectiveness was strongly dependent on the value of $(U-U_{mf})$, and on paddle velocity. The separation of carbon from sand at the sand end was found to be much superior to the separation of sand from carbon at the carbon end of the cascade. The increase in minimum fluidization velocity at the carbon-rich end was given as the primary reason for this difference.

2.3.2 Research by Muzyka[40,77,41]

Muzyka continued and expanded the scope of Minh's work by investigating the separation of coconut charcoal from salt, which again constituted a jetsam-rich system. Phenomenal separations, as measured by the ratio of the concentration of charcoal in the two ends of the cascade, were achieved under optimized conditions. The dependency of longitudinal diffusion on the convective velocity of solids, the so-called Taylor diffusivity, was also investigated. A simple mathematical model based on a mass flux balance on a vertical slab in the cascade bed was derived to explain the performance of the cascade. The model's prediction and the experimental data compared favourably.

2.3.3 Research by Jeffs[13]

Jeffs investigated the dependency of the Taylor

diffusivity on the convective velocity of solids in more detail. A more advanced mathematical model was introduced to better describe the dependency of separation effectiveness on the various operating conditions. The model is a much refined and updated version of the original simplistic model presented in Muzyka's thesis. Numerical solutions of the model yielded predicted concentration profiles which are in excellent agreement with experimental data. Jeffs also investigated very briefly the application of CCFC in the beneficiation of Kentucky coal.[42] The data were extremely limited but encouraging.

2.3.4 Research by Kaldas[43,44]

Kaldas incorporated a high voltage electrostatic field across the entire length of the CCFC. The segregation of a jetsam-rich system of acrylic-sand was studied. It was determined that the existence of an external electrostatic field could enhance separation effectiveness in the cascade. The important factors affecting the separation are the voltage of the field, the geometry of the electrostatic grid, the polarity and orientation of the electric field, the paddle speed and the air velocity. One basic disadvantage in the application of this system involves the contamination of the fluidized particles by the impregnation of the attritive fines on their surfaces, which affected the cascade separation adversely.

2.3.5 Research by Goransson[45]

Goransson studied the beneficiation of Alberta coal, using the CCFC. It was found that the separation efficiency could be greatly enhanced by the use of a dense fluidizing medium, such as a magnetite-limestone mixture. The performance of the cascade was dependent on the size of the coal particles. For the coal particles larger than about 3 mm, separations in the cascade were comparable to those of the heavy medium cyclone, which is considered the best coal cleaning device available today. For coal particles in the size range of 3 x 0.6 mm, the separation sharpness was comparable to that of a Baum jig. The dominating factors affecting the performance of the CCFC were the reflux ratios at the product and reject ends, which were a function of paddle height, paddle velocity and withdrawal rates, the density of the fluidizing medium, the length of the cascade, the ratio of product withdrawal rate to reject withdrawal rate, and the fluidizing air velocity. Separations were only slightly dependent on feed rates, with no indication of deterioration in performance when throughput rates of up to 11 tonnes per hour per meter width of cascade were used.

2.4 Commercial Fluidized Bed Separators

The use of fluidization to separate coal from its naturally occurring non-combustible contaminants and mineral ore from its impurities can be documented to the early 1920s.

In 1925, Fraser and Yancey[46] patented the first

fluidized bed separator for the removal of slate, shale and pyrite from coal. It consisted of a large cylindrical bed containing a fluidizing medium of sand. The raw crushed coal was fed into the top of the fluidized bed via a hopper. The heavy impurities were then segregated toward the bottom of the bed and discharged through a spout with a control gate and weighted valve closure to regulate withdrawal rate. The purified coal was removed from the top of the bed by an endless conveyer operating around suitable rollers and drums.

Steinmetzer[47] patented a large fluidized bed separator in which an external motor was used to apply mechanical vibration to the entire bed. Fluidization and mechanical vibration were then the basic means of segregation.

To increase the separation effectiveness, Binnix[48] introduced a separator with an elongated sloping rectangular fluidized surface. The long length of the bed had the benefit of a longer residence time for separation than previous simple fluidized bed designs. Mechanical vibration and fluidization provided the basic means of segregation in Binnix's machine. Raw coal was fed to the feed end of the bed and migrated downward along the length of the bed by gravity. As the solids slid down the bed, the heavy components would be continuously concentrated toward the bottom of the bed. At the exit section of the bed, the product and reject streams were discharged from two weirs, one located at the top stratum and the other close to the bottom of the bed. The withdrawals were facilitated by mechanical vibration.

A simple large cylindrical fluidized bed similar to Steinmetzer's separator was patented by Weintraub.[49] Feed was introduced via a dipleg into the fluidized bed containing a fluidizing medium of magnetite or sand. The product was withdrawn through a pipe extended from the bottom to the upper middle region of the fluidized bed, while the reject stream was withdrawn through a downcoming pipe close to the grid region. Unlike the Steinmetzer design, the mechanism of segregation was solely caused by fluidization.

Harms[50] patented a separator classifier similar to that of Weintraub. Vertical partitions were installed to divide the bed into different chambers. Harms claimed that the vertical partitions would inhibit mixing and enhance segregation. It was also claimed that the device could be used for drying wet feed. Entrained fines from the fluidized bed were captured by cyclones.

An interesting simple fluidized bed design separator was patented by Morgan[51] in 1937, which consisted of a cylindrical bed with a funnel-shaped conical bottom, which constituted the grid. At the centre of the conical bottom was a standpipe for the withdrawal of the heavy component-rich reject stream. The feed and product withdra[illegible] were similar to that in Weintraub's separator. The use of fluidizing medium with appropriate density and mean size was also suggested.

Recently, Baskakov, Malykh and Shiskho of the Soviet Union[52] studied the segregation of Corundum spheres in a

bed of fluidized aluminum fluoride. They concluded that the optimal fluidizing velocity was dependent on the minimum fluidization velocity of the components in accordance with the equation

$$\frac{W_{opt}}{W_{pr}} = A_1 \frac{W_{co}}{W_{pr}} + A_2 \qquad (2.5)$$

where W_{opt} is the optimal fluidization velocity for maximum segregation,

W_{co}, W_{pr} is the minimum fluidization velocity of Corundum and aluminum fluoride, respectively

and A_1 and A_2 are empirical constants.

A more sophisticated fluidized bed separator was invented by Punter[53] in 1971. It consisted of an inclined fluidized bed where the fluidized material slid down by gravity. A dividing plate, or splitter, is used at the exit end of the bed to divide the stratified outgoing stream into product, middling and reject streams. The product stream was withdrawn by pneumatic suction at the top surface of the fluidized bed above the splitter. The middling and reject streams were divided above and below the splitter into two separate bins. The separation effectiveness was dependent on the aspiration rate, the angle of the splitter, the feed rate and the fluidizing air velocity. Eveson[54] invented another separator remarkably similar to that developed by Punter. However, in Eveson's design, fluidizing medium, such as magnetite or ferro-silica, was used to facilitate segregation.

Another device for the separation of dry material was invented by Holmes[55]; it bears a remarkable resemblance to the CCFC. The basic difference between the two is that in Holme's separator, a horizontal baffle with vibrator attached was installed inside the rectangular trough to assist in causing fluidity of the mass and to prohibit the vertical exchange of solid between the upper and lower strata of the bed. This vertical exchange constitutes the principal working mechanism in the CCFC.

At the Warren Spring Laboratory, Douglas and Gayles[56,57,58] invented the pinch-sluice pneumatic separator. It consists of an inclined wedge-shaped fluidized bed with the feed solids on the upper and wide section of the fluidized bed. As solids slide down the sluice, separation in the vertical direction stratifies light and heavy constituents. The bed height also continuously increased with the reduction in cross-sectional area of the sluice. The two strata of the fluidized bed would finally be divided into product and reject streams by a horizontal partition at the outgoing port of the sluice.

Another fluidized bed separator was invented by the Warren Spring Laboratory for the continuous separation of mixtures of particles with different densities.[50,59,60,61] The separator was a rectangular trough inclined at an angle of 5 to 10 degrees. The bottom of the trough consisted of a porous grid where fluidizing air percolated through via separate wind boxes. To facilitate the removal of the heavy sink component, vibration was applied to the entire

trough. As the heavy sink component settled on the bottom surface of the trough when the bed was fluidized, because of the vibration in the trough it migrates uphill toward the upper end of the trough where it could be collected in the reject bin. The light float component was concentrated toward the lower end of the trough where it was withdrawn by an off-take vibrated screen into the product bin. Feed was introduced to the trough in the lower half section. Good separation of lithium ore from gangue materials was claimed using this device.

Yan[62] of the Mobil Oil Corporation patented a process to remove pyritic sulphur in pulverized coal. In this process, pyrites were converted to pyrrhotite, magnetite and gamma-hematite in a fluidized bed by the heated fluidizing air. These magnetized sulphur compounds could then be removed magnetically.

A novel separator, the rotating stratifier, was recently developed by Jordison[64]. It utilizes centrifugal force to enhance segregation of fluidized solids. It consists of a complicated cylindrical fluidized bed with fluidizing air admitted via vertical perforated side wall. The entire fluidized bed is made to rotate on its central axis. The heavy and/or large components concentrate on the side wall of the rotating bed while the light and/or small components are concentrated near the central core and are withdrawn by aspiration to a pneumatic transport line extending to the central core region of the bed. The heavy

tailings are discharged via an overflowing weir and an annular port in the bottom of the side wall.

The National Research Council of Canada[23] investigated the use of a continuous fluidized bed in the upgrading of germanium and iron ores. The separation effectiveness was affected by the feed rate, the location of the feed point and the fluidizing velocity. The optional fluidization velocity was usually slightly in excess of the velocity at incipient fluidization.

CHAPTER THREE

EXPERIMENTAL APPARATUS, MATERIALS, AND ANALYTICAL TECHNIQUES

3.1 Experimental Apparatus

3.1.1 Simple Cylindrical Fluidized Bed

A cylindrical, fluidized bed (Figure 3.1) was used for the determination of minimum fluidization velocity and for the determination of steady state segregation concentration profiles when the concentration of jetsam was determined as a function of bed height.

The bed was contained in a solids housing constructed from a 19 mm thick plexiglass cylinder having a diameter of 279 mm and a height of 305 mm. Above the fluidized solids housing was a tall disengaging region which was connected to an exhaust system leading outdoors. Below the fluidized solids housing was a 305 mm high windbox. Air was introduced into the windbox through a 38 mm ID pipe in a downward direction via an elbow to avoid direct impingement on the grid, which could cause non-uniformity of air distribution. To encourage even distribution of air across the cross section of the bed, the windbox was filled to the grid

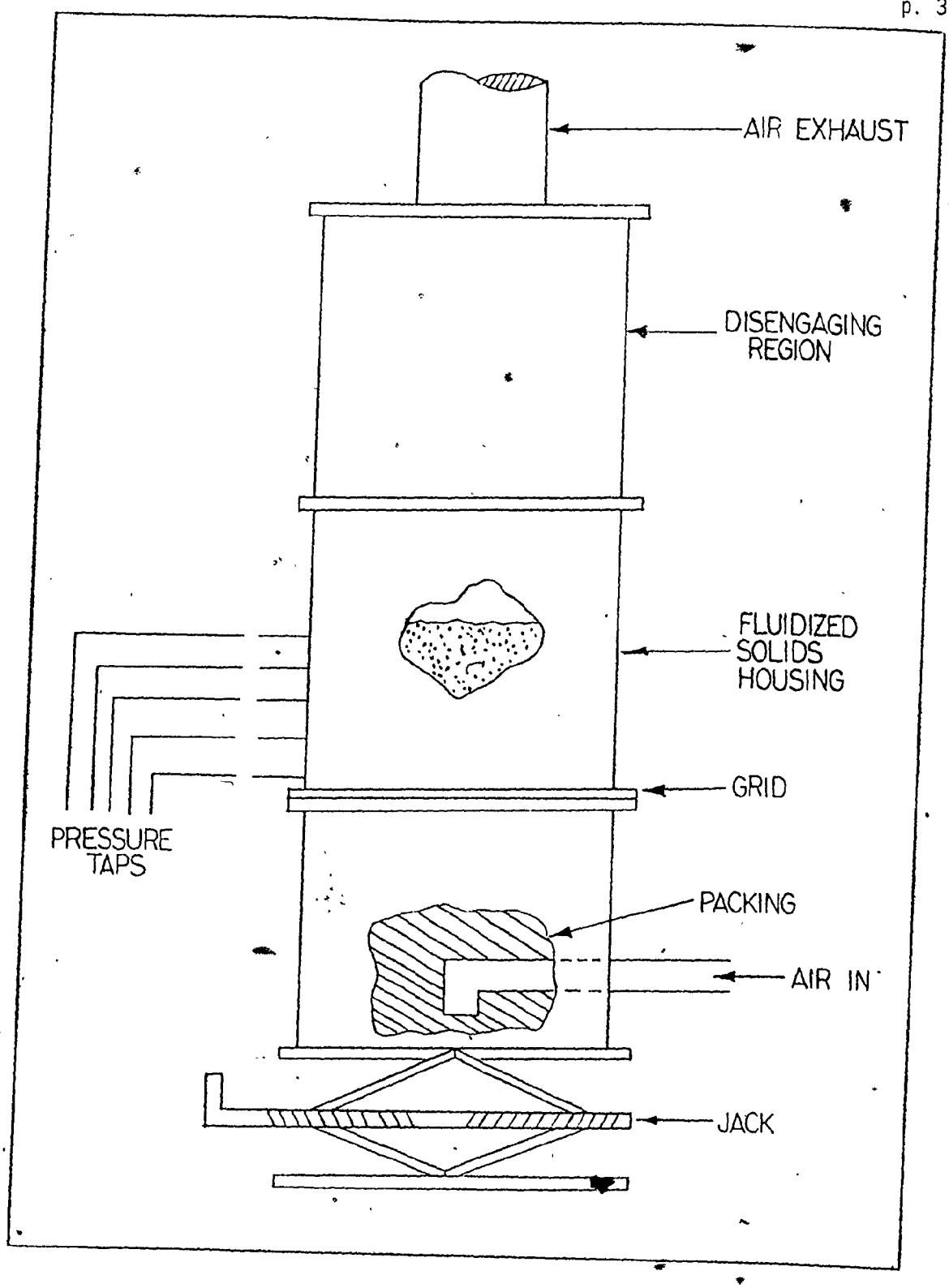

FIGURE 3.1 THE SIMPLE CYLINDRICAL FLUIDIZED BED (13)

region with 19 mm ceramic Berl saddles and 10 mm pieces of gravel. The grid used to support the solids consisted of eight sheets of chromatography paper, and a 1 mm thick porous polyethylene sheet sandwiched between two 1 mm thick perforated steel sheets. The grid assembly was tightly sandwiched between two flanges which connected the windbox to the fluidized solids section. In order to ensure uniform distributions of gas flow across the grid area the pressure drop across the grid was maintained at approximately ten to fifteen times that of the bed pressure drop, dependant on the gas velocity. Leaking of air in the grid section was not detactable.

The compressed air from a central compressor was controlled with a Watt M-4 gas pressure regulator followed by two globe valves. The volumetric flow rate was measured using sharp-edged orifice plates. The flow rate could be accurately determined from the pressure drop across the orifice plate and the upstream orifice pressure, which were measured using a water, and a mercury, manometer, respectively. The orifire meter was calibrated by Muzyka previously.(40)

To determine the pressure drop across the fluidized bed, five pressure taps were installed along the height of the bed, 58, 109, 160, 211 and 262 mm above the grid. Each tap was fitted with a polyethylene plug. The pressure at each tap was monitored with a water manometer. An identical pressure tap was installed in the windbox section.

The windbox-fluidized solids housing assembly was attached to a jack and supported on casters. The whole assembly could be lowered by the jack and wheeled away from the disengaging region for sampling, loading or solids removal purposes.

3.1.2 The Counter-Current Fluidized Cascade--Original Model

This was the original cascade designed for the separation of flotsam-rich systems. It was used for the investigation of cascade performance in the iron-sand system. Later, this model was modified to improve the effectiveness of separation, and convenience of operation (Section 3.1.3). The cascade (Figure 3.2) consisted of four detachable sections for the convenience of transportation and assembely. The working section, which was 3658 -m long, 190 mm wide and 600 mm high, contained the fluidized bed of solids, F, with a height of approximately 150 mm, and a disengagement region. Between the working section and the windbox was the grid, G, which consisted of eight sheets of chromatography paper sandwiched between two 1 mm thick perforated stainless steel sheets. The preforated grid is 20 gange thick, with 1.574 mm diameter holes. 15 holes per 100 mm^2, 33% open area, and staggered at 60^0. The working section and the windbox were tightly bolted together between flanges with the grid sandwiched in between. The tightness ensured that the leakage in the windbox was minimal. The windbox section, P, was divided into four chambers, each separated from the others by partitioning plates. The length of the windbox in the end chambers was 610 mm, and in the middle chambers was 1219 mm. The flow rate through each windbox could be controlled independently by adjusting a gate valve which was connected to each of four 38 mm ID copper pipes leading to the windboxes, I. The flow rate in each chamber was monitored using a sharp-edged orifice plate inserted in each line. The pressure drop across each orifice plate and the upstream

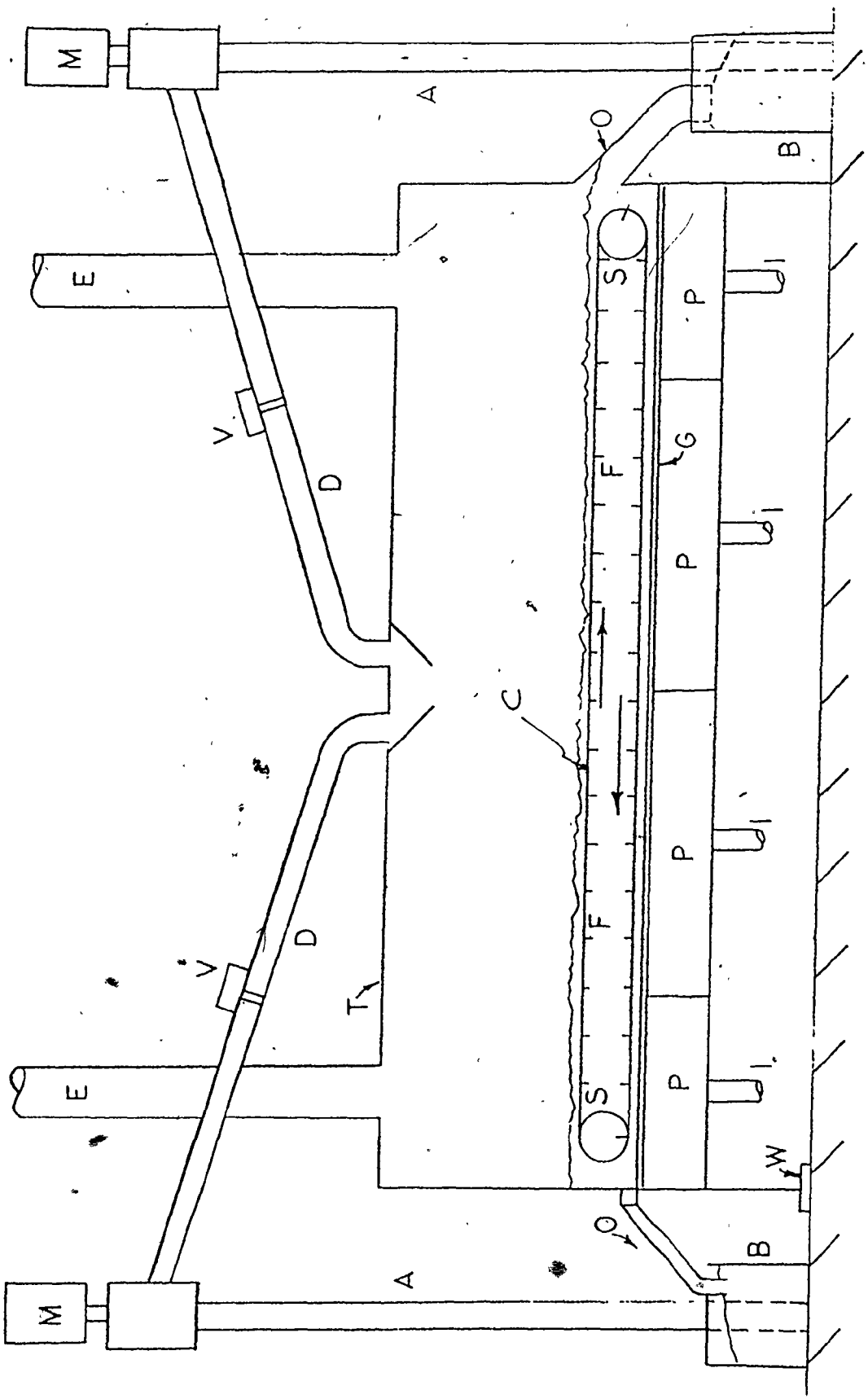

FIGURE 3.2
The Counter-Current Fluidized Cascade--Original Model

gauge pressures were monitored with water and mercury manometers, respectively. All four lines were connected to a WATT-Model M4, no. 602-12 filter and a WATT-Model M, no. 119-12 pressure regulator. The compressed air was supplied from a central compressor. De-oiling of the flowing gas is not necessary because of Chromatograph paper in the grid region of the bed.

A special endless chain (Lagos T-chain), with T-bar shaped links, C, was installed in the fluidized bed of solids. Each link (or paddle) was 38 mm deep, 6 mm thick and 170 mm. wide. The chain was supported on two 150 mm diameter steel sprockets located close to the two ends of the cascade. Affixed to each paddle was a rubber blade in order to reduce the clearance between the paddles and the gird surface. The two sprockets could be adjusted to yield optimal tension in the chain. A chain driven drive sprocket was mounted on the paddle drive sprocket shaft, on the left side of the bed.

A 1/4 HP AC electric motor coupled with a speed reducer was used to drive the chain, whose velocity could be varied by various combinations of sprockets on the motor shaft and the drive shaft of the drive sprocket. The lower half of the chain rode on a narrow steel rail traversing the length of the bed and anchored on the sides of the bed by steel cross-bars. Counter-current motion of the fluidized solids was induced when the chain was set in motion. The bed would then be divided into two strata, the lower stratum moving toward the left side and the upper stratum moving toward the right side.

There were two withdrawal ports, O, in the cascade. The one on the left end, the jetsam-rich end, was a 25 mm ID pipe located very close to the grid surface. The one on the right end, the flotsam-rich end, was a 38 mm ID pipe located in the middle of the side wall 127 mm above the grid. The two withdrawal ports were connected by flexible rubber tubing to the two cylindrial hoppers, B, at either side of the bed. The withdrawal rate on each side was controlled by variable speed augers, A (model 200, manufactured by Automatic Industrial Machines, Inc.). The speed of withdrawal was controlled by the gear boxes, M, located at the top of the auger tubes.

The two withdrawal streams were recycled back to the bed via the two downcoming 89 mm ID ABS pipes, D, with pneumatic rotating ball vibrators, V, attached to facilitate free flowing of the solids. The top of the cascade bed was covered by a removable transparent plexiglass top which facilitated visual inspection. Two 140 mm air outlets were installed onto the plexiglass top 230 mm from either end of the bed. Stove pipes, E, were attached to the air outlets and were connected to an exhaust blower. The blower was used to maintain a slight negative pressure in the disengaging section above the fluidized bed of solids in order to minimize particulate emission in the laboratory. The fluidizing air, with a small amount of attrited fines, was exhausted to the outdoors.

To determine the pressure drop across the fluidized

bed along the cascade length, five pressure taps were installed at the centre-line of each fluidized solids section, 305 mm, 1219 mm, 2438 mm, and 3353 mm from one end of the cascade. Porous polyethylene plugs were inserted into each of the taps. The pressures at the tap were monitored with water manometers. An additonal pressure tap was install in each of the four windboxes in order to monitor the grid pressure.

3.1.3 Counter-Current Fluidized Cascade--Modified Model (Figure 3.3)

To improve performance and ease of operation, the original cascade was modified. At the left end of the cascade, 483 mm from the end, the grid was inclined at an angle of 7.6^{0} to the horizontal so as to facilitate the withdrawal of material toward exit O. The exit port, O, was also modified extensively. A plexiglass outlet with a rectangular port 12.7 mm high and 190 mm wide (the same as the bed width) replaced the outlet pipe of the original model. The rectangular port was an improvement over the old design in that it caused more efficient withdrawal of material from the lower stratum of the fluidized bed. The conical hoppers, B, at either end of the bed, were also replaced by the redesigned plexiglass bins with a reduction in volume in order to minimize the undesirable accumulation of solids due to a dead zone in the original hopper.

The chain-paddle system was also modified extensively. To facilitate the control of the speed of the paddle chain, the AC electric motor was replaced by a variable speed DC

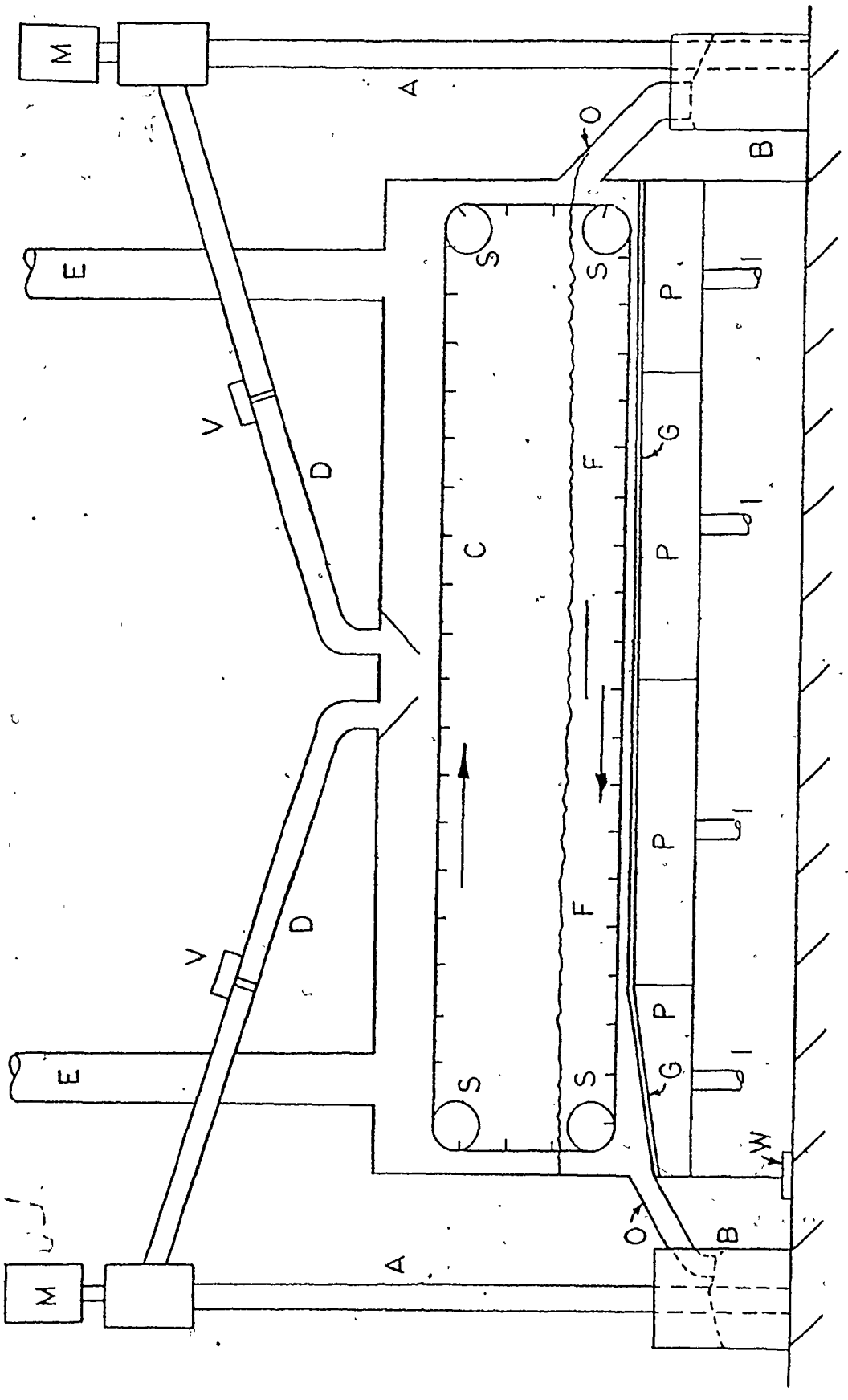

FIGURE 3.3

Counter-Current Fluidized Cascade,--Modified Model

motor. The chain was supported on 150 mm diameter sprockets at four points. The lower half of the paddle-chain rested on top of the grid as before. Motion of the upper stratum of the fluidized bed of solids to the right side, the flotsam-rich side, was now caused by gravity. To facilitate the motion of the upper stratum and to maintain the same bed height along the length of the cascade, the left side of the bed was raised slightly by a wooden block, W, in order to provide the needed inclination. The angle of inclination was frequently adjusted by the insertion of wooden blocks of different heights to maintain a uniform bed height along the length of the cascade under different chain speeds and fluidization velocities. The height of the T-bar links was also reduced to 12.7 mm by cutting. Four small holes were drilled, two on each paddle, to enable the attachment of rectangular baffles. The baffles were 76 mm. wide, and 3 mm. thick, and 125.4 mm. high stainless steel plates.

3.2 Description of the Granular Solids Systems

Various granular solids systems were used in segragation studies in simple and cascade fluidized beds.

3.2.1 Iron-Sand System

Sieve analyses of the iron and sand used in this system are given in Appendix A. Size and density properties of this system are summarized in Table 3.1 The overall concentration of iron used in the cascade was 5% by weight.

The minimum fluidization velocity for the mixture was determined to be 40.8 mm/s, and for the pure sand, 49.4 mm/s (Appendix B).

Table 3.1 Physical Properties of Iron-Sand System

Component	Iron	Sand
grain density (kg/m^3)	7800	2650
sauter mean diameter (μm)	174	233
geometric mean diameter (μm).	183	244
geometric standard deviation	4.02	3.74

3.2.2 Iron Pyrite-Coal System

Five batches of iron pyrites were used as the jetsam component in the study of pyrite removal in pyrite-coal systems. The sieve analysis of each batch is given in Appendix A. Table 3.2 is a summary of their mean sizes.

The coal used was practically pyrite-free and was provided by Energy, Mines and Resources Canada. Using standard ASTM analysis[68], the sulphur content of the coal was determined and is tabulated in Table 3.2 B. The coal was air dried and two batches with different mean sizes were prepared by crushing and sieving. A summary of the size distribution and minimum fluidization velocity of the two batches is provided in Table 3.2 C.

Detailed sieve analyses are listed in Appendix A and the plot used in the determination of minimum fluidiza-

Table 3.2 A Physical Properties of Iron Pyrites in the Pyrite-Coal System

BATCH	A	B	C	D	E
grain density (kg/m^3)	5000	5000	5000	5000	5000
designation (mesh)	100 x 0	48 x 0	48 x 0	28 x 0	14 x 0
sauter mean diameter (μm)	59	92	102	131	170
geometric mean diameter (μm)	74	116	125	174	216
geometric standard deviation	4.9	4.5	4.4	4.1	3.9

Table 3.2 B Distribution of Sulphur in Coal in the Pyrite-Coal System

pyritic sulphur	0.128 % by wt.
sulphate sulphur	0.000275 % by wt.
organic sulphur	0.418 % by wt.
overall sulphur	0.547 % by wt.

Table 3.2 C Size Distribution and Minimum Fluidization Velocity of Coal Used in Pyrite-Coal Cascade Studies

	Batch A	Batch B
sauter mean diameter (μm)	272	135
geometric mean diameter (μm)	360	153
geometric standard deviation	3.4	4.2
minimum fluidization velocity (mm/s)	98	11

tion velocity are given in Appendix B. A float-sink analysis of Batch A coal was performed; the results are given in Appendix C. From the analysis, the mean density of the coal was determined to be approximately 1425 kg/m^3.

3.2.3 Natural Coal System

With the natural coal system, the objective of the research was to investigate the effectiveness of the cascade in the removal of natural pyrites and ash from coal. The coal was obtained from Devco's Prince Mine, Nova Scotia, and was supplied by Energy, Mines and Resources Canada. Using standard ASTM analysis[69], the sulphur and ash content of the coal were determined and are summarized in Table 3.3 A.

Table 3.3 A Sulphur and Ash Content of Natural Coal System

pyritic sulphur	4.3% by wt.
total sulphur	5.2% by wt.
ash	11.7% by wt.

Sieve analysis of the coal is listed in Appendix A. A summary of the principal population parameters is given in Table 3.3 B.

The minimum fluidization velocity was determined to be 37 mm/s. The plot used in the determination of the minimum fluidization velocity is provided in Appendix B.

Table 3.3 B Natural Coal System

sauter mean diameter (μm)	167
geometric mean diameter (μm)	233
geometric standard deviation	3.79

3.2.4 Salt-Activated Charcoal System

In the sodium chloride (salt)-activated charcoal system, salt was the minor component and constituted 1% of the overall concentration by weight. The salt was the commercially available table salt from the Windsor Salt Company, hand-ground in a mortar and sieved to a size-range between 180 and 250 microns.

The activated charcoal was purchased from Barnaby-Cheney Company, Type AC 437. It was sieved to a size-range between 212 and 600 micron, with a geometric mean diameter of 375 micron. The sieve analysis is listed in Appendix A. A summary of the physical properties of this granular solids system is given in Table 3.4.

The minimum fluidization velocity for the 1% mixture was determined to be 66 mm/s (Appendix B).

3.3 Analytical Techniques

3.3.1 Sieve Analysis

Determination of size distributions were performed using standard sieve trays.

Table 3.4 Physical Properties of the Salt-Activated Charcoal System

Component	Salt	Activated Charcoal
weight fraction	0.01	0.99
sauter mean diameter (μm)		365
geometric mean diameter (μm)		376
geometric standard deviation		3.32
size range (μm)	180 < dp < 280	212 < dp < 602
grain density (kg/m^3)	2160	710
bulk density (kg/m^3)	1194	540

The computer programme used for the determination of geometric, arithmetic and sauter mean diameters of the granular solids systems, based on the data of the sieve analyses, is provided in Appendix D.

3.3.2 Iron and Sand System

The concentration of iron was determined by dissolving the iron with nitric acid, followed by titration with potassium dichromate.[69] The analytical procedures are described in detail in the reference text and will not be given here.

The accuracy of the technique was verified by carrying out the procedures with a known amount of iron powder. The uncertainty was determined to be less than 5%.

3.3.3 Pyrite-Coal System

A float-sink analysis [71,70] was used to determine the mean density of the coal. Details of the procedures can be obtained from the reference and will not be given here. The separations were carried out in standard 350 ml beakers. Media of specific gravity ranging from 1.2 to 2.02 were made by combining varsol (s.g. 0.78), perchloroethylene (s.g. 1.62) and ethylene dibromide (s.g. 2.17) in various proportions. The results are shown in Appendix C.

To determine the concentration of pyrite in the samples, a modified float-sink analysis was employed using a-tetrabromoethane (s.g. 2.96) as the separation medium. Pyrite, with a specific gravity of 5.0, can be readily separated from coal with a mean specific gravity of 1.425. After separation by the float-sink procedure, the separated pyrite was washed with ethanol and acetone. It was then dried and weighed, and the concentration of pyrite in the sample was then calculated.

To verify the accuracy of the procedure, known amounts of pyrite fines were added to the coal matrix. The weight of recovered pyrites was generally 3% to 5% less than that of the original. Thus, the uncertainty in the analytical procedure was considered to be acceptably small.

3.3.4 Natural Coal System

The ash content was determined in accordance with ASTM procedures.[68] Two methods of analysis for the deter-

mination of total sulphur in coal were used, namely, X-Ray fluorescence[72,73] and standard Eschka methods.[68]

As a result of the varying ash contents in the samples, the calibration of the X-Ray fluorescence method by internal addition was unsuccessful. Furthermore, the ASTM technique[68] for the determination of total sulphur was extremely time-consuming, hence only a limited number of samples were analyzed by the ASTM technique. However, the X-Ray fluorescence method was relatively easier, and an attempt was made to correlate the ASTM determined total sulphur concentrations with the X-Ray counts and ash contents using multiple regression.

Two sets of regressional line were used for the calculation of total sulphur. This was necessary because of modification and repair of the X-Ray machine during the course of the experiments.

For the Series A recirculation runs, the straight-through runs, and the segregation experiment in the simple fluidized bed, the regressional lines used for the determination of the percentage of total sulphur in coal are summarized in Table 3.5 A.

Equation 3.1 was used for samples with low ash content, i.e., the product stream, whereas equation 3.2 was used for samples with high ash content, i.e., the reject stream. It was found that two lines (one for high-ash reject coal, the other for low-ash product coal) gave a much lower residual than a single line. Agreement of the total

Table 3.5 A Regression Lines for the Determination of Total Sulphur (Set 1)

Regressional Line	F Ratio	F (99%)[74]
$S = 7.7157 - .3988\ (ash) - 0.7108\ (I^*) + 0.1121\ (ash \times I^*)$ (3.1)	160.5	5.39
$S = 1.8876 + 0.6619 \times 10^{-1}\ (ash) + 0.4578\ (I^*) + 0.6375 \times 10^{-2}\ (ash \times I^*)$ (3.2)	66.2	5.29

where S = percentage of total sulphur by weight (%)

ash = percentage of ash by weight (%)

I* = normalized X-Ray count (Appendix E).

sulphur percentages determined by ASTM method and those predicted by the regression lines calculated using the ash content and the normalized X-Ray count were excellent. This is evident by examining the overall F ratios, which are much greater than the critical ratio at the 99% confidence level.

Another set of regression lines was used in the Series B recirculation runs and the segregation experiment in a simple fluidized bed for the reject material. The regression lines used for the determination of percentage of total sulphur are summarized in Table 3.5 B.

Once again, the concentration of total sulphur determined by the ASTM method and those predicted by the regression lines were in excellent agreement, as indicated by the overall F ratios.

Table 3.5 B Regression Lines for the Determination of Total Sulphur (Set 2)

Regressional Line	F Ratio	F (99%)[74]
$S = 2.8456\ (ash) - 149.8030\ (I^*) + 0.6764 \times 10^{-3}\ (ash \times I^*)^2 - 0.1448 \times 10^{-1}\ (ash) + 19.9732\ (I^*)^2 - 0.6593\ (ash \times I^*) + 282.8913$	183.2	6.37
(3.3)		
$S = 0.1581\ (ash) + 2.0719\ (I^*) - 0.1592 \times 10^{-1}\ (ash \times I^*) \simeq 4.3040$	202.1	5.42
(3.4)		

To estimate the concentration of organic sulphur for the different samples, the pyritic sulphur as well as the total sulphur content of four samples were determined, using ASTM methods. The four samples were from the product and reject streams of runs 1 and 19 of Series A recirculation runs. By neglecting the sulphate sulphur, which was assumed to be very small in comparison with organic and pyritic sulphur, the organic sulphur content could be determined for the four samples. The results are summarized in Table 3.6. The total sulphur content listed in Table 3.6 was based on the total weight of the sample. The pyritic and organic sulphur contents listed in the same table were on an ash-free basis. Thus, it is not surprising that the magnitude of the pyritic sulphur content can be greater than that of the total sulphur content.

Table 3.6 Calculation of Organic Sulphur Content of Coal

Sample	Ash(%)	Total Sulphur(%)	Pyritic Sulphur (ash free basis)	Organic Sulphur(%) (ash free basis)
Run 19, reject	26.5	6.08	7.22	1.05
Run 19, product	8.34	4.38	3.05	1.68
Run 1, reject	27.2	6.21	7.36	1.17
Run 1, product	8.10	4.34	3.04	1.69

It was then assumed that the average organic sulphur content, on an ash free basis, for the reject side and the product side were 1.11% and 1.68%, respectively. However, it was not apparent why the organic sulphur of the low ash samples, on an ash-free basis, should be higher than for the high ash sample.

Because the total sulphur could be estimated from the experimentally determined values of ash content and normalized X-Ray count, and the average organic sulphur contents, on an ash-free basis, were estimated for both the product and reject streams, the pyritic sulphur of all the samples could be calculated, taking into consideration the oxidation of pyrites in the ashing process. The equations used to calculate the pyritic sulphur are as follows.

$$S_p = \frac{S - S_o'.(1-ash)}{1 - 0.627\ S_p - ash} \qquad (3.5)$$

$$S_p' = \frac{S_p}{1 - 0.627\ S_p - \text{ash}} \qquad (3.6)$$

where ash = the weight fraction of ash in the oxidized state

S = the weight fraction of total sulphur

S_o' = the weight fraction of organic sulphur on an ash-free basis

S_p = the weight fraction of pyritic sulphur

S_p' = the weight fraction of pyritic sulphur on an ash-free basis.

Equation 3.5 was used to calculate the overall pyritic sulphur content, and Equation 3.6 was used to calculate the pyritic sulphur on an ash-free basis. The derivations of the equations are provided in Appendix F.

3.3.5 Salt-Activated Charcoal System

Geometric mean diameter as well as the salt content were determined for each sample taken along the axis of the cascade in the total reflux experiment.

Size analyses of the samples were performed using 600, 500, 425, 355 and 300 micron sieves and a bottom tray. Fifteen minutes were allowed for the sieve analysis and for the salt particles, which were smaller than 300 microns in diameter, to settle into the bottom tray. After weighing the different cuts in the size analysis of the sample, all the solids were returned back to the cascade bed with the exception of material in the bottom tray, which was trans-

ferred into a 350 ml beaker. A known amount of distilled water, usually between 100 and 200 ml, was added to the solids in the beaker and the solution was stirred vigorously for three minutes.

The emulsion was then filtered with a medium porosity filter paper and the filtrate was retained for the determination of its salt concentration. The filtered activated charcoal was then rinsed with 300 ml of distilled water, dried in an oven and returned to the cascade bed. 10 ml of the dissolved NaCl solution was siphoned by a pipet and transferred to a 250 ml Erlenmeyer flask. A Mohr titration[75,76] was then carried out using 0.1 N silver nitrate solution as the titrant and potassium chromate solution as indicator. Mohr titration is described in detail in the references and will not be repeated here. From the determined concentration of salt in the filtrate and the known volume of water used for the dissolving process, the mass of salt in the sample was calculated, which in turn enabled the determination of the mass fraction of salt in the sample. An equal mass of salt was then returned to the cascade bed.

The accuracy of the analyses was verified by carrying out the procedures with a sample to which a known amount of NaCl was added. The determined and the actual NaCl contents differed by approximately 3%.

CHAPTER FOUR

EXPERIMENTAL PROCEDURES

4.1 Determination of Minimum Fluidization Velocity

The minimum fluidization velocity of granular solids systems was determined experimentally using the simple cyclindrical fluidized bed (Section 3.3.1).

Solids were loaded into the bed to a height of 165 mm. The bed was then fluidized vigorously at a superficial velocity well in excess of the minimum fluidization velocity for approximately five minutes to mix the granular solids thoroughly. After the mixing period, the reading at each of the pressure taps along the height of the bed, the pressure drops across the orifice plate, the pressure upstream of the orifice plate and the temperature of the gas above the fluidized bed of solids, were recorded. The data were used to calculate the overall pressure drop across the bed and the superficial velocity of the fluidizing air. The superficial velocity was then reduced by adjusting the globe valve and a new set of pressure data was taken again. The procedure would be repeated for a wide range of superficial air velocities, ranging from a well-fluidized bed to

a completely defluidized bed.

From the experimental data, a log-log plot of bed pressure drop versus superficial air velocity was constructed. A typical plot is provided in Figure 4.1. As can be seen, a typical plot of pressure drop versus superficial velocity consists of two discrete regions, namely, the fluidized and fixed bed regions. The intersection of the two lines occurs at the minimum fluidization velocity. However, owing to particulate interlocking, the intersection of the two lines is seldom as sharp as the idealized system of Figure 4.1. A small characteristic "hump" as shown in Figure 4.2 is often observed. A more thorough discussion of minimum fluidization velocity measurement is outlined in a text by Davidson.[4] It is interesting to note that the addition of a small amount of fines to a fluidized bed of coarse particles can often lower substantially the minimum fluidization velocity of the mixture.[8,9]

Many empirical correlations are available for the estimation of minimum fluidization velocity. From experiences with the granular solids system studied, the Wen and Yu correlation[10] usually provided predicted values of U_{mf} which were in good agreement with those measured experimentally. For a composite mixture of particles of varying sizes, the particle diameter used in the Wen and Yu correlation is usually the Sauter mean diameter of the mixture. In the absence of porosity and sphericity data, Kunii[2] suggested the following empirical correlations by modifying the original Wen and Yu correlation:

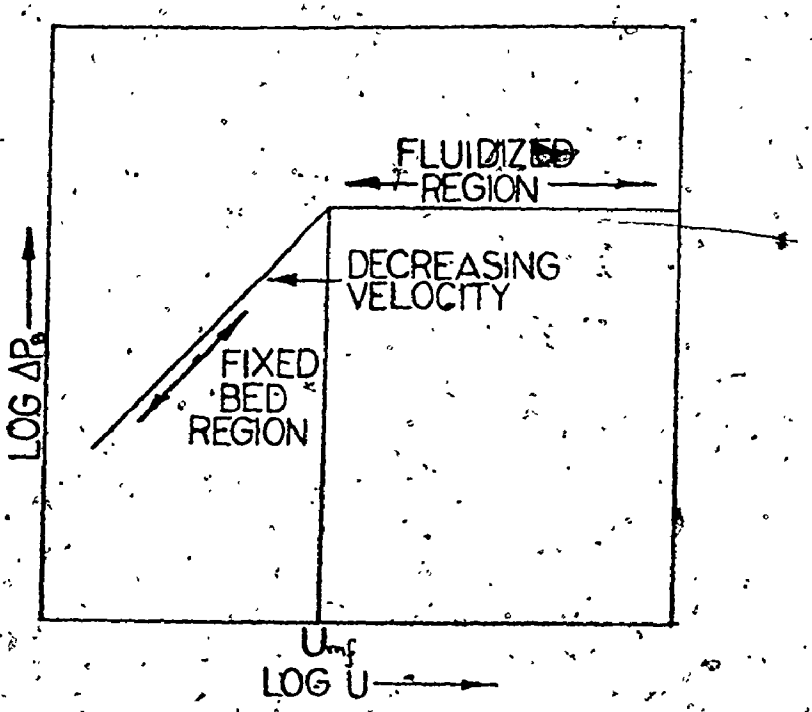

FIGURE 4.1 IDEAL PRESSURE DROP-VELOCITY CURVE (4)

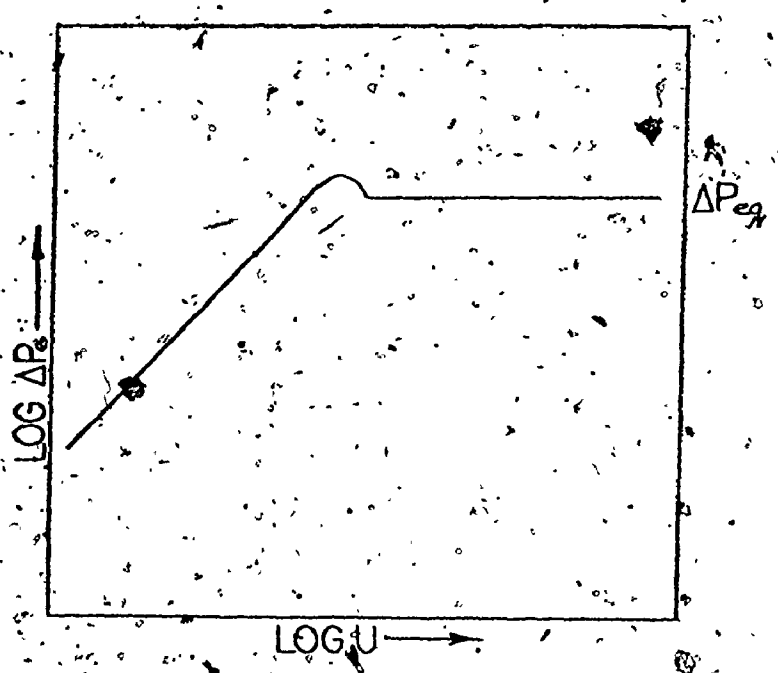

FIGURE 4.2 EFFECT OF PARTICLE INTERLOCKING ON PRESSURE DROP (4)

$$U_{mf} = \frac{dp^2 (\rho_s - \rho_g) g}{1650 \mu} \quad \text{for small particles where Rep. mf} < 20 \qquad (4.1)$$

$$U_{mf}^2 = \frac{dp(\rho_s - \rho_g) g}{24.5 \rho_g} \quad \text{for large particles where Rep. mf} > 1000 \qquad (4.2)$$

where U_{mf} = minimum fluidization velocity, m/s

Rep. mf = Reynold number of particles at minimum fluidization velocity

$$= \frac{\rho_g U_{mf} d_p}{\mu}$$

4.2 Segregation Experiments in the Cylindrical Bed

The fluidized bed used in the segregation experiments was the bed used in the determination of minimum fluidization velocity.

The granular solids were first loaded into the bed to a height of 165 mm. Air was then introduced to fluidize the bed vigorously for five minutes to premix the solids thoroughly. After the mixing period, the gas velocity was reduced to the desired superficial velocity. The system was left undisturbed at that superficial velocity for approximately fifteen minutes. It was noted by previous experimenters[13,40] that equilibrium concentration profile could be attained very rapidly, usually in less than a minute. In view of the rapidity of equilibrium profile attainment, fifteen minutes of operating time was considered to be

adequate. At the termination of the fifteen minutes run, the air flow was abruptly stopped by closing the control valve.

To facilitate sampling, the solid windbox housing assembly was separated from the disengaging section by lowering the assembly with the jack. The assembly was then wheeled aside to a more accessible location for sampling. Using aspiration, horizontal layers of the bed, with a thickness of approximately 25 mm, were taken from the bed, layer by layer, starting at the top surface of the bed. Each layer of the bed was collected and weighed. For the determination of the concentration of jetsam in each layer, a representative sample was obtained by splitting the total sample with a 2:1 sample splitter.

The reliability of obtaining a representative sample was verified by comparing the concentration of a reduced sample with that of a total sample with a known concentration. Ususally, the difference between the two values was within ±5%, which was considered acceptable. The analytical technique for the determination of the jetsam concentration in the samples varied, depending on the granular solids system. Details of the analytical technique for each system were discussed in Chapter 3. Based on the weight fraction of each layer, a normalized height of the layer could be estimated. By determining the concentration of jetsam in each layer, the equilibrium concentration profile at a specific superficial velocity was constructed for the particular

granular solids system with a known overall concentration of jetsam.

4.3 Counter-Current Fluidized Cascade Studies

Experiments were performed on the counter-current cascade to study its separation effectiveness under varying operating conditions. Three basic types of experiments were carried out with the cascade, namely, total reflux, recirculation and throughput runs. In the total reflux runs, there was no feed or withdrawal of material to or from the cascade. In the recirculation experiments, the product was recirculated from the two ends to the centre of the bed. The rates of withdrawal were controlled by variable speed augers located at the two ends of the cascade. To maintain a continuous operation, the two withdrawal streams were reintroduced to the middle of the fluidized cascade bed via downcomers. In the throughput runs, the two withdrawal streams were not returned to the bed, but were collected into two receiving storage bins. New material was continuously fed to the cascade using a vibratory feeder.

4.3.1 Total Reflux Runs

Materials were loaded into the bed to a height of 152 mm. With the exhaust blower switched on, air was then introduced into each chamber at a superficial velocity well in excess of the minimum fluidization velocity. The two

augers were then switched on to facilitate solids mixing. Fifteen minutes were allowed to completely mix the entire cascade bed. From experimental data, it was confirmed that fifteen minutes mixing time was adequate to thoroughly premix the solids in the bed. The concentration gradient along the cascade bed resulting from the previous run was destroyed after the mixing period. After the mixing period, the air flow rate to each chamber was adjusted to the desired value. The paddle-chain drive motor was then switched on. For the original cascade model, the speed of the paddle-chain could be varied by different combinations of sprockets. In the modified model of the cascade, the speed of the paddle-chain could be controlled by adjusting the speed controller. The bed was allowed to operate undisturbed for a duration of time such that each paddle of the chain had swept the length of the cascade twenty to thirty times. This time duration permitted the system to attain its steady state concentration profile.

One complication that was encountered was that the matrix particles tended to segregate along the cascade length by virtue of their size differences. This caused the large particles to accumulate toward the jetsam-rich side while the smaller particles tended to concentrate towards the flotsam-rich side. The minimum fluidization velocity of the jetsam end could therefore be significantly higher than that of the flotsam end and there would be a gradation of minimum fluidization velocity along the cascade.

While one end was well in excess of the overall minimum fluidization velocity, the other side was at less than the overall minimum fluidization velocity. The severity of this minimum fluidization velocity variation along the length of the bed could often cause defluidization of solids in the jetsam end and excessive fluidization of solids in the flotsam end. The defluidization of solids could sometimes lead to chain jamming. Thus, it was often necessary to estimate the minimum fluidization velocity in each section along the cascade bed. This could be accomplished by shutting down the air supply to all the chambers and stopping the paddle-chain by switching off the electric motor simultaneously. The minimum fluidization velocity measurement procedure was then carried out one section at a time. The procedure was identical to that discussed earlier for the cylindrical fluidized bed. The value determined by this technique, however, was not expected to be as accurate as that determined in the cylindrical bed because the fluidized solids in the cascade bed were continuous, with no partitioning wall separating one section from the other. Thus, inevitably, there would be leakage of air to the adjacent sections. From experiments, the minimum fluidization velocity determined in situ in the cascade bed and the corresponding value determined in the cylindrical bed usually differed by approximately 10%.

When the minimum fluidization velocity of each of the sections was determined, the superficial velocity at

each of the chambers could be adjusted so as to keep the same (U/U_{mf}) value, or $(U-U_{mf})$ value. The run was then repeated with this adjustment of superficial velocity in each chamber, and experimentation could proceed as described previously.

When the matrix material was composed of a narrow size range of solids, or alternatively if the superficial velocity was exceedingly high, the segregation of particles by size along the cascade was insignificant and the minimum fluidization velocity at each of the sections was, therefore, the same as the overall minimum fluidization velocity of the batch. The superficial velocity at each of the sections could, therefore, be operated at the same value.

During the run, the humidity of the exhaust air was monitored by inserting thermometers into the exhaust pipe for the measurement of wet and dry bulb temperatures.

At the completion of the run, the paddle-chain movement and air flow to all the chambers was stopped abruptly by switching off the electric motor and closing the valve in the main compressed air line simultaneously. The exhaust blower was also switched off. The plexiglass top of the bed was removed to facilitate sampling, which was accomplished using a 30 mm ID copper tube inserted perpendicularly into the bed until it touched the grid surface. Because the bed was filled with granular solids, the location of the chain-paddles could not be ascertained.

The copper tube sometimes could not be inserted all the way to the grid as it encountered a chain-paddle. In this case, the tube was withdrawn slowly from the bed so as to disturb the distribution of solids in the bed as little as possible. Another attempt would then be made at another location until the copper tube was successfully inserted throughout the entire height of the bed. With the sampling tube in place in the bed, all the solids inside the tube could be aspirated through a 6.4 mm ID copper tube into an Erlenmeyer flask. It was always checked visually that no solids remained in the sampling volume after the aspiration procedures. The aspiration vacuum was supplied by a small air sampling pump. The procedure was repeated at various locations along the bed at approximately 300 mm intervals. Analysis of the samples collected was then carried out as described in Chapter 3. From the measured concentration of jetsam in the samples, the concentration variation along the length of the cascade bed was determined. For the salt-activated charcoal system, in addition to the analysis of concentration of salt in the samples, sieve analyses were performed. From the sieve analysis, the determined geometric mean diameter of the particles in each sample could be used to estimate the minimum fluidization velocity of the sample by the Wen and Yu correlation (Section 4.1). In most cases, the estimated value and the experimentally measured value for each chamber of the fluidized bed agreed within ±6%.

4.3.2 Recirculation Runs

A total reflux run, at the same chain speed as the recirculation run, was first performed to investigate the possibility of particle segregation due to size difference. If this was observed, the minimum fluidization velocity above each chamber was measured as described in Section 4.3.1 and the superficial air velocity above each chamber was adjusted by taking into consideration the variation of the minimum fluidization velocity along the length of the bed. It should be noted that the minimum fluidization velocity estimated for each section along the cascade length for the total reflux conditions might not be the accurate estimate during the recirculation run. In the recirculation runs, material was withdrawn from the two ends of the cascade and reintroduced as feed to the middle of the bed. Thus, the solids would tend to be better mixed than with the total reflux condition because of the solids recirculation.

However, in view of the numerous combinations of withdrawal rates, chain speeds and fluidization velocities used, in situ experimental determination of the minimum fluidization velocity above each chamber, for each setting of withdrawal rate, chain speed and fluidization velocity, was impossible. Thus, the superficial velocity above each chamber was set at a level based on the minimum fluidization velocity determined for the corresponding total reflux run under the same conditions.

The premixing procedure for recirculation runs was

identical to that of the total reflux run. After the mixing period, the air flow to each chamber was reduced to the desired value. The air supply to the pneumatic vibrators on the downcomer pipes was turned on to facilitate the flow of solids. The augers at the two ends of the cascade were adjusted to the desired mass flow rate settings. The augers were individually calibrated previously by collecting and weighing the solids for a controlled time duration at each setting on the auger speed controller. Thus, by adjusting the speed controller to a prescribed setting, the mass flow rate of solids was known. Motion in the paddle-chain was then commenced by switching the electric motor on. The system was then left to operate for fifteen minutes to allow for equilibration. Samples from the product and reject ends were then collected by scooping solids from the auger wells. Usually, at each end, a large sample (approximately 350 ml) was collected in a 500 ml beaker. The samples were then reduced to approximately 50 ml using a 2:1 sample splitter, and collected in labelled sample jars. The jetsam concentration in the samples could then be determined using the analytical methods described in Chapter 3. After collecting the samples in two jars, the remainder of the samples were decanted back into the auger wells to be recirculated in the cascade. The setting of the augers could then be adjusted for a different combination of product and reject stream mass flow rates. Once again, the system was left to run for fifteen minutes and two samples, one from each end of the

cascade, were taken. This procedure was repeated for different combinations of auger withdrawal rates.

4.3.3 Throughput Runs

A limited number of throughput runs were performed. A 100 mm diameter hole was made in the plexiglass top midway along the length of the cascade. A large conical sloped metallic funnel was inserted into the hole to facilitate loading of solids. A vibratory feeder, Syntron model 5-010, FMC Corporation, was used to feed the material via the funnel into the centre of the cascade bed. The jetsam-rich reject stream withdrawal rate was controlled by the auger. The downcomer tube was used to transport the solids into a barrel. The flotsam-rich product stream withdrawal rate was controlled by means of a vibratory feeder, Syntron model BF2A, FMC Corporation.

Material withdrawn would be collected in a receiving bin which was periodically emptied into the product stream storage barrel. Solids were first loaded into the cascade bed to a height of 150 mm. The feed hopper was also fully loaded with solids. After the exhaust fan was switched on, the air flow rate to each chamber was adjusted to the desired superficial velocity. The paddle-chain was set into motion by switching on the drive motor. The left auger, the vibrator feeders in the middle and on the right side (the flotsam-rich side) of the cascade were switched on simultaneously. They were all calibrated previously and adjusted for the

appropriate feed and withdrawal rates. To avoid accumulation or depletion of solids in the bed, the feed rate was adjusted to be equal to the sum of the two withdrawal rates. A representative sample was taken from the feed prior to the run by using a 16:1 sample splitter. 300 ml samples of the reject and product streams were taken periodically during the course of the experiment.

CHAPTER FIVE

RESULTS AND DISCUSSION

5.1 The Iron-Sand System

The iron-sand system is a flotsam-rich system with iron as the jetsam component. The substantial difference in the densities of the two components suggests strong segregation. The mean particle size of iron was chosen to be smaller than that of the sand to prevent the defluidization of the heavy iron particles in the bottom stratum of the bed. The physical properties of the system were tabulated in Table 3.1.

Various analytical techniques were attempted with this system. The X-Ray fluorescence technique was abandoned because of difficulties in sample preparation due to the impossibility of homogenizing the iron in a mixture with sand. The non-uniform distribution of iron in the sample precluded an accurate concentration determination of iron by this technique. Titration using potassium dichromate was the chosen analytical method. Despite the acceptable accuracy of the titrative technique, the procedures were very time-consuming. Analytical difficulties were primarily responsible for the limited experimentation with the system.

To eliminate electrostatic effects due to charges generated by intimate solids to solids contact during fluidization, all the experiments with the iron-sand system were carried out with humidified air at a relative humidity between 35% and 50%.

Experiments with the iron-sand system can be classified into three types: runs in the simple fluidized bed; total reflux runs, and recirculation runs in the cascade. The cascade experiments were plagued by various mechanical problems which were subsequently eliminated in the modified model of the counter-current fluidized cascade (Section 3.1.2 and 3.1.3).

5.1.1 Segregation in Simple Fluidized Bed

The anticipated strong segregation of iron in the iron-sand system was confirmed by segregation experiments in the simple cylindrical fluidized bed. Even at a superficial velocity that was three times the minimum fluidization velocity of the mixture, it was evident that there was a substantial concentration of the iron towards the bottom stratum of the bed. The data are presented in Table 5.1. From the data, the mixing index was estimated to be 0.5. Using Nienow's empirical equation (equation 2.3) and assuming that the ratio of sphericity of the two components to be unity in the shape connected diameter ratio, the mixing index was estimated to be 0.3. The data from the simple fluidized bed segregation run suggested better mixing than

FIGURE 5.1 TYPICAL PLOTS OF LN(C) VERSUS Z
(IRON SAND SYSTEM)

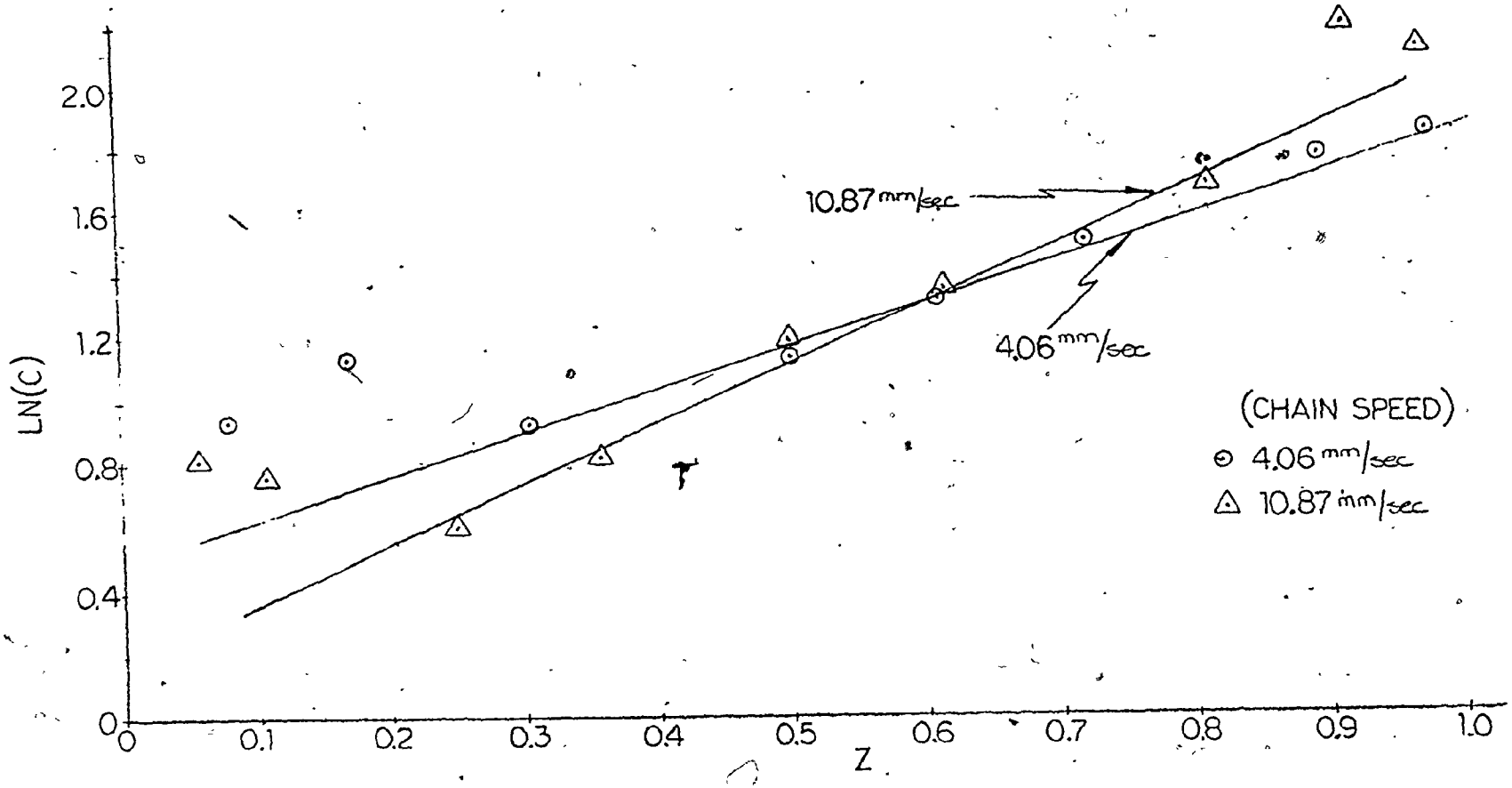

Table 5.1 Simple Fluidized Bed Segregation Run

(Iron-Sand System)

U_{mf} = 40.8 mm/sec

U/U_{mf} = 3.24

Overall concentration = 1.8% iron by weight

Estimated Mixing Index = 0.5

Normalized Bed Height, H	Concentration of Iron
1.00	0.90%
0.84	0.91
0.70	0.87
0.56	0.93
0.41	0.89
0.27	0.80
0.14	7.29

Table 5.2 A Iron-Sand System Total Reflux Run

(Chain speed = 4.06 mm/sec)

Distance from Jetsam-Rich End, Z	% Iron, C
0.0033	2.54
0.1701	3.11
0.3056	2.51
0.5000	3.10
0.6111	3.74
0.7222	4.46
0.8958	5.87
0.9757	6.38

Regression Line $Ln(C) = 1.3807\ (Z) + 0.4777$ (5.1)

Correlation Coefficient = 0.994

Beneficiation ratio = 3.98

that predicted by Nienow's empirical correlation. The size distribution of the solids, and the absence of sphericity data in the application of the empirical correlation, might contribute to the disagreements.

5.1.2 Total Reflux Experiments in the Fluidized Cascade

Experimental procedures for total reflux runs were described in Section 4.3.1. Total reflux experiments entailed the fluidization of the bed of solids in the cascade with the counter-current convective motion of the fluidized solids induced by the movement of the paddle-chain. Sufficient time, usually the time duration for the paddle-chain to sweep the length of the bed twenty to forty times, was allowed for the cascade bed to equilibrate to its steady state concentration profile. At the end of the run, the fluidizing air and the paddle-chain were shut down simultaneously, thus "freezing" the distribution of jetsam along the length of the bed. The concentration of jetsam along the length of the bed was determined by the analysis of samples withdrawn at selected locations in the bed. Details of the sampling technique were previously described in Section 4.3.1. Results of the total reflux experiments are summarized in Table 5.2 A through F; each table corresponded to a different chain speed. The superficial velocity for all the runs were kept at 128 mm/sec, approximately three times the minimum fluidizing velocity of the mixture of solids. The overall concentration of iron in the cascade

Table 5.2 B Iron-Sand System Total Reflux Run

(Chain Speed = 8.53 mm/sec)

Distance from Jetsam-Rich End, Z	% Iron, C
0.0694	2.33
0.1215	2.12
0.2361	2.05
0.3993	2.74
0.5139	3.12
0.6215	3.68
0.7396	4.63
0.8819	7.86

Regression Line $Ln(C) = 1.5650\ (Z) + 0.3549$ (5.2)

Correlation Coefficient = 0.997

Beneficiation ratio = 4.78

Table 5.2 C Iron-Sand System Total Reflux Run

(Chain Speed = 10.87 mm/sec)

Distance from Jetsam-Rich End, Z	% Iron, C
0.0592	2.24
0.1108	2.13
0.2500	1.83
0.3583	2.28
0.5000	3.27
0.6150	3.87
0.8125	5.36
0.9167	8.93
0.9692	8.34

Regression Line $Ln(C) = 1.9255\ (Z) + 0.1526$ (5.3)

Correlation Coefficient = 0.995

Beneficiation ratio = 6.86

Table 5.2 D Iron-Sand System Total Reflux Run

(Chain speed = 20.83 mm/sec)

Distance from Jetsam-Rich End, Z	% Iron, C
0.1667	2.55
0.2500	1.71
0.3333	2.31
0.4167	2.69
0.5278	3.05
0.6111	3.63
0.7222	4.88
0.8056	6.15
0.8889	8.63

Regression Line $Ln(C) = 2.1265\ (Z) + 0.0536$ (5.4)

Correlation Coefficient = 0.991

Beneficiation ratio = 8.39

Table 5.2 E Iron-Sand System Total Reflux Run

(Chain speed = 28.75 mm/sec)

Distance from Jetsam-Rich End, Z	% Iron, C
0.0764	2.14
0.1667	2.64
0.3056	2.17
0.5278	3.43
0.6146	3.82
0.7778	5.38
0.8958	7.39
0.9375	9.74

Regression Line $Ln(C) = 1.9056\ (Z) + 0.1969$ (5.5)

Correlation Coefficient = 0.998

Beneficiation ratio = 6.72

Table 5.2 F Iron-Sand System Total Reflux Run

(Chain speed = 52.78 mm/sec)

Distance from Jetsam-Rich End, Z	% Iron, C
0.0799	2.25
0.1632	3.13
0.2778	2.71
0.4722	3.31
0.6111	3.80
0.7778	4.83
0.8889	6.87
0.9514	7.24

Regression Line $Ln(C) = 1.1436\ (Z) + 0.6644$ (5.6)

Correlation Coefficient = 0.996

Beneficiation ratio = 3.14

bed was 6.3% by weight.

Similarly, in the total reflux experiments with jetsam-rich mixtures of solids investigated by other experimenters,[13,40,77,41] the concentration of the minor component appeared to be exponentially dependent on its horizontal location in the bed. When the logarithm of the concentration of iron in the sample, ln(c), was plotted against its normalized horizontal location in the bed, Z, defined as the ratio of the distance from the sampling point to the jetsam-poor end of the cascade and the length of the entire cascade, linearity was observed for the interval $0.2 < Z < 0.8$. A typical concentration profile plot of ln(c) versus Z is presented in Figure 5.1. Inspection of Figure 5.1 reveals that the data tend to lie in a straight line in the interval $0.2 < Z < 0.8$. Significant deviation from linearity was observed for $Z < 0.2$ in the jetsam-rich end of the cascade. Accumulation of jetsam in this end of the cascade would account for the deviation. The accumulation of iron in the jetsam-rich end of the cascade is an enigmatic phenomenon. A conceptual explanation is still wanting.

From the concentration profile data, least squares linear regressions of ln(c) versus Z were performed for each set of data. The regression analyses were based on data in the interval $0.2 < Z < 0.8$. The regressional lines are listed in Table 5.2 A through F. Linearity was observed in all cases. This is evident by inspecting the values of the correlation coefficients, all of which approached unity. From

FIGURE 5.1 TYPICAL PLOTS OF LN(C) VERSUS Z
(IRON SAND SYSTEM)

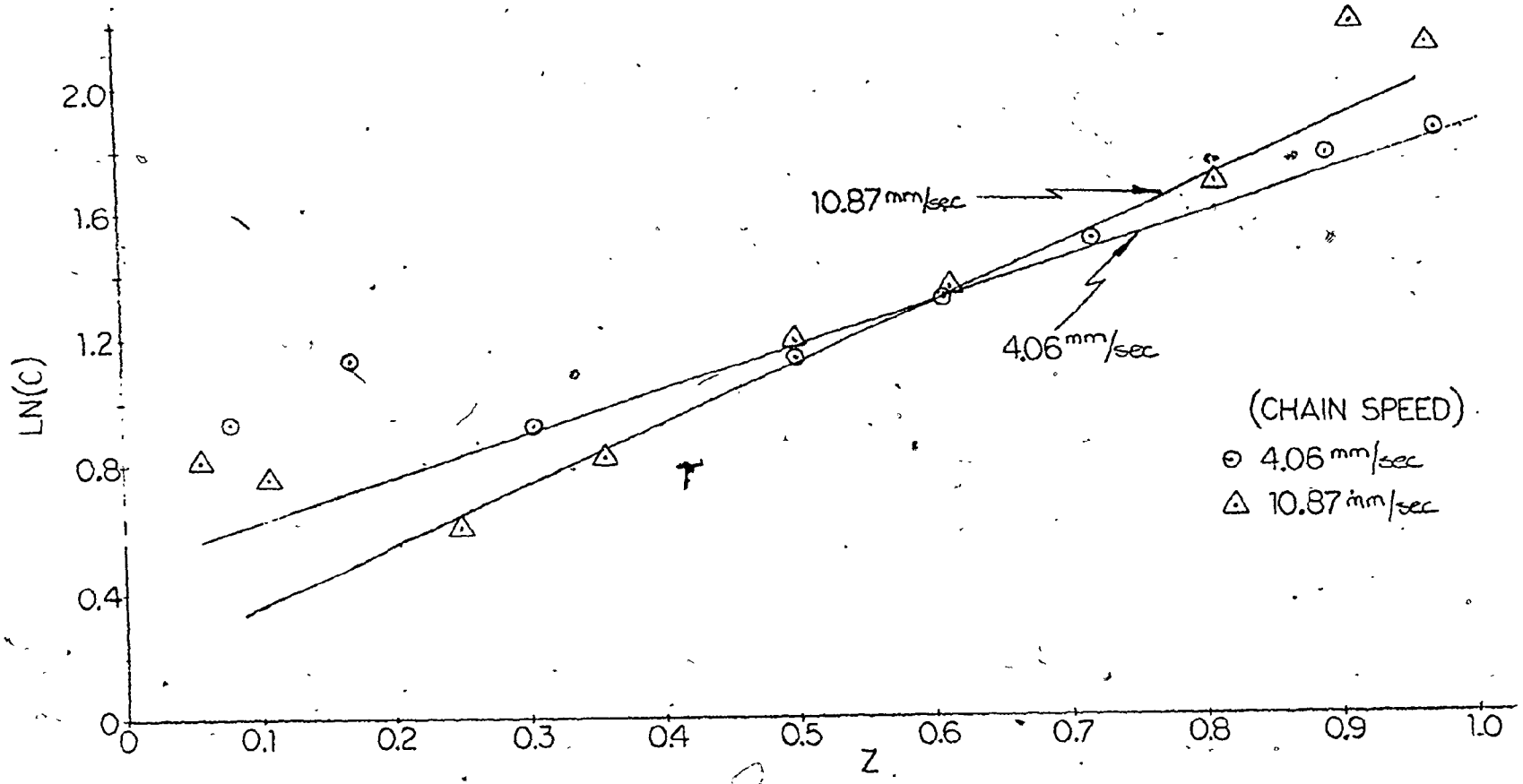

the regression line, the beneficiation ratio, which is defined as the ratio of the jetsam concentration in the two ends of the cascade, could be calculated. Figure 5.2 is a plot of the estimated beneficiation ratio versus chain speed. Inspection of the plot showed that the beneficiation ratio, which is an indicator of segregation effectiveness of the cascade, was dependent on chain speed. The optimal chain speed at which the segregation was a maximum was approximately 20 mm/sec. As the chain speed exceeded 30 mm/sec., a decline in the beneficiation ratio was observed. It was suspected that mixing in the bed could be induced by high chain speeds. Conversely, if the chain ceased in motion, the cascade would constitute an elongated simple fluidized bed. While the jetsam would still concentrate towards the bottom of the bed, the concentration of jetsam along the length of the bed should be invariant. It is interesting to note that the dependence of beneficiation ratio on the chain speed was also observed in jetsam-rich systems.[13,40,77] Experiments with other solids systems indicated that the shape of the beneficiation ratio versus chain speed plot is also dependent on the fluidization velocity. The optimal chain speed where the beneficiation ratio is maximum is contingent on the operating fluidization velocity. Experiments with the salt-activated charcoal system, which will be discussed later in this chapter, will verify this assertion.

Despite the strong segregation observed in the

FIGURE 5.2 PLOT OF BENEFICIATION RATIO VERSUS CHAIN SPEED
(IRON SAND SYSTEM)

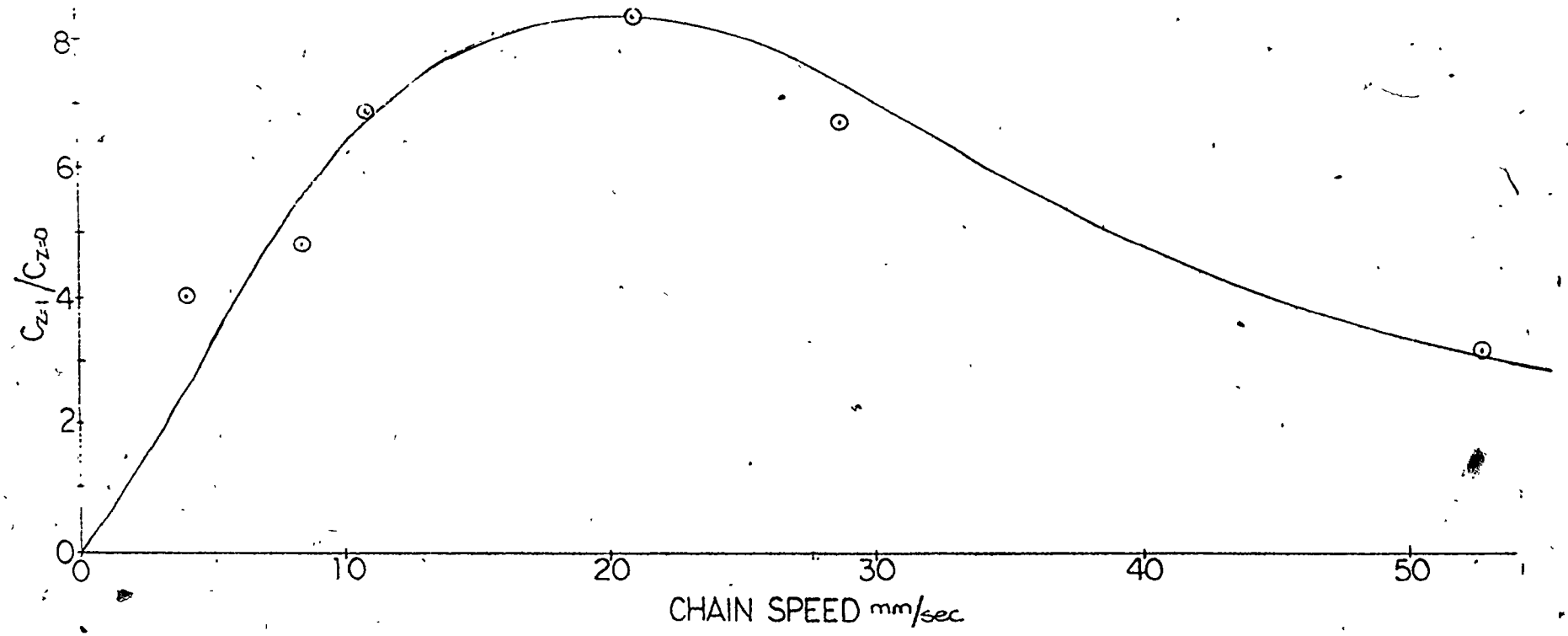

simple fluidized bed experiment, the effectiveness of separation in the cascade bed was disappointingly low. The maximum beneficiation ratio was only 8.5. Comparatively, in the jetsam-rich systems investigated by Muzyka and Jeffs,[77,13] typical values of the beneficiation ratios were at least an order of magnitude higher. However, it should be remembered that the mechanism of segregation of flotsam-rich systems is inherently different from jetsam-rich systems. Comparison of the two systems is beyond the scope of this study.

5.1.3 Effects Attributable to Particle Size

It was suspected that in the total reflux experiments, in addition to segregation by density difference, the solids might segregate by virtue of their size distribution. To investigate the severity of segregation by particle size difference, samples were taken from each end of the cascade after the completion of a typical total reflux experiment. Sieve analysis of each sample was performed and the concentration of iron in each size fraction was analyzed. The data are presented in Table 5.3. From the data, the geometric and Sauter mean diameter of the samples as well as those of their jetsam components, were calculated. The results are listed in Table 5.4. Inspection of Table 5.4 confirmed that there was indeed some segregation by size in the solids. The mean size of the sample from the jetsam-rich side was approximately ten microns larger than that

Table 5.3 Distribution of Jetsam in Iron-Sand System as a Function of Particle Size (Total Reflux Runs)

Sieve Size (micron)	Sample from Jetsam-Poor End of Cascade		Sample from Jetsam-Rich End of Cascade	
	Wt. Fraction	% Iron	Wt. Fraction	% Iron
180-297	0.1524	0.0	0.1595	0.0
125-180	0.5534	1.78	0.5905	8.62
106-125	0.2437	4.00	0.2199	21.36
90-106	0.0372	6.31	0.0242	51.36
75-90	0.0111	9.70	0.0053	71.31
0-75	0.0022	12.92	0.0006	100.00

Overall concentration of Iron

(a) Sample from Jetsam-Rich End of Cascade 11.48%

(b) Sample from Jetsam-Poor End of Cascade 2.33%

Table 5.4 Summary of Size Analyses on Samples Taken from Two Ends of Cascade

	Geom. Mean Size (μm)	Sauter Mean Size (μm)
Sample from Jetsam-Poor End	160	206
Iron only	138	170
Sample from Jetsam-Rich End	171	214
Iron only	133	166

from the other side. However, there was virtually no segregation by size of the jetsam components. The geometric mean diameter of the iron at the jetsam-rich end was in fact 133 micron, slightly smaller than the 138 micron in the opposite side. The slight difference could be attributed to analytical error.

5.1.4 Runs with Recirculation

Two sets of experiments were performed with paddle-chain speeds of 20 and 39 mm/sec. The fluidization velocity used in both cases was 125 mm/sec, approximately three times the minimum fluidization velocity of the mixture. The data are summarized in Table 5.5. In Table 5.5, the concentration of iron in the withdrawal streams at both ends of the cascade, and the ratio of the concentration of iron in the two streams (which is defined as the beneficiation ratio), are tabulated for each of nine combinations of withdrawal ratios at the two ends.

Inspection of the data reveals no clear dependency of beneficiation ratio on the withdrawal ratios. For example, at a chain speed of 20 mm/sec and for a withdrawal rate of 76 g/sec at the jetsam-rich end, as the withdrawal rate at the flotsam-rich end varied from 80.5, 163, 317 to 406 g/sec, the beneficiation ratios were correspondingly 1.28, 1.25, 1.18 and 1.44. Conversely, the beneficiation ratio appeared to be more dependent on the withdrawal rate at the jetsam-rich end. At the same withdrawal rate in the flotsam-rich

Table 5.5 Iron-Sand Recirculation Experiments

(1) Superficial Velocity = 125 mm/sec
Chain Speed = 20 mm/sec

Withdrawal rate at flotsam-rich end, g/sec	Withdrawal rate at jetsam-rich end, g/sec	FR* % Iron	JR** % Iron	Beneficiation ratio
80.5	76	3.34	4.13	1.23
163		3.35	4.20	1.25
317		3.24	3.82	1.18
406		3.12	4.48	1.44
80.5	157	3.28	3.81	1.16
163		3.55	4.23	1.19
317		3.48	3.91	1.12
406		3.36	3.97	1.18
80.5	283	3.27	3.46	1.06
163		3.66	3.59	1.00
317		3.53	3.91	1.11
406		3.12	3.63	1.17

(2) Superficial Velocity = 125 mm/sec
Chain Speed = 39 mm/sec

Withdrawal rate at flotsam-rich end, g/sec	Withdrawal rate at jetsam-rich end, g/sec	FR* % Iron	JR** % Iron	Beneficiation ratio
80.5	76	2.34	5.44	2.32
163		2.54	5.28	2.08
317		2.66	5.33	2.00
406		2.70	5.77	2.14
80.5	156	2.74	4.69	1.71
163		3.01	4.22	1.40
317		3.16	4.09	1.29
406		3.24	4.36	1.35
80.5	283	2.69	4.28	1.59
163		3.20	4.34	1.35
317		3.28	3.80	1.16
406		3.41	3.85	1.13

*FR = Flotsam Rich Withdrawal

**JR = Jetsam Rich Withdrawal

side, the beneficiation ratio decreased with the increase in the withdrawal rate of the jetsam-rich side. An example of this dependency can be found at the chain speed of 39 mm/sec and a withdrawal rate of 80.5 mm/sec at the flotsam-rich end, where the beneficiation ratio decreased from 2.32 to 1.71 and from 1.71 to 1.59 as the withdrawal rate at the jetsam-rich end increased from 76 to 156 and from 156 to 283 g/sec. A statistical analysis of the dependency of beneficiation ratio on the withdrawal ratios on either end of the cascade could not be attempted because of the limited available data.

In general, the results of the recirculation runs were disappointing. Despite the fact that the system is a strongly segregated one, the highest beneficiation ratio attained was only 2.32. Inspection of the data also revealed that the concentration of iron in the two withdrawal streams was consistently lower than the overall concentration of the bed, at 6.3%. Apparently, a significant portion of the jetsam must have accumulated in the bed, and was thus prevented from circulating. It was suspected that the most likely area for the accumulation of jetsam was near the grid region of the bed in the jetsam-rich end of the cascade. This speculation was verified by aspirating the entire one-third of the bed in the jetsam-rich end and then determining the iron concentration of a sample, which showed a disproportionately high concentration of iron. The withdrawal port in the jetsam-rich end could also contribute

to the accumulation of jetsam. The port was a small circulator pipe located close to the grid surface. The pure jetsam layer in the bottom of the grid was rather shallow in depth and might be beneath the opening of the port. Jetsam could also accumulate in the "dead zones" on either side of the withdrawal port. Furthermore, jetsam was also proven to be accumulating in the bottom of the conical auger wells in the two ends of the cascade. The excessively larger volume of the conical auger wells, coupled with the mechanical vibrations from the augers, may have been responsible for accumulation in the wells. Most of the problems with jetsam accumulation were alleviated in the modified version of the cascade. The installation of the rectangular port with an opening traversing the width of the bed, the inclination of the grid surface in the jetsam-rich end, and the redesigned auger wells as described in Section 3.3.1, all contributed to the reduction of jetsam accumulation in the cascade bed.

Despite the limited experimentation, the results with the iron-sand system revealed deficiencies in the original design of the cascade, and provided insights for the construction of the modified version of the cascade, which was significantly more versatile and better performing than the original.

5.2 Iron Pyrite-Coal System

The counter-current fluidized cascade may find applications in coal beneficiation. Of the three basic forms of sulphur in coal, namely, pyrite, organic and sulphate sulphur, there is no known commercially viable physical method for the removal of organic and sulphate sulphur. There is, however, a variety of physical methods for the removal of pyritic sulphur. Wet washing and mechanical jigs are typical of the more popular cleaning methods in pyritic sulphur removal. Since a substantial difference in density exists between the pyrite and its coal matrix, it was thought that the cascade might be applicable in the removal of pyritic sulphur from coal.

Experiments with this system constituted the first concerted investigation of coal beneficiation using the counter-current fluidization cascade. In this system, the coal was a low sulphur coal, 0.5% sulphur by weight, provided by Energy, Mines and Resources Canada. ASTM analytical procedures were followed for the determination of the sulphur content of the coal; the sulphur distribution is provided in Table 3.2 B. Two batches of coal fines with different mean sizes were prepared by crushing and screening. Batches of fine iron pyrite with different mean sizes were added to either batch of coal to make artificial mixtures of coal and pyrite. The objective of the experiment was to investigate the performance of the cascade in the removal of pyrite under varying experimental conditions. Different combinations

of paddle speed (chain speed), fluidization velocity, coal feed rate, relative withdrawal rate of rejects and product streams, and mean size of coal and pyrite were used in an attempt to study their effect on the pyrite removal efficiency. In the absence of a reliable theoretical model describing the rheology of the solids in the cascade, statistical methods were used to interpret the experimental data.

During the course of the experiments, it became apparent that some of the pyrite was prevented from circulating by accumulating in the "dead" zones of the cascade and auger hoppers. To alleviate the problem, modifications were made in the cascade bed and in the hoppers. It should be pointed out that the paddle-chain drive mechanism was modified at the beginning of the experimental program. (Details of the modifications were described in Section 3.1.3.) The analytical technique was relatively simple. Using a heavy medium, tetrabromethane (s.g. 2.90), as the flotation agent, the pyrite was separated from the coal fines. The concentration of pyrite in the sample could then be determined gravimetrically after the separation. The procedures are described in Section 3.3.4.

5.2.1 Pyrite E - Coal A System

A batch of material with a pyrite concentration of 6% by weight was loaded into the cascade bed to a height of 170 mm. The geometric mean size of coal, batch A, and

pyrite, lot E, were 360 and 216 micron, respectively. This constitutes the coarsest mixture of pyrite and coal studied. Earlier on, it was detected that there was a significant size variation of the fluidized solids along the length of the cascade. The phenomenon of segregation by size was observed in a typical total reflux cascade experiment with a paddle speed of 39 mm/sec and at a fluidization velocity of 196 mm/sec, approximately twice the minimum fluidization velocity of the overall solids mixture. While the jetsam end of the cascade was poorly fluidized, almost to the point of complete defluidization, the opposite flotsam end was fluidized excessively. Apparently, the minimum fluidization velocity of the solids varied along the axis of the bed. After the total reflux run, the minimum fluidization velocity of the solids in each of four quadrants of the bed was determined, first by an in-situ approach as described in Section 4.3.1, and also by removing the materials from the central regions of each quadrant for the determination of the minimum fluidization velocity in the simple fluidized bed. The minimum fluidization velocity values determined by either method agreed fairly well to within 10%. The fluidization velocities used in the recirculation runs in the four quadrants of the cascade were set at 53, 53, 122 and 262 mm/sec, at approximately 1.25 times the minimum fluidization velocity. Higher fluidization velocities could not be attempted because of the limited capacity of the air supply. At a chain speed of 39 mm/sec, a series of recir-

culation runs was performed. The results are given in Table 5.6.

It is important to note that the order of each experiment is identical to the run number given in Table 5.6. Inspection of the results revealed a disproportionately high concentration of pyrite in the rejects stream in the early experiments, which then dwindled with time. It was suspected that not all the pyrite leaving the cascade was reintroduced back to the cascade. The pyrite leaving the cascade was assumed to be accumulating in the auger wells, and was thus prevented from re-entering the cascade bed. This would result in an overall dilution of pyrites in the cascade with time. The pyrite-coal system is a strongly segregating system, and the vibration induced by the auger motor in the auger well could lead to settling of the pyrite towards the bottom of the auger well. This problem was compounded by the fact that the auger well was basically a simple conical bin with a large volume. Subsequent aspiration and analyses of samples from the auger well confirmed the accumulation of pyrite. Other potential areas for pyrite accumulation were in the "dead" zones in the cascade bed between the jetsam end wall and the point at which the chain rose to meet the sprocket, and in-between the perforated plates in the air distribution grid. Sampling and analyses confirmed the accumulation of jetsam in those areas.

In fact, the effect of the rejects and products

withdrawal rate on pyrite removal efficiency could not be ascertained from the results in Table 5.6. It is possible that the dilution of jetsam in the cascade bed as a result of its accumulation in the auger wells might have a more significant effect on the concentration of pyrite in the rejects stream. The fact that the pyrite concentration remained low and roughly constant at 0.2 to 0.3% in the products stream gives some credence to this speculation. An experiment was performed at a reject and product withdrawal rate of 27 and 169 kg/hr, respectively, and at a paddle speed of 39 mm/sec. Samples were taken from the reject stream as a function of time. The results are summarized in Table 5.7. Inspection of Table 5.7 reveals the same trend as exhibited in the previous runs, Table 5.6, with the high pyrite concentration in the beginning followed by a gradual reduction with time. It is quite evident that the reduction in pyrite concentration in the rejects stream with time was caused by the accumulation of pyrite, as previously discussed in this section.

Despite the limited scope of experimentation with this system, the results clearly indicated that the coarse pyrite, in admixture with the coal fines with a geometric mean diameter of 360 μm could readily be removed by the cascade. With the difficulties encountered in maintaining the pyrite in circulation, it was decided that further experimentation was not warranted.

Table 5.6 Results of Recirculation Runs in Coal A - Pyrite E System

Run No.	Rejects (Kg/hr)	Products (Kg/hr)	Pyrites in Rejects	Pyrite in Products
1	27	169	26.9%	0.21%*
2	27	392	14.8	0.34 *
3	27	460	9.2	0.34 *
4	40	169	7.4	0.19
5	40	392	7.8	-
6	40	460	9.6	0.19 *
7	151	169	1.8	0.29
8	151	392	5.7	0.27
9	151	460	3.9	0.32

* Determined by ASTM chemical analysis; all other pyrite concentrations were determined gravimetrically after separation by float-sink technique.

Table 5.7 Pyrite Concentration at Rejects Outlet as a Function of Time (Pyrite E - Coal A System)

Time (minutes)	Concentration (%)
5	6.28
8	6.03
12	4.35
15	4.98
20	3.07

Table 5.8 Distribution of Pyrite Along the Fluidized Cascade (Pyrite A - Coal B System)

Distance from flotsam-end wall	Concentration
355 mm	2.09%
760	2.61
1370	4.21
1770	3.50
2290	4.82
2900	4.85
3220	4.99
3420	6.70

5.2.2 Pyrite A - Coal B System

A batch of material containing 5.9% pyrite A by weight in admixture with coal, batch B, was loaded into the cascade bed to a height of 170 mm. The geometric mean sizes of batch B coal and pyrite A were 153 and 74 microns, respectively. Other physical properties of the component are given in Section 3.2.2. This system constituted the finest mixture of pyrite and coal studied.

Before experimentation with this mixed solids system, the auger wells at the products and rejects sides of the cascade were modified in order to minimize the volume for jetsam accumulation. A total reflux run was performed at U/U_{mf} equal to 2.10 and a paddle speed of 39 mm/sec. Segregation by size was not apparent in the experiment. The superficial velocities used in the four quadrants of the cascade were identical, as the minimum fluidization velocity was assumed to be invariant along the axis of the bed. Results of the longitudinal assay of the concentration of pyrite in this total reflux run are presented in Table 5.8. The results indicated that pyrite was still lost from circulation, presumably by accumulating in the grid region of the cascade. A series of runs was attempted with the flotsam end of the cascade raised up by 50 mm to facilitate the movement of pyrite toward the jetsam-rich exit. Additional coal was loaded into the bed in order to make up for the reduction of bed height in the flotsam end. The average pyrite concentration was reduced to 4.64%. Results of the

runs are summarized in Table 5.9. Inspection of Table 5.9 reveals that the problem associated with the loss of pyrite from circulation was still unresolved.

Another attempt was made to alleviate the problem of jetsam accumulation in the "dead" zone of the bed. It was thought that the angle of tilt of the cascade bed was insufficient to cause the movement of solids in the lower stratum of the bed towards the rejects side of the cascade. A modification was made in the cascade to increase the angle of tilt by inclining the grid surface at 7.6^{o} to the horizontal, 483 mm from the end wall of the jetsam-rich end. The circular pipe withdrawal port in the jetsam end was also replaced by a slotted outlet in order to facilitate the outflow of the reject material. Details of the modifications were described in Section 3.1.3.

Two lengthy series of recirculation runs were performed with the modified cascade. The first series was performed at a value of U/U_{mf} equal to 2.0, with the chain speed varied from 16.6 to 68.6 mm/sec. In the second series, the ratio U/U_{mf} was maintained at 1.5 and the chain speed varied from 22.4 to 68.6 mm/sec. Inspection of Table 5.10 and 5.11 reveals that the loss of pyrite from circulation was still a problem. The pyrite concentration in the rejects was frequently lower than the overall pyrite concentration of 4.64%. It was likely that the loss of pyrite was due to its accumulation in the auger tube housing. The volume of the auger housing was fairly substan-

Table 5.9 Recirculation Runs for Coal B - Pyrite A System with the Cascade Tilted Towards the Jetsam End

(unmodified cascade)

Rejects Withdrawal Rate (kg/hr)	% Pyrite	Products Withdrawal Rate (kg/hr)	% Pyrite	Chain Speed
19	3.68	39	1.02	39.0 mm/s
	3.94	84	1.18	
	3.98	112	0.99	
59	2.77	39	1.25	
	3.44	84	1.24	
	3.37	112	1.11	
154	3.03	39	1.16	
	2.34	84	1.60	
	2.45	112	1.09	
19	4.56	39	0.71	20.5 mm/s
	4.47	84	0.84	
	4.45	112	1.04	
59	3.07	39	1.04	
	2.83	84	1.13	
	3.10	112	1.15	
154	2.53	39	0.92	
	2.28	84	0.92	
	2.82	112	1.06	

Table 5.10 Recirculation Runs for Coal B - Pyrite A System in Modified Fluidized Cascade (U/U_{mf} = 2.0)

Rejects Withdrawal Rate (kg/hr)	% Pyrite	Products Withdrawal Rate (kg/hr)	% Pyrite	Chain Speed
11.5	2.45	39	0.82	16.6 mm/s
	2.73	84	0.72	
	2.56	112	0.91	
19.1	2.38	39	0.97	
	2.66	84	0.91	
	1.89	112	0.76	
31.7	1.92	39	0.87	
	2.43	84	1.06	
	2.31	112	0.86	
11.5	2.62	39	0.59	22.4
	3.27	84	1.00	
	3.16	112	1.08	
19.1	2.98	39	0.73	
	2.61	84	0.54	
	2.99	112	1.02	
31.7	3.20	39	0.65	
	2.29	84	0.51	
	1.89	112	0.76	
11.5	4.10	39	0.64	26.0
	3.46	84	0.79	
	3.42	112	0.62	
19.1	2.93	39	0.69	
	2.91	84	0.73	
	2.86	112	0.82	
31.7	3.42	39	0.82	
	2.56	84	0.60	
	3.36	112	0.69	

Table 5.10 (Continued)

Rejects Withdrawal Rate (kg/hr)	% Pyrite	Products Withdrawal Rate (kg/hr)	% Pyrite	Chain Speed
11.5	2.78	39	0.75	32.7 mm/s
	2.68	84	0.60	
	2.05	112	0.96	
19.1	2.70	39	0.97	
	2.26	84	0.76	
	2.66	112	0.93	
31.7	2.28	39	0.96	
	3.13	84	0.66	
	2.13	112	0.86	
11.5	3.62	39	0.73	41.5
	3.79	84	0.64	
	2.95	112	0.45	
19.1	3.01	39	0.45	
	1.94	84	0.48	
	2.64	112	0.54	
31.7	2.39	39	0.80	
	2.08	84	0.59	
	2.86	112	0.51	
11.5	2.72	39	0.84	68.6
	2.54	84	0.65	
	2.99	112	0.77	
19.1	3.00	39	0.52	
	1.74	84	0.67	
	2.02	112	1.01	
31.7	3.01	39	0.56	
	1.82	84	0.78	
	2.41	112	1.18	

Table 5.11 Recirculation Runs for Coal B - Pyrite A System in Modified Fluidized Cascade ($U/U_{mf} = 1.5$)

Rejects Withdrawal Rate (kg/hr)	% Pyrite	Products Withdrawal Rate (kg/hr)	% Pyrite	Chain Speed
0		112	1.00	68.6 mm/s
11.5	2.10	39	0.53	
	1.61	84	0.48	
	2.98	112	0.88	
19.1	2.31	39	0.53	
	1.04	84	1.24	
	1.31	112	0.92	
0	3.58	112	0.85	41.5
11.5	3.47	39	0.40	
	2.33	84	0.80	
	2.78	112	0.52	
19.1	2.76	39	0.51	
	3.01	84	0.69	
	2.34	112	0.87	
31.7	2.50	39	0.45	
	2.74	84	0.79	
	2.76	112	0.64	
0	3.32	112	0.54	26.0
11.5	3.79	39	0.42	
	3.37	84	0.45	
	2.90	112	0.27	
19.1	2.71	39	0.25	
	3.22	84	0.25	
	3.10	112	0.42	

Table 5.11 (Continued)

Rejects Withdrawal Rate (kg/hr)	% Pyrite	Products Withdrawal Rate (kg/hr)	% Pyrite	Chain Speed
31.7	3.04	39	0.32	
	2.72	84	0.42	
	2.22	112	0.44	
0	4.70	112	0.77	22.4 mm/s
11.5	3.79	39	0.61	
	3.49	84	0.50	
	3.83	112	0.80	
19.1	3.47	39	0.73	
	3.51	84	0.72	
	3.18	112	0.70	
31.7	2.86	39	0.72	
	3.12	84	0.83	
	3.03	112	0.98	

tial; vibration caused by the movement of the conveyer screw would cause the pyrite to concentrate towards the bottom portion of the auger housing. However, it was found that steady state occurred after approximately thirty minutes, starting from a thoroughly premixed bed. The steady state was also relatively unperturbed by changes in products and/or rejects withdrawal rates. Thus, before the first samples of the products and rejects were taken, the bed was usually allowed to run undisturbed for one hour in order to reach steady state. After resetting the augers for a different combination of products and rejects withdrawal, fifteen to twenty minutes were allowed before samples were taken. This procedure was adopted for all the runs.

Multiple regression analysis was used to study dependence of the separation effectiveness of the cascade on various operating conditions. D_1, the concentration of pyrites in the product stream; D_2, the concentration of pyrites in the rejects stream, and D_3, the beneficiation ratio equal to the quotient of D_2 and D_1, were the three dependent variables. The four primary independent variables were G, the total feed rate in kg/hr; P_r, the fraction of the feed originating at the products end of the cascade; CS, the speed of the paddle chain in mm/sec; and N_f, the fluidization number ($= U/U_{mf}$). Since it was presumed that, at a constant G, P_r and N_f setting, an optimal chain speed would exist where the pyrite concentration in the rejects as well as the beneficiation ratio would be maximized, and

the pyrite concentration in the products minimized, an extra term defined as the square of the chain speed, CS^2 was included in the list of independent variables. Results of the regression analysis are summarized in Table 5.12. The statistical significance of the fit was evaluated by comparing the calculated F ratio, defined as the ratio of the sum of squares attributed to the regression divided by the sum of squares of deviation from the regression, with the critical F ratio obtained from standard statistical tables at a specified confidence level. At the 1%, 2.5% and 5% significance level, the critical F ratio corresponding to 5 degrees of freedom associated with the regression, namely, the five independent variables F, P_r, CS, CS^2 and N_f, and the 81 degrees of freedom associated with deviation from regression were 9.18, 6.10 and 4.42, respectively. When the dependent variables D_1, D_2 and D_3 were regressed with the five aforementioned independent variables, the F ratios were calculated to be 5.27, 7.60 and 7.60, respectively. Thus, it appeared that the regression equations for dependent variables D_2 and D_3 were significant at the 2% level, while D_1 was only significant at the 3 to 4% level.

Some conclusions could be drawn from the magnitude and size of the regression coefficients. Inspection of the regression equations in Table 5.12 revealed that an increase in feed rate, G, and fluidization number, N_f, would lead to a decrease in D_2 and D_3, the concentration of

Table 5.12 Multiple Regression Analysis on Cascade Recirculation Results Using Coal B with Pyrite lot A

System	Dependent Variable	Regression Coefficient: Intercept	G(kg/hr)	P_r	CS(mm/s)	CS^2	N_f	F Ratio	$F_{0.05}$
	D_1	0.6946	0.003232	-0.2522	-0.01483	0.0002123		2.41	5.76
N_f= 1.5	D_2	2.4390	-0.01238	2.944	-0.003941	-0.000389		29.50	5.76
	D_3	3.466	-0.05073	9.497	0.06388	-0.001795		2.54	5.76
	D_1	1.223	0.001351	-0.2350	-0.02224	0.0002385		2.54	5.76
N_f=2.0	D_2	1.518	-0.007756	1.676	0.03928	-0.0004918		2.54	5.76
	D_3	0.06003	-0.01551	2.806	0.1688	-0.001877		3.88	5.76
N_f=1.5 &	D_1	0.5512	0.001876	-0.1671	-0.02122	0.0002473	0.2588	5.27	4.42
N_f=2.0	D_2	2.171	-0.008145	1.608	0.03418	-0.0005705	-0.1334	7.60	4.42
Inclu-sive	D_3	7.304	-0.02467	3.650	0.1573	-0.002129	-3.114	7.60	4.42

D_1 = % pyrite in products

D_2 = % pyrite in rejects

D_3 = Beneficiation Ratio ($=D_2/D_1$)

$F_{0.05}$ = F Ratio for 95% confidence

pyrite in the rejects and the beneficiation ratio. Conversely, it would result in the increase of D_1, the concentration of pyrites in the products. An increase in the fractional withdrawal of the feed as products, P_r, would lead to an increase in D_2 and D_3 while D_1 would be decreased. This is conceptually accurate. As in most coal cleaning devices, an increase in throughput usually results in a deterioration in beneficiation. An increase in fluidization number, as expected, leads to enhanced mixing in the fluidized bed, with a detrimental effect on separation efficiency. The last point from the regression analysis is interesting. It was predicted that an increase in product recovery P_r would be advantageous to the beneficiation. This could be construed as an encouraging assessment of the cascade in coal beneficiation.

In all the regressions, the dependent variables were found to be only marginally dependent on G. When the feed rate was increased, there was only a slight decrease in the beneficiation ratio. This is encouraging, for it implies the possibility of a substantial increase in the feed rate, with only a slight decrease in the beneficiation ratio. It should also be remembered that the feed in this experiment was a mixture of the products and rejects stream recirculated from the two ends of the cascade. The product withdrawal rate was usually higher than that of the rejects. As a result, associated with the increase in G there was usually a decrease in the pyrite content in the

feed. A decrease in the mean size of the feed was also likely. If the feed composition were to remain constant, as in the case of a true throughput experiment in which the products and the rejects are not recirculated, the degradation in the performance of the cascade as a consequence of the increase in feed rate should not be severe. Inevitably, a point will be reached at which the feed rate will be excessive and the pyrite removal ability of the cascade will be affected by the increased feed rate. Unfortunately, this could not be verified, as the limited capacity of the augers did not permit high throughput rates.

The effect of chain speed on the dependent variables could be found by taking the partial derivatives of the dependent variables with respect to the chain speed, CS.

$$\frac{\partial D}{\partial CS} = a_3 + 2a_4\, CS \qquad (5.7)$$

$$\frac{\partial^2 D}{\partial CS^2} = 2a_4 \qquad (5.8)$$

where D is the dependent variable, and a_3, a_4 are the coefficients in the regression equations. By equating the first derivative to zero, the chain speed at which the dependent variable would be at a maximum or minimum is $a_3/2a_4$. The sign of the second derivative determines the existence of maximum or minimum at the optimal chain speed. The optimal chain speed in which D_1 is at a minimum, D_2 a maximum and D_3 a maximum, may not be coincident. Inspection of Table 5.13

Table 5.13 Optimum Chain Speed Values (mm/s) Computed from Regression Analysis

	Based on % Pyrites in Products (Minimum)	Based on % Pyrites in Rejects (Minimum)	Based on Beneficiation Ratio (Maximum)
Data with N_f=1.5	38.0	5.1	17.8
Data with N_f=2.0	46.6	39.9	45.0
All data combined	42.9	30.0	36.9

Table 5.14 Size Analyses on Pyrite from the Rejects and Product Streams of the Cascade

(Coal B, Pyrite lot A)

N_f = 2.1 Chain Speed = 39 mm/s

Reject Withdrawal Rate (kg/hr)	Sample	Product Withdrawal Rate (kg/hr)	Sample
19.1	A	39	B
14.6	C	144	D

Sample	Geometric Mean Diameter µm	Geometric Standard Deviation
A	84.0	4.8
B	67.6	5.0
C	80.8	4.8
D	78.4	4.9

The size analyses of the total samples A and B, coal and pyrite inclusive, showed that A has a geometric mean diameter of 163 µm, and B of 148 µm.

showed that all three optimal chain speeds were different in all three cases.

Experiments were carried out to investigate whether there was a significant size difference between the pyrite in the products and rejects streams. Using two combinations of products and rejects withdrawal rates, the geometric mean size of the pyrite samples were determined by sieve analysis, after separation from the coal fines by using tetrabromoethane. The results are summarized in Table 5.14. At the low products and rejects withdrawal rates, there was indeed a detectable size difference of the pyrites originated from the opposite ends of the cascade, as indicated by the mean sizes of sample A and B. However, the difference diminished at the higher products and rejects withdrawal rates. The geometric mean sizes of pyrites sample C and D were virtually identical.

It is likely that the separation effectiveness of the cascade would be significantly better if the working section were to be lengthened. The pyrite concentration in the rejects stream is considered too low to warrant disposal and should be beneficiated further. To confirm the possibility of further beneficiation, segregation experiments in a simple cylindrical fluidized bed were performed on materials withdrawn from the products and rejects sides of the cascade. The overall pyrite concentration of the sample from the jetsam side was 4.4%. The corresponding concentration of the flotsam side was 0.7%. Two fluidization

velocities were used, at N_f = 2.0 and 1.43. The results are summarized in Table 5.15 and 5.16. The concentrations presented in Tables 5.15 and 5.16 were the average concentrations of the sampled layers of the bed, and not the local concentration. Substantial segregation of pyrite from coal was observed in both experiments, confirming that further beneficiation in terms of pyrite removal was possible. From sampling, it was observed that, in all cases, there was formation of a concentrated pyrite layer in the bottom grid region of the bed. Improved beneficiation could be realized by the use of a cascade with a longer working section, or alternatively, by reintroducing the rejects and products streams into other cascades for further pyrite removal. The results from the simple fluidized bed segregation runs were interesting, and were only in partial agreement with the findings of Rowe and his coworkers.[12,21] For most flotsam-rich systems studies, Rowe observed that the bed was completely mixed above the pure jetsam layer in the bottom of the bed. When the overall concentration of jetsam in the bed was increased, the resultant concentration profile showed an increase in the thickness of the jetsam layer in the bottom of the bed; the concentration of jetsam above the pure jetsam layer was not affected significantly. Inspection of Tables 5.15 and 5.16 revealed the existence of a concentration gradient in the bulk of the bed above the bottom layer of jetsam. With the higher overall jetsam content, the concentration of pyrite in the bulk of the bed

Table 5.15 Segregation of Pyrite from Coal from the Product End of the Cascade, in a Simple Fluidized Bed
(Coal B, Pyrite lot A)

Overall weight concentration of pyrite = 0.7%

Test #1 N_f = 2.0

Normalized Height of Layer	% Pyrite
0 - 0.13	2.17
0.13 - 0.3	0.49
0.3 - 0.5	0.32
0.75 - 1.0	0.22

Test #2 N_f = 1.43

Normalized Height of Layer	% Pyrite
0 - 0.17	1.34
0.17 - 0.3	0.63
0.3 - 0.5	0.44
0.75 - 1.0	0.35

Table 5.16 Segregation of Pyrite from Coal from the Rejects End of the Cascade, in a Simple Fluidized Bed (Coal B, Pyrite lot A)

Over all weight concentration of pyrite = 4.4%

Test #1 N_f = 2.0

Normalized Height of Layer	% Pyrite
0 - 0.16	15.6
0.16 - 0.32	4.0
0.32 - 0.48	3.1
0.8 - 1.0	1.4

Test #2 N_f = 1.43

Normalized Height of Layer	% Pyrite
0 - 0.17	13.3
0.17 - 0.33	3.4
0.33 - 0.5	3.3
0.83 - 1.0	1.4

Table 5.17 Recirculation Run of Coal B - Combined Pyrites (Lots A, B, C) in Modified Fluidized Cascade

Chain Speed = 33 mm/sec

U/U_{mf}	Rejects Withdrawal Rate (kg/hr)	% Pyrite	Products Withdrawal Rate (kg/hr)	% Pyrite
2.1	11.5	18.1	39	0.52
		20.4	84	0.69
		18.3	143	0.73
1.5	11.5	13.0	39	0.59
		14.6	84	0.65
		18.0	143	0.68
2.1	14.6	15.2	39	0.70
		11.0	84	0.63
		13.7	143	0.44

was proportionately higher. The effect of fluidization velocity on the concentration profile was also minimal. On the other hand, Rowe observed that the segregation/mixing of jetsam in a fluidized bed was very sensitive to the fluidization velocity; segregation appeared to be most prominent at a superficial velocity close to the minimum fluidization velocity of the mixed solids and deteriorated progressively as the superficial velocity was increased. It is not clear why the findings here were not in good agreement with those of Rowe. The heterodispersed nature of the solids in our system may contribute partially to the discrepancy.

5.2.3 Combined Pyrite (lots A, B, C) - Coal B System

An artificial mixture of coal and pyrite containing a relatively high concentration of heterodispersed pyrite was prepared by adding coarse pyrite from lots B and C to the previous system. The geometric mean size of pyrite from lots B and C were 117 and 125 micron, respectively, as compared with the 74 micron for lot A. The overall concentration of pyrite was increased to 9.3% by weight. The objective was to investigate the effect of the increase in mean size of jetsam and/or the increase in the overall concentration of pyrite on the performance of the cascade in the removal of pyrite from coal.

Results of a series of recirculation runs are presented in Table 7.17. Inspection of the results immediately revealed a substantial improvement in the performance of the

cascade. As compared with the previous Pyrite A - Coal B system, the concentration of pyrite in the rejects was substantially higher, while the concentration in the products was virtually unchanged. As a result, the beneficiation ratios were substantially higher. After separation from the coal fines using tetrabromoethane, the geometric mean sizes of the pyrite originating from the products and rejects strata were determined by sieve analysis. Owing to the dilute nature of the products stream, pyrite originating from the product streams from different runs were combined in order to obtain a large enough sample for sieve analysis. Samples G, I and K from the rejects streams were also combined because the samples were not sufficiently large for sieve analysis. The results of the size analysis are summarized in Table 5.18. The pyrite in the rejects was substantially larger, because of the presence of the coarser pyrites B and C. It seems that the cascade could remove the coarse pyrites very significantly, as virtually all the coarser pyrite appeared in the rejects. The removal of the original fine pyrite, lot A, was not measurably affected by the addition of the new coarser pyrite. The increase in the overall concentration could also contribute to the improvement in beneficiation. The resultant increase in the thickness of the pure jetsam layer in the bottom stratum of the cascade could facilitate more efficient pyrite removal.

Because of the limited number of experiments performed for this system, statistical regression analysis was not attempted in the correlation of the data.

Table 5.18 Size Analyses on Pyrites from the Rejects and Product Streams of the Cascade (Coal B, Pyrite A, B, C combined)

N_f = 2.1 Chain Speed = 33 mm/s

Rejects Withdrawal Rate (kg/hr)	Sample	Products Withdrawal Rate (kg/hr)	Sample
11.5	A	39	B
	C	84	D
	E	144	F
14.6	G	39	H
	I	84	J
	K	144	L

Sample	Geometric Mean Diameter	Geometric Standard Deviation
A	129	4.4
C	130	4.4
E	140	4.3
B,D,F combined	94	4.7
G,I,K combined	126	4.4
H,J,L combined	60	5.1

5.3 Natural Coal System

The objective of the study was to investigate the performance of the cascade as a separation device in the removal of naturally occurring pyrite and ash from coal. The coal was from Devco's Prince Mine in Nova Scotia. Analysis showed that it contained 5.2% sulphur, 4.3% pyrite sulphur and 11.7% ash by weight. The coal was first air dried and then crushed by Mikro Pulvinger System (manufactured Ducon-Mikrapul Ltd., Ont.), and particles below 125 micron were removed by screening. The physical properties of the system are described in Section 3.2.3. The effect of the different combinations of paddle height, chain speed and withdrawal rates of the products and rejects, on the performance of the cascade was investigate. There were two series of recirculation runs performed; in Series A, the paddle height was identical to that used in the synthetic iron pyrite -coal system (40 mm); in Series B, the paddle height was reduced to 13 mm. A limited number of straight-through runs were also performed in which the product and reject streams were not recirculated; coal was continously fed into the mid-section of the cascade, products and rejects from the two ends of the cascade were collected in separate bins for further processing or analysis.

The analytical procedures used for the determination of ash and pyritic sulphur are discussed in Section 3.3.4. Basically, the sulphur content of the sample was detemined form the regressional lines correlating the ASTM[68] deter-

mined sulphur contents with the X-Ray fluorescence count rates and the ash contents of a number of samples. This was a compromise, as the ASTM's Eschka technique, however accurate, was also extremely time-consuming whereas the X-Ray counting technique and the gravimetric determination of ash by combustion were relatively easy. Considering the statistical significance of the regression lines as indicated by the F ratio, the accuracy of the sulphur content as determined by this technique should be reasonable. The estimation of the pyritic sulphur content of the samples, on an ash-free basis, was discussed in Section 3.3.4.

The scope of the investigation on the natural coal system, despite its importance and some encouraging results obtained, was limited owing to budgetary and manpower limitations.

5.3.1 Recirculation Experiments

Segregation by size in the cascade runs was quite pronounced. The mean particle size of coal varied from 160 microns at the product side to 360 microns at the reject side. To keep the cascade uniformly fluidized along the axis, the superficial velocity above the four wind chambers was maintained at 18, 21, 73 and 85 mm/sec, estimated to be twice the minimum fluidization velocity of the solids in each quadrant of the cascade. The height of the bed, when defluidized, was 180 mm. Results of Series A, with the paddle height of 40 mm, and Series B, with the paddle height of

13 mm, are given in Tables 5.19 and 5.20. There was a total of 36 experiments in Series A and 16 in Series B. Beneficiation, both with respect to sulphur and ash, was observed in all cases. Inspection of Table 5.19 and 5.20 revealed that the beneficiation performance with the larger paddles was in general superior to that with shallow paddles.

At first glance, it might be surprising to find that the pyritic sulphur concentration exceeded that of total sulphur. This was because the pyritic sulphur content was calculated on an ash-free basis whereas the total sulphur was calculated inclusively. In general, the removal of ash appeared to be better than the removal of sulphur. In Series A, a typical beneficiation ratio for ash was 3.0 versus 1.5 for sulphur. The same trend could be observed in Series B but with inferior results. On an ash-free basis, a typical beneficiation ratio for pyritic sulphur in Series A was 2.5. The ash and pyritic sulphur contents of the rejects did not appear to be affected measurably by the variation in chain speed and the products and rejects withdrawal rates. It is quite possible that a substantial portion of the pyritic sulphur was not liberated and was still incorporated within the coal matrix, with little tendency to segregate from the coal solids when fluidized. In fact, liberation of pyrite and ash from coal may be the limiting factor in the beneficiation. Simple bed segregation experiments on material withdrawn from the product stream, to be discussed in Section 5.3.3, were supportive

Table 5.19 Results of Series A Recirculation Runs (Natural Coal System)

Run Number	CS (mm/sec)	W (kg/m-hr)	P_r (%)	Product Coal			Reject Coal		
				% Ash	% Sulphur	PSAF* (%)	% Ash	% Sulphur	PSAF* (%)
1	23	677	75	8.10	4.34	3.09	27.2	6.21	7.79
2		763	78	8.03	4.47	3.24	27.1	6.35	7.99
3		1702	90	8.04	4.47	3.24	26.3	6.27	7.76
4		1134	45	8.61	4.52	3.33	25.9	6.15	7.53
5		1220	49	8.28	4.49	3.28	25.0	6.00	7.20
6		2159	71	8.23	4.48	3.26	25.1	5.64	6.69
7		1528	33	8.40	4.50	3.29	23.1	5.57	6.37
8		1614	37	8.29	4.49	3.28	22.8	5.49	6.23
9		2553	60	8.42	4.50	3.30	23.5	5.44	6.23
10	33	677	75	9.00	4.53	3.36	26.7	6.53	8.21
11		763	78	8.78	4.54	3.36	26.1	6.65	8.31
12		1702	90	8.67	4.65	3.48	24.4	6.29	7.55
13		1134	45	8.71	4.53	3.35	22.8	5.86	6.75
14		1220	49	8.73	4.50	3.31	23.1	6.19	7.26
15		2159	71	8.98	4.56	3.40	24.0	6.19	7.36
16		1528	33	8.97	4.56	3.40	21.9	5.81	6.59
17		1614	37	9.09	4.66	3.52	20.9	6.00	6.75
18		2553	60	8.98	4.55	3.38	21.4	5.83	6.56

* PSAF = Ash-free Pyritic Sulphur

Table 5.19 (Continued)

Run Number	CS (mm/sec)	W (kg/m-hr)	P_r (%)	Product Coal			Reject Coal		
				% Ash	% Sulphur	PSAF* (%)	% Ash	% Sulphur	PSAF* (%)
19	42	677	75	8.34	4.38	3.15	26.5	6.08	7.50
20		763	78	8.45	4.51	3.31	27.0	6.39	8.03
21		1702	90	8.25	4.49	3.27	26.3	6.20	7.66
22		1134	45	8.53	4.51	3.31	24.6	6.22	7.48
23		1220	49	8.63	4.52	3.33	23.8	5.72	6.66
24		2159	71	8.48	4.51	3.31	24.8	6.13	7.37
25		1528	33	8.61	4.53	3.34	22.7	6.10	7.08
26		1614	37	8.44	4.51	3.31	23.5	6.17	7.27
27		2553	60	8.67	4.53	3.34	23.1	6.08	7.10
28	69	677	75	7.87	4.46	3.22	27.1	6.36	8.00
29		763	78	8.27	4.48	3.26	26.1	5.68	6.86
30		1702	90	8.17	4.48	3.26	26.9	5.88	7.25
31		1134	45	8.50	4.50	3.30	24.6	5.28	6.11
32		1220	49	8.45	4.49	3.29	24.7	5.65	6.66
33		2159	71	8.49	4.50	3.30	23.2	5.22	5.89
34		1528	33	8.39	4.50	3.29	23.1	5.62	6.44
35		1614	37	8.60	4.50	3.31	23.8	5.40	6.20
36		2553	60	8.39	4.49	3.28	25.0	5.80	6.91

* PSAF = Ash-free Pyritic Sulphur

Table 5.20 Results of Series B Recirculation Runs (Natural Coal System)

Run Number	CS (mm/sec)	W (kg/m-hr)	P_r (%)	Product Coal			Reject Coal		
				% Ash	% Sulphur	PSAF*(%)	% Ash	% Sulphur	PSAF* (%)
37	23	677	75	9.58	4.82	3.74	14.8	5.77	5.86
38		1702	90	9.27	4.74	3.62	15.0	6.19	6.42
39		1134	45	9.80	4.87	3.81	14.1	5.55	5.53
40		2159	71	9.52	4.89	3.81	12.5	5.31	5.10
41	33	677	75	9.80	4.80	3.73	17.1	5.75	6.04
42		1702	90	9.40	4.70	3.58	15.1	5.64	5.72
43		1134	45	9.93	5.33	4.36	12.9	5.29	5.11
44		2159	71	9.58	4.83	3.86	12.6	5.57	5.43
45	42	677	75	10.40	4.97	3.96	14.1	5.44	5.38
46		1702	90	9.66	4.79	3.71	17.3	5.77	6.08
47		1134	45	9.72	4.74	3.65	12.7	5.23	5.02
48		2159	71	9.73	4.73	3.64	13.0	5.34	5.17
49	69	677	75	9.55	4.94	3.87	16.5	5.83	6.09
50		1702	90	9.01	4.65	3.80	16.7	5.97	6.29
51		1134	45	9.27	4.85	3.75	13.3	5.92	5.93
52		2159	71	9.15	4.73	3.60	14.3	5.84	5.91

of this assertion.

From previous experience with the cascade on other granular solids systems, there were concerns that the jetsam, namely, the pyrite and ash, could be accumulating in the auger wells and other "dead" zones of the cascade and was thus prevented from circulating. By assuming an exponential profile for the jetsam concentration along the axis of the cascade,[77,41,40] the total mass of ash and pyritic sulphur in the cascade bed could be estimated by integration using the concentration of jetsam in the products and rejects as the limits of integration. The validity of assuming an exponential profile was affirmed by cascade experiments with the iron sand system, previously described in Section 5.1, and the salt-activated charcoal system, to be discussed later in this chapter. The jetsam in the auger well was added to the integrated mass. The mass balances computed for ash and pyritic sulphur yielded standard relative errors of 4.8% and 4.9%, respectively, for those components. In view of the possible uncertainties associated with the analyses and sampling procedures, the mass balances were surprisingly consistent. Details of the calculation are presented in Appendix G.

From simple bed segregation experiments (Section 5.3.3) it appeared that the non-liberated ash content in the coal was approximately 7%. By assuming that the non-liberated ash content in the coal was homogeneous throughout the cascade bed at 7%, the liberated ash content in the

product and reject streams could be estimated by subtraction. If an exponential profile of liberated ash was assumed, a mass balance on the ash could again be performed by adding the integrated liberated ash to the non-liberated ash in the bed as well as the auger wells. Calculation revealed a standard relative error of 3.9%, a slight improvement over the previous mass balance where the liberated and non-liberated ash were not treated separately.

A packaged statistical regressional program, the Statistical Program for Social Science (SPSS), was used to correlate the results of the recirculation runs. The dependent variables, namely, the percentage ash, percentage total sulphur and percentage pyritic sulphur on an ash-free basis, and beneficiation ratio based on ash, sulphur or pyritic sulphur, were regressed with the independent variables CS, the chain speed in mm/sec; P_r, the fraction of the feed orginating at the product end of the cascade; and W, the total feed rate per unit width of the cascade bed in kg/mhr.

Initially, all first and second powers and products of the independent variables were included as independent variables, but only those whose inclusion was significant at the 5% confidence level were retained. A summary of the regression analyses is given in Table 5.21. Comparison of the calculated F ratios in Table 5.21 and standard statistical tables revealed that with beneficiation ratio and ash as the dependent variables, the regression equations were

Table 5.21 Results of Regression Analysis on Data from Natural Coal System

Series	Dependent Variable	Intercept	CS (mm/s)	CS^2 $(mm/s)^2$	P_r	P_r^2	W (kg/m-hr)	P_rxC (mm/s)	F Ratio *
A	Beneficiation Ratio (ash)	2.65			0.92		-20×10^{-4}		26.3 (0.28)
	(total sulphur)	1.35	-1.41×10^{-3}		0.196		-5.5×10^{-5}		12.6 (0.077)
	(pyritic sulphur, ash-free)	2.12	-2.44×10^{-3}		0.640		-1.7×10^{-4}		23.3 (0.19)
B	Beneficiation Ratio (ash)	0.92	3.78×10^{-3}		0.858		-1.15×10^{-4}		7.9 (0.19)
	(total sulphur)	1.00		9.06×10^{-5}	0.522			-9.86×10^{-3}	9.5 (0.08)
	(pyritic sulphur, ash-free)	1.62	-2.14×10^{-2}	2.64×10^{-4}					9.1 (0.16)
A	% ash in rejects	22.96			6.24		-1.44×10^{-3}		46.5 (1.75)
	% ash in products	7.39	5.80×10^{-2}	-6.5×10^{-4}					6.2 (0.29)
B	% ash in rejects	11.20			7.60		-1.46×10^{-2}		11.1 (1.67)
	% ash in products	8.80	6.6×10^{-2}	-7.94×10^{-4}			-2.69×10^{-4}		10.2 (0.33)
A	% total sulphur in rejects	5.04	5.40×10^{-2}	-6.45×10^{-4}					7.0 (0.34)
	% total sulphur in products	Regression not significant at 5% level							
B	% total sulphur in rejects	6.25	-5.27×10^{-2}	6.19×10^{-3}	0.654				7.6 (0.28)
	% total sulphur in products	Regression not significant at 5% level							

* Standard deviation given in brackets

Table 5.21 Results of Regression Analysis of Data from Natural Coal System (Continued)

Series	Dependent Variable	Intercept	CS (mm/s)	CS^2 $(mm/s)^2$	P_r	P_r^2	W (kg/m-hr)	$P_r xC$ (mm/s)	F Ratio *
A	% pyritic sulphur (ash-free) in rejects	6.75	-8.20×10^{-3}		1.73		-4.3×10^{-4}		18.6 (0.57)
	% pyritic sulphur (ash-free) in products	3.00	1.10×10^{-2}	-1.25×10^{-4}					3.23 (0.073)
B	% pyritic sulphur (ash-free) in rejects	5.99	-6.24×10^{-2}	7.51×10^{-4}	1.143				7.80 (0.42)
	% pyritic sulphur (ash-free) in products	Regression not significant at 5% level							

* Standard deviation given in brackets

all significant at the 1% confidence level. In general, for both Series A and B, the ash beneficiation ratios were not dependent on CS; they decreased with W and increased with P_r. The beneficiation ratio for pyritic sulphur increased with reduction in CS and W, and increased with P_r in Series A. Series B exhibited the same trend, except for the fact that it was virtually independent of W. The beneficiation ratio based on total sulphur exhibited similar dependency as the Series A beneficiation ratio based on pyritic sulphur. In Series B, however, it did not appear to be dependent on CS.

When ash was treated as the dependent variable, the percentage of ash in the rejects was not found to be dependent on CS. For both Series A and B, it increased with P_r and decreased with W. For the product stream, chain speed, CS, appeared to be the only dominating independent variable. The ash content in the products increased with CS.

No regression equation was obtained for the percentage of total sulphur in the product stream, as none of the independent variables was significant at the 5% confidence level. For the rejects stream, the signs of the coefficient of CS in Series A and B were reversed, implying that for Series A, the total sulphur content increased with CS, while the trend was reversed for Series B. The reasons for the difference are not clear.

When the percentage of pyritic sulphur on an ash-free basis was the dependent variable, the regression equation

for the products was barely significant at the 5% confidence level for Series A; in Series B, the regression equation was not statistically significant. For the rejects, the regression equations were quite acceptable, with a relatively large F ratio. In general, the pyritic sulphur in the rejects increased with P_r and decreased with CS and W.

Despite the fact that most of the regression lines were statistically significant, it should be pointed out that the dependency of the various dependent variables on the independent variables was not very marked. For example, according to the regression equation the ash beneficiation ratio at $P_r = 0.9$ and $W = 0$ equalled 3.48, whereas at the highest feed rate studies, i.e. W = 2553 kg/m-hr, the beneficiation ratio was 2.97 at the same value of P_r. The regression coefficients were also generally smaller in the natural coal system than in the synthetic mixture of iron pyrites and coal, implying that the effect of the independent variables on the cascade performance for the natural coal system was less pronounced. In fact, cascade performance was generally rather insensitive to the operating conditions. This phenomenon was particularly noticeable for the product stream. This insensitivity could well be attributed to the degree of liberation of ash and pyrites from the coal matrix. The observation that the beneficiation ratios were relatively insensitive to the throughput rate, W, was encouraging as implying a higher throughput capability for the cascade without deterioration in efficiency. However, it is quite pos-

sible that cascade performance may be affected by the fact that, in recirculation runs, the overall jetsam composition in the cascade was invarient, regardless of the operating conditions. In a true throughput run, in which the products and rejects are not recirculated, cascade performance may well be different.

In the synthetic iron pyrite-coal system, the paddle speed CS appeared to be of considerable importance. In this system, this was not true. In fact, the paddle speed CS was often forced out from many regression analyses as it was not significant at the 5% confidence level. It may be that the range of paddle speed studied was too limited and was away from the region where it could affect the beneficiation effectiveness of the cascade. An explanation is still wanting with regard to the inferior performance of the shallow paddles in Series B, as compared to Series A with the broader paddles. It is thought that the smaller paddles would more efficiently sweep a higher concentration of rejects material. It could be that the movement of the shallow paddles created a local mixing action near the grid region with adverse effect on the sweeping of the reject material.

Despite the limited scope of the investigation, it was demonstrated that the cascade could have applications in coal beneficiation. The ash and sulphur content in the rejects was still too low to warrant disposal. However, beneficiation does not have to be a single-pass process. The rejects could still be processed in subsequent passes

in another cascade of similar design. This concept will be tested in the straight-through experiments, to be discussed in the next section. Performance of the cascade is limited by the length of the working section. If the cascade were to be lengthened, the ash and pyrites removal efficiency would be significantly increased. The removal of pyrites and ash could be limited by the degree of liberation of impurities in the crushing process. Undoubtedly, more pyrite and ash would be liberated by crushing the coal to a finer mesh size. The penalty is that the finer solids tend to be well-mixed when fluidized. An experimental program could be planned to ascertain the optimal mesh size of the coal for maximum ash and pyritic sulphur removal.

5.3.2 Straight-through Runs

In contrast with the recirculation runs in which the feed composition was dependent on the composition and flowrate of the recirculated product and reject streams, the straight-through runs were characterized by an independently controlled feed composition. The products and rejects were not recirculated, but were collected in separate bins as finished products or for futher purification. In fact, the straight-through runs resemble a real beneficiation process in which the run-of-the-mill coal is crushed and partially cleaned before combustion.

Three cascade passes were made, called the rougher, cleaner, and scavenger passes. The coal processed in the

rougher pass contained 5.2% pyritic sulphur, or a pyrite content of 9.7%, on an ash-free basis. The ash content was approximately 12%. Products and rejects from the rougher pass were used as feed in the cleaner pass and the scavenger pass, respectively. It was expected that the feed in the rougher and scavenger passes would be relatively high in jetsam material. In order to optimize the performance of the cascade, the large paddles, 40 mm in height, were used in those passes in order to effectively sweep the thicker jetsam layer in the bottom stratum of the cascade bed. Conversely, the shallow paddles, 13 mm in height, were used in the cleaner pass because it was reasoned that the smaller paddles would probably be more appropriate for sweeping the shallower jetsam layer in the bottom stratum of the cascade. The results are summarized in Table 5.22. Sampling was a problem in the straight-through runs. To assume homogeneity in the feed, product and reject streams with respect to ash and pyritic sulphur content would be presumptuous. To obtain a representative sample of each stream by sample splitting technique would be impractical and potentially error-prone in view of the quantity of coal processed. Consequently, it was decided to withdraw 500 gram samples from each of the three streams during each pass at ten-minute intervals. The samples were then reduced so as to provide an appropriate size for analysis. Concentration data presented in Table 5.22 are averages of all the samples in each stream.

Table 5.22 Results of Straight Through Runs
(Natural Coal System)

	Rougher Pass	Cleaner Pass	Scavenger Pass
Feed Rate (tonne/m-hr)	1.54	1.16	1.54
Product Recovery (%)	68.7	72.8	69.7
Rejects Side			
% Ash	19.5	14.8	30.3
% Sulphur	6.03	5.81	7.16
% Pyritic Sulphur (ash-free basis)	6.64	5.91	9.74
% Pyrite (ash-free basis)	12.42	11.06	18.22
Products Side			
% Ash	10.6	9.75	14.0
% Sulphur	5.08	4.85	5.44
% Pyritic Sulphur (ash-free basis)	4.11	3.78	4.80
% Pyrite (ash-free basis)	7.68	7.07	8.98

Inspection of Table 5.22 revealed reasonable beneficiation in all three passes. The product recovery in all the passes was approximately 70%. After processing the cleaned product of the rougher pass, with an initial ash content of 10.6% and pyritic sulphur on an ash-free basis of 4.11%, the ash content was reduced to 9.75%. The reduction in pyritic sulphur was only marginal, at a concentration of 3.78%. The difference between the products from the cleaner pass and the original feed in the rougher pass in ash and ash-free pyritic sulphur were 1.5% and 2-3%, respectively. When the rejects from the rougher pass containing 19.5% ash and 6.64% pyritic sulphur, were processed in the scavenger pass, the product stream was significantly cleaner at 14% ash and 4.8% pyritic sulphur. The reject from the scavenger pass was actually quite dirty with ash and pyritic sulphur contents of 30% and 9.74%, respectively. The rejects of the cleaner pass, with 14.8% ash and 5.91% pyritic sulphur, were still too clean to warrant disposal and should be processed further.

The beneficiation performance of the cascade is encouraging considering that the products from the cleaner pass were 27% and 19% respectively lower in pyritic sulphur and ash as compared with the original coal. The rejects from the scavenger pass were 87% and 150%, respectively, higher in pyritic sulphur and ash than the original coal. The beneficiation ratio between the products from the cleaner pass and the rejects from the scavenger pass with respect

to ash and pyritic sulphur were substantial, at 3.1 and 2.6, respectively. Undoubtedly, further beneficiation by additional passes was still possible. The beneficiation performance of the cascade could also be improved by the lengthening of the working section.

5.3.3 Simple Fluidized Bed Segregation Runs

In view of the negligible variation in the ash and pyritic sulphur content of the product stream in the recirculation runs, Section 5.3.1, it was speculated that the liberation of ash and pyrite from coal may be the limiting factor. It was also believed that the concentration of impurities in the reject stream could be substantially increased, if the working section of the cascade were to be lengthened. Thus, it was important to study the simple bed segregation characteristics of the product and rejects materials from a typical recirculation run. The results are summarized in Tables 5.23 and 5.24. Inspection of Table 5.23 confirmed that the jetsam-rich coal from the reject end of the cascade could still be refined further. At either superficial velocity, segregation was clearly observed even though segregation appeared to be slightly greater at the lower fluidization velocity. However, at the lower velocity, a slight gradient in the concentration of ash and pyritic sulphur with bed height was observed. At the higher velocity, the gradient in jetsam concentration disappeared.

The results of the simple bed segregation runs with

Table 5.23 Results of Simple Fluidized Bed Segregation Experiments on Coal Withdrawn from the Jetsam-Rich Side

Test #1 N_f = 2.0 U_{mf} = 86 mm/sec

Distance above grid (mm)	% Ash	% Sulphur**	% Pyritic Sulphur *
108 - 133	12.86	5.13	4.91
83 - 108	13.44	5.15	4.98
51 - 83	12.98	5.13	4.92
25 - 51	13.27	5.15	4.96
0 - 25	55.18	8.08	19.0

Test #2 N_f = 1.5 U_{mf} = 86 mm/sec

Distance above grid (mm)	% Ash	% Sulphur**	% Pyritic Sulphur *
102 - 127	9.96	4.65	4.14
76 - 102	10.11	4.58	4.06
51 - 76	10.66	4.79	4.35
25 - 51	20.85	8.78	6.44
0 - 25	59.11	8.50	22.6

** total sulphur, as is

* on an ash-free basis

Table 5.24 Results of Simple Fluidized Bed Segregation Experiment on Coal Withdrawn from Flotsam-Rich Side

Test #1 N_f = 2.0 U_{mf} = 18 mm/sec

Distance above grid (mm)	% Ash	% Sulphur**	% Pyritic Sulphur *
102 - 127	6.89	4.42	3.12
76 - 102	7.02	4.44	3.15
51 - 76	7.17	4.43	3.15
25 - 51	7.57	4.45	3.19
0 - 25	9.64	4.56	3.44

Test #2 N_f = 1.5 U_{mf} = 18 mm/sec

Distance above grid (mm)	% Ash	% Sulphur**	% Pyritic Sulphur *
102 - 127	6.94	4.42	3.12
76 - 102	7.07	4.43	3.14
51 - 76	7.29	4.43	3.15
25 - 51	7.70	4.44	3.19
0 - 25	9.26	4.56	3.41

the low ash, low sulphur material from the product end of the cascade, Table 5.24, were in essence a confirmation that the liberation of ash and pyritic sulphur in coal was the limiting factor in the beneficiation. Although there was still a weak segregation of ash, there was virtually no segregation in the pyritic sulphur. It could be concluded that although there was still a marginal amount of liberated ash in the product material, there was almost complete absence of liberated pyrite in the material. The absence of segregation in the simple bed, at both fluidizing velocities, implied the impossibility of attaining a higher purity in the products without further liberation by crushing.

5.4 Salt-Activated Charcoal System

The salt-activated charcoal system was another mixed solids system chosen to study cascade performance using a flotsam-rich system under varying conditions of fluidization velocity and paddle velocity. The jetsam used was a commercially available table salt sieved to a size range between 180 and 250 micron. The geometric mean size of the activated charcoal was 375 micron. The solids system was previously described in Section 3.2.4. The greatest merit of this solids system over those previously studied was in the ease and accuracy of the analyses. The iron pyrite-coal and iron-sand systems were plagued by the time-consuming analytical procedures. In the case of the natural coal system, the problem of analysis was also compounded by the limited liberation of the jetsam ash and pyrite from the coal solids. The present system, in addition to the advantages in the analytical procedures, has the characteristic that the densities of salt and activated charcoal resemble that of ash and coal. Thus, the cascade experiment on the salt-activated charcoal system simulates the removal of the liberated ash from coal in the natural coal system.

Simple bed and total reflux cascade runs were performed. In the simple bed experiments, steady state jetsam concentration profiles as a function of bed height were investigated at various overall salt concentrations and fluidization velocities. In the total reflux experiments, the operating variables were paddle height, fluidization

velocity and chain speed. In many ways, experimentation with the salt-activated charcoal system was similar to that of the iron pyrite-coal and iron-sand systems. The difference was that the investigation with the present system was more thorough than with the previous systems, as a result of the simpler analytical procedures. In previous studies, the fluidization velocity was characterized by the fluidization number, N_f. In the present system, this was replaced by the excess fluidization velocity, $U-U_{mf}$. In accordance with the two phase fluidization theory,[13] $U-U_{mf}$ equals the gas flow to the bubble phase of the fluidized bed and should be conceptually more meaningful than the fluidization number. Neinow's empirical equation for the estimation of mixing index[20] also used the excess fluidization velocity.

5.4.1 Single Bed Segregation Experiments

Three nominal salt concentrations, 0.015%, 0.1% and 1% by weight, were used in combination with excess fluidization velocities of 92, 69 and 46 mm/sec. To minimize segregation by size of the activated charcoal matrix, the activated charcoal used in the series of experiments was the same as that described in Section 3.2.5 but with the solids below 300 micron and above 500 micron removed by sieving. The minimum fluidization velocity of the activated charcoal was 63 mm/sec. The curve used in the determination of the minimum fluidization velocity can be found in Appendix B.

Results of the runs listed in Table 5.25 A, B and C

Table 5.25 A Simple Bed Segregation Run (Salt-Activated Charcoal System) at 0.015% Salt

$U-U_{mf}$ = 92 mm/sec		$U-U_{mf}$ = 69 mm/sec		$U-U_{mf}$ = 46 mm/sec	
H*	Ci (%)	H*	Ci (%)	H*	Ci (%)
1.000	0.014	1.000	0.004	1.000	0.012
0.843	0.015	0.885	0.011	0.849	0.013
0.665	0.013	0.695	0.012	0.702	0.012
0.495	0.012	0.534	0.013	0.536	0.013
0.342	0.015	0.351	0.015	0.363	0.017
0.224	0.024	0.186	0.031	0.176	0.038

Table 5.25 B Simple Bed Segregation Run (Salt-Activated Charcoal System at 0.1% Salt

$U-U_{mf}$ = 92 mm/sec		$U-U_{mf}$ = 69 mm/sec		$U-U_{mf}$ = 46 mm/sec	
H*	Ci (%)	H*	Ci (%)	H*	Ci (%)
1.000	0.066	1.000	0.037	1.000	0.034
0.835	0.065	0.873	0.050	0.901	0.045
0.597	0.070	0.699	0.057	0.729	0.047
0.500	0.079	0.515	0.063	0.528	0.070
0.338	0.091	0.373	0.123	0.326	0.123
0.162	0.249	0.185	0.277	0.161	0.340

Table 5.25 C Simple Bed Segregation Run (Salt-Activated Charcoal System) at 1% Salt

$U-U_{mf}$ = 92 mm/sec		$U-U_{mf}$ = 69 mm/sec		$U-U_{mf}$ = 46 mm/sec	
H*	Ci (%)	H*	Ci (%)	H*	Ci (%)
1.000	0.571	1.000	0.315	1.000	0.223
0.858	0.590	0.894	0.415	0.895	0.464
0.713	0.586	0.725	0.449	0.722	0.601
0.537	0.626	0.574	0.570	0.549	0.607
0.384	0.848	0.430	0.771	0.400	0.775
0.220	2.353	0.249	2.535	0.241	2.521

*H = normalized height from grid surface

correspond to salt concentrations of 0.015%, 0.1% and 1%, respectively. In the tables, X is the normalized height of each of the six sampled layers based on the weight fraction of layers. C_i is the salt concentration of each layer.

The results from the simple bed segregation experiments were in general encouraging. At the concentration of salt studied, segregation was observed at the three fluidization velocities. However, it should be pointed out that effective segregation in a simple fluidized bed does not necessarily imply satisfactory jetsam removal in the fluidized cascade. Experiences with the iron-sand system justified this assertion.

5.4.2 Total Reflux Experiments

Segregation by size was quite marked for the salt-activated charcoal system in total reflux experiments, necessitating the estimation of the minimum fluidization velocity in each of the four sections of the cascade bed in order to maintain the constant $U-U_{mf}$ value throughout the cascade. As a result of the many combinations of fluidization velocity, chain speed and paddle height studied, in-situ U_{mf} determination by the bed pressure drop versus fluidization velocity techniques would be impractical. The U_{mf} values listed in Tables 5.26 and 5.27 for each of the four sections were determined by the Wen and Yu equation (equation 4.1) using the experimentally determined geometric mean diameter of the solids from the mid-sections of the

Table 5.26 Results of Total Reflux Experiments on Salt-Activated Charcoal System (Paddle Height = 25.4 mm)

Run #	Operating Conditions: U_{mf} in each quadrant (mm/s) 1	2	3	4	$U-U_{mf}$ (mm/s)	chain speed (mm/s)	Linear Regression: Ln(C) = A (Z) + B A	B	CC***	BR*	C_{exp} (%)	JR**(%)
1	46.00	44.00	37.30	32.00	92.0	68.58	-5.664	1.518	0.999	288.3	0.80	19.7
2	"	"	"	"	"	41.45	-5.728	1.329	1.000	307.4	0.66	34.3
3	"	"	"	"	"	32.66	-5.621	1.424	0.994	276.1	0.74	26.3
4	"	"	"	"	"	22.35	-5.618	1.459	0.998	275.4	0.76	23.7
5	"	"	"	"	"	10.16	-4.227	0.993	0.998	68.52	0.63	37.1
6	39.32	39.32	39.32	39.32	"	2.54	-3.130	0.927	0.990	22.87	0.77	22.8
7	46.00	46.00	37.30	32.00	6.90	68.58	-5.305	1.424	0.997	301.3	0.78	22.1
8	"	"	"	"	"	41.45	-5.729	1.392	0.997	307.6	0.70	30.0
9	"	"	"	"	"	32.66	-5.441	1.108	0.995	230.6	0.55	44.6
10	"	"	"	"	"	22.35	-6.008	1.285	0.989	406.6	0.60	40.0
11	"	"	"	"	"	2.54	-5.538	1.292	0.996	254.2	0.65	34.6
12	"	"	"	"	46.0	68.58	-3.743	1.132	0.989	42.2	0.81	19.1
13	"	"	"	"	"	41.45	-4.787	1.065	0.997	120.0	0.60	39.9
14	"	"	"	"	"	32.66	-5.303	1.173	0.992	200.9	0.61	39.3
15	"	"	"	"	"	22.35	-5.717	1.330	0.986	304.0	0.66	34.1
16	"	"	"	"	"	2.54	-5.629	0.471	0.989	278.5	0.28	71.7
17	"	"	"	"	"	2.54	-5.754	0.601	0.993	315.4	0.32	68.4
18	"	"	"	"	69.0	22.35	-5.921	1.259	0.995	392.6	0.59	40.7

* Beneficiation Ratio ** Jetsam Accumulation *** Correlation Coefficient

Table 5.27 Results of Total Reflux Experiments on Salt-Activated Charcoal System (Paddle Height = 12.7 mm)

Run #	Operating Conditions: U_{mf} in each quadrant (mm/s) 1	2	3	4	$U-U_{mf}$ (mm/s)	Chain Speed (mm/s)	Linear Regression Ln(C) = A (Z) + B: A	B	CC***	BR*	C_{exp} (%)	JR**(%)
19	36.85	36.85	36.85	36.85	92.0	20.32	-4.567	1.113	0.994	96.2	0.66	34.0
20	"	"	"	"	"	10.16	-4.000	1.009	0.997	54.6	0.67	32.7
21	"	"	"	"	"	5.08	-3.366	0.990	0.998	29.0	0.77	22.8
22	"	"	"	"	"	2.54	-1.930	0.654	0.972	6.9	0.85	14.8
23	"	"	"	"	"	55.9	-5.337	1.202	0.998	207.9	0.62	38.0
24	43.01	40.81	34.99	31.00	69.0	20.32	-5.347	1.184	0.990	209.9	0.61	39.2
25	"	"	"	"	"	10.16	-5.568	1.246	0.989	261.9	0.62	37.8
26	"	"	"	"	"	5.08	-5.440	1.045	0.996	230.5	0.52	48.0
27	"	"	"	"	"	2.54	-5.346	1.293	0.990	209.8	0.68	32.1
28	"	"	"	"	"	55.9	-5.152	0.897	0.993	172.8	0.47	52.7
29	"	"	"	"	46.0	20.32	-4.948	0.403	0.988	140.9	0.30	70.0
30	"	"	"	"	"	10.16	-5.012	0.598	0.994	150.2	0.36	64.0
31	"	"	"	"	"	5.08	-5.828	0.860	0.987	339.6	0.40	60.0
32	"	"	"	"	"	2.54	-5.838	0.959	0.993	343.1	0.45	55.4
33	"	"	"	"	"	8.00	-5.222	0.545	0.990	185.3	0.33	67.2
34	"	"	"	"	"	14.00	-4.982	0.408	0.999	146.0	0.30	70.0
35	"	"	"	"	"	55.9	-4.704	1.036	0.980	112.6	0.59	40.9

* Beneficiation Ratio ** Jetsam Accumulation *** Correlation Coefficient

four sections. Experimentally, the minimum fluidization velocity values predicted from equation 4.1 and the in-situ experimentally determined minimum fluidization velocity values agreed to within ±10%.

Results of the total reflux experiments for the 25.4 mm paddle and the 12.7 mm paddle are summarized in Tables 5.26 and 5.27, respectively. Sieve analyses of the samples taken along the axis of the cascade bed for each run are tabulated in Appendix I. Table 5.26 reveals that for the series of experiments with the larger paddle, the minimum fluidization velocity in each quadrant of the cascade was insensitive to the various combinations of $U-U_{mf}$ and chain speed. For most runs, the minimum fluidization velocities in the four quadrants were 46, 44, 37 and 33 mm/sec, respectively; the exception was when $U-U_{mf}$ = 92 mm/sec and the chain speed equaled 2.54 mm/sec. In this case, the minimum fluidization velocity of the four quadrants were essentially identical at 39 mm/sec. Apparently, for that combination of the highest fluidization velocity and lowest paddle chain speed, segregation by size was negligible. A similar situation was encountered with the smaller 12.7 mm paddles. In Table 5.27, the highest $U-U_{mf}$ setting of 92 mm/sec essentially precluded segregation by size, the minimum fluidization velocity of the four sections were identical at 37 mm/sec. At other $U-U_{mf}$ settings, the minimum fluidization velocities of the four quadrants were 46, 44, 37 and 32 mm/sec, respectively, regardless of the operating chain speed. The reduc-

tion of segregation by size at the highest fluidization velocity is consistant with the expectation of enhanced mixing associated with the higher gas velocity.

Experimental concentration profiles were found when the concentration of salt of the samples was plotted against its normalized axial distance in the cascade. A typical plot of ln (C_i) versus the normalized distance, Z, is presented in Figure 5.3. C_i is defined as the percent salt by weight. In the present investigation, the work was primarily focused on the segregation of jetsam salt in admixture with activated charcoal. The segregation of activated charcoal by size was only of interest here because of its effect on the minimum fluidization velocity of the solids along the length of the cascade.

Linear regressions of ln (C_i) versus Z were performed for all the runs. The regression equations are summarized in Tables 5.26 and 5.27 for the two series of experiments with different paddle heights. The excellent linearity of the experimental data is evident in the values of the correlation coefficient associated with each regression line. In all cases, the correlation coefficients approached 1.0. For some unknown reasons, the linearity of the exponential jetsam concentration profile in this solids system was remarkably better than that observed in the iron-sand system.

If the assumption is made that the regression line may be extrapolated beyond the working position of the cas-

FIGURE 5.3 TYPICAL CONCENTRATION PROFILE OF SALT-ACTIVATED CHARCOAL SYSTEM

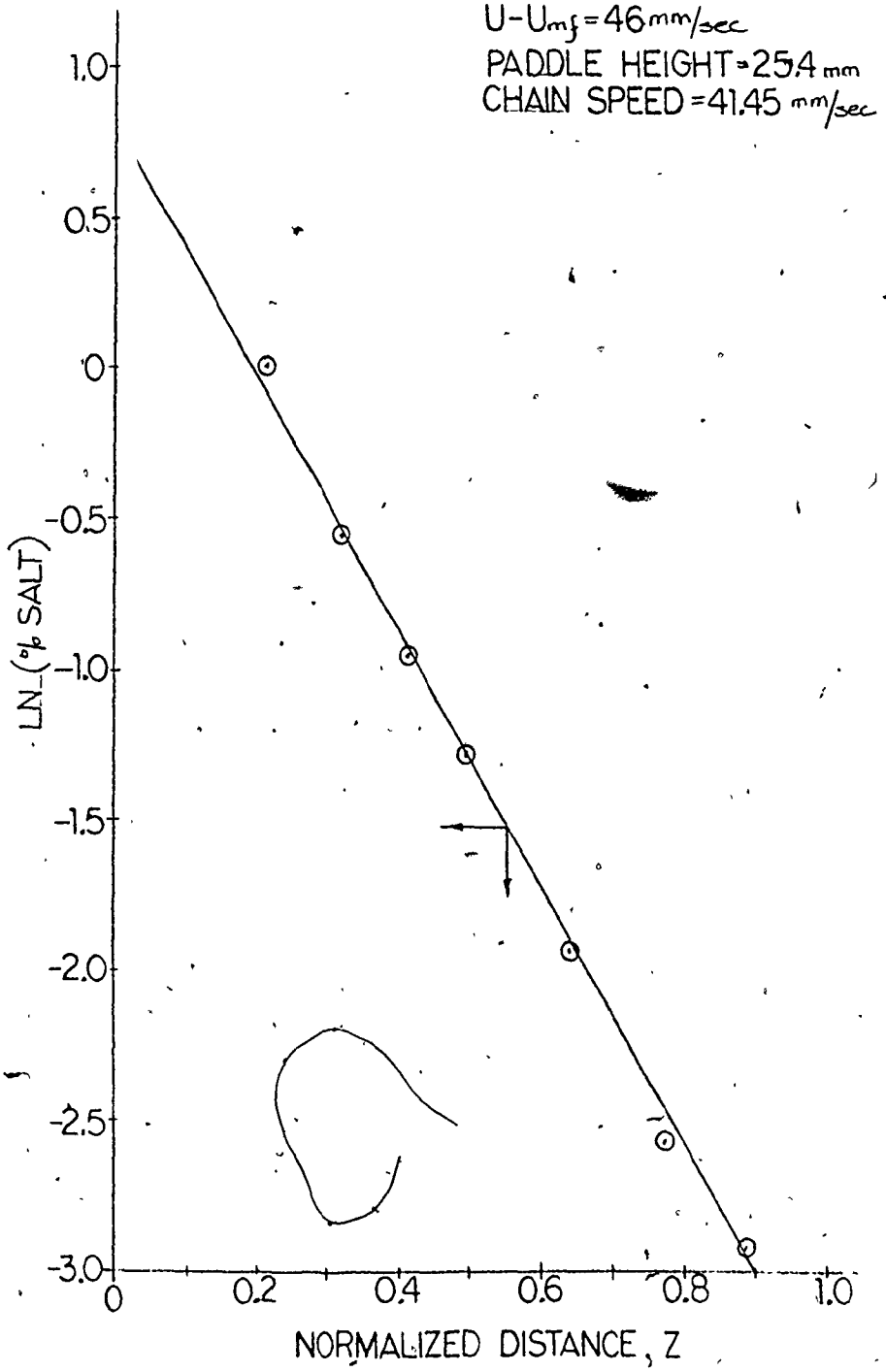

cade where the samples were taken after the completion of each total reflux experiment, the beneficiation ratio may be estimated from the slope of the regression line, A, and equals exp(-A). The calculated beneficiation ratios are tabulated in Tables 5.26 and 5.27 for runs using 25.4 mm and 61.7 mm paddles, respectively. There appeared to be a remarkable variation in the magnitude of the beneficiation ratios. For example, the beneficiation ratio equaled 407 for the 25.4 mm paddles at $U-U_{mf}$ = 69 mm/sec and a chain speed of 22.35 mm/sec. At a $U-U_{mf}$ value of 92 mm/sec and a chain speed of 2.54 mm/sec, the beneficiation ratio for the smaller 12.7 mm paddles was only 6.9. The combination of high fluidization velocity and low chain speed with the resultant poor beneficiation is to be expected. Conceptually, as the chain velocity dwindles and approaches the motionless condition, the cascade is essentially an elongated rectangular simple fluidized bed. When coupled with the high fluidization velocity, mixing would prevail and the jetsam concentration profile should be uniform across the length of the cascade.

In general, the results in Table 5.26 and 5.27 affirmed the superior performance of the larger paddles. In most cases, at the identical $U-U_{mf}$ and chain speed settings, the beneficiation ratios for the larger paddles were better than the corresponding values for the smaller paddles. A similar trend was previously observed with the natural coal systems under recirculation conditions.

The beneficiation ratios are plotted against the chain speed in Figures 5.4 and 5.5 for the 25.4 mm and the 12.7 mm paddles, respectively. The figures show the familiar skewed bell-shaped profiles; the steepness of the curves were dependent on the $U-U_{mf}$ setting. It is interesting to note that the bell-shaped curve is by no means unique to the flotsam-rich system. Previous investigations on the application of the counter-current fluidized cascade in the removal of flotsam materials from a jetsam-rich system showed similar profiles[13,39,40,77,43] despite the fact that flotsam-rich and jetsam-rich systems are inherently different. Examination of Figures 5.4 and 5.5 show the peaks of the curves to be progressively shifting towards the y-axis as the fluidization velocity was reduced. The steepness and severity of the skewness of the curves are dependent on the $U-U_{mf}$ value. For the 12.7 mm paddles, the same trend is observed in Figure 5.5, with a steep rise in the beneficiation ratio at low chain speed. The curve peaked at a chain speed of 5 mm/sec; thereafter it rapidly declined as the chain speed increased to approximately 8 mm/sec and leveled off at a beneficiation ratio of 150. Undoubtedly, if the chain speed were to be significantly higher than 55 mm/sec, the induced mixing as a result of the excessively high chain speed would eventually lead to a drop in the beneficiation ratio. Mechanical problems prohibited experimentation at chain speed significantly above 55 mm/sec; therefore the concept could not be verified.

FIGURE 5.4 PLOT OF BENEFICIATION RATIO VERSUS PADDLE SPEED

(SALT-ACTIVATED CHARCOAL SYSTEM)

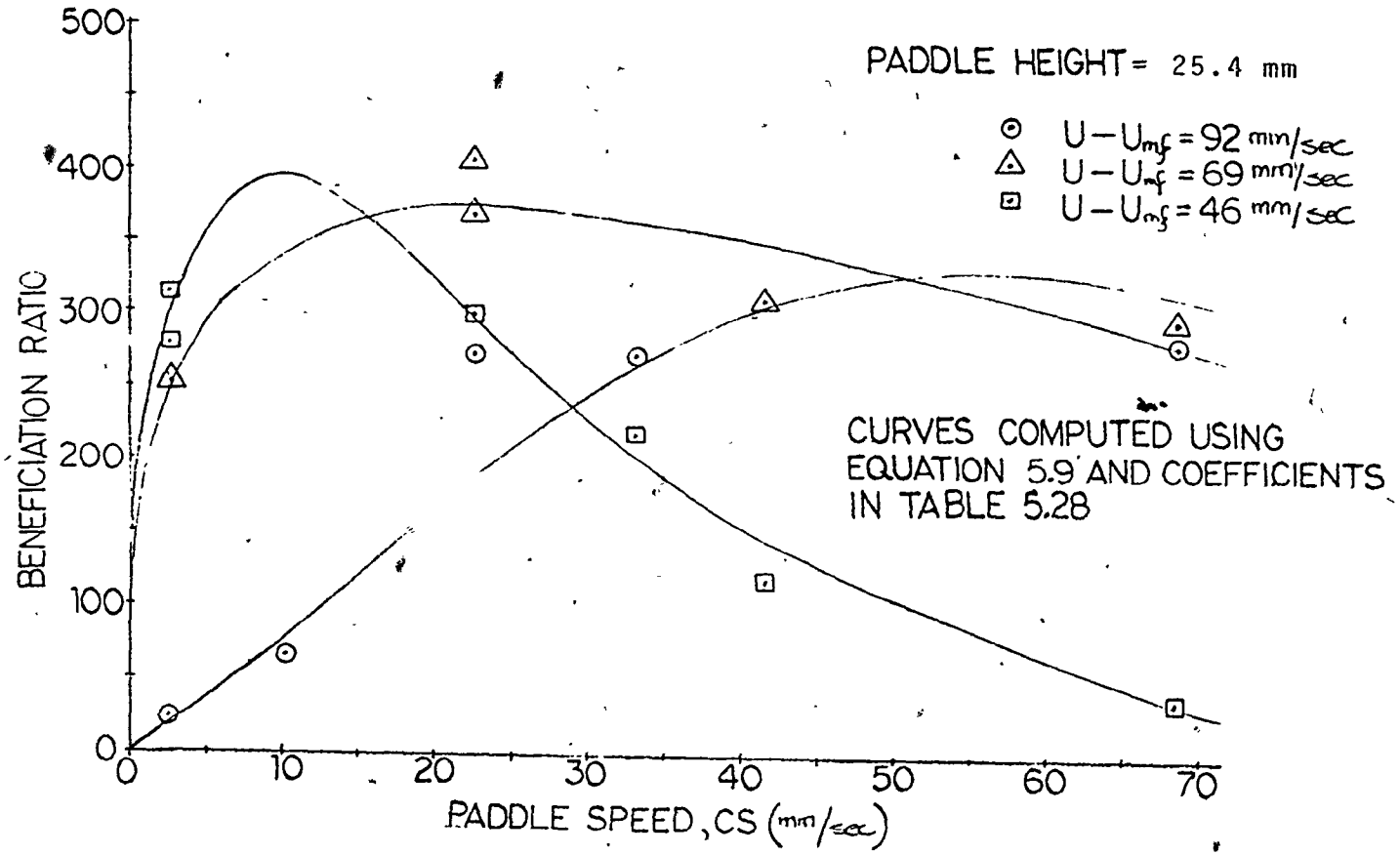

FIGURE 5.5 PLOT OF BENEFICIATION RATIO VERSUS CHAIN SPEED

(SALT ACTIVATED CHARCOAL SYSTEM)

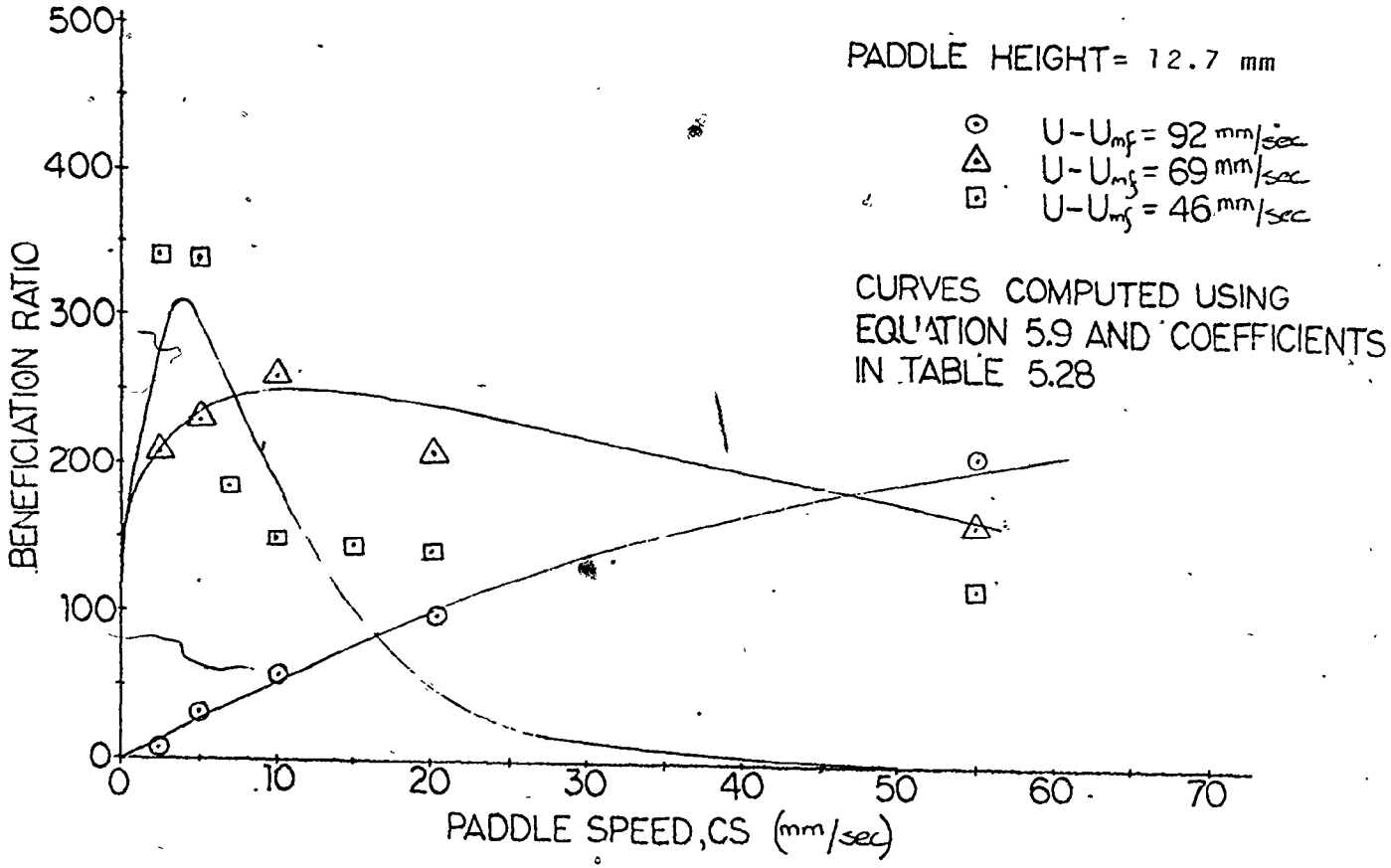

Judging from the height of the curves, the larger 25.7 mm paddles generally out-performed the smaller 12.7 paddles. However, to generalize about the effect of the paddle height on the beneficiation ratio based on experimentation with two paddle heights would be imprudent. It is also worth noting that at the optimum chain speed the maximum beneficiation ratio for the three fluidization velocities was comparable in the case of the taller 25.4 mm paddles. For the smaller 12.7 mm paddles, however, the maximum beneficiation ratios for the higher $U-U_{mf}$ setting were appreciably smaller than that corresponding to the lower $U-U_{mf}$ setting. The deterioration of beneficiation ratio with the increase in fluidization velocity is in agreement with the simple bed segregation experiment, Section 5.4.1, where enhanced mixing was observed at higher fluidization velocity. The fact that for the 25.4 mm paddles the maximum beneficiation ratio was relatively insensitive to fluidization velocity in the ranges of fluidization velocities studied, is difficult to understand.

The statistical regression procedure outlined by Ingelo's article[65] was attempted in an effort to find the dependency of the beneficiation ratio on the principal independent variables of $U-U_{mf}$, chain speed and paddle height, but to no avail. An alternative route was tried in which the beneficiation ratio at a specific fluidization velocity and paddle height was correlated with the chain speed, CS, in mm/sec. Various experimental functions were attempted, including the log-normal, Weibull and other distributions.[74]

The function given in equation 5.9 gave the best fit to the experimental data:

$$\text{Beneficiation Ratio} = A_1(CS)^{A_2} \exp(-A_3(CS)) \qquad (5.9)$$

In Equation 5.9, A_1, A_2 and A_3 are empirical constants and CS is the chain speed in mm/sec. The constants A_1, A_2 and A_3 were optimized to yield the best fit between the data and the curve of beneficiation ratio versus CS as defined by the function. An optimization routine, MINW, written by Professor J. Dickenson and supported by SACDA, was used to determine the optimal values of the empirical constants that would yield the least squares error of the difference between the experimentally determined beneficiation ratio and the value of the beneficiation ratio as predicted by Equation 5.9. MINW is a proprietary packaged computer program and is therefore not listed in the thesis.

The empirical coefficients A_1, A_2 and A_3 determined by the optimization program MINW for the six combinations of paddle height and $U-U_{mf}$ are listed in Table 5.28. The curves in Figures 5.4 and 5.5 are based on the regression lines of Table 5.28. Inspection of Figures 5.4 and 5.5 showed that in most cases, the curves fit the data well. The exception was for the 12.7 mm paddles at $U-U_{mf}$ = 46 mm/sec. At this combination of the short paddle height and low fluidization velocity, the equation with the optimized empirical coefficient failed to fit the data well; this is especially apparent in the "tail" section corresponding to high chain speed. Apparently, Equation 5.9 is still inherently deficient

Table 5.28 Summary of Regression Analyses (Salt-Activated Charcoal System

Regression Equation

$$\text{Beneficiation Ratio} = A_1(CS)^{A_2}(\exp(-A_3CS)) \qquad (5.9)$$

Paddle Height (mm)	$U-U_{mf}$ (mm/sec)	Regression Coefficients A_1	A_2	A_3
25.4	92	1.903	1.837	0.04095
	69	198.3	0.3045	0.0137
	46	203.3	0.5720	0.06089
12.7	92	4.298	1.1112	0.0107
	69	186.4	0.1826	0.01576
	46	228.6	0.7334	0.1810

in its representation of beneficiation ratio as a function of chain speed. It was so chosen because of the difficulties in finding better empirical functions to represent the dependency more satisfactorily. However, it should be stressed once again that with the exception of the aforementioned set of data, Equation 5.9 with the optimized coefficients did in fact fit most of the experimental data very well.

It is interesting to note that besides using MINW, the coefficient A_1, A_2 and A_3 could be optimized by an alternate route. If Equation 5.9 were to be linearized by taking the logarithm of both sides of the equation, the coefficients of the linearized equation could be determined by linear multiple regression. From the coefficients of the linearized equation, A_1, A_2 and A_3 could again be calculated. Using this route and applying the multiple regression program in the packaged SPSS programs, it was discovered that the values of the empirical constants A_1, A_2 and A_3 were similar to those determined by MINW. The SPSS determined values of the coefficients were not listed because the curves based on the new coefficients did not fit the data as well as those derived from the MINW optimization program. Nevertheless, it should be pointed out that SPSS is a very efficient computer software package. The cost in computation by the SPSS route was substantially lower than the MINW route.

Equation 5.9 consists of two counteracting terms, one that expresses the increase in beneficiation ratio with chain speed, and a term that expresses the exponential

deterioration in beneficiation ratio. Conceptually, as the chain is set in motion, the paddles continually sweeping the bottom stratum of the cascade bed induce the convective flow of jetsam-rich materials to the left side resulting in the enrichment of jetsam towards one side of the cascade. Thus, beneficiation should improve if the chain were to be traveling at a higher speed. Conversely, when the velocity of the chain is exceedingly high, the mechanical agitation created by the movement of the paddles inevitably induces mixing. The two counteracting effects result in a beneficiation ratio curve characterized by a rapid growth in the beneficiation ratio at low or moderate chain speed followed by a gradual decrease of the beneficiation ratio at the higher chain speeds. The peak in the curve occurs at a chain speed of A_2/A_3; this was derived by differentiating Equation 5.9 with respect to chain speed, CS, and by equating the derivative to zero. Despite its simplicity, Equation 5.9 is conceptually meaningful.

5.4.3 Jetsam Accumulation Considerations

It should be pointed out that had the accumulation of salt in the "dead" zones of the cascade been insignificant, the integration of the exponential jetsam distribution profile over the normalized length of the bed would yield a mean jetsam concentration, C_{exp}, which should be essentially identical to the nominal concentration of jetsam in the cascade. From integration, it can be shown that:

$$C_{exp} = e^{B}/A(e^{A} - 1) \qquad (5.10)$$

where A, B are the slope and intercept of the linear regression line defining the exponential jetsam concentration profile versus the normalized bed length. The values of A and B were previously tabulated in Tables 5.26 and 5.27 for the 25.4 mm and 12.7 mm paddles, respectively. Values of C_{exp} as determined by Equation 5.10 for the two series of runs with different paddle heights are listed in Table 5.26 and 5.27. Inspection of the tables reveals that C_{exp} is not invariant. Past experience with the iron-sand and iron pyrite-coal systems indicated the most likely place for jetsam accumulation to be in the jetsam-rich end of the cascade, in the space between the point where the chain lifts off from the grid surface to join the chain sprocket and the end wall of the cascade. It is not clear why jetsam would accumulate there, in violation of the exponential profile that was so strikingly linear throughout the working section of the cascade swept by the paddle chain, considering the end zone of the bed was as fluidized as the remaining sections of the bed. Complicated solids movement induced by the presence of internals in the end zones, such as the relatively massive chain sprockets and the non-vertical placement of the paddles as the chain lifts to meet the upper sprocket could be the cause of the phenomenon.

Accumulation of jetsam in the jetsam-rich end could be calculated by subtracting C_{exp} from the nominal concentra-

tion of salt in the cascade, 1% salt by weight. The calculated percentages of jetsam accumulation were listed in Tables 5.26 and 5.27 for the two series of experiments with different paddle heights. The jetsam accumulations were also plotted versus the chain speed in Figure 5.6 for the series with the 25.4 mm paddles and in Figure 5.7 for the 12.7 mm paddles. Inspection of Figure 5.7 revealed two parabolic curves, the curve for $U-U_{mf}$ equal to 46 mm/sec was situated above the curve for $U-U_{mf}$ equal to 92 mm/sec. Despite the considerable scattering of the data at $U-U_{mf}$ equal to 69 mm/sec, the data were sandwiched in the space between the other two curves. For the series with the 25.4 mm paddles, Figure 5.6 revealed the same trend as that observed in Figure 5.7 for the shorter paddles. The scattering of the data points at $U-U_{mf}$ equal to 92 mm/sec was considerable but the data were generally located below the two curves with the smaller fluidization velocities.

Thus, it appeared that jetsam accumulation in the jetsam-rich side of the cascade was dependent on chain speed and fluidization velocity and diminished when the fluidization velocity was increased.

FIGURE 5.6 PLOT OF JETSAM ACCUMULATION VERSUS CHAIN SPEED

(SALT-ACTIVATED CHARCOAL SYSTEM)

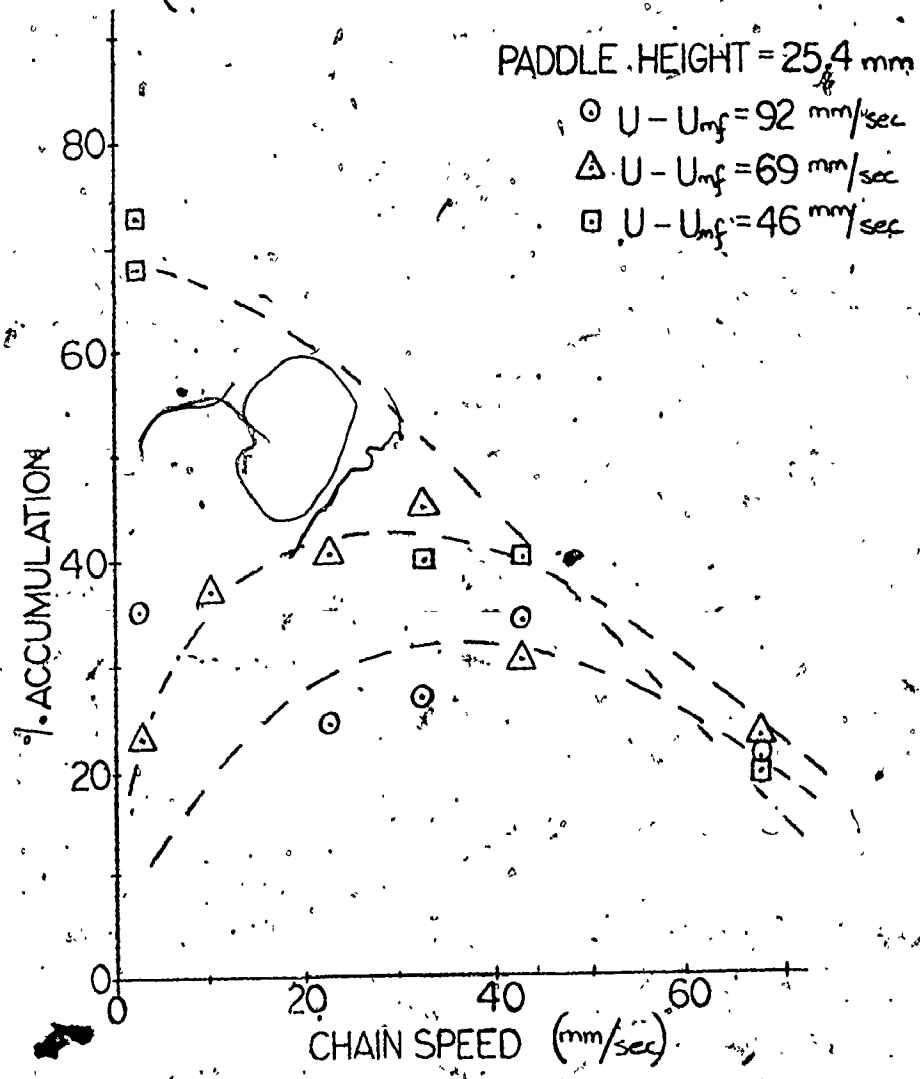

FIGURE 5.7 PLOT OF JETSAM ACCUMULATION VERSUS CHAIN SPEED

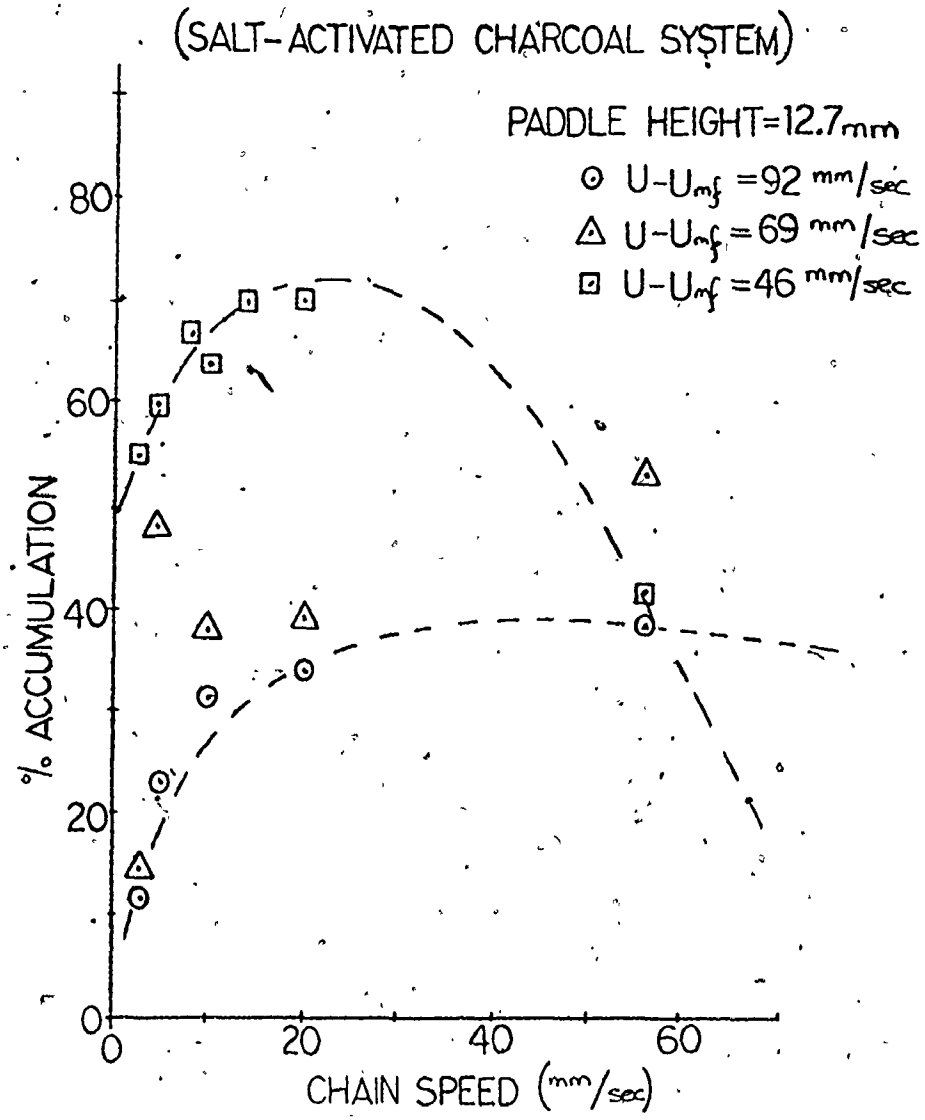

CHAPTER SIX

THEORETICAL CONSIDERATIONS FOR FLOTSAM-RICH SYSTEM

6.1 Muzyka-Beeckmans-Jeffs Model for Jetsam-Rich System

The first theoretical model on the counter-current cascade was proposed by Muzyka and Beeckmans for the jetsam-rich system.[77] Despite the fact that this thesis is concerned with flotsam-rich systems, the model proposed by Muzyka et al. will be briefly discussed, as the theoretical model proposed later in this chapter for flotsam-rich systems is a modified version of the original model.

Similarity between the operating counter-current exchange principle in the separation of a minor component in the counter-current fluidized cascade and the conventional distillation tower was previously discussed in Chapter 1. In the Muzyka-Beeckmans-Jeffs model, the flux of the minor flotsam component from the lower layer into the upper layer of a fluidized bed was approximated by the product of the mass transfer coefficient, K; and the difference between the flotsam concentration in the upper layer of the cascade bed, Y, and the equilibrium flotsam concentration in the upper

portion of a simple fluidized bed with identical overall composition, $\bar{X}$. This approximation is analogous to that used in interphase mass transfer theory in binary or multi-component distillation. The mixing induced by the turbulent motion of the fluidized solids in the cascade was approximated by the introduction of D, the turbulent diffusivity. Axial diffusion of either the flotsam or jetsam component in the cascade was assumed to be the primary factor in the reduction of axial concentration gradients in the cascade, which was created by the combined effect of the segregation of the different components in the fluidized bed, and the horizontal convective motion of the fluidized solids in the cascade due to the sweeping paddle movement.

A second order differential equation was formulated relating the convective, diffusive and vertical exchanges and transports, based on a flux balance of the flotsam component in the lower stratum of the cascade bed. Using the theoretical model, and assigning assumed values to the vertical mass transfer coefficient, K, and the diffusivity, D, the beneficiation ratio of the flotsam component could be calculated at varying paddle speeds. The theoretical beneficiation ratio versus paddle speed curves approximated the general trend of the experimental data. The fit between the theoretical curve and the experimental data was only moderately successful.

Further work by Beeckmans and co-workers revealed

that the diffusivity was a function of the horizontal velocity of the fluidized solids.[79,81] The dependency of the diffusivity on the horizontal solids velocity resembles that of the dispersion of tracers in a flowing liquid, i.e., the Taylor diffusivity. The dependency of turbulent diffusivity on the horizontal velocity of the flowing fluidized solids will be discussed later in this chapter.

6.2 Modified Theoretical Model for Flotsam-Rich Systems

The theoretical model presented here for flotsam-rich systems is a modified version of the Múzyka-Beeckmans-Jeffs model.[77] (The latter is valid for jetsam-rich systems.) Despite some differences in the assumptions used in the development, the principles of the two models are similar.

In Figure 6.1, H is the height of the cascade bed, αH is the height of the bed in the lower stratum, swept to the jetsam side of the cascade by the paddles at a mean velocity of V_h. The upper stratum of the bed with a height of $(1-\alpha)H$, is moving to the opposite flotsam end of the bed at a velocity of V_L. Subscripts h and L imply heavy and light, as the heavy jetsam tends to concentrate in the bottom of the bed. The volumetric concentrations of jetsam in the two strata of the cascade were designated Y and X, by analogy with binary component distillation. Thus, the overall jetsam

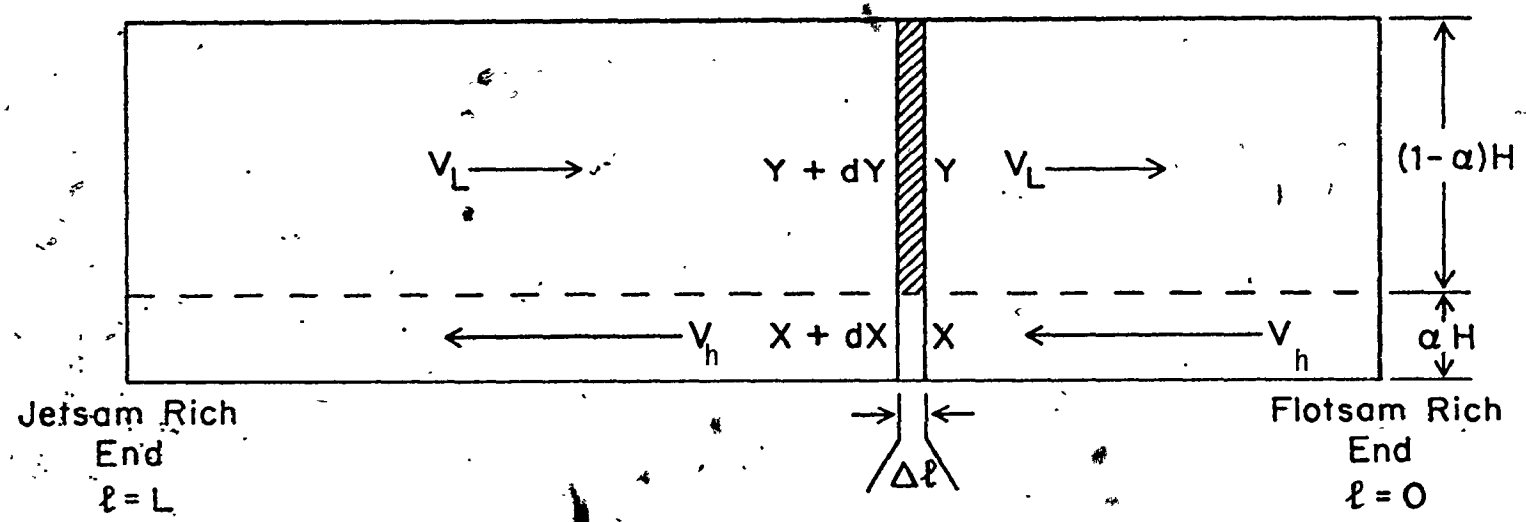

FIGURE 6.1 SCHEMATIC DIAGRAM OF FLUIDIZED CASCADE MODEL

concentration, $\bar{X}$, equals

$$\bar{X} = \alpha X + (1-\alpha)Y \qquad (6.1)$$

The mean velocities of the two strata are also related by the following equation:

$$V_h = \frac{(1-\alpha)}{\alpha} V_L \qquad (6.2)$$

If an assumption is made that the longitudinal mixing of the jetsam component in the upper stratum, F_d, is equal to the product of turbulent diffusivity, D, and the concentration gradient of the jetsam component, the diffusive transport of the jetsam, in the direction of the concentration gradient, is

$$F_d = D(1-\alpha)H \frac{dY}{d\ell} \qquad (6.3)$$

In the absence of a comprehensive theory on the mechanism of segregation of the jetsam component in the fluidized beds, the transport of jetsam from the bottom into the top portion of the bed, F_v, is approximated by the expression

$$F_v = K(Y-Y^*)\ \Delta\ell \qquad (6.4)$$

In equation 6.4, K is the vertical mass transfer coefficient, and Y* is the equilibrium jetsam concentration that the upper portion of a simple fluidized bed would attain with the same overall jetsam concentration and under the same fluidization velocity. Equation 6.4 is established by

analogy with vapour-liquid mass transfer in distillation towers. Rowe[21] observed that for most flotsam-rich systems, homogeneity of the jetsam concentration prevailed above the pure jetsam layer in the bottom grid region of the fluidized bed. Thus, Y* can be expressed as a function of the overall jetsam concentration $\bar{X}$,

$$Y^* = S\bar{X} \tag{6.5}$$

At a distance ℓ from the flotsam-rich end (Figure 6.1), the flux of jetsam into the upper stratum of the bed (the shaded area in Figure 6.1), is equal to the sum of convective and diffusive transport,

$$\text{Flux in} = -V_L(1-\alpha)HY\Big|_{\ell} - D(1-\alpha)H\frac{dY}{d\ell}\Big|_{\ell} \tag{6.6}$$

At a distance $(\ell+\Delta\ell)$ from the flotsam-rich side, the outgoing flux of jetsam from the shaded element is expressed in equation 6.7.

$$\text{Flux out} = -V_L(1-\alpha)HY\Big|_{\ell+\Delta\ell} - D(1-\alpha)H\frac{dY}{d\ell}\Big|_{\ell+\Delta\ell} \tag{6.7}$$

At steady state, the difference between the two fluxes must be equal to the flux of jetsam from the bottom stratum into the upper element, F_v.

$$V_L(1-\alpha)HY\Big|_{\ell+\Delta\ell} - V_L(1-\alpha)HY\Big|_{\ell} + D(1-\alpha)H\frac{dY}{d\ell}\Big|_{\ell+\Delta\ell}$$

$$- D(1-\alpha)H\frac{dY}{dl}\Big|_{\ell} = K(Y-Y^*)\Delta\ell \tag{6.8}$$

Dividing equation 6.8 through by $\Delta\ell$ and letting $\Delta\ell \to 0$, a second order ordinary differential equation is obtained.

$$D\frac{d^2Y}{d\ell^2} + V_L\frac{dY}{d\ell} + \frac{K}{(1-\alpha)H}(Y^*-Y) = 0 \qquad (6.9)$$

Thus, equation 6.9 relates the diffusive, convective, and vertical transport of jetsam in the elemental volume in the upper stratum of the bed. At steady state, the horizontal flux of jetsam in both strata must be the same and, assuming zero diffusive mixing in the jetsam layer (because of the presence of paddles), we find

$$(1-\alpha)HV_L Y + (1-\alpha)HD\frac{dY}{d\ell} = \alpha HV_h X \qquad (6.10)$$

By combining equations 6.2 and 6.10, and simplifying, the relationship between the jetsam concentration in the two strata can be established.

$$X = Y + \frac{D}{V_L}\frac{dY}{d\ell} \qquad (6.11)$$

Incorporating equations 6.11, 6.5 and 6.1 into equation 6.9, simplifying and rearranging, gives equation 6.12:

$$\frac{d^2Y}{d\ell^2} + \left[\frac{V_L}{D} + \frac{KS\alpha}{H(1-\alpha)V_L}\right]\frac{dY}{d\ell} + \frac{K(S-1)}{D(1-\alpha)H}Y = 0 \qquad (6.12)$$

Equation 6.12 is the basic equation describing the axial distribution of jetsam in the upper stratum of the cascade. A general solution to equation 6.12 is

$$Y = C_1 \text{Exp}(M_1 \ell) + C_2 \text{Exp}(M_2 \ell) \qquad (6.13)$$

From experience with the iron-sand, and salt-activated charcoal systems, it was observed that the overall

jetsam concentration, $\bar{X}$, is an exponential function of the axial distance in the cascade (see Section 5.1 and 5.4). Assuming that the jetsam concentration in the upper stratum of the cascade bed would also exhibit a similar dependency on the axial distance, we write

$$Y = Y_0 \, \mathrm{Exp}(M_1 \ell) \qquad (6.14)$$

In equation 6.14, Y_0 is the value of Y at $\ell = 0$, and M_1 is the root of the characteristic equation, equation 6.13, as well as the slope of the ln(Y) versus ℓ plot. If equation 6.14 is valid, one possible assumption would be that the combined effect of C_2 and M_2 rendered the second term of equation 6.13 negligible. The assumption of a logarithmic dependency of Y with the axial distance is reasonable, considering that $\bar{X}$ and Y are related by equation 6.1. By using equation 6.14, and after differentiation and simplification, equation 6.12 becomes

$$M_1^2 + \left(\frac{V_L}{D} + \frac{KS\alpha}{H(1-\alpha)V_L}\right) M_1 + \frac{K(S-1)}{D(1-\alpha)H} = 0 \qquad (6.15)$$

Thus, M_1 can be calculated as a function of V , D, K, S, H and α.

$$M_1 = \left[\left(\frac{V_L}{D} + \frac{KS\alpha}{H(1-\alpha)V_L}\right)^2 - \frac{4K(S-1)}{D(1-\alpha)H}\right]^{\frac{1}{2}} / 2.0 - \left(\frac{V_L}{D} + \frac{KS\alpha}{H(1-\alpha)V_L}\right) / 2.0 \qquad (6.16)$$

Using equations 6.1, 6.11 and 6.14, the overall jetsam concentration, $\bar{X}$, can be expressed as

$$\bar{X} = Y_0 \, \mathrm{Exp}(M_1 \ell) \left[1 + \frac{\alpha D}{V_L} M_1\right] \qquad (6.17)$$

It can be shown that the beneficiation ratio, defined as the ratio of jetsam concentration at the two ends of the cascade, can be calculated by equation 6.18:

$$\text{Beneficiation Ratio} = \text{Exp}(M_1 L) \qquad (6.18)$$

where L is the total length of the cascade bed.

The horizontal velocity of the fluidized solids in the upper stratum of the bed, V_L, can be calculated by specifying the paddle speed, CS, and the dimensionless paddle height, .

$$V_L = CS \frac{(\alpha)}{(1-\alpha)} \qquad (6.19)$$

6.2.1 Considerations of Diffusivity

The diffusivity presented in the Muzyka-Beeckmans-Jeffs model of the counter-current cascade was later found to be dependent on the horizontal velocity of the flowing fluidized solids.[79,81] In a paper by Muzyka and Beeckmans[79], the diffusivity D was estimated by applying the original Muzyka-Beeckmans-Jeffs model to the experimental data of a jetsam-rich system, based on assumed values of K, the vertical mass transfer coefficient. Channel flow experiments of flowing fluidized solids were also made, using both segregating and non-segregating tracers. The concept of diffusivity measurement was based on the analogy with the dispersion of a narrow pulse of tracer injected into a liquid flowing through a tube.

Taylor[82,83] showed that an initially infinitely narrow pulse of tracer will broaden about a point travelling at the mean fluid velocity, and that the distribution is Gaussian. Furthermore, the variance of the distribution is given by

$$\sigma^2 = 2D_t\, t \qquad (6.20)$$

D_t is the so-called Taylor diffusivity coefficient.

When the initial tracer distribution is not infinitely narrow, the Taylor diffusivity coefficient may be calculated by the rate of change of the variance, σ^2, with time, t.

$$D_t = \tfrac{1}{2}\left(\frac{d\sigma^2}{dt}\right) \qquad (6.21)$$

Even though Taylor dispersion was derived for the flow of liquid in conduits, and is inherently different from the turbulent diffusion in flowing fluidized solids, the two situations are similar in that the convective displacement in the axial direction occurs in the presence of a concentration gradient, and a non-uniform transverse velocity distribution.

Based on limited experimental data, Muzyka and Beeckmans proposed the following empirical equation to describe the relationship between the turbulent diffusivity and the mean horizontal convective velocity of the flowing fluidized solids:

$$\ln(D_t - D_0) = a_0 + a_1 \ln(\bar{U}) + a_2 \ln^2(\bar{U}) \qquad (6.22)$$

a_0, a_1 and a_2 are empirical constants, D_t is the Taylor diffusivity at the fluidized solids convective velocity of

$\bar{U}$, and D_0 is the lateral diffusivity in the simple fluidized bed in the complete absence of horizontal motion.

A recent paper on Taylor diffusivity in channel flow of fluidized solids was presented by Beeckmans and Jeffs[81]. Two partial differential equations were established to describe the distribution of tracer in a fluidized channel as a function of the axial, vertical and transverse directions. The exchange of material between the wake and the emulsion phase was calculated based on Kunii and Levenspiel's expression[78], and Rowe's empirical equations for the prediction of bubble diameter as a function of the vertical position in the fluidized bed[80]. Using appropriate boundary conditions, the calculated Taylor dispersion coefficients were reasonably consistent with experimental values. It is important to note that both theoretical and experimental data suggest a linear log-log plot of $(D_t - D_0)$ versus $\bar{U}$ under the conditions studied. Therefore, the third term of equation 6.22 could practically be ignored. The dependence of diffusivity on the horizontal velocity of the flowing fluidized solids will be incorporated into the model outlined in Section 6.2 for the analysis of the data of the salt-activated charcoal system.

6.3 Application of the Cascade Model to Experimental Data

An attempt was made to apply the model developed in Section 6.2 to the experimental data of the salt-activated charcoal system. The salt-activated charcoal system was chosen primarily because it was the most thoroughly investi-

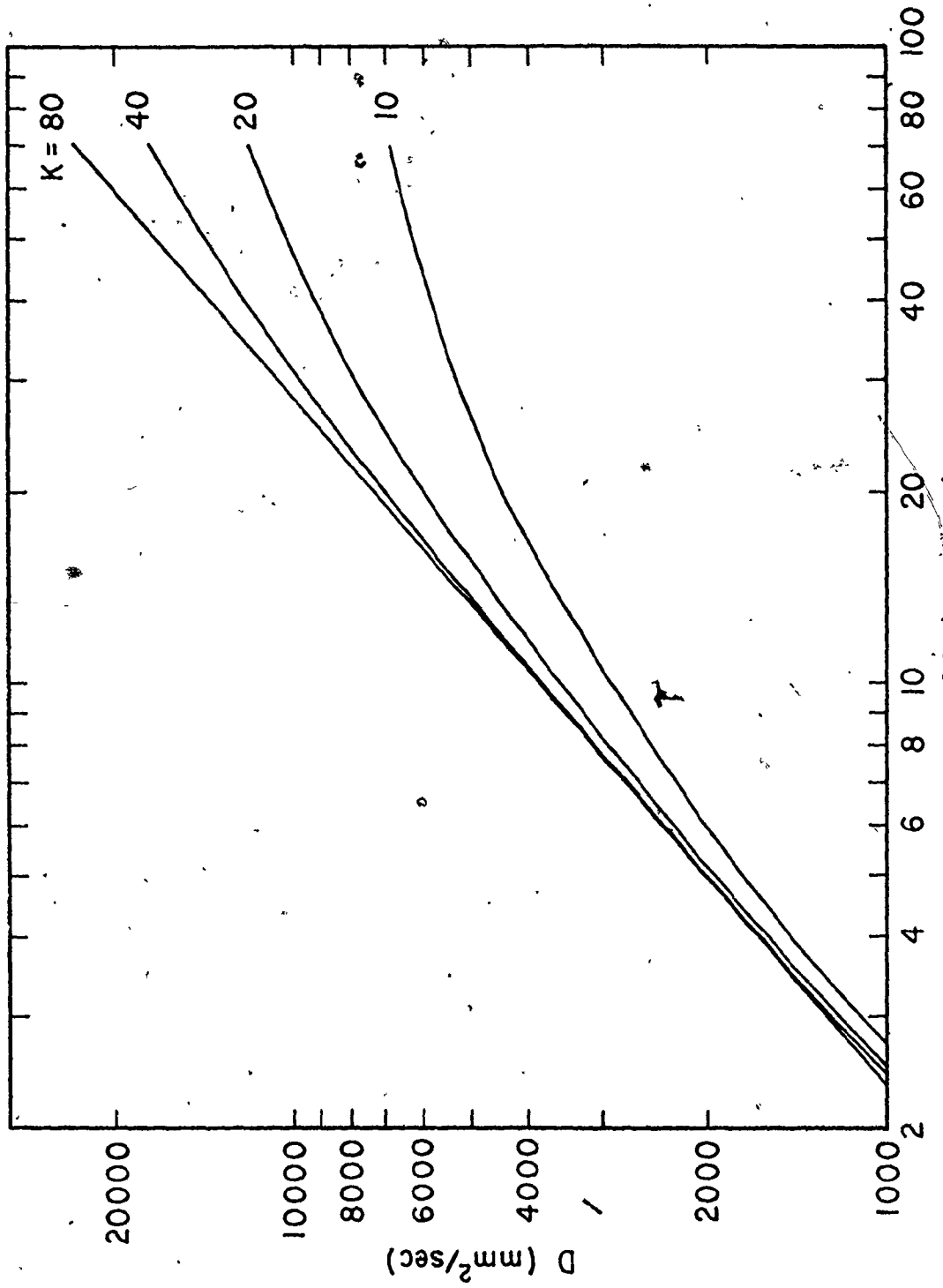

FIGURE 6.2D PLOT OF D VERSUS CS ($\bar{U}-U_{mf}$ = 69 mm/s, 12.7 mm PADDLES)

gated system in this thesis.

Using the data from the simple fluidized bed segregation experiments previously discussed in Section 5.4.1, parameter S, which was defined in Equation 6.5, was calculated. A sample calculation is provided in Appendix J. A summary of the values of S is given in Table 6.1. Inspection of Table 6.1 shows that S is dependent on the overall concentration of jetsam, $\bar{X}$, and on the excess fluidization velocity, $U-U_{mf}$. Unfortunately, only three overall concentrations were studied in the simple bed segregation experiments and this is insufficient to ascertain the relationship between S and $\bar{X}$. It is also important to note that S is calculated on the assumption that the jetsam is distributed uniformly in the upper portion of the simple fluidized bed. Inspection of Table 5.25A, B and C reveals some degree of non-uniformity of the jetsam concentration in the upper stratum of the simple fluidized bed. In view of the absence of a reliable correlation between S and $\bar{X}$, an average value of S for each $U-U_{mf}$ setting was used in conjunction with the model of Section 6.2

Using experimental values of the beneficiation ratio obtained at various combinations of paddle heights, excess fluidization velocities, and paddle speeds (Tables 5.26 and 5.27), the diffusivity D was calculated for each discrete data point. By rearranging Equation 6.16, D can be calculated as

Table 6.1 S as a Function of $\bar{X}$ and $U-U_{mf}$

$\bar{X}$* (%)	$U-U_{mf}$=92 mm/s	$U-U_{mf}$=69 mm/s	$U-U_{mf}$=46 mm/s
0.015	0.88	0.76	0.76
0.1	0.72	0.64	0.55
1.0	0.63	0.64	0.62
Average:	0.74	0.64	0.62

* $\bar{X}$ = overall salt concentration in simple fluidized bed in weight percents.

$$D = \frac{2aV_L - 2(2M_1+a)V_L - b}{4M_1(M_1+a)}$$

where $$a = \frac{KS\alpha}{H(1-\alpha)V_L}$$

$$b = \frac{4K(S-1)}{(1-\alpha)H} \qquad (6.23)$$

Different values of K were selected, and the diffusivity D was calculated for each run in Tables 5.26 and 5.27. According to Beeckmans and co-workers,[81] linearity should prevail when (D_t-D_0) is plotted versus V_L on a log-log plot. D_t, D_0 are defined in Equation 6.22 and V_L is defined in Equation 6.19. The average velocity of the fluidized solids in the upper stratum of the cascade, V_L, flowing in opposite direction to that of the paddle chain, is directly proportional to the paddle speed, CS, as defined in Equation 6.19. Since the normalized paddle height, α, is constant for each of the two series of experiments with different paddle heights, D is plotted versus CS in place of V_L in Figure 6.2 A through F for the six combinations of paddle height and excess fluidization velocities. In the figures, the discrete data points are deleted for clarity.

In this work there are no experimental data on D_0, but from previous work it has been shown that D_0 is very small in comparison with D_t[81]. The linearity of D versus CS on a log-log plot should therefore not be significantly affected.

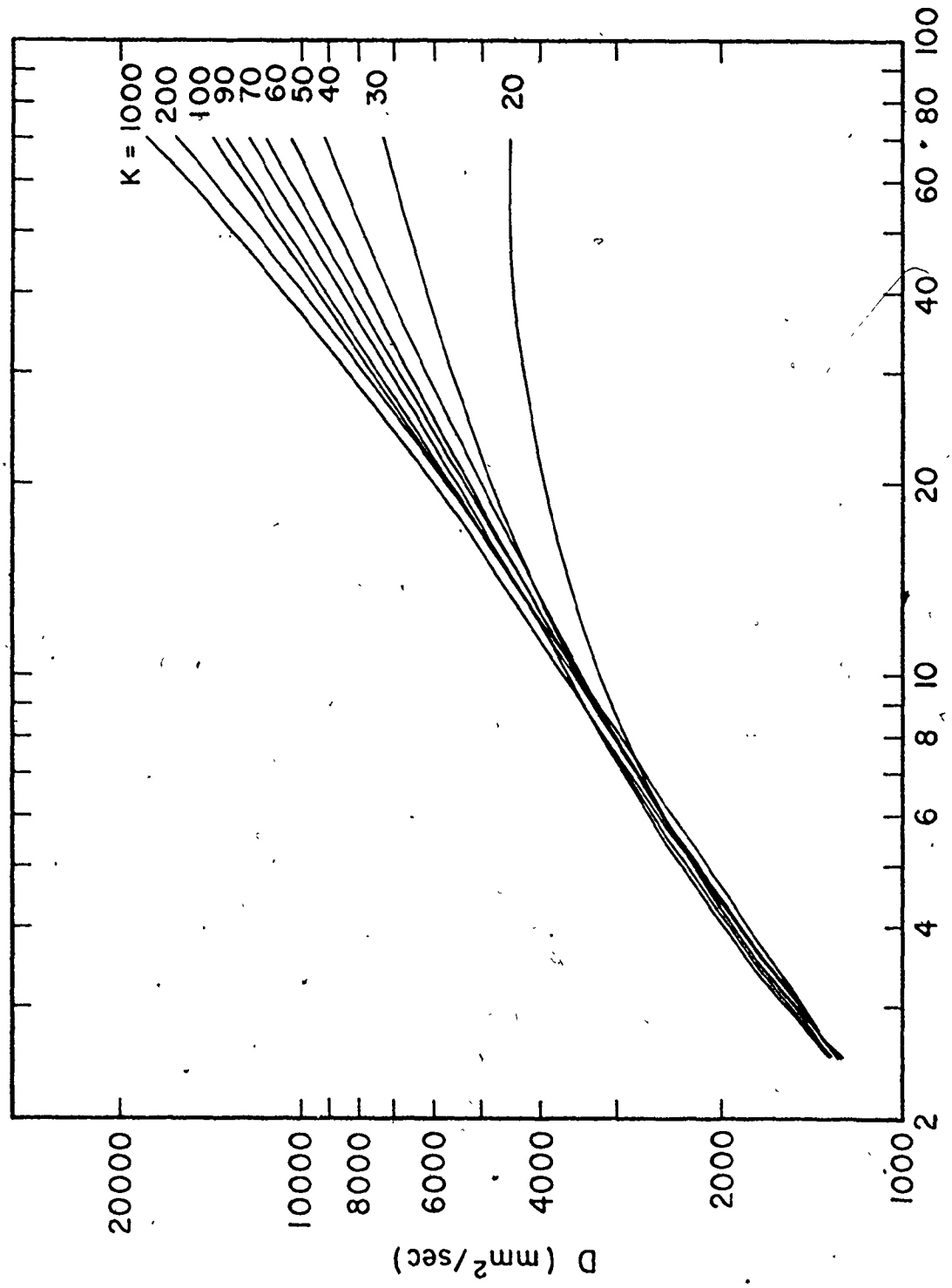

FIGURE 6.2A PLOT OF D VERSUS CS ($U-U_{mf}$ = 92 mm/s, 25.4 mm PADDLES)

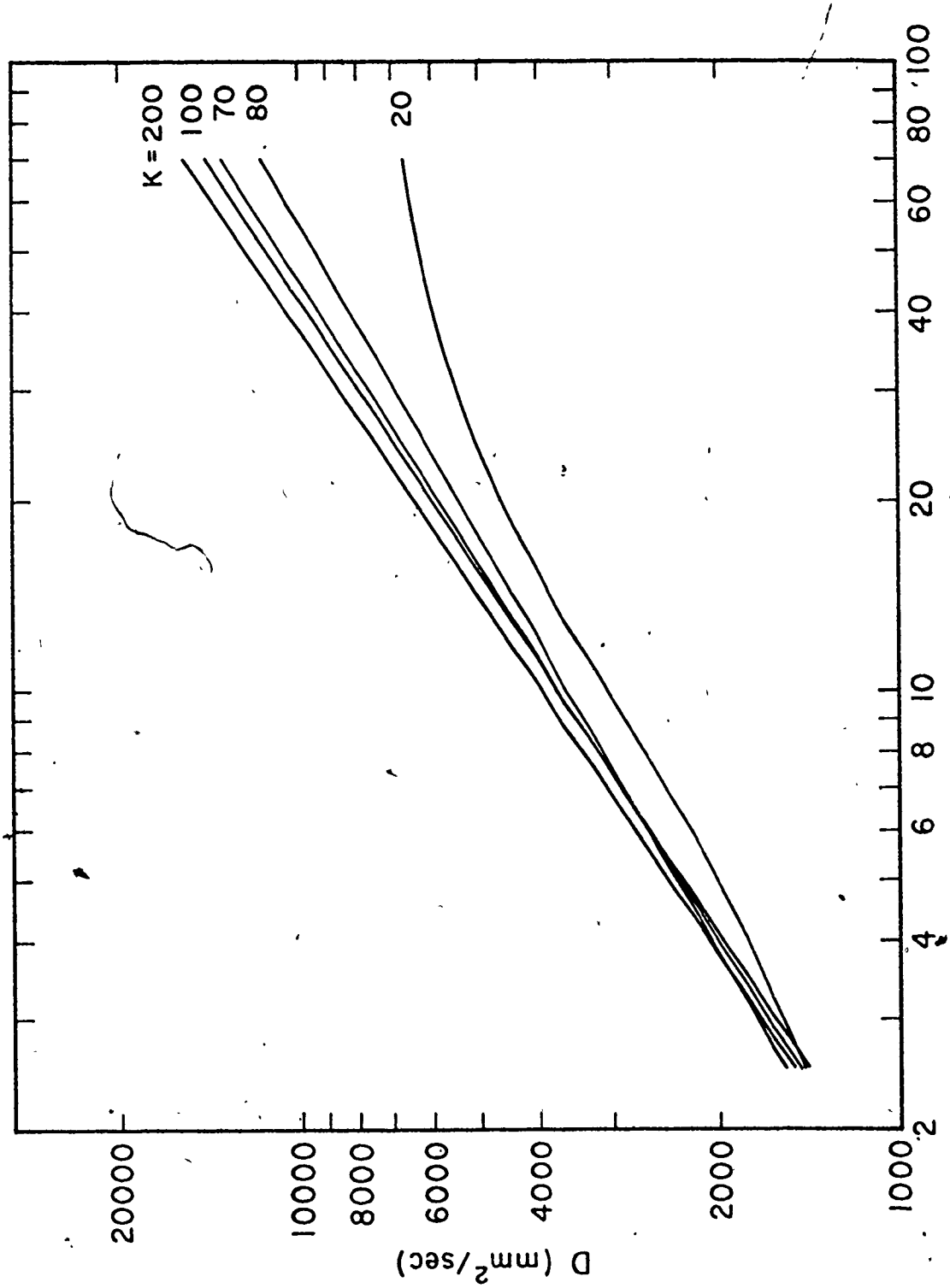

FIGURE 6.2B PLOT OF D VERSUS CS ($U-U_{mf}$ = .92 mm/s, 12.7 mm PADDLES)

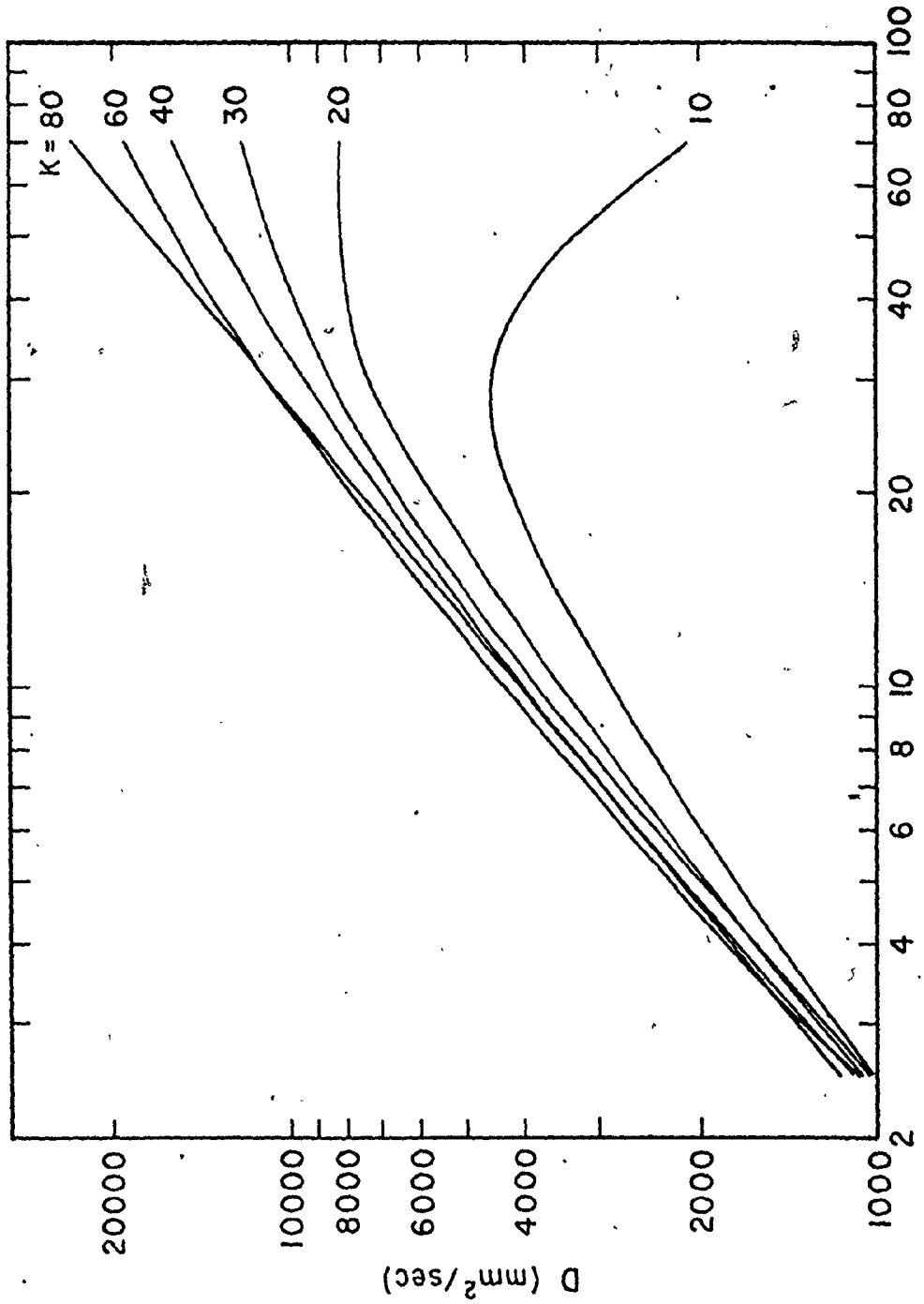

FIGURE 6.2C PLOT OF D VERSUS CS ($U-U_{mf}$ = 69 mm/a, 25.4 mm PADDLES)

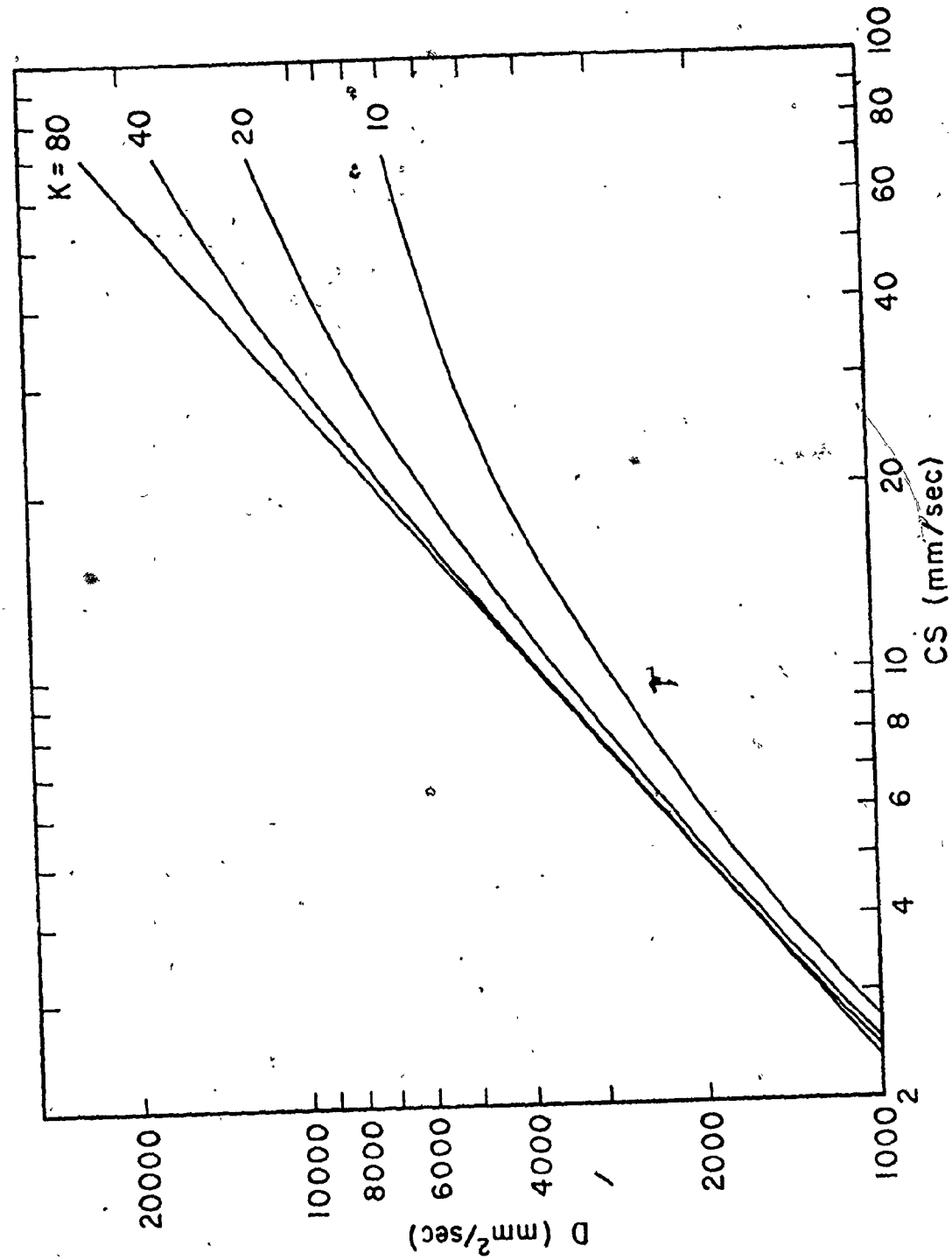

FIGURE 6.2D PLOT OF D VERSUS CS ($U-U_{mf}$ = 69 mm/s, 12.7 mm PADDLES)

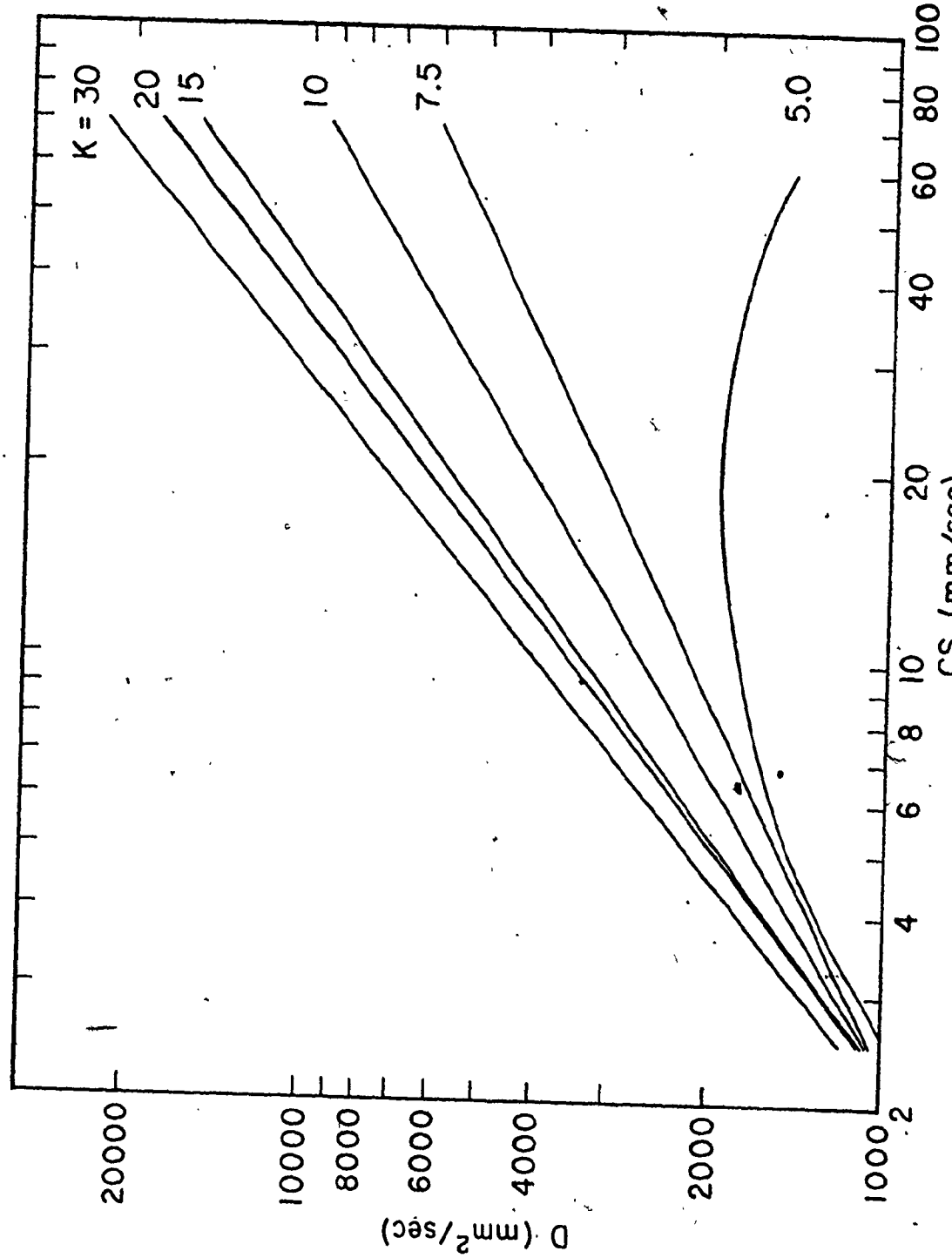

FIGURE 6.2E PLOT OF D VERSUS CS ($U-U_{mf}$ = 46 mm/s, 25.4 mm PADDLES)

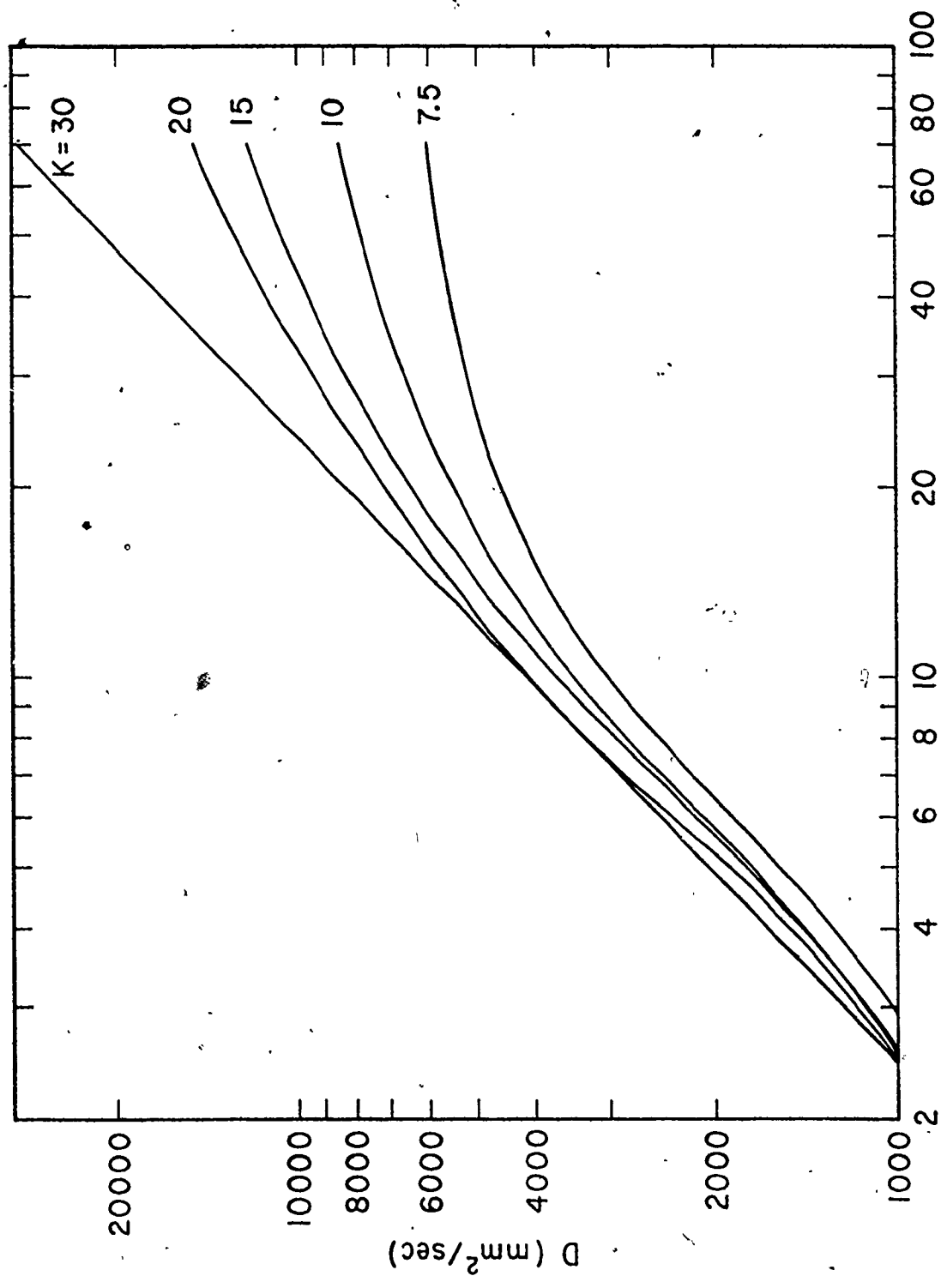

FIGURE 6.2F PLOT OF D VERSUS CS $(U-U_{mf}$ = 46 mm/s, 12.7 mm PADDLES)

Table 6.2A Regression Analyses of Calculated Diffusivity Data at $U-U_{mf}$ = 92 mm/s

Paddle Height (mm)	K Assumed (mm/s)	A_1	A_2	cc
25.4	20	991.93	0.4058	0.9413
	30	823.83	0.5373	0.9887
	40	754.65	0.6009	0.9957
	70	673.64	0.6835	0.9986
	100	642.84	0.7175	0.9987
	200	607.53	0.7582	0.9981
	300	595.86	0.7721	0.9978
	1000	579.58	0.7919	0.9973
12.7	50	925.10	0.5850	0.9883
	60	903.79	0.6024	0.9880
	70	888.47	0.6151	0.9877
	80	876.86	0.6249	0.9874
	90	867.79	0.6325	0.9872
	100	860.49	0.6387	0.9870
	1000	823.12	0.6834	0.9862

$$D = A_1 \, Exp(A_2 x \ln(CS)) \qquad (6.23)$$

Table 6.2B Regression Analyses of Calculated Diffusivity Data at $U-U_{mf}$ = 69 mm/s

Paddle Height (mm)	K Assumed (mm/s)	A_1	A_2	cc
25.4	30	528.77	0.7657	0.9722
	40	543.65	0.8173	0.9951
	50	524.63	0.8491	0.9968
	60	511.78	0.8710	0.9977
	70	502.50	0.8870	0.9983
	80	495.45	0.8992	0.9986
	90	489.92	0.9089	0.9988
12.7	10	628.41	0.6057	0.9829
	30	498.40	0.8410	0.9985
	40	475.42	0.8784	0.9992
	50	462.80	0.9022	0.9995
	70	447.64	0.9312	0.9998
	80	442.73	0.9406	0.9999

$$D = A_1 \, Exp(A_2 x \ln(CS)) \qquad (6.23)$$

Table 6.2C Regression Analysis of Calculated Diffusivity Data at $U-U_{mf}$ = 46 mm/s

Paddle Height (mm)	K Assumed (mm/s)	A_1	A_2	cc
25.4	7.5	639.44	0.5194	0.9991
	10	577.44	0.6529	0.9990
	15	527.74	0.7806	0.9984
	30	479.64	0.9169	0.9979
	40	466.82	0.9542	0.9978
	60	453.37	0.9937	0.9976
12.7	7.5	646.45	0.6176	0.9564
	15	541.69	0.8004	0.9868
	30	403.97	1.0070	0.9950

$$D = A_1 \, Exp(A_2 \times \ln(CS)) \qquad (6.23)$$

Figures 6.2 A through F reveal that the linearity of D versus CS on log-log plots occurred at discrete values of K. Least squares linear regression analyses of ln (D) versus ln (CS) were performed for various assumed values of K. The results are summarized in Tables 6.2 A, B and C for the excess fluidization velocities of 92, 69 and 46 mm/s, respectively.

Inspection of the tables revealed that when the value of the specified K is sufficiently high, linearity of ln (D) versus ln(CS) is observed. For this reason, linearity as judged by the values of the correlation coefficients in the regression lines cannot be used as the sole criterion in determination of K. Nevertheless, this condition of linearity could be used as a criterion for the estimation of the lower limit for K.

The determination of K is, unfortunately, quite subjective and needs further explanations. Since K quantifies the vertical transport of jetsam, we expect the value of K to be invarient with paddle height, and to increase with the excess fluidization velocity, $U-U_{mf}$. For the 127 mm paddles at $U-U_{mf}$ = 46 mm/s, Figure 6.2F, linearity of the diffusivity plot first occurred when K is equal to 30 mm/s. For the taller paddles at the same excess fluidization velocity, linearity of the diffusivity plot, Figure 6.2 E, is apparent when K is equal to or greater than 7.5 mm/. Since K is assumed

be invarient with paddle height, a value of 30 mm/s was assigned to K at that excess fluidization velocity for both paddles. In the same manner, using Figure 6.2 C and D, K was chosen to be at least 80 mm/s at the excess fluidization velocity of 69 mm/s. As we expect the value of K at the excess fluidization velocity of 92 mm/s to be higher than that at 69 mm/s, and excellent linearity of the diffusivity plots were also observed when K is equal to 100 mm/s. For both paddles at the highest excess fluidization velocity of 92 mm/s K is estimated to be 100 mm/s.

It is important to note that K may be affected by the combined effect of paddle height and the horizontal convective velocity of the fluidized solids, especially at high chain speed. As the relationship is not known, we assumed K to be invarient with chain speed. In view of the fact that the assumptions have not been tested, the procedures for the determination of K should only be considered as an approximation.

For the six combinations of two paddle heights, and three excess fluidization velocities, calculated values of diffusivities D are summarized in Tables 6.3 A through F. Linearity of D versus CS on log-log plot at each of the chosen K's is excellent. Figure 6.4 A and B are the log-

Table 6.3A Diffusivity as Estimated from Experimental Data

$(U-U_{mf}$ = 92 mm/s, 25.4 mm Paddles)

K = 100 mm/s
α = 0.1693
S = 0.74

CS* (mm/s)	BR**	D** (mm^2/s)	V_L ** (mm/s)
2.54	22.9	1248	0.52
10.16	68.5	3591	2.07
22.35	275.4	5561	4.56
32.66	276.1	7760	6.66
41.45	307.4	9267	8.45
68.58	288.3	13817	13.90

* Experimental ** Calculated

Table 6.3B Diffusivity as Estimated from Experimental Data

$U-U_{mf}$ = 92 mm/s, 12.7 mm Paddles

K = 100 mm/s
α = 0.0847
S = 0.74

CS* (mm/s)	BR*	D** (mm^2/s)	V_L ** (mm/s)
2.54	6.9	1840	0.23
5.08	29.0	2094	0.47
10.16	54.6	3469	0.94
20.32	96.2	5869	1.88
55.9	207.9	12118	5.17

* Experimental ** Calculated

Table 6.3C Diffusivity as Estimated from Experimental Data

($U-U_{mf}$ = 69 mm/s, 25.4 mm Paddles)

K = 80 mm/s
α = 0.1693
S = 0.64

CS* (mm/s)	BR*	D** (mm^2/s)	V_L** (mm/s)
2.54	254.2	1120	0.52
22.35	406.6	8051	4.56
22.35	372.6	8185	4.56
32.66	230.6	12459	6.66
41.45	307.6	14197	8.45
68.58	301.3	20519	13.98

* Experimental ** Calculated

Table 6.3D Diffusivity as Estimated from Experimental Data

($U-U_{mf}$ = 69 mm/s, 12.7 mm Paddles)

K = 80 mm/s
α = 0.0847
S = 0.64

CS* (mm/s)	BR*	D** (mm^2/s)	V_L** (mm/s)
2.54	209.8	1055	0.23
5.08	230.5	2047	0.47
10.16	261.9	3897	0.94
20.32	209.9	7756	1.88
55.90	172.8	19131	5.17

* Experimental ** Calculated

Table 6.3E Diffusivity as Estimated from Experimental Data

$(U-U_{mf}$ = 46 mm/s, 25.4 mm Paddles)

K = 30 mm/s
α = 0.1693
S = 0.62

CS* (mm/s)	BR*	D** (mm^2/s)	V_L** (mm/s)
2.54	315.4	1144	0.52
2.54	278.5	1170	0.52
22.35	304.0	7591	4.56
32.66	200.9	10761	6.66
41.45	120.0	14291	8.45
68.58	42.2	26649	13.98

* Experimental ** Calculated

Table 6.3F Diffusivity as Estimated from Experimental Data

$(U-U_{mf}$ = 46 mm/s, 12.7 mm Paddles)

K = 30 mm/s
α = 0.0847
S = 0.62

CS* (mm/s)	BR*	D** (mm^2/s)	V_L** (mm/s)
2.54	343.1	1027	0.23
5.09	339.6	1990	0.47
8.00	185.3	3392	0.74
10.16	150.2	4395	0.94
14.00	146.0	5837	1.30
20.32	140.9	7982	1.88
55.90	112.6	16847	5.17

* Experimental **Calculated

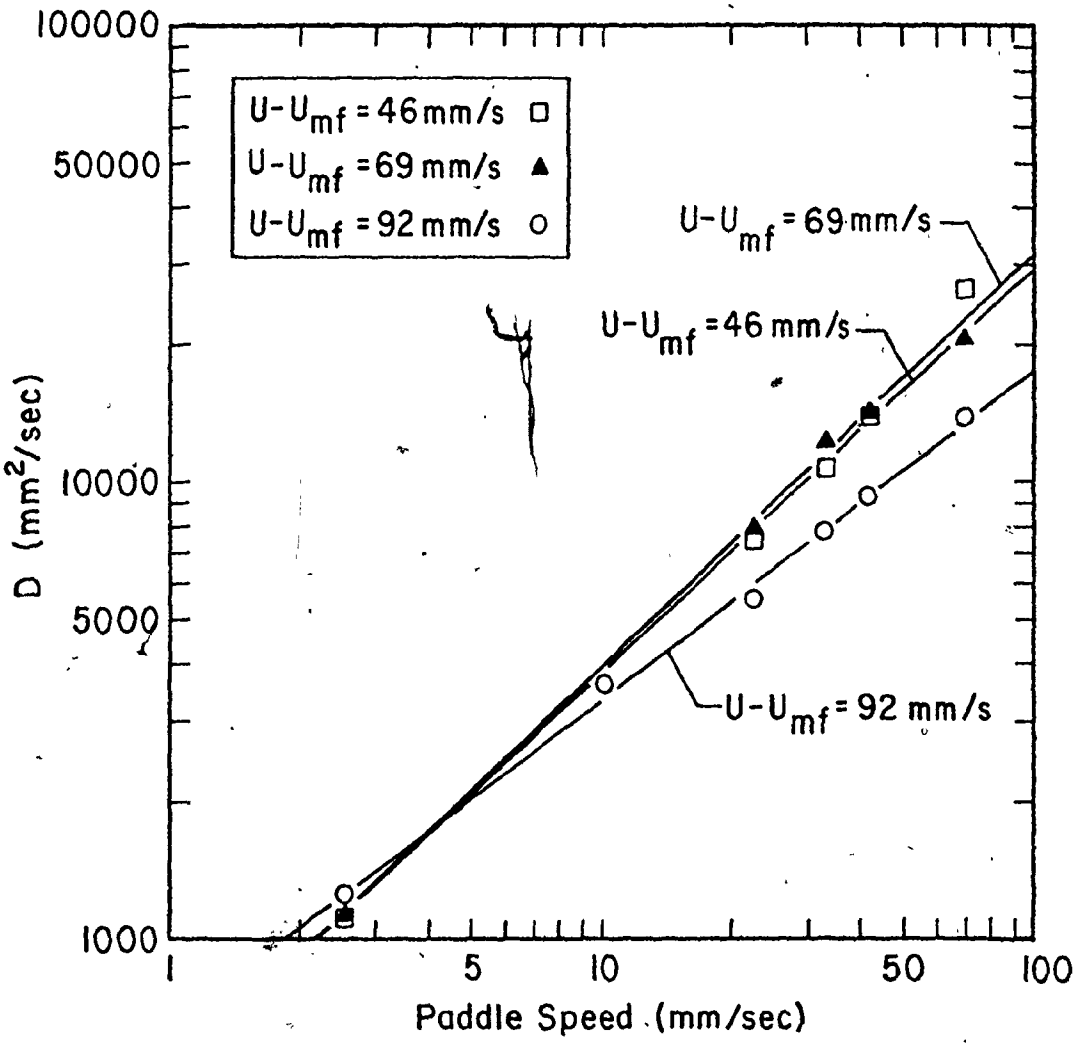

FIGURE 6.3A PLOT OF D VERSUS PADDLE SPEED

(25.4 mm PADDLES)

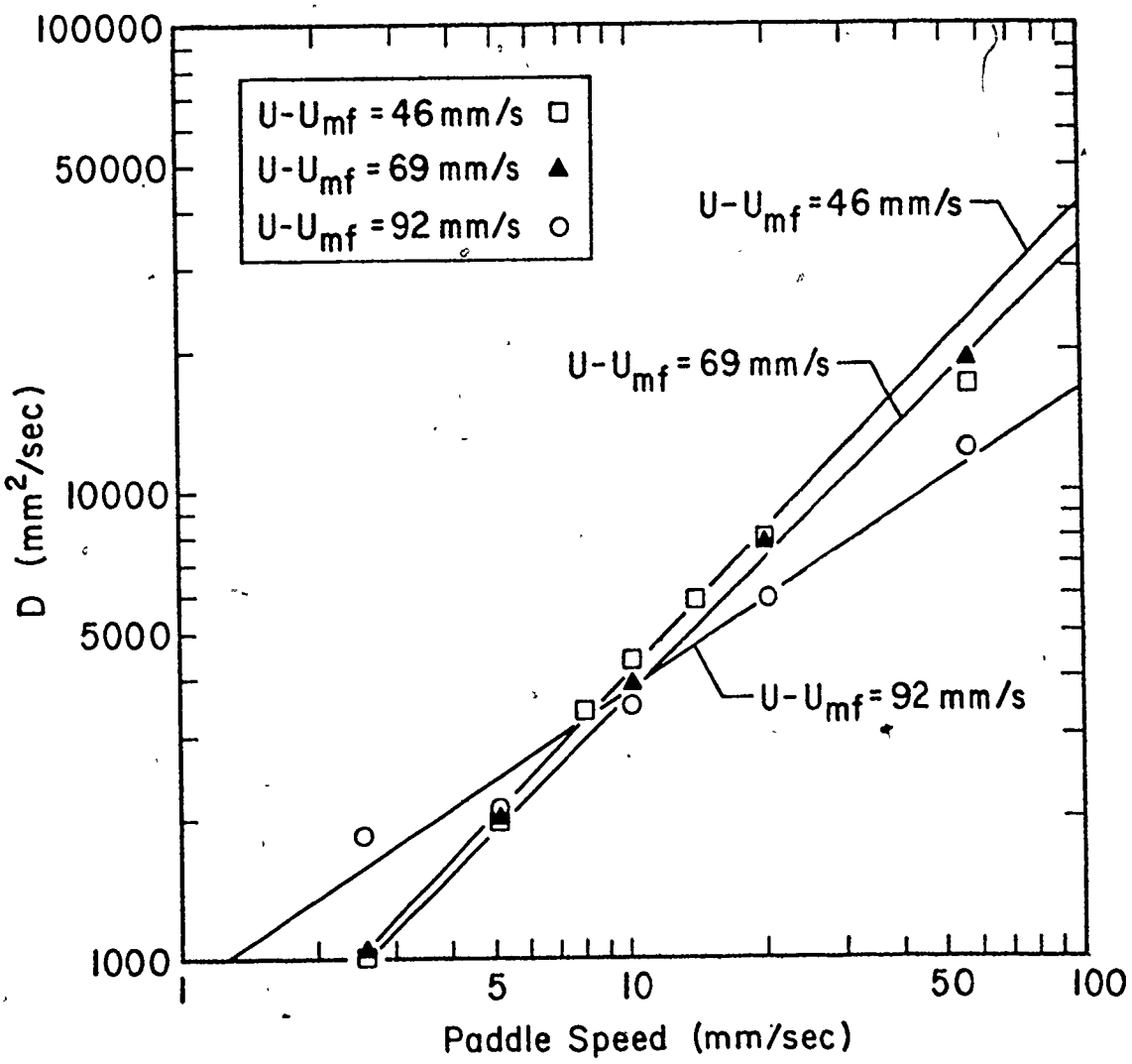

FIGURE 6.3B PLOT OF D VERSUS PADDLE SPEED

(12.7 mm PADDLES)

log plots of D versus CS for the series of experiments with the 25.4 and 12.7 mm paddles respeotively. The linear lines in the figures are obtained from the regression lines summarized in Table 6.4. All the correlation coefficients in Table 6.4 approach unity and therefore confirm the linearity of ln(D) versus ln(CS).

For the two series of experiments with different paddle heights, Figures 6.3 A and B exhibited similar dependency of D on the paddle speed, CS. The highest fluidization velocity, $U-U_{mf}$ = 92 mm/s, is characterized by high diffusivity at chain speed below 5 mm/s. The higher diffusivity at the higher fluidizatioin velocity and low paddle speed is conceptually accurate. As the paddle speed approaches zero, the cascade is essentially a rectangular simple fluidized bed. In simple fluidized bed, increase in fluidization velocity should increase the turbulent diffusivity of the fluidized solids.

Figures 6.4 A, B and C are the plots of D versus V_L at the three excess fluidization velocities. The lines drawn in the figures are obtained from least squares linear regression of the discrete data points. A summary of the regression lines is provided in Table 6.5. The figures show that for the same flow velocity of the fluidized solids in the upper stratum, the smaller paddle is usually characterized by higher diffusivity. Perhaps a disturbance in the jetsam-rich lower stratum of the cascade bed is created by the movement of the smaller paddles close to the grid region,

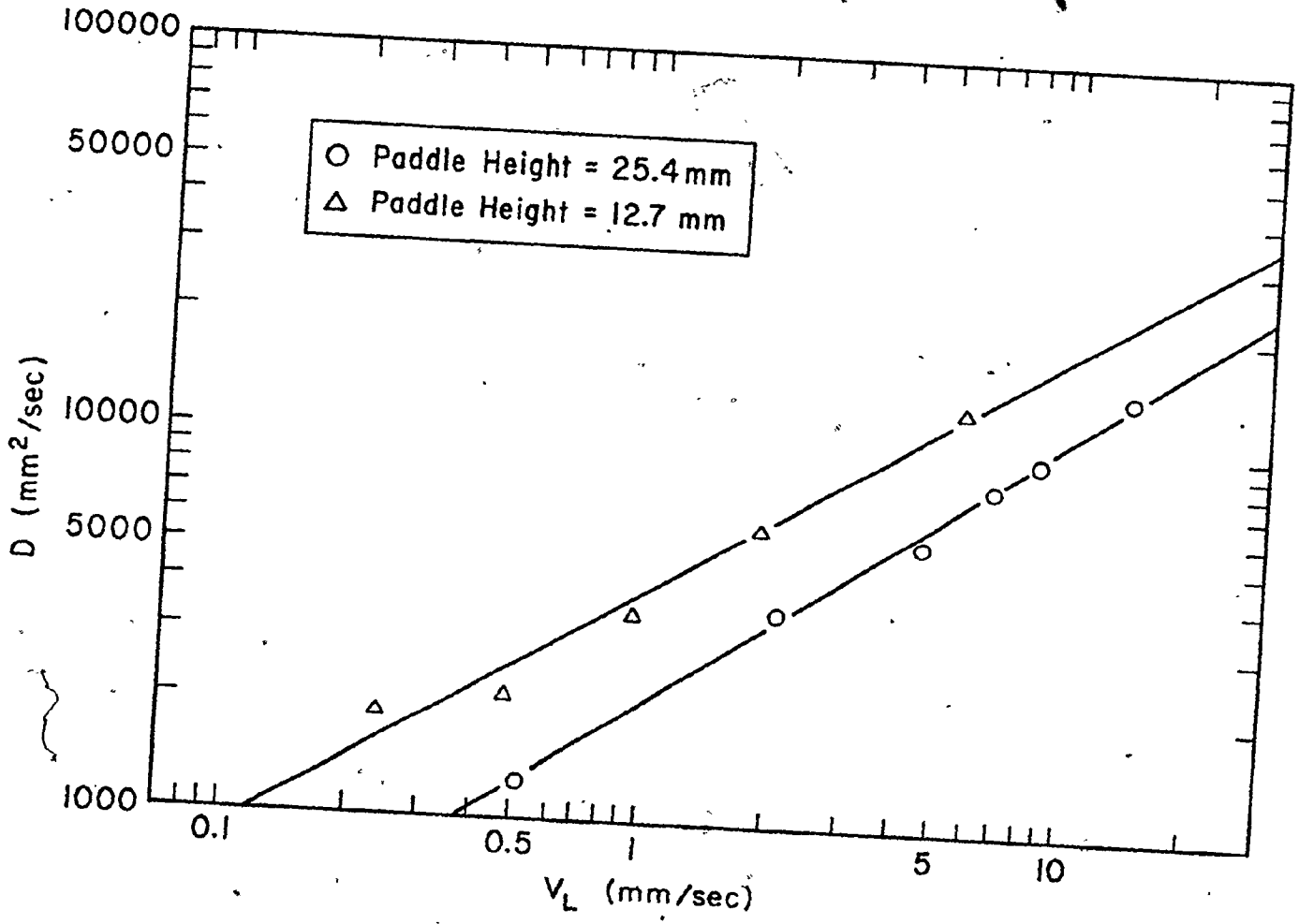

FIGURE 6.4A PLOT OF D VERSUS V_L , $(U-U_{mf} = 92$ mm/s)

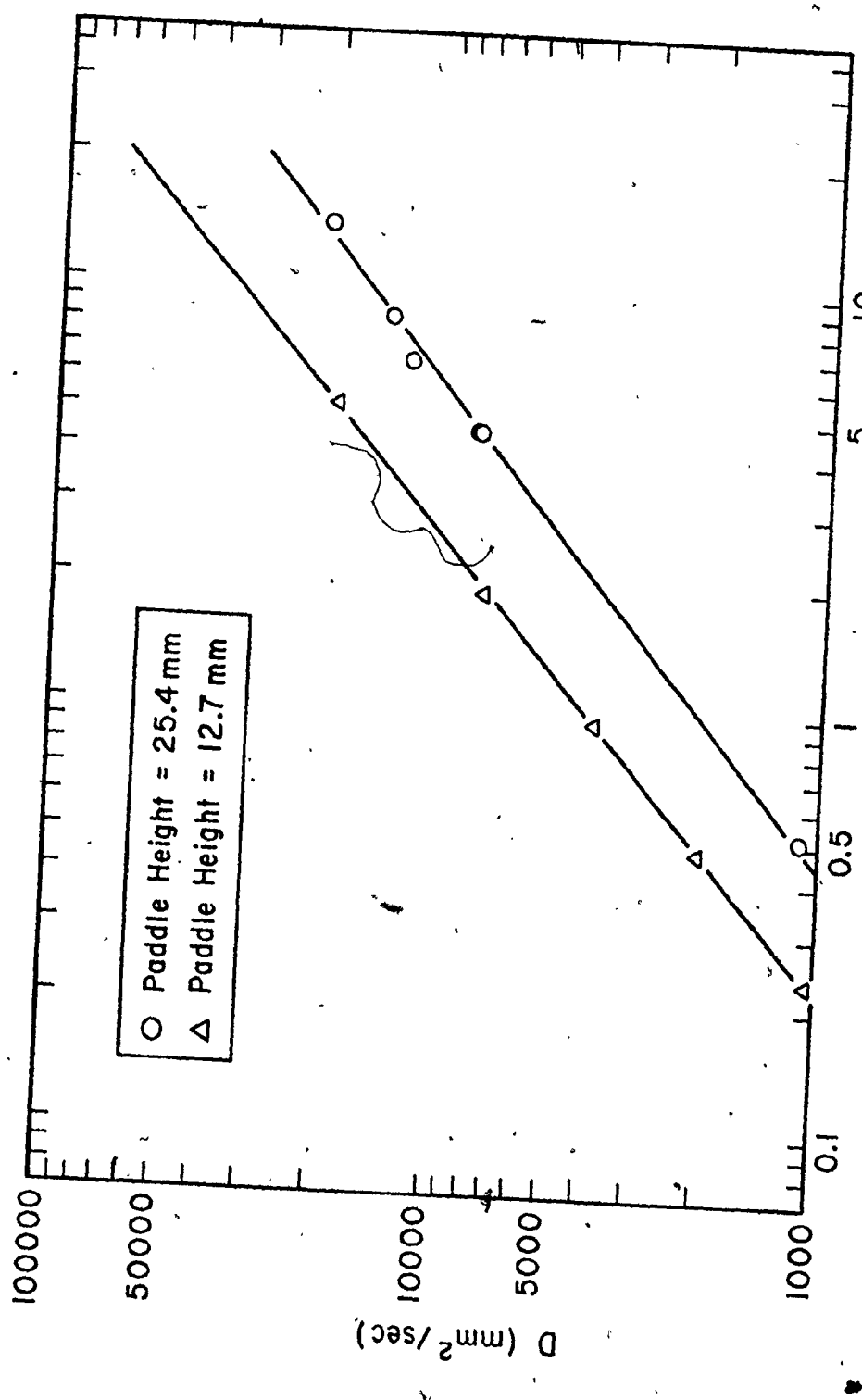

FIGURE 6.4B PLOT OF D VERSUS V_L $(U-U_{mf} = 69$ mm/s)

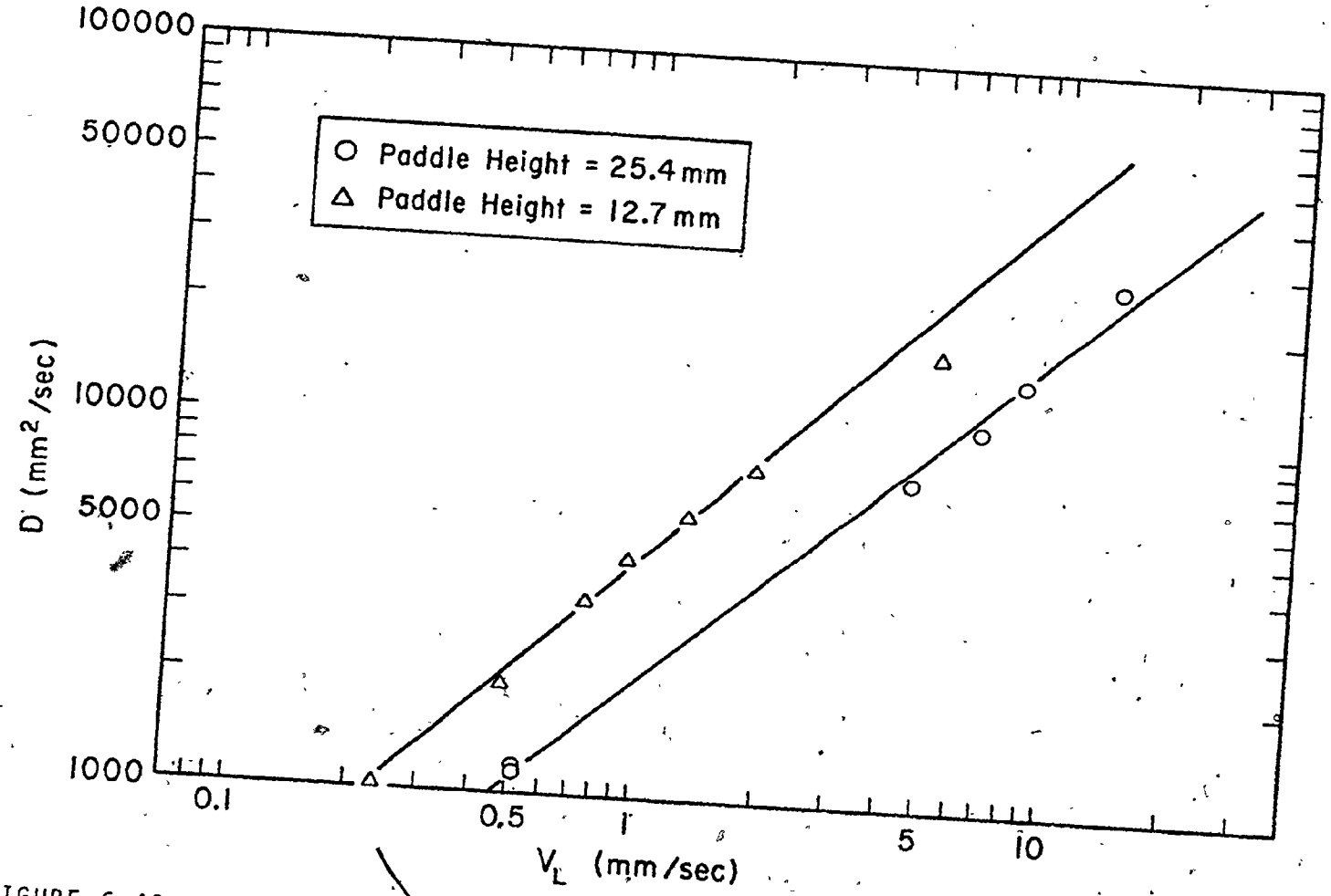

FIGURE 6.4C PLOT OF D VERSUS V_L $(U-U_{mf} = 46$ mm/s)

Table 6.4- Selected Regression Lines of ln(D) Versus ln(CS)

$$D = A_1 \, Exp(A_2 \times \ln(CS)) \qquad (6.23)$$

(A) Series A (Paddle Height = 25.4 mm)

$U-U_{mf}$ (mm/s)	A_1	A_2	CC*
92	642.84	0.7175	0.9987
69	495.45	0.8992	0.9986
46	479.64	0.9169	0.9979

(B) Series B (Paddle Height = 12.7 mm)

$U-U_{mf}$ (mm/s)	A_1	A_2	CC*
92	860.50	0.6387	0.9870
69	442.73	0.9406	0.9999
46	403.97	1.0070	0.9985

* Correlation Coefficient of regression line

Table 6.5 Regression Lines of ln(D) Versus ln(V_L)

$$D = A_1 \text{ Exp}\cdot(A_2 \times \ln(V_L)) \qquad (6.24)$$

(A) Series A (Paddle Height = 25.4 mm)

$U-U_{mf}$ (mm/s)	A_1	A_2	CC*
92	2012	0.7175	0.9987
69	2071	0.8992	0.9986
46	2061	0.9169	0.9979

(B) Series B (Paddle Height = 12.7 mm)

$U-U_{mf}$ (mm/s)	A_1	A_2	CC*
92	3937	0.6387	0.9870
69	4155	0.9406	0.9999
46	4441	1.0069	0.9985

* Correlation Coefficient of regression line

and will therefore contribute to the higher dispersion of the solids at the same chain speed. More theoretical and experimental work is required to better explain the effect of the paddle height, as well as the paddle velocity, on the dispersion of jetsam in the counter-current fluidized cascade.

At this point, the beneficiation ratio can be computed from the estimated values of K, S and the established relationships between diffusivity and paddle speed, using Equations 6.16 and 6.18. The calculated beneficiation ratios were plotted versus paddle speed for the two series of experiments with the 25.4 and the 12.7 mm paddles. The plots are given in Figures 6.5A and B. In general, the plots resemble the statistically fitted curves of Figures 5.4 and 5.5. The fits between the discrete data points and the theoretical curves were reasonable, despite some scattering of the experimental points. The sharp increase in the beneficiation ratio at low paddle speed, followed by a gradual decline at higher paddle speed for the series of experiments with the lower fluidization velocity, as well as the gradual increase in the beneficiation ratio with paddle speed for the series of experiments with the highest fluidization velocity, was predicted by the model of Section 6.2. The model also predicts the existence of an optimal paddle speed where the beneficiation curve reaches a maximum,

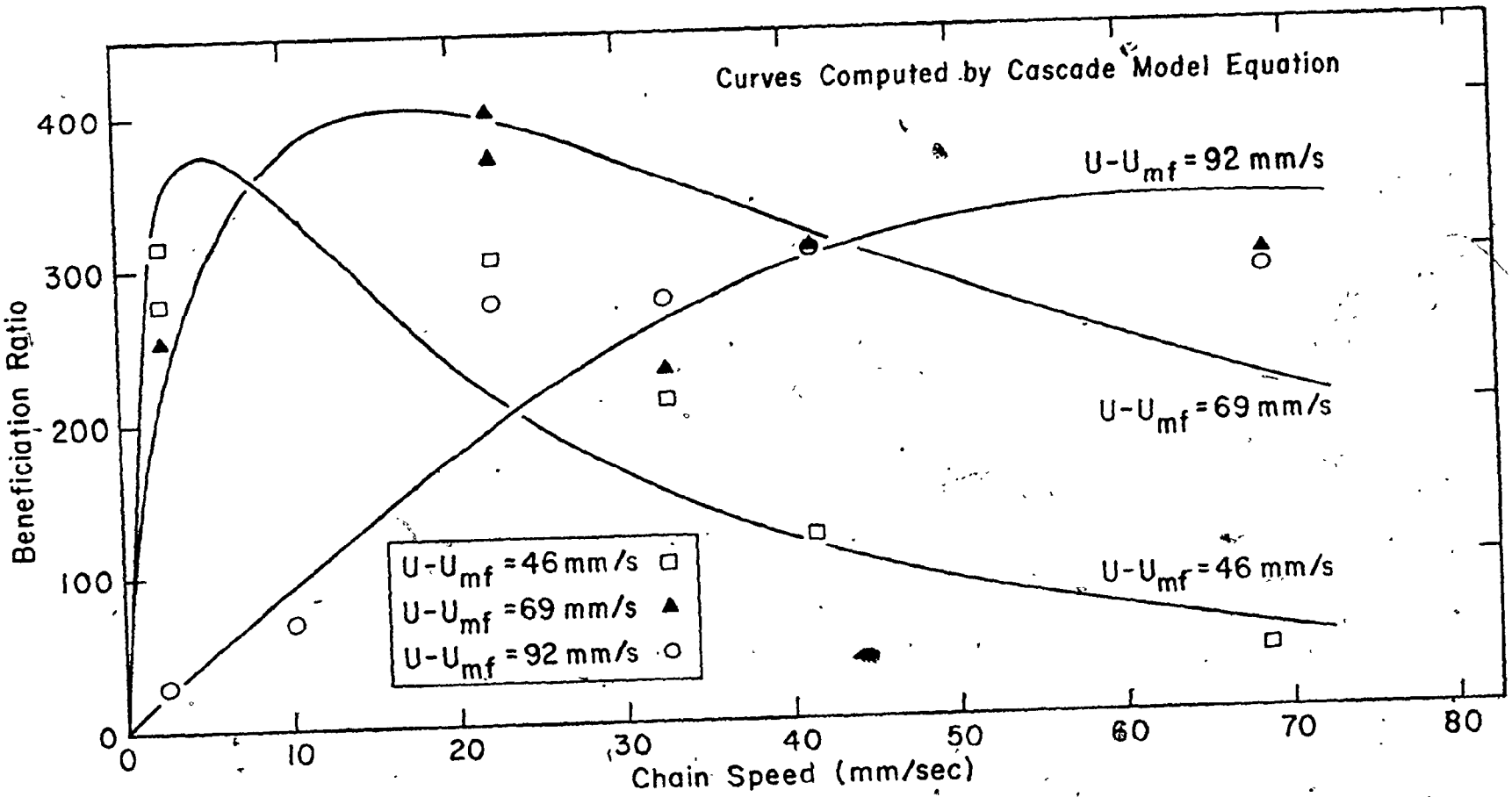

FIGURE 6.5A PLOT OF BR VERSUS CS (SALT-ACTIVATED CHARCOAL SYSTEM) (25.4 mm PADDLES)

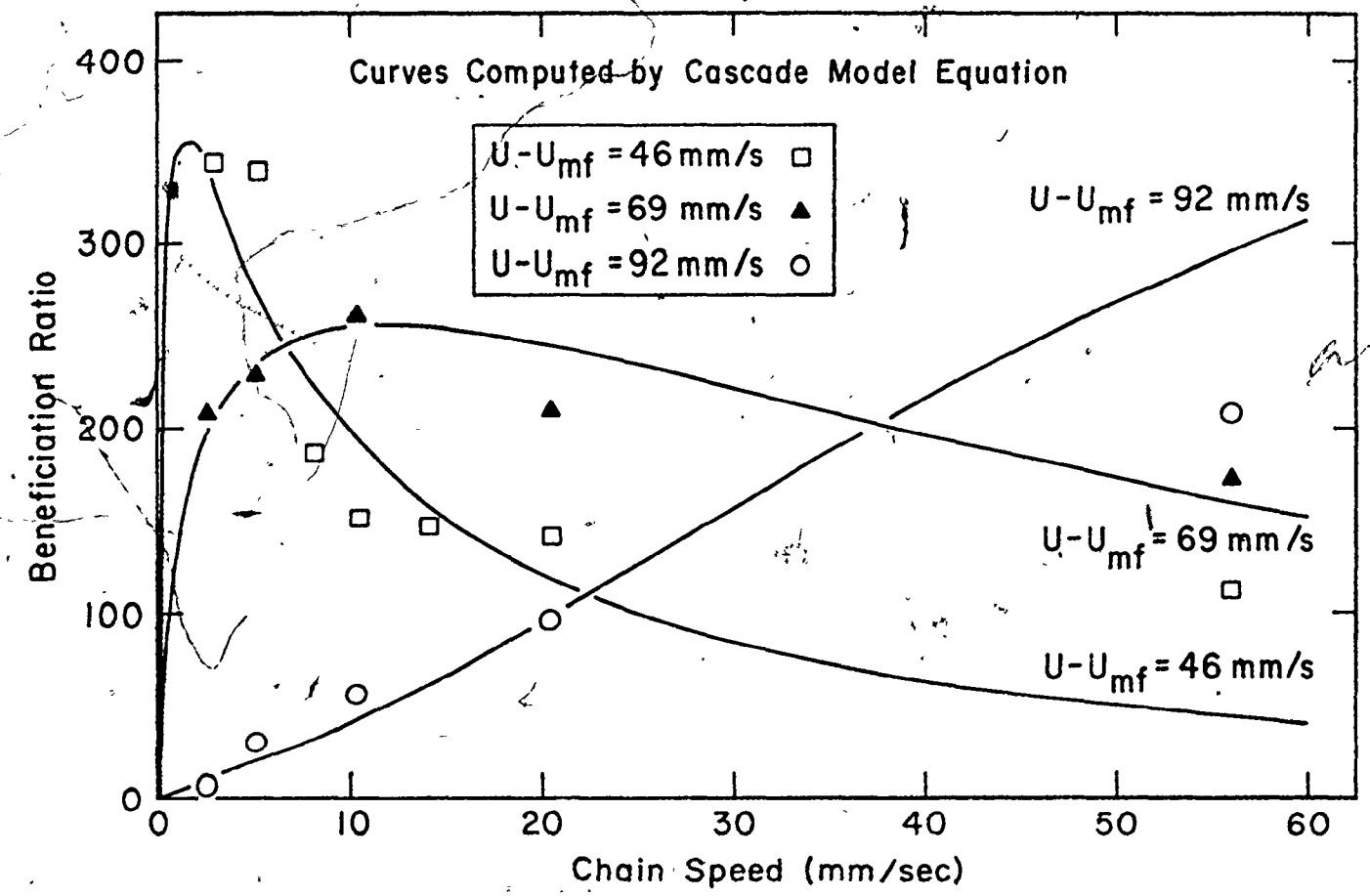

FIGURE 6.5B PLOT OF BR VERSUS CS (SALT-ACTIVATED CHARCOAL SYSTEM) (12.7 mm PADDLES)

in agreement with the experimental data at the same fluidization velocity, i.e., the same K, the model predicted inferior perfomance for the shorter paddles, due to its higher diffusivity which adversely affected the performance of the cascade in the separation of solids.

It therefore appears that the theoretical model presented in Section 6.2 can reasonably describe the separation performance of the cascade. However, it should be remembered that in the development and application of the present theoretical model, assumptions were made because of the absence of experimental measurements. For example, we approximated the neutral plane of the horizontal velocity profile of the fluidized solids in the cascade to be located at the upper edge of the paddles. It is possible that the location of the neutral plane is dependent on the chain speed and fluidization velocity.

When applying the theoretical model to the experimental data of the salt-activated charcoal system, the vertical mass transfer coefficient of jetsam, K, was determined quite subjectively. Experimental measurement of the diffusivity was not available. Otherwise, the procedure for the determination of K could be significantly improved. Furthermore, the validity of approximating the vertical jetsam transport by Equation 6.4 has not been tested. Thus, we should not be overly concerned with the accuracy or the physical significance of the estimated values of paramenter K. The equation was

introduced because of the lack of understanding on the mechanisms of segregation of the jetsam component in fluidized bed. More theoretical and experimental work is neede in order to incorporate into the present theoretical model a better approximation of the vertical transport of jetsam in the cascade.

Despite the assumptions, the present theoretical model appears to be promising. When combined with the concept of linear dependency of the log-log plot of the axial diffusivity versus the horizontal convective velocity of the fluidized solids, the model can reasonable describe the separation performance of the counter-current fluidized cascade in flotsam-rich systems.

CHAPTER SEVEN

CONCLUSIONS AND RECOMMENDATIONS

7.1 Conclusions

The experimental data were in general encouraging in their affirmation of the counter-current cascade as a dry pneumatic device in the separation of solids of different densities.

The fundamental working principle of the cascade is based on the vertical partial segregation of mixed solids of different densities at low fluidization velocity. Separation is enhanced by the counter-current motion in the upper and lower strata of the fluidized bed of solids induced by the sweeping movement of the paddles attached to an endless chain; while one end would be enriched in flotsam, jetsam will concentrate in the opposite end of the cascade.

Multiple regression technique was used to investigate the separation performance of the cascade as a function of the various independent variables. Paddle height, paddle speed and fluidization velocity appeared to be the dominating factors in the cascade separation efficiency. The importance of particle size distribution of the solids was also apparent

in the iron-sand and iron pyrite-coal system. Contrary to segregation in simple fluidized beds, density differences between the components in the binary mixed solids system alone did not always result in good separation in the cascade; solids systems with small mean particle size tend to be difficult to separate, despite the existence of a substantial density difference.

A theoretical model was proposed to describe the performance of the cascade under total reflux conditions. Incorporated into the model is the dependency of turbulent diffusivity on the horizontal flow velocity of the fluidized solids, based on a paper by Beeckmans et al.[81]. Reasonable agreement between the theoretical model and the experimental data is observed.

Application of the cascade in coal beneficiation appeared to be promising. Experiments with the synthetic iron pyrite-coal and natural coal systems have demonstrated the potential of the cascade as a dry coal beneficiation device. In the former system, the removal of coarse pyrite from coal was virtually complete; the removal of fine pyrite, however, was less effective. In the natural coal system, partial removal of ash and pyrite from fine coal was demonstrated. It was also shown that the beneficiation efficiency of the cascade could be improved by a multi-pass process. The purity of the products, however, appeared to be limited by the liberation of the impurities from the

coal matrix.

An explanation is still wanting for the accumulation of jetsam in the reject side of the cascade. The accumulation was especially acute at low fluidization velocity.

7.2 Recommendations

The overall concentration of jetsam in the cascade bed and the bed height are two independent variables whose effect on the cascade performance has not been explored in this study. An experimental program is recommended to study the effect of the aforementioned variables on the performance of the cascade.

The mean sizes and size distributions of both the jetsam and flotsam components in the binary mixed solids system appeared to have a significant effect on the jetsam removal ability of the cascade. The importance of the mean sizes of the components was demonstrated by the experiments with the synthetic iron pyrite-coal system. The investigative work in this area should be expanded in order to gain more fundamental understanding of the cascade. Furthermore, the possibility of alleviating the problem of limited liberation of pyrite and ash from the coal fines by reducing the size of the coal fines should be examined in more detail.

The combined effect of paddle height, paddle speed and fluidization velocity on the performance of the cascade was briefly addressed in the study of the salt-activated charcoal system; this work should be expanded and continued.

The salt-activated charcoal system is a good candidate for experimentation because of the relative ease and accuracy in the analytical procedures. The work in the present study was restricted to total reflux conditions because of the lack of time. Recirculation and/or straight-through experiments should be included as part of a comprehensive experimental program.

Finally, regression analysis on data from the natural coal system indicated that the beneficiation performance of the cascade was insensitive to the throughput rate. New higher capacity feeders and product and reject withdrawal systems would be required to establish the range of throughput rates in which the performance of the cascade would be affected. Throughput rate is of primary importance in coal beneficiation. A more concerted effort should be made for a thorough investigation of this important variable.

APPENDIX A

Sieve Analyses of Granular Solids Systems

A.1 Iron-Sand System

A.1.1 Component Iron

Size Passing (microns)	Greater Than (microns)	Weight Fraction
75	0	0.0024
90	75	0.0035
106	90	0.0297
125	106	0.0610
150	125	0.1697
180	150	0.2380
212	180	0.2494
355	212	0.2466
417	355	0.0001

Geometric Mean Diameter 183 microns
Geometric Standard Deviation 4.021

Sauter Mean Diameter 174 microns

A.1.2 Component Sand

Size Passing (microns)	Greater Than (microns)	Weight Fraction
75	44	0.0001
90	75	0.0006
125	90	0.0208
150	125	0.0443
180	150	0.1025
212	180	0.1859
355	212	0.5695
425	355	0.0621
495	425	0.0146

Geometric Mean Diameter 244 microns
Geometric Standard Deviation 3.739

Sauter Mean Diameter 233 microns

A.2 Iron pyrite-Coal System

A.2.1 Component Pyrites

A.2.1.1 Pyrite A

Size Passing (microns)	Greater Than (microns)	Weight Fraction
44	0	0.1717
90	44	0.3330
106	90	0.1501
125	106	0.1612
150	125	0.1521
180	150	0.0122
208	180	0.0198

Geometric Mean Diameter 74 microns
Geometric Standard Deviation 4.90

Sauter Mean Diameter 59 microns

A.2.1.2 Pyrite B

Size Passing (microns)	Greater Than (microns)	Weight Fraction
90	0	0.3286
150	90	0.2754
212	150	0.2703
250	212	0.1073
300	250	0.1027
425	300	0.0115
600	425	0.0055
701	600	0.0014

Geometric Mean Diameter 117 microns
Geometric Standard Deviation 4.50

Sauter Mean Diameter 92 microns

A.2.1.3 Pyrite C

Size Passing (microns)	Greater Than (microns)	Weight Fraction
90	0	0.2192
150	90	0.3079
212	150	0.2855
250	212	0.1074
300	250	0.0789
425	300	0.0011

Geometric Mean Diameter 125 microns
Geometric Standard Deviation 4.40

Sauter Mean Diameter 102 microns

A.2.1.4 Pyrite D

Size Passing (microns)	Greater Than (microns)	Weight Fraction
44	0	0.0299
106	44	0.2043
150	106	0.1450
212	150	0.2011
300	212	0.1796
425	300	0.1732
600	425	0.0665
701	600	0.0005

Geometric Mean Diameter 174 microns
Geometric Standard Deviation 4.10

Sauter Mean Diameter 131 microns

A.2.1.5 Pyrite E

Size Passing (microns)	Greater Than (microns)	Weight Fraction
150	0	0.2055
250	150	0.4975
300	250	0.0530
425	300	0.0997
600	425	0.0560
1180	600	0.0527
1700	1180	0.0348
1981	1700	0.0008

Geometric Mean Diameter 216 microns
Geometric Standard Deviation 3.90

Sauter Mean Diameter 170 microns

A.2.2 Component Coal

A.2.2.1 Coal A

Size Passing (microns)	Greater Than (microns)	Weight Fraction
125	0	0.0454
212	125	0.2215
355	212	0.2455
425	355	0.0759
707	425	0.2091
850	707	0.0662
1180	850	0.0908
1400	1180	0.0284
1651	1400	0.0173

Geometric Mean Diameter 360 microns
Geometric Standard Deviation 3.40

Sauter Mean Diameter 272 microns

A.2.2.2 Coal B

Size Passing (microns)	Greater Than (microns)	Weight Fraction
53	0	0.0172
90	53	0.0956
106	90	0.0787
125	106	0.0939
150	125	0.1246
180	150	0.1609
212	180	0.2124
250	212	0.1324
355	250	0.0844

Geometric Mean Size 153 microns
Geometric Standard Deviation 4.198

Sauter Mean Diameter 135 microns

A. 3 Natural Coal System

Size Passing (microns)	Greater Than (microns)	Weight Fraction
125	0	0.2104
300	125	0.3596
355	300	0.0925
425	355	0.0882
500	425	0.0716
600	500	0.0687
710	600	0.0577
850	710	0.0336
991	850	0.0176

Geometric Mean Diameter 233 microns
Geometric Standard Deviation 3.79

Sauter Mean Diameter 167 microns

A.4 Salt-Activated Charcoal System

A.4.1 Component Salt

180 microns $\leq D_p \leq$ 250 microns

A.4.2 Component Activated Charcoal

Size Passing (microns)	Greater Than (microns)	Weight Fraction
106	0	0.0003
180	106	0.0007
212	180	0.0018
250	212	0.0258
300	250	0.1552
355	300	0.2457
425	355	0.2625
500	425	0.1829
600	500	0.1184
707	600	0.0066

Geometric Mean Diamter 376 microns
Geometric Standard Deviation 3.321

Sauter Mean Diameter 365 microns

APPENDIX B

Bed Pressure Drop versus Superficial Air Velocity Plots used in The Determinations of U_{mf} for The Various Granular Solids Systems

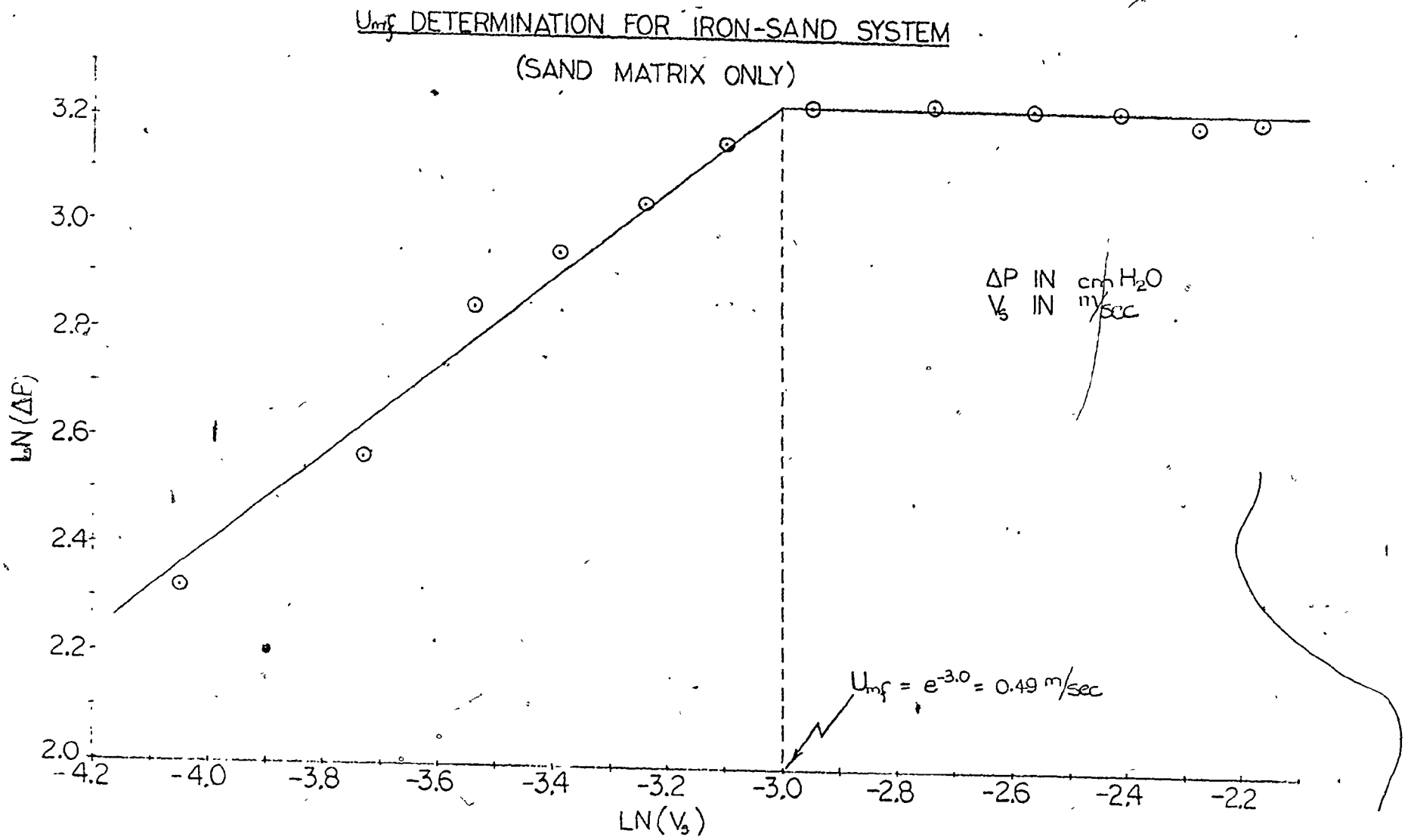
U_{mf} DETERMINATION FOR IRON-SAND SYSTEM
(SAND MATRIX ONLY)
3.2
3.0
2.8
2.6
2.4
2.2
2.0
LN(ΔP)
ΔP IN cm H_2O
V_s IN m/sec
$U_{mf} = e^{-3.0} = 0.49$ m/sec
-4.2
-4.0
-3.8
-3.6
-3.4
-3.2
-3.0
-2.8
-2.6
-2.4
-2.2
LN(V_s)

U_{mf} DETERMINATION FOR IRON-SAND SYSTEM
(5% IRON BY WEIGHT)

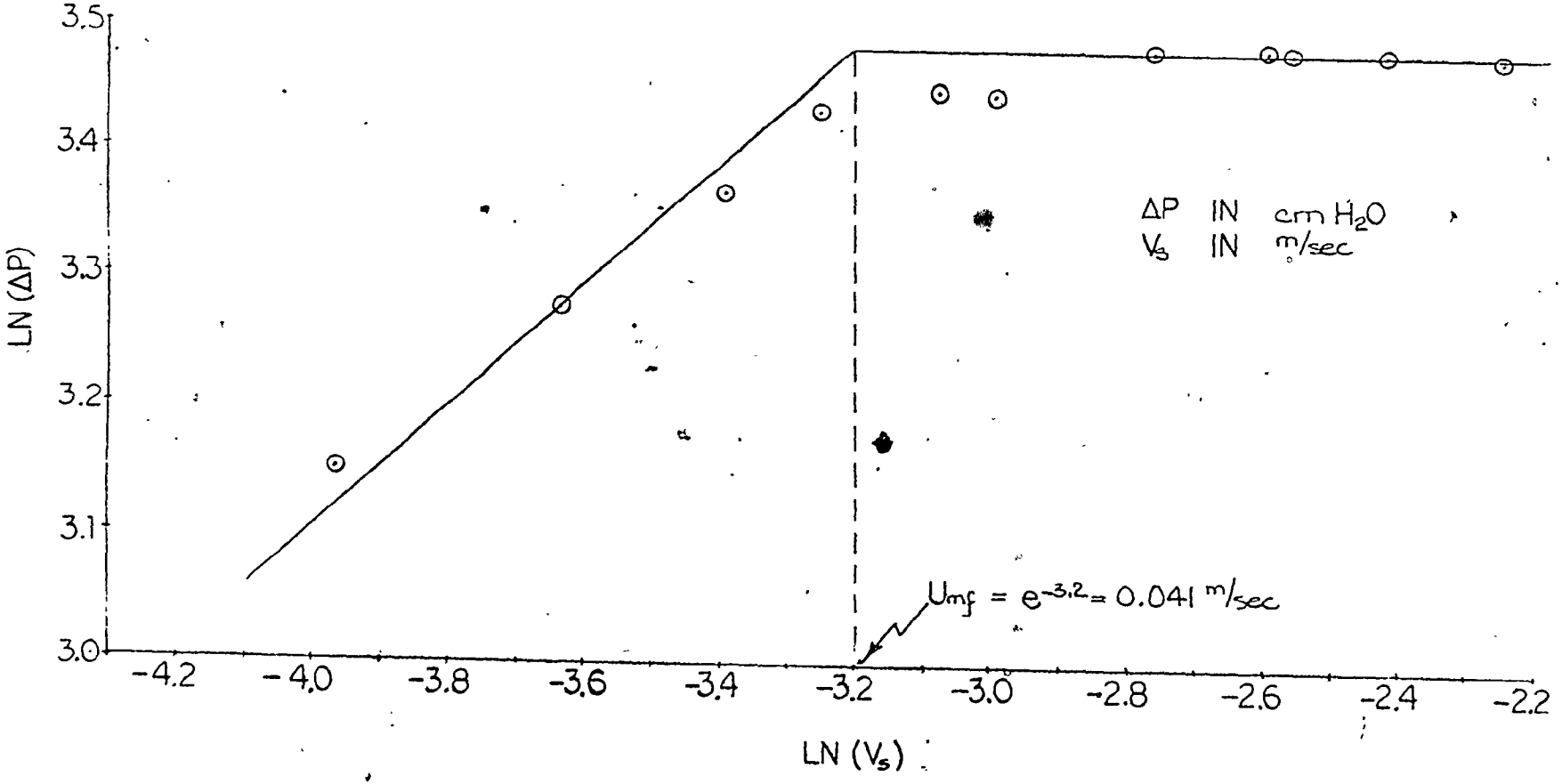

U_{mf} DETEMINATION FOR IRON PYRITE-COAL SYSTEM
(COAL A)

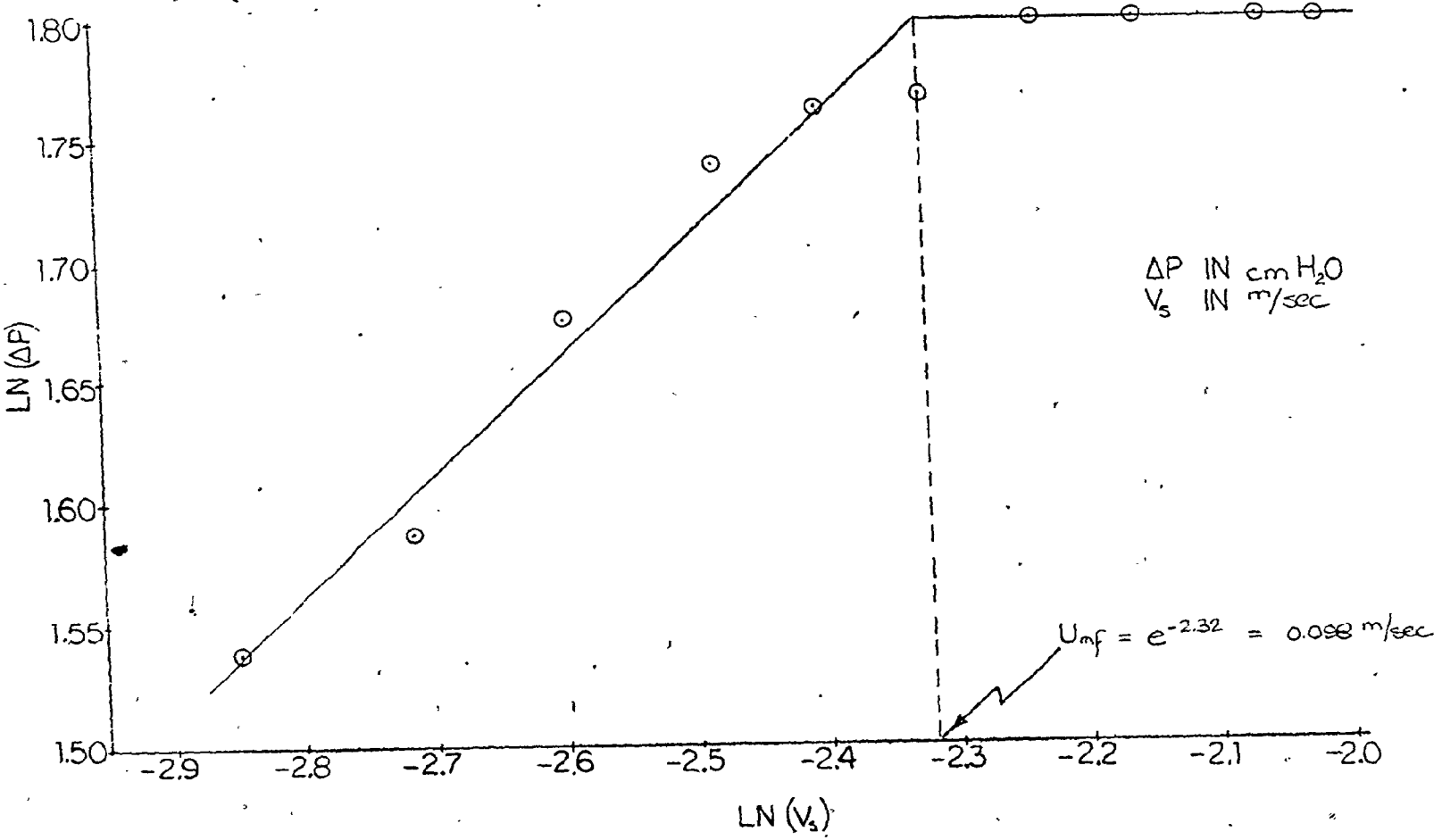

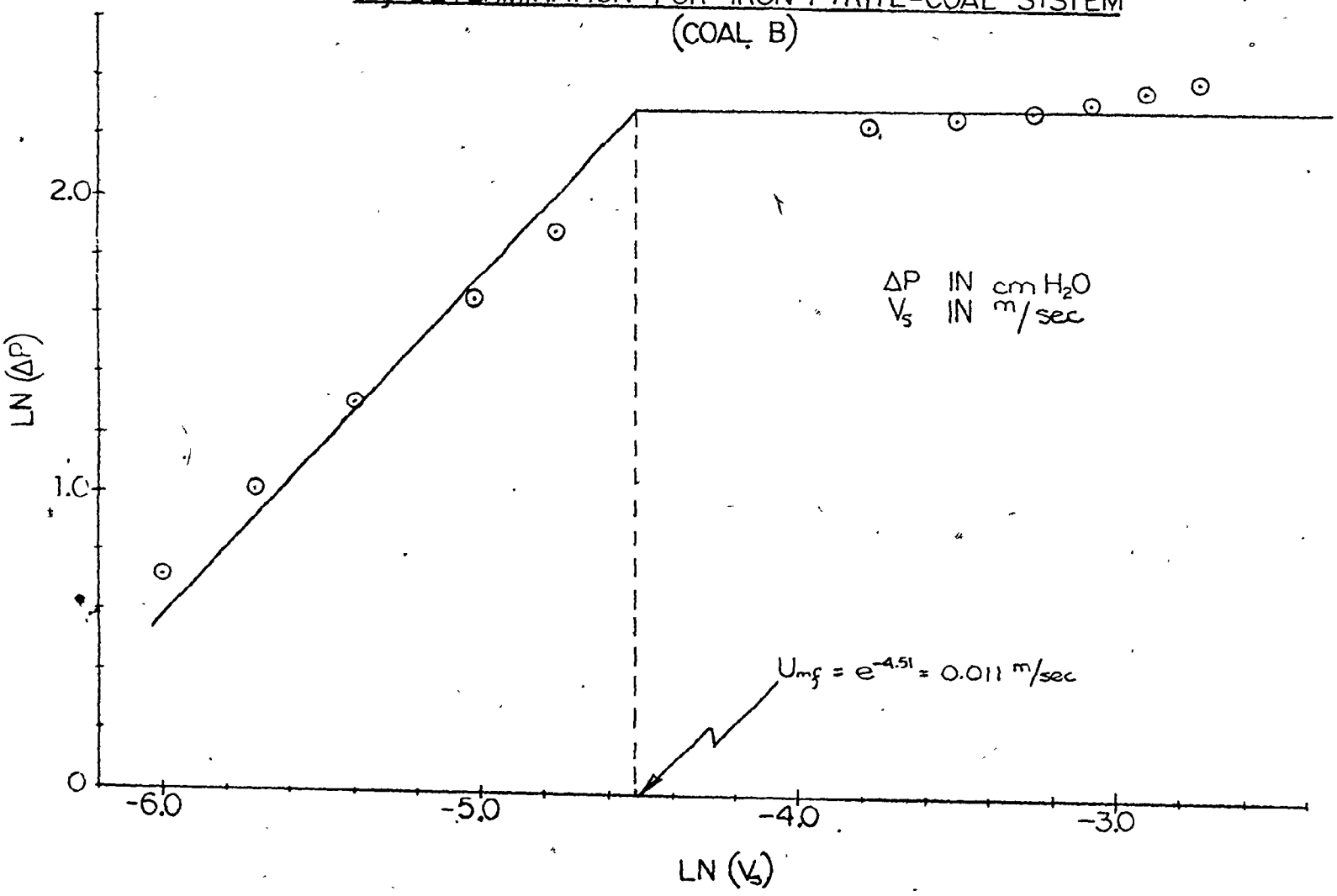
U_{mf} DETERMINATION FOR IRON PYRITE-COAL SYSTEM
(COAL B)
2.0
1.0
0
LN (ΔP)
ΔP IN cm H_2O
V_s IN m/sec
$U_{mf} = e^{-4.51} = 0.011$ m/sec
-6.0
-5.0
-4.0
-3.0
LN (V_s)

U_{mf} DETERMINATION FOR NATURAL COAL SYSTEM

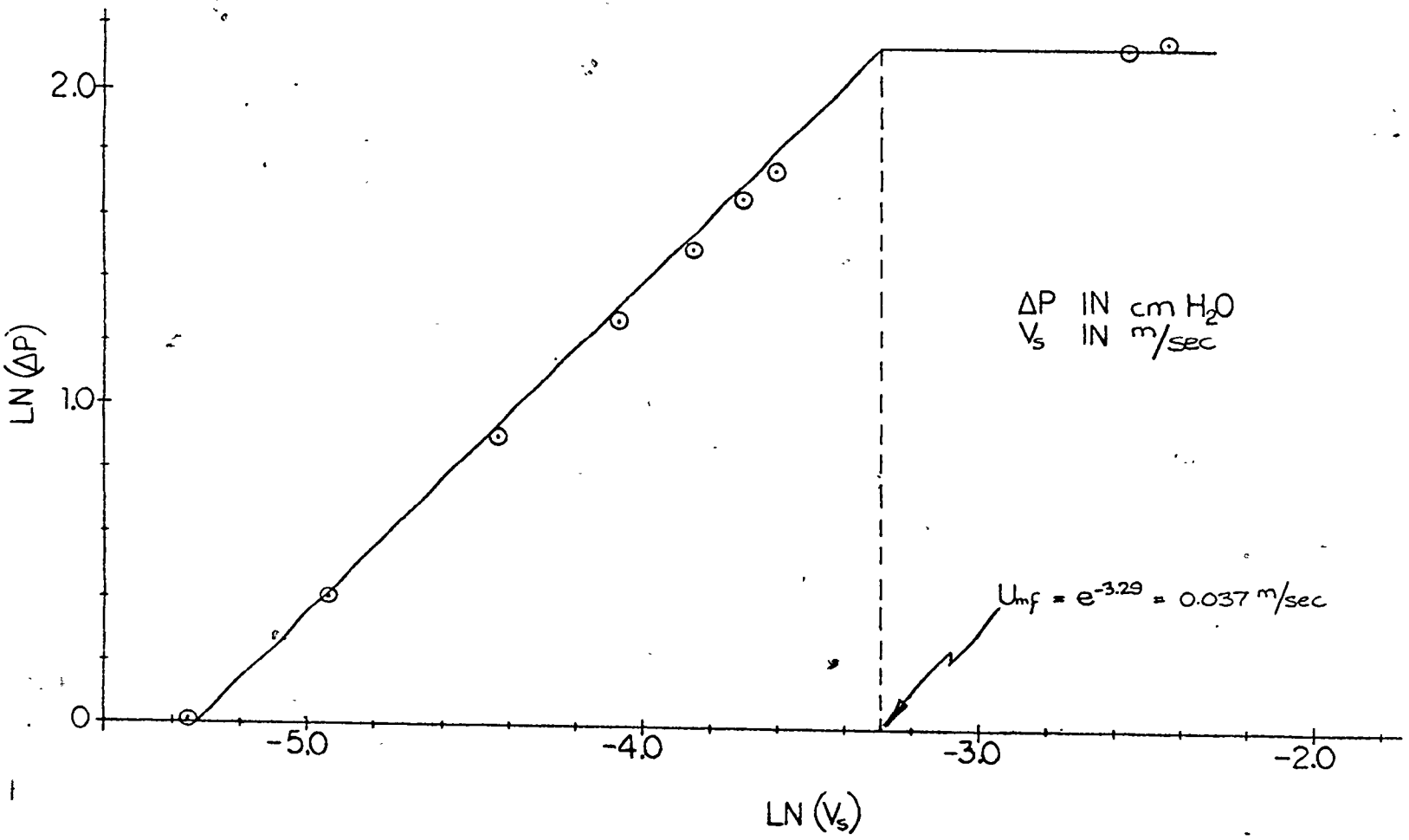

U_{mf} DETERMINATION FOR SALT-ACTIVATED CHARCOAL SYSTEM

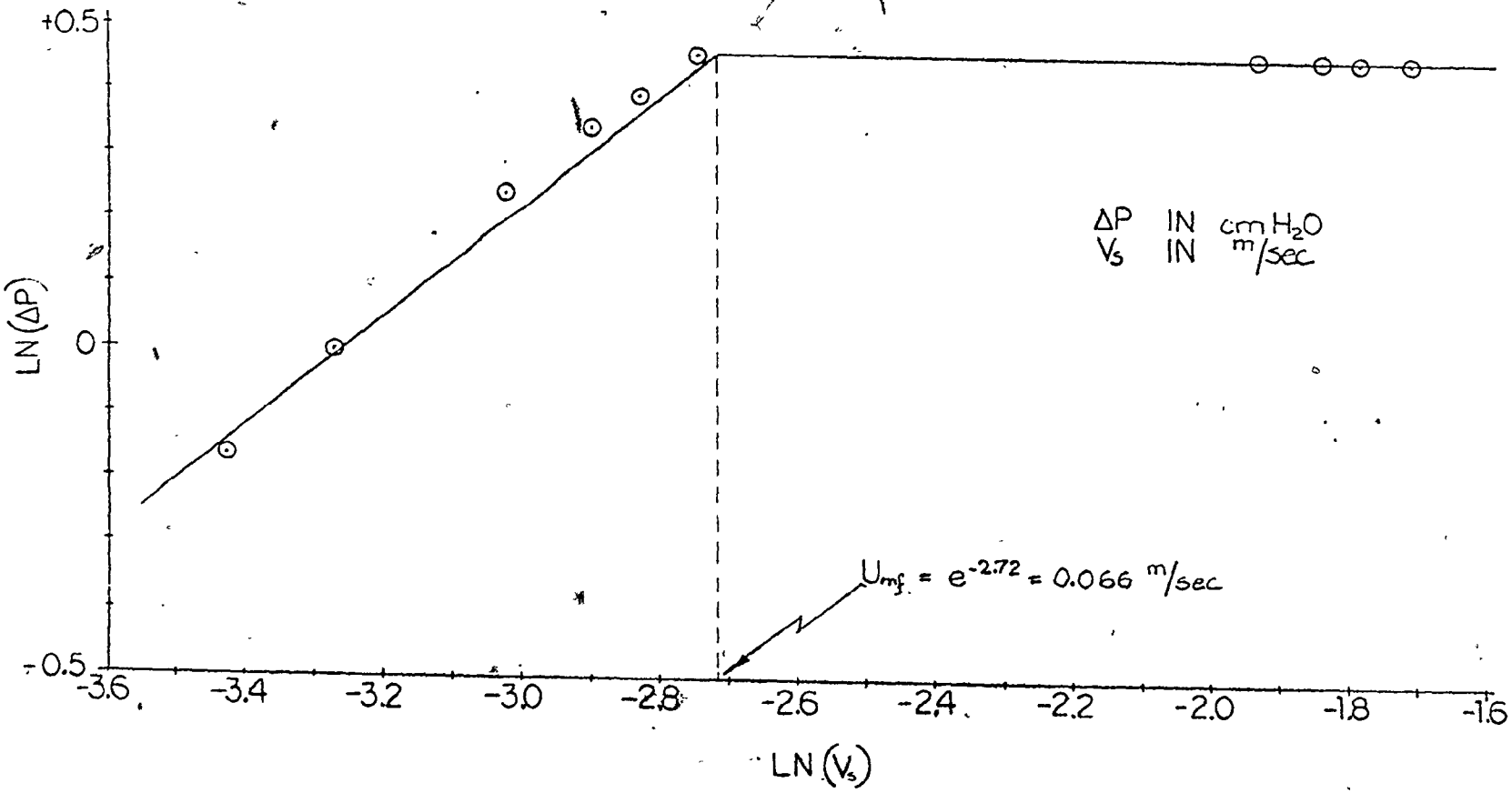

APPENDIX C

Float-Sink Density Analysis for Coal A in Iron pyrite-Coal System

FLOAT-SINK ANALYSIS OF COAL

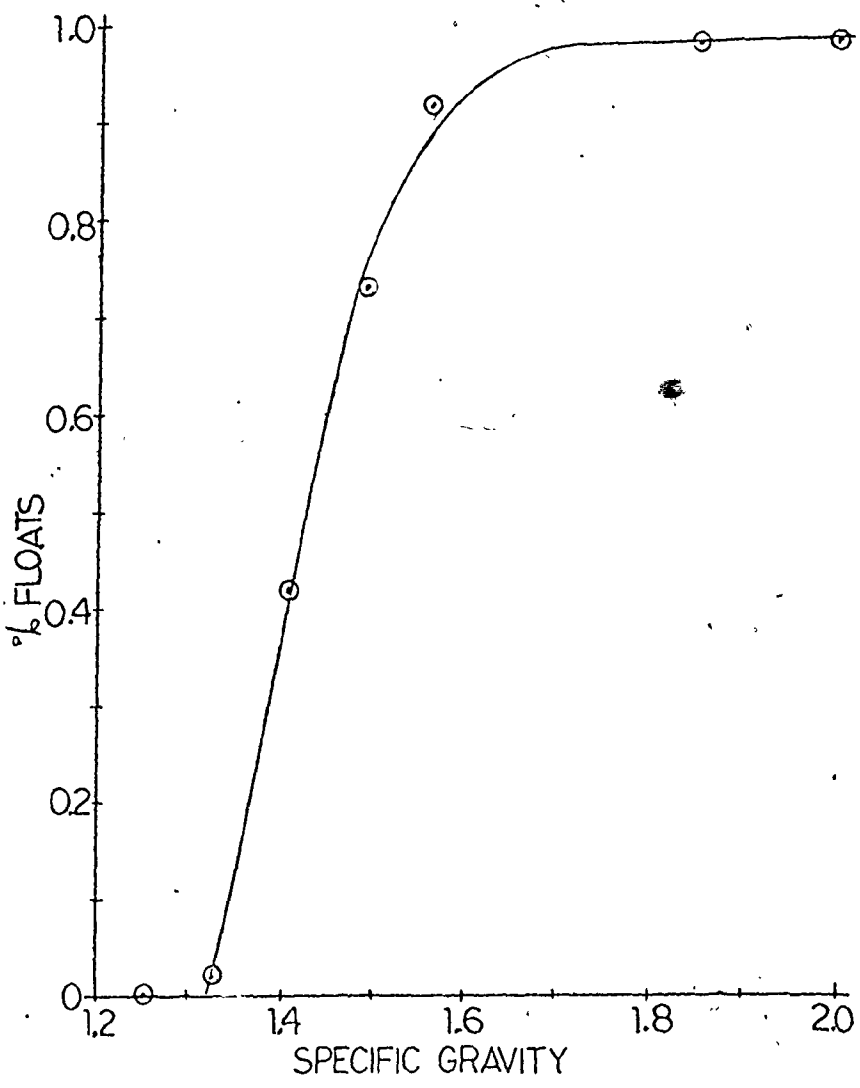

APPENDIX D

Listings of Computer Program SIEV1 used in Sieve Analyses of Granular Solids Systems

PROGRAM SIEV1

SIEVE ANALYSIS PROGRAM SIEV1

```
// FOR
*  LIST SOURCE PROGRAM
*  IOCS(CARD,1403 PRINTER)
C       SIEVE ANALYSIS PROGRAM
C       PROGRAM CALCULATES DISCRETE WEIGHT
C       DISTRIBUTION FUNCTION PSIW, DISCRETE NUMBER
C       DISTRIBUTION FUNCTION PSI, CUMULATIVE
C       WEIGHT FUNCTION FW, SPECIFIC SURFACE,
C       AND VARIOUS POPULATION PARAMETERS FROM
C       RAW SIEVE ANALYSIS DATA.  PROGRAM ALSO
C       CALCULATES POWER LAW SLOPES AT LOWER END OF
C       DISTRIBUTION CURVE
C
C       CARD 1 (I10,3F10.0,10A4)
C       NUMBER OF DATA POINTS, PARTICLE SPECIFIC GRAVITY, SHAPE FACTOR
C       LAMBDA, OPENING SIZE OF SMALLEST SCREEN WHICH
C       PASSES COMPLETE SAMPLE (MICRONS) ,SAMPLE NAME
C       FIRST SET (8F10.0) VALUES OF SCREEN OPENINGS
C       IN MICRONS WHICH RETAIN CUTS I (IN ASCENDING ORDER)
C       SECOND SET (8F10.0) WEIGHTS OF CUTS I
      DIMENSION XM(20),DX(20),PSI(20),W(20),W3(20),X(20),PSIW(20),SW(20)
     1,AK(4) ,ANM(10)
      READ (2,1) N,RHOP,SFAC,XO ,ANM
      WRITE (5,12) ANM
   12 FORMAT (1H1,//20X,'SIEVE ANALYSIS',5X,10A4)
      WRITE (5,13) RHOP,SFAC
   13 FORMAT(//,' PARTICLE SPECIFIC GRAVITY =',F8.2,'   SHAPE FACTOR LAM
     1BDA =',F6.2)
    1 FORMAT(I10,3F10.2,10A4)
      READ (2,2) (X(I),I=1,N)
      READ (2,2) (W(I),I=1,N)
    2 FORMAT (8F10.0)
      WRITE (5,14)
   14 FORMAT (//,'      FRACTION      SIZE PASSING (MICRONS)     GREATER
     1THAN (MICRONS)          WEIGHT          CUMULATIVE WEIGHT FUNCTION'//)
      B =10000.
      WT = 0.
      DO 40 I=1,N
   40 WT = WT+W(I)
      SW(1) =0.
      DO 21  I =2,N
   21 SW(I) =SW(I-1) +W(I-1)/WT
      N1 = N-1
      WRITE (5,15) (I,X(I+1),X(I),W(I),SW(I),I=1,N1)
      WRITE(5,15) N,XO,X(N),W(N),SW(N)
   15 FORMAT (I10,4F24.4)
      DO 10 I=1,N
   10 X(I) =X(I)/B
      XO = XO/B
      DX(N) =XO-X(N)
      XM(N) =(XO +X(N)) /2.
      DO 3  I =1,N1
      XM(I) = (X(I+1)+X(I))*.5
    3 DX(I) = X(I+1)-X(I)
      SUM3 = 0
      DO 4 I=1,N
      W3(I) = W(I)/XM(I)**3
    4 SUM3 = SUM3+W3(I)
      DO 5 I=1,N
      PSIW(I) = W(I)/DX(I)/WT
    5 PSI(I) = W3(I)/DX(I)/SUM3
      B3 = WT/SUM3
      C1 =0
      C2 = 0
      DG =0
      SIGG =0
      DO 6 I=1,N
      DG =DG +PSI(I)*ALOG(XM(I))*DX(I)
      C1 =C1 +PSI(I)*XM(I)*DX(I)
    6 C2 = C2+PSI(I)*XM(I)**2*DX(I)
```

SIEVE ANALYSIS PROGRAM SIEV1 (Continued)

```
      DVA = D3/D2
      S = 6.*SFAC/RHOP/DVA
      D3 = D3**(1./3.)
      D2 = SQRT(D2)
      DG =EXP(DG)
      DO 25   I =1,N
   25 SIGG =SIGG +PSI(I)*(DG -ALOG(XM(I)))**2*DX(I)
      SIGG =SQRT(ALOG(SIGG))
      DO 440   I =1,N
      XM(I) =XM(I)*B
  440 DX(I) =DX(I)*B
      D1 =D1*B
      D2 =D2*B
      D3 =D3*B
      DVA =DVA*B
      DG =DG*B
      WRITE (5,11)
   11 FORMAT(//'      FRACTION      XM(MC)          DX(MC)          PSI
     1        PSIW'//)
      WRITE (5,7) (I,XM(I),DX(I),PSI(I),PSIW(I),I=1,N1)
      WRITE(5,7) N,XM(N),DX(N),PSI(N),PSIW(N)
    7 FORMAT (I10,4E15.4)
      WRITE (5,8) D2,D3,DVA,S
    8 FORMAT (//' MEAN SQUARED DIAMETER =',F10.2,'  MICRONS       MEAN CU
     1BED DIAMETER =',F10.2,'  MICRONS'/'  SAUTER MEAN DIAMETER ='F10.2,
     2 '  MICRONS,        SPECIFIC SURFACE AREA ='F10.2,'  CM2/G')
      WRITE(5,26) D1,DG,SIGG
   26 FORMAT(//,' ARITHMETIC MEAN DIAMETER =',F10.2,'  MICRONS       GEOM
     1ETRIC MEAN DIAMETER ='F10.2,'  MICRONS'/'  GEOMETRIC STANDARD DEVI
     2ATION ='F10.4)
      AW = W(N)
      BW = X(N)
      DO 30 I=1,4
      J = N-I
      AV = W(J)
      BV = X(J)
   30 AK(I) = (ALOG(AW)-ALOG(AV))/(ALOG(BW)-ALOG(BV))-1.
      WRITE (5,31)AK
   31 FORMAT (//20X,' K PARAMETER ESTIMATES'/5X,4E12.4)
      STOP
      END
```

APPENDIX E

Sulphur Analysis by X-Ray Fluorescence Techniques

E.1 Sample Preparation

Because the X-Rays emitted from the X-Rays Fluorescence machine can only penetrate the surface of the sample to a depth of 1/100 microns, the surface of the sample should be homogeneous and representative of the entire sample. Error can be minimized if the grain size of the sample is at most 1/5 of the penetration depth. Thus, all the samples were ground in a tungsten ball mill using tungsten balls. The grinding time was always kept at fifteen minutes per sample in order to be consistent. The ground coal powder was then pelletized at high pressure in an aluminum cap.

E.2 Count Measurements

Using the lithium flouride crystal, the angle for sulphur determination was taken at 46.15 degrees. Background reading was taken at 47.5 degrees. The counting period was kept at 20 seconds. After taking the reading at 46.15 degrees for each sample, the pure sulphur reference was rotated in place, and the count rate was again taken. This procedure was to minimize the effect of drift within the apparatus. The background count rate for the sample and the pure sulphur reference were then taken by setting the angle of incidence at 47.5 degrees. The procedures were repeated for each sample.

To calculate the sulphur content of the samples, Equations 3.1, 3.2, 3.3 or 3.4 were used. (see Section 3.3.5) The normalized X-ray count, I* in the equations, was calculated by Equation E.1.

$$I^* = (I-I_B)/(I-I_B)_S \times 100 \qquad (E.1)$$

In Equation E.1, $(I-I)$ and $(I-I_B)_S$ are the differences in the scintillation count rates between the principal and the background radiation for the sample and for the pure sulphur reference respectively. The count rates were measured in photons/sec..

APPENDIX 'F

Calculation of the Concentration of Pyritic Sulphur on an Ash Free Basis

Variables	Definitions
P	Pyrite fraction, as is
M	Minerals fraction, excluding pyrites, as is
C	Carbon fraction, as is
S	Total sulphur, as is
S_o	Organic sulphur, as is
S_p	Pyritic sulphur, as is
A	Weight fraction of ash after combustion

(all primed quantities imply on an ash free basis)

$$1 = P + M + W + C \qquad (F.1)$$

Molecular weight of pyrite (FeS_2) = 119.97

Molecular weight of sulphur (S) = 32.06

Molecular weight of Fe_2O_3 = 159.70

After ashing the coal sample, the pyrites will be oxidized to iron oxide, Fe_2O_3. The reaction is

$$2FeS_2 \rightarrow 7/2O_2 + Fe_2O_3 + 2SO_2$$

Thus,

$$P/S_p = 119.97/(32.06X2) = 1.871$$

$$P = 1.871 S_p \qquad (F.2)$$

$$S = S_o + S_p \qquad (F.3)$$

$$A = (159.7)/(119.97X2)\ P + M \qquad (F.4)$$

By substitution, using Equation F.2,

$$A = 1.244\ S_p + M$$

By rearrangement,

$$M = A - 1.244 S_p \qquad (F.5)$$

Substituting into Equation F.1 and rearranging,

$$W + C = 1 - 0.627\ S_p - A \qquad (F.6)$$

On an ash free basis, the organic sulphur

$$S_o' = S_o / (1 - 0.627\, S_p - A) \qquad (F.7)$$

$$S_p' = S_p / (1 - 0.627\, S_p - A) \qquad (F.8)$$

But,

$$S_p = S - S_o = S - S_o' (1 - 0.627\, S_p - A) \qquad (F.9)$$

By rearranging Equation F.9 ,

$$S_p = \frac{S - S_o' (1 - A)}{(1 - 0.627\, S_o')} \qquad (F.10)$$

Since S_o' is known, Table 5.7, Equation F.10 can be used to calculate S_p . Using Equation F.8, the pyritic sulphur on an ash free basis, S_p' , can be calculated.

Note that Equations F.10 and F.8 are identical to Equations 3.5 and 3.6 of Chapter 3.

APPENDIX G

Mass Balance Considerations on Ash and Pyritic Sulphur in Natural Coal System

The exponential concentration profile of the jetsams (ash or pyritic sulphur), can be expressed in Equation G.1.

$$C = C_0 \, EXP(A_1 \, Z) \qquad (G.1)$$

In Equation G.1, C is the jetsam concentration in the normalized axial position of Z, C_0 is the jetsam concentration in the flotsam end of the cascade at $Z = 0$, and A_1 is the empirical constant corresponding to the slope of the LN(C) versus Z regression line.

Integration of Equation G.1 should yield the total mass of jetsam in the cascade bed. The integrated mass of jetsam in the cascade bed, M_1 , can be calculated by Equation G.2 ;

$$M_1 = V_b \, / \, LN(C_1 \, / \, C_0) \, X \, (C_1 - C_0) \qquad (G.2)$$

where V_b is the volume of the cascade bed, and C_1 and C_0 are the jetsam concentration in the reject and product ends of the cascade respectively. All the concentrations are expressed in weight of jetsam per unit bed volume.

The total mass of jetsam in the auger wells, M_2 , can be calculated by using Equation G.3;

$$M_2 = V_a (C_1 + C_0) \qquad (G.3)$$

where V_a is the volume of the solids hold-up in the auger wells. From experiment, it was determined that

$$V_a = 0.045 \, V_b \, . \qquad (G.4)$$

Thus, the total mass of jetsam in the entire system equals the sum of M_1 and M_2 and can be calculated by Equation G.5.

$$\text{Total Jetsam Mass} = M_1 + M_2$$

$$= V_b \, X \, ((C_1 - C_0)/LN(C_1/C_0) + 0.045(C_1 + C_0)) \qquad (G.5)$$

Since all the concentration data in this thesis were expressed in mass percentages, to use Equation G.5, the mass percentages of the reject and product stream, c_1 and c_0, must first be converted to C_1 and C_0 on a per unit bed volume basis. The conversion can be performed by using Equation G.6a and b.

$$C_1 = c_1 / (c_1/\rho_j + (100 - c_1)/\rho_f) \qquad \text{(G.6a)}$$

$$C_0 = c_0 / (c_0/\rho_j + (100 - c_0)/\rho_f) \qquad \text{(G.6b)}$$

In Equations G.6a and G.6b, ρ_j, ρ_f are the bulk densities of the jetsam and flotsam components respectively.

APPENDIX H

Calculation of Superficial Velocity by the Orifice Equation (13)

In all of the experiments run for this research project, sharp-edged orifice plates were used to monitor the air flowrates through the pipes. From these data the volumetric flow in any particular run could be determined with the aid of the orifice equation (67).

$$Q_{ori} = C_o \, Y \, A_2^* \left[\frac{2 \, \Delta P_{ori}}{\rho_G (1-\beta^4)} \right]^{\frac{1}{2}} \qquad \ldots(H.1)$$

where Q_{ori} = actual volumetric flowrate of gas upstream from the orifice plate

A_2 = orifice cross-sectional area

ΔP_{ori} = orifice pressure drop

Y = expansion factor

C_o = discharge coefficient

β = D_{ORF}/D_p where D_{ORF} is the diameter of the orifice opening

The expansion factor Y is described by (for air)

$$Y = 1 - \frac{1 - P_{UP\ ORF}/P_{D\ ORF}}{1.404} \left[0.41 + 0.35\beta^4 \right]$$

The discharge coefficient C_o is a function only of β for orifice Reynolds numbers ($4\rho_g \, Q_{ORF}/\mu \, D_{ORF} \, \pi$) greater than 10^4 and can be expressed as -

$$C_o = 0.5798\ e^{0.1195\beta} \qquad \ldots(H.2a)$$

for $0.22 < \beta < 0.45$

and

$$C_o = 0.4429\ e^{0.4429\ \beta} \qquad \ldots(H.2b)$$

for $0.45 < \beta < 0.70$

The actual flow at the grid was found using equation B.3

$$Q_G = \frac{(P_{UP\ ORF})\ (Q_{ORF})}{(P_{ATM} + P_G)} \qquad \ldots(H.3)$$

Actual superficial velocities at the grid were computed from either Equation B.1 or B.3 by substituting Q_G into

$$u = \frac{Q_G}{A} \qquad \ldots(H.4)$$

where A is the chamber cross-sectional area in the cascade.

A computer program written for a TI-57 calculator was used to carry out this calculation.

APPENDIX I

Data from Salt-Activated Charcoal System

Run #1

paddle height = 25.4 mm
u-umf = 92 mm/sec
chain speed = 68.58 mm/sec

section	1	2	3	4
umf(mm/sec)=	46	44	37.3	32

sieve analysis (sample weight in grams)

size (micron)	1	2	3	4	5	6	7	8
600	.12	.12	.27	.31	.32	.31	.37	.50
500	3.76	4.16	6.07	6.95	6.89	9.81	12.67	15.09
425	9.56	10.19	13.27	14.47	16.17	18.83	20.21	25.73
355	19.65	20.71	24.35	23.01	24.28	25.08	27.73	29.22
300	24.10	23.38	22.48	23.72	22.26	21.60	20.95	22.82
0	21.11	21.88	20.82	18.56	18.41	17.94	17.47	20.81

sample	distance z	% salt	geom. mean (micron)	standard deviation
1	0.875	0.0934	296.8	3.550
2	0.767	0.0582	297.6	3.547
3	0.604	0.1557	312.5	3.500
4	0.513	0.2317	321.3	3.473
5	0.406	0.4764	324.7	3.463
6	0.319	0.7870	335.2	3.432
7	0.185	1.4404	344.4	3.406
8	0.123	2.3803	344.9	3.404

Run #2

paddle height = 25.4 mm
u-umf = 92 mm/sec
chain speed = 41.45 mm/sec

section =	1	2	3	4
umf(mm/sec)=	46	44	37.3	32

sieve analysis (sample weight in grams)

size (micron)	1	2	3	4	5	6	7	8
600	.23	.20	.13	.21	.26	.41	.35	.36
500	4.18	4.82	5.32	6.70	7.73	9.36	10.21	11.12
425	10.20	11.05	12.76	14.00	15.98	18.58	19.63	19.33
355	21.31	20.80	21.67	23.89	22.54	23.77	23.71	25.23
300	22.90	24.38	22.04	20.80	22.32	21.46	20.17	20.73
0	19.83	20.07	19.38	18.97	17.69	18.81	18.73	17.84

sample	distance z	% salt	geom. mean (micron)	standard deviation
1	0.868	0.0669	303.8	3.527
2	0.732	0.0576	305.8	3.521
3	0.645	0.0899	311.4	3.503
4	0.520	0.1934	319.1	3.479
5	0.395	0.4120	326.8	3.456
6	0.281	0.7591	331.1	3.444
7	0.192	1.2470	334.0	3.435
8	0.138	1.6586	338.6	3.422

Run #3

paddle height = 25.4 mm
u-umf = 92 mm/sec
chain speed = 32.66 mm/sec

section =	1	2	3	4
umf(mm/sec)=	46	44	37.3	32

sieve analysis (sample weight in grams)

size (micron)	1	2	3	4	5	6	7	8
600	.15	.12	.23	.23	.26	.33	.54	.58
500	3.91	4.39	4.80	6.45	6.94	8.13	9.42	11.78
425	10.22	11.09	11.53	14.60	14.88	17.38	18.64	21.75
355	20.53	21.65	22.27	22.24	22.65	22.69	24.36	24.32
300	21.29	22.38	21.03	22.13	21.13	19.91	19.07	20.23
0	20.12	18.92	19.93	20.52	19.14	18.53	19.03	19.54

sample	distance z	% salt	geom. mean (micron)	standard deviation
1	0.894	0.0383	300.9	3.537
2	0.786	0.0596	308.1	3.514
3	0.645	0.0879	307.4	3.516
4	0.503	0.2645	314.1	3.495
5	0.418	0.3851	319.6	3.478
6	0.305	0.6720	327.3	3.455
7	0.222	1.1552	331.4	3.443
8	0.140	2.1604	337.7	3.425

Run #4

paddle height = 25.4 mm
u-umf = 92 mm/sec
chain speed = 22.35 mm/sec

section =	1	2	3	4
umf(mm/sec)=	46	44	37.3	32

sieve analysis (sample weight in grams)

size (micron)	1	2	3	4	5	6	7	8
600	.16	.14	.19	.37	.24	.42	.30	.39
500	3.98	4.50	5.54	6.44	6.46	7.48	8.12	10.16
425	10.54	11.29	12.70	14.33	14.05	15.66	17.76	20.52
355	20.52	20.94	21.54	23.46	22.95	22.61	22.12	24.39
300	23.52	22.34	22.63	21.03	22.67	22.19	21.70	18.62
0	18.03	19.75	19.37	19.48	17.98	17.50	18.17	20.32

sample	distance z	% salt	geom. mean (micron)	standard deviation
1	0.897	0.0444	308.1	3.513
2	0.785	0.0567	305.7	3.521
3	0.618	0.1248	312.0	3.501
4	0.479	0.2815	317.7	3.484
5	0.435	0.3741	321.1	3.473
6	0.310	0.7011	326.9	3.456
7	0.227	1.1865	328.3	3.452
8	0.140	2.1359	331.0	3.444

Run #5

paddle height = 25.4 mm
u-umf = 92 mm/sec
chain speed = 10.16 mm/sec

section	1	2	3	4
umf(mm/sec)=	46	44	37.3	32

sieve analysis (sample weight in grams)

size (micron)	1	2	3	4	5	6	7	8
600	.07	.10	.12	.17	.15	.19	.19	.24
500	4.01	4.09	4.39	5.29	5.27	5.43	5.78	6.48
425	10.94	12.14	12.19	13.26	13.64	14.16	14.76	15.56
355	20.38	21.84	21.52	22.96	21.51	22.07	22.75	23.69
300	22.94	22.50	21.84	22.17	21.74	21.62	21.26	20.28
0	19.06	18.74	18.53	18.30	18.73	19.10	19.77	20.52

sample	distance z	% salt	geom. mean (micron)	standard deviation
1	0.868	0.0680	305.3	3.522
2	0.784	0.1030	309.7	3.509
3	0.645	0.1561	310.7	3.505
4	0.538	0.3094	316.4	3.488
5	0.420	0.4688	314.3	3.494
6	0.309	0.6866	315.0	3.492
7	0.222	1.0270	315.2	3.491
8	0.139	1.5558	316.4	3.488

Run #6

paddle height = 25.4 mm
u-umf = 92 mm/sec
chain speed = 2.54 mm/sec

section	1	2	3	4
umf(mm/sec)=	39.32	39.32	39.32	39.32

sieve analysis (sample weight in grams)

size (micron)	1	2	3	4	5	6	7	8
600	.16	.23	.20	.18	.23	.25	.20	.23
500	4.83	5.55	5.49	5.39	5.42	6.07	5.40	6.94
425	12.77	13.87	13.63	13.68	13.80	14.52	13.62	16.15
355	21.83	23.03	22.03	23.01	22.48	22.45	22.49	23.30
300	23.56	22.47	23.01	21.92	21.97	21.76	20.87	22.40
0	17.79	18.11	18.25	20.34	17.83	19.27	19.28	19.49

sample	distance z	% salt	geom. mean (micron)	standard deviation
1	0.868	0.1480	315.4	3.491
2	0.701	0.3440	318.6	3.481
3	0.614	0.3325	316.9	3.486
4	0.505	0.5428	311.5	3.503
5	0.420	0.7150	318.6	3.481
6	0.307	0.9704	316.8	3.486
7	0.223	1.1137	313.8	3.496
8	0.138	1.6937	320.8	3.474

Run #7

paddle height = 25.4 mm
u-umf = 69 mm/sec
chain speed = 68.58 mm/sec

section =	1	2	3	4
umf(mm/sec)=	46	44	37.3	32

sieve analysis (sample weight in grams)

size (micron)	1	2	3	4	5	6	7	8
600	.11	.07	.13	.19	.17	.21	.21	.31
500	2.36	3.04	3.69	5.14	6.05	7.31	8.14	9.58
425	7.36	8.63	10.48	12.85	15.14	17.14	18.34	21.03
355	18.11	18.79	19.48	22.77	21.97	22.68	25.42	28.19
300	22.18	23.18	23.85	22.95	23.50	24.64	21.25	21.74
0	21.75	21.06	19.68	18.81	17.46	17.24	16.43	18.89

sample	distance z	% salt	geom. mean (micron)	standard deviation
1	0.895	0.0406	285.0	3.589
2	0.785	0.0742	292.1	3.565
3	0.671	0.1040	301.7	3.534
4	0.559	0.1908	314.0	3.495
5	0.451	0.3813	322.4	3.469
6	0.368	0.6289	328.8	3.450
7	0.276	0.9861	336.0	3.429
8	0.141	1.9512	336.2	3.429

Run #8

paddle height = 25.4 mm
u-umf = 69 mm/sec
chain speed = 41.45 mm/sec

section	=	1	2	3	4
umf(mm/sec)	=	46	44	37.3	32

sieve analysis (sample weight in grams)

size (micron)	1	2	3	4	5	6	7	8
600	.09	.12	.09	.19	.32	.31	.38	.53
500	2.53	3.07	3.59	5.23	6.20	7.66	9.55	11.00
425	7.90	8.67	9.62	12.96	14.38	17.78	20.82	22.44
355	18.33	19.07	20.23	22.73	21.45	24.15	26.21	28.18
300	22.15	21.08	22.77	22.79	23.32	20.56	22.22	21.32
0	20.17	22.11	20.06	19.04	17.13	18.63	17.74	18.68

sample	distance z	% salt	geom. mean (micron)	standard deviation
1	0.906	0.0308	290.8	3.569
2	0.796	0.0492	289.0	3.576
3	0.684	0.0727	299.3	3.542
4	0.571	0.1479	313.7	3.496
5	0.459	0.2752	322.7	3.469
6	0.324	0.5708	327.5	3.454
7	0.212	1.1578	338.2	3.423
8	0.123	2.2828	341.1	3.415

Run #9

paddle height = 25.4 mm
u-umf = 69 mm/sec
chain speed = 32.66 mm/sec

section	1	2	3	4
umf(mm/sec)=	46	44	37.3	32

sieve analysis (sample weight in grams)

size (micron)	1	2	3	4	5	6	7	8
600	.10	.10	.15	.20	.22	.26	.42	.37
500	2.46	2.83	3.65	4.57	5.24	7.59	8.83	9.87
425	7.04	7.80	9.92	12.02	12.78	16.81	18.51	22.02
355	16.03	18.27	19.59	21.84	22.62	23.73	26.83	26.56
300	20.68	20.48	24.48	21.53	22.23	22.39	20.72	21.78
0	19.16	18.47	20.44	21.59	19.57	17.62	17.53	17.37

sample	distance z	% salt	geom. mean (micron)	standard deviation
1	0.905	0.0402	288.1	3.578
2	0.811	0.0430	295.4	3.554
3	0.697	0.0672	299.0	3.542
4	0.585	0.0965	302.9	3.530
5	0.506	0.1839	311.8	3.502
6	0.364	0.4693	328.6	3.451
7	0.256	0.7648	335.5	3.431
8	0.139	1.4317	341.3	3.414

Run #10.

paddle height = 25.4 mm
u-umf = 69 mm/sec
chain speed = 22.35 mm/sec

section	=	1	2	3	4
umf(mm/sec)	=	46	44	37.3	32

sieve analysis (sample weight in grams)

size (micron)	1	2	3	4	5	6	7	8
600	.07	.16	.18	.23	.20	.28	.34	.51
500	2.84	3.51	4.06	5.22	6.75	8.35	9.30	11.22
425	8.36	10.20	10.50	13.46	15.34	17.20	19.10	21.17
355	19.06	18.82	20.72	22.05	23.71	24.26	23.93	27.29
300	23.82	24.27	24.29	22.20	22.03	20.92	21.16	19.59
0	20.07	20.44	18.96	19.15	17.89	16.41	17.16	19.16

sample	distance z	% salt	geom. mean (micron)	standard deviation
1	0.883	0.0905	294.3	3.558
2	0.774	0.0491	298.3	3.545
3	0.659	0.0556	306.0	3.520
4	0.520	0.1225	313.5	3.500
5	0.411	0.2891	324.1	3.464
6	0.299	0.6151	334.6	3.433
7	0.215	0.9538	336.4	3.428
8	0.123	2.0645	338.5	3.422

Run #11

paddle height = 25.4 mm
u-umf = 69 mm/sec
chain speed = 2.54 mm/sec

section =	1	2	3	4
umf(mm/sec)=	46	44	37.3	32

sieve analysis (sample weight in grams)

size (micron)	1	2	3	4	5	6	7	8
600	.12	.13	.15	.22	.21	.31	.30	.28
500	3.99	4.40	5.30	5.58	5.69	6.04	6.19	8.41
425	11.55	11.95	12.78	14.08	17.55	14.63	14.96	18.42
355	21.66	22.12	22.68	22.15	22.20	22.43	22.51	24.11
300	22.21	21.00	23.10	22.27	20.94	19.79	20.31	20.47
0	19.77	20.08	17.94	18.29	17.91	18.87	19.15	20.28

sample	distance z	% salt	geom. mean (micron)	standard deviation
1	0.888	0.0405	305.5	3.522
2	0.772	0.0458	306.3	3.519
3	0.661	0.1016	316.6	3.487
4	0.519	0.2264	317.7	3.484
5	0.404	0.3873	323.8	3.165
6	0.322	0.5911	318.0	3.483
7	0.209	0.9598	318.1	3.483
8	0.121	2.1097	325.0	3.462

Run #12

PADDLE HEIGHT = 25.4 MM
U-UMF = 46 MM/SEC
CHAIN SPEED = 68.58 MM/SEC

SECTION	1	2	3	4
UMF(MM/SEC)=	46	44	37.3	32

SIEVE ANALYSIS (SAMPLE WEIGHT IN GRAMS)

SIZE (Micron)	1	2	3	4	5	6	7	8
600	.17	.16	.22	.32	.29	.42	.38	.54
500	4.22	6.25	7.22	7.73	8.19	8.94	10.30	12.94
425	9.45	13.44	14.98	16.42	16.47	17.59	20.27	21.85
355	19.27	22.34	23.52	23.84	24.30	25.33	23.82	31.23
300	22.53	22.51	22.48	22.15	20.63	20.71	22.37	22.41
0	19.52	19.73	19.27	19.29	18.41	18.87	18.62	24.32

sample	distance z	% salt	geom. mean (micron)	standard deviation
1	0.880	0.0933	301.1	3.536
2	0.729	0.2007	314.1	3.495
3	0.600	0.3799	320.6	3.475
4	0.519	0.4591	323.9	3.465
5	0.423	0.5527	327.5	3.454
6	0.321	0.8016	329.9	3.447
7	0.210	1.3671	335.2	3.432
8	0.097	2.5071	330.7	3.445

Run #13

paddle height = 25.4 mm
u-umf = 46 mm/sec
chain speed = 41.45 mm/sec

section	=	1	2	3	4
umf(mm/sec)	=	46	44	37.3	32

sieve analysis (sample weight in grams)

size (micron)	1	2	3	4	5	6	7	8
600	.08	.10	.21	.23	.30	.27	.25	.36
500	2.99	4.34	6.02	6.98	8.20	9.03	10.72	12.35
425	7.18	9.90	13.05	14.83	15.99	17.81	20.12	22.63
355	16.83	20.86	20.85	23.92	24.74	24.76	26.42	28.17
300	20.01	20.93	23.22	21.64	21.70	22.31	21.71	23.64
0	19.14	20.58	18.54	18.39	18.10	17.75	18.86	20.85

sample	distance z	% salt	geom. mean (micron)	standard deviation
1	0.885	0.0530	290.6	3.570
2	0.770	0.0761	300.1	3.539
3	0.633	0.1428	315.5	3.491
4	0.491	0.2753	322.6	3.469
5	0.409	0.3808	328.1	3.453
6	0.319	0.5722	332.8	3.439
7	0.213	1.0100	336.2	3.429
8	0.125	1.8182	337.0	3.427

Run #14

paddle height = 25.4 mm
u-umf = 46 mm/sec
chain speed = 32.66 mm/sec

section	1	2	3	4
umf(mm/sec)=	46	44	37.3	32

sieve analysis (sample weight in grams)

size (micron)	1	2	3	4	5	6	7	8
600	.07	.20	.23	.22	.32	.33	.36	.45
500	2.74	3.81	4.91	6.56	7.85	9.43	10.53	11.67
425	7.50	9.70	11.30	13.33	15.74	18.21	20.85	22.59
355	18.15	19.48	20.35	23.39	24.40	25.79	26.56	27.89
300	20.45	22.71	21.85	20.44	20.60	20.85	20.95	21.56
0	21.43	20.43	20.44	19.07	18.53	16.76	18.16	19.75

sample	distance z	% salt	geom. mean (micron)	standard deviation
1	0.881	0.0748	286.1	3.585
2	0.798	0.0574	298.5	3.544
3	0.631	0.1109	304.3	3.525
4	0.515	0.1619	317.2	3.485
5	0.433	0.2773	325.6	3.460
6	0.310	0.6844	337.8	3.424
7	0.209	1.1340	339.0	3.421
8	0.142	1.6452	339.1	3.421

Run #15

paddle height = 25.4 mm
u-umf = 46 mm/sec
chain speed = 22.35 mm/sec

section	1	2	3	4
umf(mm/sec)=	46	44	37.3	32

sieve analysis (sample weight in grams)

size (micron)	1	2	3	4	5	6	7	8
600	.17	.17	.20	.24	.32	.34	.48	.64
500	2.81	3.67	5.16	6.36	7.46	9.73	10.18	13.15
425	7.84	9.28	11.67	14.87	15.68	18.17	20.66	24.01
355	17.82	20.34	23.35	22.75	23.82	24.98	26.51	30.31
300	22.90	22.53	25.16	22.31	21.23	21.32	22.18	23.81
0	20.61	20.29	21.42	18.31	17.01	15.76	16.51	19.67

sample	distance z	% salt	geom. mean (micron)	standard deviation
1	0.869	0.0668	290.3	3.571
2	0.743	0.0594	298.5	3.544
3	0.659	0.0739	306.3	3.519
4	0.519	0.1240	320.9	3.474
5	0.435	0.2391	329.0	3.450
6	0.295	0.5889	340.8	3.416
7	0.212	1.1262	343.0	3.409
8	0.114	2.0032	[illegible].0	3.407

Run #16

paddle height = 25.4 mm
u-umf = 46 mm/sec
chain speed = 2.54 mm/sec

section =	1	2	3	4
umf(mm/sec)=	46	44	37.3	32

sieve analysis (sample weight in grams)

size (micron)	1	2	3	4	5	6	7	8
600	.06	.13	.10	.14	.19	.00	.23	.30
500	2.42	3.08	3.65	5.29	5.19	.00	7.57	8.31
425	8.33	9.26	10.91	14.02	13.52	.00	16.99	17.59
355	19.22	20.26	21.79	22.81	21.63	.00	22.63	23.89
300	24.03	23.66	23.42	21.75	20.92	.00	17.18	17.93
0	20.30	20.22	17.91	17.29	18.70	.00	17.37	17.87

sample	distance z	% salt	geom. mean (micron)	standard deviation
1	0.895	0.0196	292.8	3.563
2	0.734	0.0343	297.5	3.547
3	0.645	0.0375	309.3	3.510
4	0.524	0.0647	320.2	3.476
5	0.423	0.1313	314.2	3.495
6	0.309	0.2949	.0	0.000
7	0.223	0.5241	328.8	3.451
8	0.138	0.7450	330.6	3.441

Run #17

paddle height = 25.4 mm
u-umf = 46 mm/sec
chain speed = 2.54 mm/sec

section =	1	2	3	4
umf(mm/sec)=	46	44	37.3	32

sieve analysis (sample weight in grams)

size (micron)	1	2	3	4	5	6	7	8
600	.08	.10	.17	.15	.13	.17	.23	.27
500	2.71	3.26	4.04	5.09	5.41	5.99	7.09	7.31
425	8.73	9.64	11.32	13.27	13.94	15.32	16.27	17.25
355	20.40	20.60	21.73	22.76	23.09	22.90	22.76	24.01
300	23.21	23.14	22.55	20.69	21.02	20.68	20.48	19.10
0	20.32	19.68	18.82	18.98	18.18	17.41	17.69	18.74

sample	distance z	% salt	geom. mean (micron)	standard deviation
1	0.884	0.0349	295.2	3.555
2	0.767	0.0268	300.1	3.539
3	0.659	0.0408	308.2	3.513
4	0.522	0.0686	313.6	3.496
5	0.435	0.1430	317.8	3.483
6	0.326	0.2551	323.2	3.467
7	0.244	0.4875	326.0	3.459
8	0.159	0.8192	325.6	3.460

Run #18

paddle height = 25.4 mm
u-umf = 69 mm/sec
chain speed = 22.35 mm/sec

section	1	2	3	4
umf(mm/sec)=	46	44	37.3	32

sieve analysis (sample weight in grams)

size (micron)	1	2	3	4	5	6	7	8
600	.14	.08	.10	.16	.17	.16	.13	.23
500	2.33	2.81	3.18	4.22	5.18	6.02	7.07	7.97
425	7.54	8.74	9.50	11.57	13.50	15.47	16.87	19.29
355	18.00	18.70	19.81	20.81	22.21	23.40	24.57	25.55
300	21.91	22.06	21.80	22.68	21.49	21.55	20.11	19.61
0	20.80	20.18	19.84	18.88	17.92	18.22	17.52	18.69

sample	distance z	% salt	geom. mean (micron)	standard deviation
1	0.873	0.0662	287.6	3.580
2	0.787	0.0402	293.5	3.561
3	0.671	0.0551	297.9	3.546
4	0.557	0.1194	308.0	3.514
5	0.453	0.2252	316.9	3.486
6	0.364	0.4271	321.5	3.472
7	0.256	0.8942	328.2	3.452
8	0.144	1.4189	330.4	3.446

Run #19

paddle height = 12.7 mm
u_{mf} = 92 mm/sec
chain speed = 20.32 mm/sec

section	1	2	3	4
u_{mf}(mm/sec)=	36.85	36.85	36.85	36.85

sieve analysis (sample weight in grams)

size (micron)	1	2	3	4	5	6	7	8
600	.09	.10	.12	.14	.15	.19	.19	.23
500	2.45	2.92	3.65	3.76	4.14	4.53	5.05	6.09
425	9.16	10.08	10.90	11.34	12.62	13.63	14.15	15.96
355	18.71	20.52	21.63	22.22	21.07	20.98	22.23	23.24
300	22.24	23.10	22.88	21.52	21.13	21.40	19.43	19.66
0	22.70	21.42	20.07	20.72	20.17	19.40	19.98	19.72

sample	distance z	% salt	geom. mean (micron)	standard deviation
1	0.884	0.1358	286.9	3.582
2	0.771	0.0860	295.3	3.554
3	0.660	0.1770	303.0	3.529
4	0.519	0.2420	302.4	3.531
5	0.437	0.4276	305.6	3.521
6	0.352	0.5690	310.3	3.506
7	0.269	0.9871	311.3	3.503
8	0.155	1.5901	317.9	3.483

Run #20

paddle height = 12.7 mm
u-umf = 92 mm/sec
chain speed = 10.16 mm/sec

section =	1	2	3	4
umf(mm/sec)=	36.85	36.85	36.85	36.85

sieve analysis (sample weight in grams)

size (micron)	1	2	3	4	5	6	7	8
600	.08	.13	.16	.18	.15	.20	.18	.16
500	3.21	3.67	4.15	4.38	4.37	4.56	4.95	5.64
425	10.83	11.91	11.96	13.44	12.80	12.61	13.51	14.96
355	19.90	21.20	22.26	21.90	21.29	21.65	22.05	22.94
300	21.85	22.56	21.85	21.97	19.99	20.45	21.09	19.64
0	22.12	20.47	19.37	20.48	20.05	19.05	19.92	21.05

sample	distance z	% salt	geom. mean (micron)	standard deviation
1	0.881	0.1423	294.2	3.557
2	0.800	0.1023	303.1	3.529
3	0.660	0.2253	308.1	3.513
4	0.520	0.3406	307.7	3.514
5	0.433	0.4755	306.7	3.517
6	0.352	0.6476	310.2	3.506
7	0.243	1.0086	310.5	3.505
8	0.155	1.5166	311.4	3.503

Run #21

paddle height = 12.7 mm
u-umf = 92 mm/sec
chain speed = 5.08 mm/sec

section =	1	2	3	4
umf(mm/sec)=	36.85	36.85	36.85	36.85

sieve analysis (sample weight in grams)

size (micron)	1	2	3	4	5	6	7	8
600	.08	.10	.13	.21	.12	.10	.14	.14
500	3.02	3.25	3.46	4.04	3.94	3.93	4.00	4.84
425	10.58	10.98	11.02	12.07	11.85	12.20	11.86	13.69
355	21.70	20.68	21.14	22.16	21.33	20.42	21.09	22.33
300	22.47	21.67	22.24	21.56	21.18	20.50	19.79	20.46
0	20.85	21.53	20.71	20.37	21.27	21.56	21.54	20.75

sample	distance z	% salt	geom. mean (micron)	standard deviation
1	0.892	0.1300	298.8	3.543
2	0.808	0.1757	296.9	3.549
3	0.670	0.2785	300.4	3.537
4	0.527	0.4961	305.3	3.522
5	0.417	0.6454	301.2	3.535
6	0.334	0.9430	299.8	3.539
7	0.222	1.1514	300.0	3.539
8	0.138	1.7061	308.2	3.512

Run #22

paddle height = 12.7 mm
u-umf = 92 mm/sec
chain speed = 2.54 mm/sec

section =	1	2	3	4
umf(mm/sec)=	36.85	36.85	36.85	36.85

sieve analysis (sample weight in grams)

size (micron)	1	2	3	4	5	6	7	8
600	.11	.11	.20	.17	.12	.16	.16	.15
500	3.78	4.01	4.32	4.16	4.14	4.53	4.12	4.54
425	11.86	12.47	12.96	12.38	12.77	13.04	12.62	13.15
355	21.24	22.33	22.56	22.15	20.90	22.96	21.58	21.54
300	23.46	23.30	20.72	23.33	20.76	21.82	20.20	22.25
0	21.52	20.92	20.30	20.36	22.18	21.09	22.45	21.34

sample	distance z	% salt	geom. mean (micron)	standard deviation
1	0.881	0.3316	300.8	3.536
2	0.771	0.3866	304.7	3.523
3	0.659	0.6596	308.1	3.513
4	0.520	0.6902	306.4	3.518
5	0.438	0.8600	300.2	3.538
6	0.316	1.1255	306.6	3.518
7	0.213	1.0589	299.8	3.539
8	0.157	1.4792	305.0	3.523

Run #23

PADDLE HEIGHT = 12.7 MM
U-UMF = 92 MM/SEC
CHAIN SPEED = 55.9 MM/SEC

SECTION	1	2	3	4
UMF(MM/SEC)=	36.85	36.85	36.85	36.85

SIEVE ANALYSIS (SAMPLE WEIGHT IN GRAMS)

SIZE (micron)	1	2	3	4	5	6	7	8
600	.04	.01	.05	.06	.12	.11	.16	.13
500	1.40	1.46	2.08	2.54	3.03	3.98	4.59	5.65
425	5.49	6.37	7.83	9.79	10.47	13.38	14.85	17.31
355	16.46	17.03	18.37	20.87	21.26	23.04	23.10	24.67
300	20.74	21.54	22.31	22.01	20.15	20.92	20.54	19.61
0	24.74	24.33	23.99	22.95	22.10	21.21	20.12	21.52

sample	distance z	% salt	geom. mean (micron)	standard deviation
1	0.873	0.0806	268.0	3.649
2	0.789	0.0537	272.2	3.633
3	0.645	0.1018	279.9	3.606
4	0.511	0.1980	289.9	3.572
5	0.427	0.3410	294.1	3.556
6	0.307	0.6453	305.3	3.522
7	0.224	0.9465	311.9	3.502
8	0.139	1.7357	314.8	3.493

Run #24

paddle height = 12.7 mm
u-umf = 69 mm/sec
chain speed = 20.32 mm/sec

section =	1	2	3	4
umf(mm/sec)=	43.01	40.81	34.99	31

sieve analysis (sample weight in grams)

size (micron)	1	2	3	4	5	6	7	8
600	.06	.08	.08	..14	.17	.21	.31	.37
500	2.09	2.52	2.91	3.70	4.60	5.65	6.43	7.86
425	7.64	8.45	9.37	11.54	13.67	15.56	17.74	21.21
355	18.43	19.19	20.24	21.90	23.37	24.10	23.91	24.92
300	21.79	23.70	22.79	22.83	21.96	19.28	20.80	20.17
0	25.46	22.54	22.70	20.18	18.56	19.93	18.37	19.51

sample	distance z	% salt	geom. mean (micron)	standard deviation
1	0.828	0.0387	276.0	3.620
2	0.743	0.0497	287.4	3.581
3	0.631	0.1628	290.3	3.571
4	0.522	0.1747	304.1	3.526
5	0.437	0.3194	315.0	3.492
6	0.324	0.5863	316.4	3.488
7	0.210	0.9211	325.6	3.460
8	0.157	1.5264	328.9	3.450

Run #25

paddle height = 12.7 mm.
u-umf = 69 mm/sec
chain speed = 10.16 mm/sec

section	1	2	3	4
umf(mm/sec)=	43.01	40.81	34.99	31

sieve analysis (sample weight in grams)

size (micron)	1	2	3	4	5	6	7	8
600	.06	.05	.09	.12	.14	.17	.22	.27
500	2.16	2.48	3.24	3.73	4.74	5.17	6.14	8.51
425	7.80	8.65	10.91	11.81	13.11	14.70	16.36	19.80
355	18.79	19.14	20.37	21.08	21.92	22.61	22.81	25.79
300	23.57	23.56	22.07	21.72	22.35	20.38	19.60	20.40
0	22.13	22.37	21.43	20.59	17.99	19.75	18.31	20.80

sample	distance z	% salt	geom. mean (micron)	standard deviation
1	0.881	0.0510	285.8	3.586
2	0.735	0.0536	287.9	3.579
3	0.686	0.0673	296.9	3.549
4	0.570	0.1257	302.4	3.532
5	0.460	0.2694	314.9	3.492
6	0.376	0.4024	313.6	3.496
7	0.243	0.7144	322.3	3.470
8	0.125	2.3115	326.5	3.458

Run #26

paddle height = 12.7 mm
u-umf = 69 mm/sec
chain speed = 5.08 mm/sec

section	=	1	2	3	4
umf(mm/sec)	=	43.01	40.81	34.99	31

sieve analysis (sample weight in grams)

size (micron)	1	2	3	4	5	6	7	8
600	.11	.11	.13	.13	.15	.16	.21	.20
500	2.34	2.58	2.91	3.14	3.84	4.07	4.49	5.24
425	8.36	9.55	9.88	10.39	12.17	11.90	13.19	14.66
355	20.26	19.68	20.09	20.53	22.26	21.55	21.29	21.93
300	23.28	23.91	23.47	22.19	19.65	21.40	19.82	19.43
0	21.99	22.02	20.74	21.05	21.78	18.94	19.59	19.97

sample	distance z	% salt	geom. mean (micron)	standard deviation
1	0.868	0.0420	289.3	3.574
2	0.787	0.0451	291.6	3.567
3	0.702	0.0567	296.5	3.551
4	0.590	0.1020	297.1	3.545
5	0.480	0.2269	300.7	3.537
6	0.366	0.3445	308.4	3.513
7	0.256	0.7697	309.1	3.510
8	0.143	1.3134	312.4	3.500

Run #27

paddle height = 12.7 mm
u-umf = 69 mm/sec
chain speed = 2.54 mm/sec

section	1	2	3	4
umf(mm/sec)=	43.01	40.81	34.99	31

sieve analysis (sample weight in grams)

size (micron)	1	2	3	4	5	6	7	8
600	.12	.14	.12	.17	.15	.11	.18	.15
500	2.84	2.99	3.87	3.76	4.29	4.49	4.49	5.32
425	10.25	10.35	11.40	11.81	12.50	12.96	12.95	13.92
355	19.60	21.12	21.23	20.60	22.28	22.41	21.95	22.15
300	20.88	22.52	23.22	21.46	21.28	20.96	19.97	20.49
0	22.18	20.89	19.65	20.76	19.76	18.92	20.20	20.19

sample	distance z	% salt	geom. mean (micron)	standard deviation
1	0.873	0.0924	291.6	3.567
2	0.763	0.0487	297.8	3.547
3	0.625	0.1323	305.2	3.523
4	0.513	0.2901	301.6	3.534
5	0.429	0.4370	308.1	3.513
6	0.314	0.7319	311.6	3.503
7	0.203	1.0114	307.5	3.515
8	0.145	1.5674	311.1	3.504

Run #28

paddle height = 12.7 mm
u-umf = 69 mm/sec
chain speed = 55.9 mm/sec

section	1	2	3	4
umf(mm/sec)=	43.01	40.81	34.99	31

sieve analysis (sample weight in grams)

size (micron)	1	2	3	4	5	6	7	8
600	.07	.02	.05	.07	.09	.15	.15	.24
500	1.20	1.29	2.00	2.37	3.21	4.37	5.20	5.70
425	4.87	5.44	7.76	8.97	11.38	14.37	16.54	18.18
355	15.06	16.19	18.19	19.64	21.43	23.86	24.04	25.61
300	21.49	21.48	21.32	20.47	21.59	22.12	20.78	20.11
0	25.26	25.72	23.96	23.61	21.66	18.97	18.52	18.96

sample	distance z	% salt	geom. mean (micron)	standard deviation
1	0.873	0.0860	263.6	3.665
2	0.763	0.0503	265.6	3.660
3	0.616	0.0797	278.9	3.610
4	0.511	0.1750	284.3	3.590
5	0.452	0.2393	297.9	3.550
6	0.306	0.4880	314.8	3.490
7	0.223	0.8234	320.8	3.470
8	0.138	1.2439	324.1	3.460

Run #29

paddle height = 12.7 mm
u-umf = 46 mm/sec
chain speed = 20.32 mm/sec

section	1	2	3	4
umf(mm/sec)=	43.01	40.81	34.99	31

sieve analysis (sample weight in grams)

size (micron)	1	2	3	4	5	6	7	8
600	.04	.05	.07	.12	.25	.23	.21	.27
500	1.53	1.60	2.61	3.83	5.04	6.14	7.17	6.70
425	5.73	5.85	8.51	11.56	14.53	16.67	18.76	18.01
355	16.12	16.31	19.14	20.76	22.18	23.77	23.89	25.10
300	21.74	23.18	21.58	21.85	19.64	21.09	19.06	20.79
0	25.22	24.57	21.65	19.79	18.62	15.86	18.33	17.20

sample	distance z	% salt	geom. mean (micron)	standard deviation
1	0.909	0.0499	268.1	3.648
2	0.800	0.0531	271.3	3.636
3	0.660	0.0655	288.9	3.576
4	0.522	0.1237	304.1	3.526
5	0.411	0.2038	316.0	3.489
6	0.324	0.3489	330.9	3.444
7	0.214	0.6619	328.2	3.452
8	0.157	0.8859	330.6	3.445.

Run #30

paddle height = 12.7 mm
u-umf = 46 mm/sec
chain speed = 10.16 mm/sec

section	1	2	3	4
umf(mm/sec)=	43.01	40.81	34.99	31

sieve analysis (sample weight in grams)

size (micron)	1	2	3	4	5	6	7	8
600	.02	.07	.01	.13	.15	.28	.30	.29
500	1.51	2.16	3.01	4.45	5.16	6.74	7.49	8.10
425	6.37	7.70	9.29	12.86	14.34	16.13	17.53	18.94
355	16.76	18.42	19.82	22.92	22.98	23.71	24.22	24.21
300	23.63	23.90	24.13	22.08	19.98	20.31	18.85	20.54
0	23.94	22.76	21.46	20.56	18.27	15.79	16.80	15.92

sample	distance z	% salt	geom. mean (micron)	standard deviation
1	0.882	0.0526	274.4	3.626
2	0.774	0.0371	283.9	3.593
3	0.631	0.0901	293.8	3.560
4	0.493	0.1233	307.6	3.515
5	0.409	0.2240	317.4	3.485
6	0.323	0.3804	331.7	3.442
7	0.212	0.6689	332.3	3.440
8	0.156	0.8168	337.8	3.424

Run #31

paddle height = 12.7 mm
u-umf = 46 mm/sec
chain speed = 5.08 mm/sec

section	1	2	3	4
umf(mm/sec)=	43.01	40.81	34.99	31

sieve analysis (sample weight in grams)

size (micron)	1	2	3	4	5	6	7	8
600	.03	.05	.07	.07	.17	.19	.21	.24
500	1.45	1.80	2.33	3.12	3.80	5.23	5.52	6.03
425	5.94	7.01	9.16	10.28	12.08	14.77	15.40	16.96
355	15.79	18.55	18.74	21.23	22.61	23.34	22.57	23.20
300	22.98	24.71	23.55	21.79	21.22	19.76	19.00	18.41
0	24.49	22.62	21.61	20.12	19.35	17.43	18.02	18.54

sample	distance z	% salt	geom. mean (micron)	standard deviation
1	0.876	0.0662	270.3	3.640
2	0.763	0.0313	282.5	3.597
3	0.680	0.0580	289.9	3.572
4	0.569	0.0687	299.7	3.540
5	0.482	0.0959	307.8	3.514
6	0.315	0.3837	321.1	3.473
7	0.203	0.7711	320.3	3.476
8	0.147	1.1460	322.5	3.469

Run #32

paddle height = 12.7 mm
u-umf = -46 mm/sec
chain speed = 2.54 mm/sec

section =	1	2	3	4
umf(mm/sec)=	43.01	40.81	34.99	31

sieve analysis (sample weight in grams)

size (micron)	1	2	3	4	5	6	7	8
600	.05	.07	.15	.14	.18	.19	.25	.24
500	1.66	1.98	2.86	3.27	4.62	5.78	6.16	6.30
425	6.54	7.59	9.63	10.67	14.09	15.79	15.79	16.39
355	18.27	19.76	20.41	20.67	22.64	23.73	22.68	23.56
300	24.21	22.75	22.37	20.84	20.95	20.48	18.57	19.02
0	24.14	23.60	20.99	20.14	17.67	16.55	18.11	18.44

sample	distance z	% salt	geom. mean (micron)	standard deviation
1	0.876	0.0546	277.1	3.616
2	0.764	0.0309	282.2	3.599
3	0.623	0.0668	295.3	3.555
4	0.513	0.1331	300.0	3.539
5	0.428	0.1677	317.6	3.484
6	0.317	0.4462	326.7	3.457
7	0.260	0.7094	322.1	3.471
8	0.148	0.9712	322.9	3.468

4 4

OF / DE

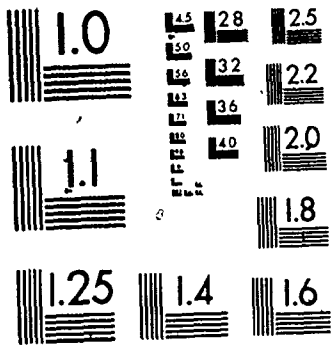

Run #33

paddle height = 12.7 mm
u-umf = 45 mm/sec
chain speed = 8 mm/sec

section	1	2	3	4
umf(mm/sec)=	43.01	40.81	34.99	31

sieve analysis (sample weight in grams)

size (micron)	1	2	3	4	5	6	7	8
600	.01	.06	.02	.07	.10	.09	.10	.11
500	1.09	1.44	1.90	2.62	3.58	4.94	5.16	5.63
425	4.77	5.33	7.33	9.94	12.04	15.05	15.45	16.73
355	15.70	17.09	18.90	20.38	22.58	22.18	23.03	24.94
300	23.83	23.14	23.08	21.98	21.02	20.74	19.81	19.87
0	24.54	24.99	21.87	20.87	19.42	17.32	17.81	17.58

sample	distance z	% salt	geom. mean (micron)	standard deviation
1	0.871	0.0459	267.3	3.651
2	0.784	0.0365	270.0	3.641
3	0.676	0.0439	284.7	3.590
4	0.563	0.0693	295.1	3.555
5	0.454	0.1670	306.8	3.517
6	0.312	0.3547	320.1	3.476
7	0.227	0.6034	320.3	3.476
8	0.144	0.7646	325.2	3.461

Run #34

paddle height = 12.7 mm
u-umf = 46 mm/sec
chain speed = 14 mm/sec

section =	1	2	3	4
umf(mm/sec)=	43.01	40.81	34.99	31

sieve analysis (sample weight in grams)

size (micron)	1	2	3	4	5	6	7	8
600	.03	.01	.07	.08	.08	.10	.17	.18
500	1.08	1.25	1.84	2.89	3.46	4.54	5.12	5.46
425	4.22	4.89	6.55	9.64	11.39	14.05	15.56	16.42
355	14.11	15.68	18.19	20.31	21.38	23.54	23.80	24.45
300	21.98	22.66	21.59	21.67	21.18	19.74	19.39	19.93
0	25.49	25.36	23.12	20.97	18.67	18.17	17.95	18.02

sample	distance z	% salt	geom. mean (micron)	standard deviation
1	0.868	0.0568	269.2	3.678
2	0.784	0.0503	285.3	3.659
3	0.671	0.0533	278.3	3.612
4	0.533	0.1044	294.8	3.556
5	0.451	0.1631	306.4	3.519
6	0.310	0.3100	316.2	3.488
7	0.225	0.4704	320.7	3.475
8	0.141	0.7784	322.9	3.468

Run #35

PADDLE HEIGHT = 12.7 MM
U-UMF = 46 MM/SEC
CHAIN SPEED = 55.9 MM/SEC

SECTION =	1	2	3	4
UMF(MM/SEC)=	43.01	40.81	34.99	31

SIEVE ANALYSIS (SAMPLE WEIGHT IN GRAMS)

SIZE (micron)	1	2	3	4	5	6	7	8
600	.03	.03	.04	.07	.10	.18	.15	.14
500	.82	1.20	1.90	2.75	3.87	4.83	5.47	5.86
425	3.60	4.96	7.10	10.15	12.79	15.45	16.87	18.38
355	12.59	15.24	17.60	19.80	22.10	24.24	24.77	27.75
300	20.64	22.35	19.42	21.05	20.98	20.65	22.53	22.11
0	26.15	25.41	24.79	22.25	19.72	19.76	18.47	20.80

sample	distance z	% salt	geom. mean (micron)	standard deviation
1	0.680	0.0686	252.8	3.706
2	0.783	0.0633	264.3	3.662
3	0.645	0.1032	273.3	3.630
4	0.530	0.1652	291.2	3.568
5	0.420	0.3306	307.4	3.516
6	0.307	0.7468	315.3	3.491
7	0.225	1.1620	322.6	3.469
8	0.141	1.5865	321.0	3.474

Run #36

paddle height = 12.7 mm
u-umf = 46 mm/sec
chain speed = 2.54 mm/sec

section =	1	2	3	4
umf(mm/sec)=	43.01	40.81	34.99	31

sieve analysis (sample weight in grams)

size (micron)	1	2	3	4	5	6	7	8
600	.09	.14	.17	.19	.11	.13	.18	.18
500	3.54	3.89	4.16	4.12	4.10	4.29	4.12	4.83
425	11.10	11.55	12.38	12.24	12.23	12.83	12.56	14.00
355	22.06	22.29	22.72	22.36	21.62	21.57	21.74	22.06
300	23.26	23.00	21.85	22.08	20.22	21.07	20.79	20.15
0	21.41	21.60	20.87	20.80	21.72	20.88	21.94	22.07

sample	distance z	% salt	geom. mean (micron)	standard deviation
1	0.881	0.3443	300.0	3.539
2	7.708	0.4211	301.3	3.535
3	0.661	0.5922	305.2	3.522
4	0.520	0.6699	304.9	3.524
5	0.437	0.8328	300.9	3.536
6	0.350	0.9695	304.8	3.524
7	0.268	1.1533	301.5	3.535
8	0.156	1.6208	305.0	3.523

APPENDIX J

Sample Calculation for Parameter S

From Table 5.25A, at $(U-U_{mf})$ = 92 mm/s,

Normalized Height from Grid	C_i (%)
1.0	0.014
0.843	0.015
0.665	0.013
0.495	0.012
0.342	0.015
0.224	0.024

$$Y^* = \frac{[\,0.014(1-0.843)+0.015(0.843-0.665)+0.013(0.665-0.495)+0.012(0.495-0.342)+0.015(0.342-0.224)\,]}{(1-0.224)}\ \%$$

$$= 0.0147\%$$

$$\bar{X} = 0.024(0.224)+[\quad] = 0.01681\%$$

S(based on weight) = 0.0147/0.01681 = 0.874

On an volumetric basis, assume density of salt =2.2
density of AC =1.4

$$Y^* = \frac{0.0147/2.2}{0.0147/2.2+(100-0.0147)/1.4} = 0.0000936\%$$

$$\bar{X} = \frac{0.01681/2.2}{0.01681/2.2+(100-0.01681)/1.4} = 0.0001070\%$$

S(based on volume) = 0.0000936/0.000107 = 0.875

Therefore, S based on weight and S based on volume is almost identical because of the low weight concentration.

APPENDIX K

Computer Programs DIFF and CASCAD for the Calculations of Diffusivity and Beneficiation Ratio based on Cascade Theoretical Model

```
      PROGRAM DIFF(INPUT,OUTPUT,TAPE5=INPUT,TAPE6=OUTPUT)
      REAL K,M1
      READ(5,*)K,S,U,H,PH
      ALPHA=PH/H
      WRITE(6,101)K,S,U,PH,H,ALPHA
  101 FORMAT(///,10X,"K= ",F10.4,/,10X,"S= ",F10.4,
     1/,10X,"U-UMF=",F10.4,/,10X,"PH= ",F10.4,
     2/,10X,"H= ",F10.4,/,10X,"ALPHA= ",F10.4)
  190 READ(5,*)CS,BR
      IF(CS.LE.1.E-3)GOTO 300
      VL=CS*PH/(H-PH)
      A=K*S*ALPHA/(H*(1.-ALPHA)*VL)
      B=4.*K*(S-1.)/((1.-ALPHA)*H)
      M1=ALOG(BR)/3658.
      D=2.*A*VL-2.*(2.*M1+A)*VL-B
      D=D/(4.*M1*(M1+A))
      WRITE(6,102)CS,BR,VL,D
  102 FORMAT(5X,"CS= ",F10.2,5X,"BR= ",F10.2,
     15X,"VL= ",F10.4,5X,"D= ",F10.2)
      GOTO 190
  300 CONTINUE
      STOP
      END
```

```
      PROGRAM CASCAD(INPUT,OUTPUT,TAPE5=INPUT,TAPE6=OUTPUT)
C
C     EDWARD W. CHAN NOV.25,82
C     CASCADE MODEL ON FLOTSAM PICH SYSTEM
C     PGM TO CAL BENEFICIATION RATIO BASED ON ASSUMED DIFFUSIVITY
C     DATA, MASS TRANSFER CONSTANT K, AND AS A FUNCTION OF CHAIN SPEED
C
      REAL K, M1,INT,L,PH
 1002 READ(5,*)UMUMF,PH,K,S,SLOPE,INT
      IF(UMUMF.LE.1.E-3)GOTO 1003
      H=150.
      L=3658.
      WRITE(6,101)UMUMF,PH,K,S,SLOPE,INT
  101 FORMAT(///,10X,"U-UMF=",F10.1,/,10X,"PH    =",F10.1,/,10X,"K     =",
     1F10.1,/,10X,"S     =",F10.2,/,10X,"SLOPE=",F10.4,/,10X,"INT   =",
     2F10.4)
      ALPHA=PH/H
       DO 1001 I=2,70
      CS=FLOAT(I)
      VL=CS*PH/(H-PH)
      D=EXP(INT)*EXP(SLOPE*ALOG(CS))
      CONST1=VL/D+K*S*ALPHA/H/(1.-ALPHA)/VL
      CONST2=4.*K*(S-1.)/D/(1.-ALPHA)/H
      M1=(CONST1*CONST1-CONST2)**0.5-CONST1
      M1=M1/2.
      BP=EXP(M1*L)
      WRITE(6,102)CS,VL,D,BP
  102 FORMAT(/,5X,"CS=",F5.1,5X,"VL=",F10.3,5X,"D=",F10.2,5X,"BP=",
     1F10.2)
 1001 CONTINUE
      GOTO 1002
 1003 CONTINUE
      STOP
       END
```

REFERENCES

1. MacDonald, I. F., EL-Sayed, M., Mow, K., and Dullien, "Flow through Porous Media - the Ergun Equation Revisited", Ind. Eng. Chem. Fundam., Vol. 18, No. 3, 1979 (pp. 199-207).

2. Kunii, D. and Levenspiel, O., "Fluidization Engineering". Huntington: Kreiger Publishing Co., 1977, p. 70.

3. Ibid, p. 112.

4. Davidson, J. F. and Harrison, D. (editors), "Fluidization". London: Academic Press, 1971, p. 28.

5. Ibid, p. 183.

6. Zenz, I. A. and Othner, D. F., "Fluidization and Fluid-Particle Systems". New York: Rheinhold Publishing Corp., 1960, p. 232.

7. Broadhurst, T. E. and Becker, H. A., "Onset of Fluidization and Slugging in Bed of Uniform Particles", AICHE Journal, Vol. 21, No. 2 (March, 1975), pp. 238-247.

8. Chen, J.L.P. and Keairns, D. L., "Particle Segregation in a Fluidized Bed", Can. J. Chem. Eng., Vol. 53 (Aug. 1975), p. 395.

9. Cheung, L., Nienow, A. W. and Rowe, P. W., "Minimum Fluidization Velocity of a Binary Mixture of Different Sized Particles", Chem. Eng. Sci., Vol. 29, 1974, pp. 1301-1303.

10. Wen, C. Y. and Yu, Y. H., AICHE Journal, Vol. 12, 1966, p. 610.

11. Gibilaro, L. G. and Rowe, P. N., "A Model for a Segregating Gas Fluidized Bed", Chem. Eng. Sci., Vol. 29, 1974, pp. 1403-1412.

12. Nienow, A. W., Rowe, P. N. and Cheung, L.Y.L., "A Quantitative Analysis of the Mixing of Two Segregating Powders of Different Density in a Gas Fluidized Bed", Power Technology, Vol. 20, 1978, pp. 89-97.

13. Jeffs, J. A., "Effect of Convection in a Bed of Fluidized Solids", U.W.O. - M.E.Sc. Thesis, 1980.

14. Nienow, A. W., Rowe, P. N. and Cheung, L.Y.L., "The Mixing/Segregation Behaviour of a Dense Powder with Two Sizes of a Lighter Ore in a Gas Fluidized Bed", "Fluidization", Combridge Unversity Press, 1970.

15. Nienow, A. W., Naimer, N. "Continuous Mixing of Two Particulate Species of Different Density in a Gas Fluidized Bed", Trans. I. Chem. E., Vol. 58, 1980 pp 181-186.

16. Rowe, P. N., Partridge, B. A., Cheney, A. G., Henwood, G. A. and Lyall, E., "The Mechanisms of Solids Mixing in Fluidized Beds", Trans. Instn. Chem. Engrs., Vol. 43, 1965, T271-286.

17. Rowe, P. N., Nienow, A. W. and Agbim, A. J., "The Mechanism by Which Particles Segregate in Gas Fluidized Bed - Binary System of Near Spherical Particles", Trans. Instn. Chem. Engrs., Vol. 50, 1972 pp 310-323

18. Nienow, A. W., Rowe, P. N. and Agbim, A. J., "A Note on the Liquid-Like Properties of Gas Fluidized Bed", Trans. Instn. Chem. Engr., Vol. 51, 1973 pp 260-264

19. Piccinini, N., Bernard, A., Campagna, P. and Vallana, I., "Segregation Phenomenon in Spouted Bed", The Canadian Journal of Chem. Engr., Vol. 55, April 1977 pp 122-125

20. Lai, I., Hersey, J. and Staniforth, J., "Segregation and Mixing of Fine Particles in an Ordered Mixture", Powder Technology, Vol. 28, 1981, pp. 17-23.

21. Rowe, P. N., Nienow, A. W. and Agbim, A. J., "A Preliminary Quantitative Study of Particle Segregation in a Gas Fluidized Bed - Binary System of Near Spherical Particles", Trans. Instn. Chem. Engr., Vol. 50, 1972 pp 324-333

22. Chiba, S., Nienow, A. W., Chiba, T. and Kobayashi, H., "Fluidized Binary Mixtures in Which the Denser Component May Be Flotsam", Powder Technology, Vol. 26, 1980, pp. 1-10.

23. Capes, C. E. and Sutherland, J. P., "Ore Separations in a Packed Fluidized Bed", I & EC Process Design and Development, Vol. 5, No. 3, July 1966, pp. 330-336.

24. Rowe, P. N. and Sutherland, K. S., "Solids Mixing Studies in Gas Fluidized Bed. Part II: The Behaviour of Deep Beds of Dense Materials", Trans. Instn. Chem. Engrs., Vol. 42, 1964 T55-763

25. Chechetkin, A. V.; Pavlou, V. A., Apostolova, G. V., Dementev, A. I. and Romanova, T. T., "Effect of the Size of Solid-Phase Particles on the Intensity of Their Mixing in the Fluidization of a Polydispersed Material", Theoretical Foundations of Chem. Egr. (USSR), Vol. 8(5), 1974, pp. 752-754.

26. Hussain, I. D., Maitra, P. P. and Jackson, R., "Heat Transfer to an Endothermic Gas-Solid Reaction Using a Particulate Heat Transfer Medium", to be published soon. A copy of the manuscript can be obtained from Professor R. Jackson, Dept. of Ch.E., U. of Houston, Houston, Texas 77004, USA.

27. Iya, S. K. and Geldart, D., "Flow of Coarse Particles Through a Fluidized Bed of Fines", Ind. Eng. Chem. Process Des. Dev., Vol. 17, No. 4, 1978.

28. Nienow, A. W., Rowe, P. N. and Chiba, T., "Mixing and Segregation of a Small Proportion of Large Particles in Gas Fluidized Beds of Small Ones", AIChE Symp. Ser. 74, N176: 45, 1978.

29. Rowe, P. N. and Nienow, A. W., "Particle Mixing and Segregation in Gas Fluidized Beds. A Review", Powder Technology, 15, 1976, pp. 141-147; also presented in Chem. Eng. Congress (Pa.Ch.E.C. 1977).

30. Burgess, J. M., Fane, A. and Fell, C., "Measurement and Prediction of the Mixing and Segregation of Solids in Gas Fluidized Bed", Proceedings Pachec '77, 1977.

31. Tanimoto, H., Chiba, S., Chiba, T. and Kobayashi, H., "Mechanism of Solid Segregation in Gas Fluidized Bed", in Fluidization (J. R. Grace and J. M. Matsen, ed.), 1980, p. 381.

32. Chiba, S., Tanimoto, H., Kobayashi, H. and Chiba, T., "Measurement of Solid Exchange Between the Bubble Wake and the Emulsion Phase in a Three Dimensional Gas Fluidized Bed", Journal of Chem. Engin. of Japan, Vol. 12, No. 1, 1979, pp. 43-45.

33. Chiba, T. and Kobayashi, H., "Solid Exchange Between the Bubble Wake and the Emulsion Phase in a Gas Fluidized Bed", Journal of Chem. Engin. of Japan, Vol. 10, No. 3, 1977, pp. 206-210.

34. Yoshida, K., Kameyama, H. and Shimizu, I., "Mechanism of Particle Mixing and Segregation in Gas Fluidized Bed", Fluidization (J. R. Grace and J. M. Matsen, ed.), 1980, p. 389.

35. Yoshida, K. and Kunii, D., "Stimulus Response of Gas Concentration in Bubbling Fluidized Beds", Journal of Chem. Engin. of Japan, Vol. 1, No. 1 , 1968, pp. 11-16.

36. Beeckmans, J. M. and Bergstrom, L., "Segregation Mechanisms in Gas Fluidized Beds", to be published shortly. A copy of the paper may be obtained from Professor Beeckmans, U. of Western Ontario, London, Ontario, Canada.

37. Bergstrom, L., "The Fundamental Mechanisms of Mixing and Segregation in GasFluidized Beds", Diplôme d"Etudes Approfondies - Thesis, Universite de Technologie de Compiegne, Compiegne, France, 1980.

38. Minh, T. O., "Solids Segregation in Gas-Fluidized Cascade", U.W.O. - M.E.Sc. Thesis, 1978.

39. Beeckmans, J. M. and Minh, T. O., "Separation of Mixed Granular Solids Using the Fluidized Counter-Current Cascade Principle", Canadian Journal of Chem. Engin., Vol. 55, Oct. 1977, pp. 493-496.

40. Muzyka, D. W., "Solid Separation in a Counter-Current Fluidized Cascade", U.W.O. - M.E.Sc. Thesis, 1979.

41. Muzyka, D. W. and Beeckmans, J. M., "Effect of Convective Velocity on Longitudinal Diffusivities in a Fluidized Cascade Separator", Canadian Journal of Chem. Engin., Vol. 57, Oct. 1979, pp. 586-589.

42. Jeffs, J. A., "Segregation of Ash from Coal in a Fluidized Cascade", U.W.O. - ES400 Project Report, 1978.

43. Kaldas, A., "Electrostatic Fluidized Cascade", U.W.O. - M.E.Sc. Thesis, 1980.

44. Kaldas, A., "Literature Survey on Mixing and Separation in Fluidized Bed", U.W.O. - ES601 Project Report, 1979.

45. Goransson, M. E., "Coal Beneficiation in Counter-Current Fluidized Cascade", Diplime d'Etudies Approfondies - Thesis, Universite deTechnologie de Compiegne, Compiegne, France.

46. Fraser, T. and Yancey, H. F., "Process of Separating Loosely Mixed Materials", U.S. Patent 1534846, April 21, 1925.

47. Steinmetzer, J. N., "Apparatus for the Separation of Dry Materials", U.S. Patent 2006119, June 25, 1935.

48. Binnix, D. B., "Pneumatic Stratification with Vibratory Draw-off", U.S. Patent 3278029, Oct. 11, 1966.

49. Weintraub, M., Deurbrouck, A. W., "Separation of Particulate Solids of Varying Densities in a Fluidized Bed", U.S. Patent 3774759, Nov. 27, 1973.

50. Harms, V., "Progressive Classifying of Treating Solids in a Fluidized Bed Thereof", U.S. Patent 2586818, Feb. 26, 1952.

51. Morgan, J. D., "Process and Mechanism for Separating Intermixed Divided Materials", U.S. Patent 2069325, Feb. 2, 1937.

52. Baskakov, A. P., Malykh, G. A. and Shishko, I. I., "Separation of Materials in a Fluid Bed with Continuous Feeding and Discharge", The Soviet Chemical Industry, 6:6, 1974, pp 393-395.

53. Punter, T. J., "Fluidized Bed Recovery System for Particulate Material", Breitish Patent: 1-370-801, April 30, 1971.

54. Eveson, G. I., "Improvement Relating to the Dry-Cleaning of Large or Small Coal or Other Particulate Materials Containing Components of Different Specific Gravities", British Patent: 1037279, July 27, 1966.

55. Holmes, C.W.H., "Apparatus for Separation of Dry Materials", U.S. Patent 1944643, Jan. 23, 1934.

56. "Dryflo Separators - A New Principle for Dry Concentration and Classification of Mineral", a Publication from Dryflo Separators Limited, New Barnet, Herts., Telex: 25292.

57. Pearson, D. and Webb, M., "The Salvage and Recycling of Useful Matereials", The Chemical Engineers, Feb. 1973.

58. Douglas, E. and Sayles, C. P., "Dry Sorting Using Pneumatically Fluidized Powders", AIChE Symposium Series, No. 116, Vol. 67, 1971.

59. Douglas, E. and Walsh, T., "New Type of Dry, Heavy-Medium Gravity Separator", Transactions/Section C of the Institution of Mining and Metallurgy, Vol. 75, C225, 1966.

60. Douglas, E. and Jackson, D. V., "Waste Reclamation 1, A Source of Raw Materials", J. of Environmental Planning and Pollution Control, Vol. 1, No. 2, 1972, pp 12-18.

61. "Pneumatic Coal Cleaning Process", a Publication from Birtley Engineering Limited, BSA House, 54 St. James St., London, S.W. 1.

62. Yan, T. Y., "Magnetic Desulfurization of Airborne Pulverized Coal", U.S. Patent 4052170, Oct. 4, 1977.

63. Chen, J. L. P. and Keairns, D. L., "Particle Separation from a Fluidized Mixture. Simulation of the Westinghouse Coal Gasification Combustion /Gasifier Operation", Ind. Eng. Chem. Process Deo. Dev., Vol. 17, No. 2, 1978, pp. 135-141.

64. Jordison, F., "Rotating Stratifier", U.S. Patent: 3844414, Oct. 29, 1974.

65. Ingels, R. M., "How to Use the Computer to Analyze Test Data", Chemical Enquiry, August 11, 1980.

66. Levenspiel, O., "Chemical Reaction Engineering", New York: John Wiley and Sons Publishing Co., 1972, p. 308.

67. Perry, R. H. and Chilton, C. H., "Chemical Engineers' Handbook", New York: McGraw Hill Book Company, Fifth Edition, 1973.

68. Book of ASTM Standard, Designation D271-70.

69. Christian, G. O., "Analytical Chemistry", Waltham, Mass.: Xerox College Publications, 1970.

70. "Book of ASTM Standard", Designation E277-69.

71. Picard, J. L. and Rosenhart, C.F.J., "Procedure for Float-Sink Analysis", Divisional Report FMP 67/14 WRL, Dept. of Energy, Mines and Resources of Canada - Mines Branch, Ottawa, 1966.

72. Jenkins, R., An Introduction to X-Ray Spectrmetry, New York: Heyden and Son Limited, 1974.

73. Abugor, B. D., "Coal Beneficiation in a Countercurrent Fluidized Cascade", U.W.O. - M.E.Sc. Thesis, 1978.

74. Sterling, T. D. and Pollack, S. V., "Introduction to Statistical Data Processing", Prentice Hall Company, Englewood Cliffs, New Jersey, 1968, p. 645.

75. Kolthoff, I. M., "Quantitative Inorganic Analysis", New York: McMillan Book Company, 1969-1971, pp. 542-544.

76. Murphy, D. M. and Rousseau, V., "Foundation of College Chemistry", New York: Ronalt Press Company, 1969.

77. Muzyka, D. W., Beeckmans, J. M. and Jeffs, J. A., "Solid Separation in a Counter Current Fluidized Cascade: Jetsam Rich Mixture at Total Reflux", Canadian Journal of Chem. Engin., Vol 56, June 1978, pp. 286-291.

78. Kunii, D. and Levenspiel, O., "Fluidization Engineering." Huntington: Kreiger Publishing Co., 1977, p. 157.

79. Muzyka, D. and Beeckmans, J.M., "Effect of Convective Velocity on Longitudinal Diffusivities in a Fluidized Cascade Separator", Canadian Journal of Chem. Engin., Vol. 57, Oct. 1979, pp. 586-590.

80. Rowe, P.N., "Prediction of Bubble Size in a Gas Fluidized Bed", Chemical Engineering Science, Vol. 31, 1976, pp. 285-288.

81. Beeckmans, J.M. and Jeffs,A., "Taylor Dispersion in Fluidized Channel Flow", Chemical Engineering Science, Vol. 37, 1982, pp. 863-867.

82. Taylor, G., Proc. Roy. Soc. 1953, A219, 186.

83. Taylor, G., Proc. Roy. Soc. 1954, A223, 446.

END

2010983

FIN